ABSTRACT

MIELKE, BENJAMIN THOMAS. Advanced Fiber Strengthening Systems for Concrete Structures. (Under the direction of Dr. Sami H. Rizkalla).

For a number of recent years, repair and strengthening of civil infrastructure has become in great demand due to the deterioration of concrete structures caused by corrosion of the steel reinforcement and the need for increasing the load carrying capacity of structures and bridges. This research project investigates the use of innovative strengthening systems using different types of fiber reinforced polymer materials in combination with different adhesive materials for strengthening and repair of reinforced concrete structures. Some of the advantages of these innovative strengthening systems are they have a high fire resistance due to the use of cementitious materials as the adhesive and use high strength carbon fiber rods to greatly increase the ultimate load carrying capacity. This report summarizes the results of 14 reinforced concrete slabs strengthened with different FRP strengthening systems, and two control unstrengthened slabs that were used to measure the effectives of the different strengthening systems examined in this study. The following is a summary of the experimental program, test results, and the research findings based on the completed experimental program. The research presented in this report explores new and advanced fiber strengthening systems for concrete structures. The fibers used are:

- Carbon fiber strands, commercially known as FORCA carbon strands provided by Nippon Steel Materials Co., Ltd
- Carbon fiber grid provided by Fyfe Company, LLC
- Glass fiber grids provided by PPG Company

The research program explores the use of these fibers with cementitious material as the adhesive material instead of the traditional epoxy material which does not have good fire resistance. The two cementitious adhesive materials explored were:

- Grancrete PCW provided by Grancrete Inc.
- Tyfo C-Matrix provided by Fyfe Company, LLC

The load carrying capacity, ductility, and mode of failure of the strengthened slabs were observed and used to evaluate four parameters that are critical in determining the

effectiveness of the strengthening system. The four parameters investigated in the experimental program includes the application technique that is used to apply the strengthening system, the type of fiber used in the strengthening system, the effect the type of adhesive used has on the strengthening system, and the effect the fiber reinforcement ratio has on the proposed strengthening systems. It is believed that these four parameters influence the ultimate load carrying capacity and failure mode the most. The research findings indicate that the use of near surface technique gives comparable results to those that use the externally bonded technique and therefore may be a useful alternative to using the externally bonded technique. The findings also indicate that the use of carbon fibers generally increase the ultimate load carrying capacity more than the glass fibers and have a similar reduction in ductility, signifying that carbon fibers are more effective than glass fibers. When comparing the cementitious materials to the traditional epoxy adhesive, the findings indicate that the cementitious materials allow for a more ductile failure mode while obtaining similar ultimate load carrying capacities as the epoxy, and when you combine this with the potential benefits of having a higher fire resistance, it presents a desirable alternative to the traditional epoxy strengthening system. The findings also indicate that the fiber reinforcement ratio, more specifically the spacing between the FRP fibers, is an important parameter, especially when cementitious materials are used as the adhesive. The research shows that as the spacing between the fibers are increased; a stronger bond is formed that meets the bond strength requirement of the ACI 440.2R-08 committee report for externally bonded strengthening systems.

Advanced Fiber Strengthening Systems for Concrete Structures

by
Benjamin Thomas Mielke

A thesis submitted to the Graduate Faculty of
North Carolina State University
in partial fulfillment of the
requirements for the degree of
Master of Science

Civil Engineering

Raleigh, North Carolina

2011

APPROVED BY:

_____	_____
Dr. Rudolf Seracino	Dr. James Nau

_____
Dr. Sami H. Rizkalla
Chair of Advisory Committee

DEDICATION

I dedicate this thesis to all those who supported me and believed in me, through the good times and the bad. They include my parents, my brother, all the students at the CFL and NC State who helped me through this, and my fellow church members at Good Shepherd Lutheran Church and Holy Trinity Lutheran Church. Without your constant love and support, I wouldn't be the person I am today. Thank you.

BIOGRAPHY

Benjamin Thomas Mielke was born in Anchorage, Alaska in and was raised in Raleigh, North Carolina. He attended Leesville Road High school where he received his high school diploma. Benjamin was accepted to the Department of Civil Engineering at North Carolina State University and began his college career in the fall of 2005. He graduated Magnum cum Laude in December 2009 with a Bachelor of Science degree from the Department of Civil Engineering. After graduation, he immediately started graduate school at North Carolina State University under the direction of Dr. Sami H. Rizkalla. While enrolled in the graduate program, he worked on two main projects. The first one is described in this thesis, which is the Use of Advanced Fiber Strengthening Systems for Infrastructure, and the other is the ICC Acceptance Testing of CFRP Strengthening Systems for Reinforced Concrete Structures. After graduation, Benjamin wishes to join a well-respected structural engineering firm as a designer, earn his PE, and become a project manager.

ACKNOWLEDGMENTS

I would first like to thank my advisor, Dr. Sami Rizkalla, for his guidance and support during this project. Without continued direction from you I would not be where I am today. I would also like to thank Dr. Rudolf Seracino and Dr. James Nau for being a member of my advisory committee. Your time, effort, and advice were invaluable during this process.

Special thanks to the industrial members of the Center for Integration of Composites into Infrastructure (CICI) who shared the sponsorship of this research program. In particular the following members:

- Nippon Steel Materials Co., Ltd.
- Fyfe Company, LLC
- Grancrete Inc.

These companies provided the technical support I needed to make this project a success. Special thanks goes to Jeff Selph who was always ready and willing to help with casting of Grancrete.

Thanks also to the staff of the Constructed Facilities Laboratory, North Carolina State University. They include Greg Lucier, the Constructed Facilities Lab Manager, for his constant guidance and advice, lab technicians Jerry Atkinson and Johnathan McEntire, who helped me with any of the technical problems I had during my project, and administrative assistant Denise Thoesen who helped me clear all the administrative hurdles.

Last but certainly not least, I would like to thank all the students at the CFL who helped me through this process, whether it be helping me with the casting of my specimens, discussing academic theories, or just being there for moral support, I definitely could not have done this without you. I would like to acknowledge Adolfo Obregon-Salinas for teaching me all that he knew; Tyler Storm who shared an office with me and helped me deal with Adolfo; and to

Curtis Kennedy, David Ragan, Ty Rutledge and Amy Byrum, who were all there for me when I needed them the most. Without them I would have never made it through. Last but not least, special thanks go to my brother, Brian, who worked side by side with me to help me complete this project. Without your help I would have never finished on time and your constant support and encouragement got me through the most trying two years of my life. Thank you all.

TABLE OF CONTENTS

LIST OF TABLES

LIST OF FIGURES

CHAPTER 1 -INTRODUCTION

1.1 Background

Research in the field of civil infrastructure has focused on providing industry with a repair/strengthening system that can be used effectively and efficiently. The deterioration of civil infrastructure and the need to increase the load carrying capacity of these structures has led to a need for these repair and strengthening systems. Researchers first explored the use of a steel plate and epoxy strengthening system to strengthen and repair these structures. While this strengthening system did work, there were several complications that arose when using these systems. These complications included the fact that the steel plates were heavy, which made them hard to handle, and the steel plates had a tendency to corrode. To address these complications, researchers turned to Fiber Reinforced Polymer (FRP) sheets. FRP sheets have the advantage of being light weight, easy to handle, resistant to corrosion, and stronger than the steel plates. Since the 1980's, researchers and engineers have focused on using these FRP strengthening systems to strengthen and repair civil infrastructure. They have looked at several key parameters that affect the performance of these FRP strengthening systems. Some of these parameters include bond length, surface preparation, and concrete strength. With continued research, industry has been able to better predict the performance of these systems.

1.2 Objectives

The objective of this experimental program is to investigate the use of advanced FRP strengthening systems for repair and strengthening of reinforced concrete structures. The research includes the study of the various parameters which are believed to influence the effectiveness of the proposed FRP strengthening system. The parameters examined in this research are the application technique, type of fiber, type of adhesive, and the fiber reinforcement ratio. To study the effect of these parameters, fourteen reinforced concrete slabs were strengthened with an FRP strengthening system and tested in four-point bending. The two other unstrengthened slabs were used as control specimens. Two application techniques were studied, the externally bonded technique and the near surface mounted

technique. Three different types of fibers were investigated, a carbon fiber strand sheet, a carbon fiber grid, and a glass fiber grid. The adhesives used were two cementitious materials and an epoxy. The effect of using different fiber reinforcement ratios, and more specifically the spacing between the fibers, was also studied. Spacing refers to the center-line to center-line distance between the fibers and is critical when using a cementitious adhesive to ensure that the cementitious adhesive is able to penetrate between the fibers and form a strong bond with itself and the concrete surface. Pull-off test will also be conducted to study the affect these parameters have on the bond strength between the fibers, adhesive, and concrete surface.

1.3 Scope

In addition to the introductory chapter, the second chapter in this thesis will provide background information on the repair of civil infrastructure with the use of FRP strengthening systems. More specifically, this chapter will explore two different application techniques. The first one is the externally bonded technique, which has been used since the strengthening of structures was first considered and has been widely researched. The other method is the near surface mounted technique, which is a more recent and innovative technique that has been suggested in recent studies to be more efficient than the externally bonded technique.

The third chapter in this thesis will describe the experimental program. The material properties of the concrete, reinforcing steel, and FRP material that were used in the experimental program will be described. The details of the flexural strengthening of the reinforced concrete slabs will also be provided. The test setup as well as the instrumentation will also be described.

The fourth chapter will explore the experiment results and discuss any findings that were made. The four parameters affecting the performance of the strengthening systems will be investigated and the results of the findings discussed. Predictions of the ultimate load carrying capacity will be compared to the experimental results and the accuracy of these

predictions will be discussed. Predictions were made using ACI 440.2R-08 design guidelines.

The fifth chapter will be a summary of the experimental program and will describe the conclusions that were drawn as a result of the two phases of the experimental program. Recommendations for future work will also be presented in this chapter.

CHAPTER 2 -LITERATURE REVIEW

2.1 Introduction

Aging, deteriorating civil engineering infrastructure and the demand to increase the load carrying capacity of reinforced concrete structures and bridges has led to the need for a rehabilitating and/or strengthening system that is cost effective in comparison to replacing these structures. The rehabilitation and strengthening systems are also desired to be simple and can be constructed in a short amount of time. Research has been conducted to explore different strengthening systems that could be used to strengthen these reinforced concrete structures. Steel plates bonded to the surface with an epoxy adhesive were first considered and used to increase the capacity for reinforced concrete structures. Steel was selected due to its high strength and ductile behavior at failure. There were several complications that arose when using the steel plate strengthening system. The first is that the steel plates are usually very long and heavy; therefore, it was difficult to erect and apply in the field. The other complication was the presence of voids in the epoxy layer that allowed tainted water and other potentially corrosive liquids to be in contact with the steel and cause corrosion. There was also concern with debonding of these heavy steel plates when bonded to the concrete. Researchers concluded that there was a need for new material to replace the steel plates. This vision led to the use of the new advanced composite material in the form of Fiber Reinforced Polymers (FRP) as alternative materials for these strengthening systems. The advantages to using FRP as a replacement to steel became apparent in the late 1980s. The advantages of FRP materials are its non-corrosive characteristics, high strength to weight ratio and high tensile strength. When compared to steel plates, FRP is much lighter, which leads to an easier, quicker, and more economical installation cost than steel strengthening. FRP materials can increase the yield load carrying capacity as well as significantly increase the ultimate load carrying capacity more than the steel due to its higher strength characteristics when compared to steel. The research explored the different application techniques that can be used to apply these new materials. An application technique that ensured full utilization of the FRP reinforcements of the concrete member was desired. The first application

technique that was used to apply these FRP and epoxy strengthening systems was the externally bonded technique, similar to what was used for the application of steel plates. The externally bonded (EB) technique involves laying a FRP sheet or plate on the cleaned and prepared concrete surface and bonding the FRP with an epoxy or other cementitious material as the adhesive. This technique was very successful and has been extensively researched and used in the field. However, there have been some concerns in recent years that this system is not efficient enough and does not allow for the full utilization of the FRP material. Therefore, recent studies have focused on a different technique, which has been referred to as the Near Surface Mounted (NSM) technique. The following literature reviews selected details of these two different application techniques, their strengths and weaknesses, the different failure modes that can be associated with each, as well as discusses possible research that should be considered in the future.

2.2 Externally Bonded (EB) Technique

The externally bonded (EB) technique is the oldest technique used to attach the FRP material to the concrete surface. Through extensive research and field application, it has proven to be a very effective and economical strengthening technique. The externally bonded technique is a multi-step process that begins with the preparation of the concrete surface. This is one of the most important steps in the strengthening process. It is critical to remove all loose particles from the concrete substrata and expose the aggregate in order to ensure a full bond between the adhesive and the concrete substrata. This is usually done with a rough-disk grinder or sandblasting as shown in Figure 1.

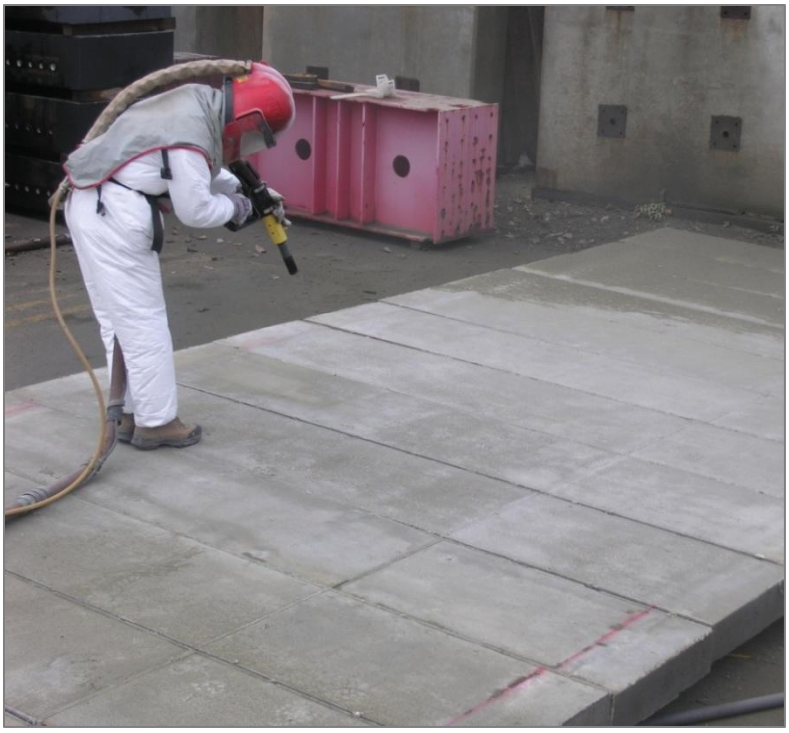

Figure 1: The use of Sandblasting as a Surface Preparation Technique

After cleaning the surface, establish some roughness of the surface and remove all loose particles with pressurized air. A layer of adhesive is then applied to the prepared surface. The most common type of adhesive used is a two-part epoxy, consisting of a hardener and resin, that when combined, form a very strong adhesive. Once this layer of adhesive is placed on the prepared concrete surface, it is followed by laying down the FRP plate or sheets. One of the most common and effective fiber used for flexural strengthening is carbon FRP (CFRP). CFRP has many desirable material characteristics including high strength, noncorrosive properties, as well as the carbon fibers' ability to form a strong bond with the adhesive and the prepared surface. The only drawback of the carbon fiber materials is its high cost in comparison to glass fiber. The high cost has encouraged research to explore alternative fibers for the strengthening systems. Glass fiber reinforced polymer (GFRP) materials were also considered due to its desirable characteristic of high rupture strain. However, it is typically not recommended for flexural strengthening due to its low elastic modulus and therefore deflection of the strengthened member may become one of the major

criteria for the design. Once this FRP sheet or plate has been applied to the adhesive, a second layer of adhesive is applied on top of the FRP sheet to complete the saturation of the fibers. These steps are shown in Figure 2. Once the adhesive has cured and gained its full strength, the strengthening system can now be used to carry the designed additional loads.

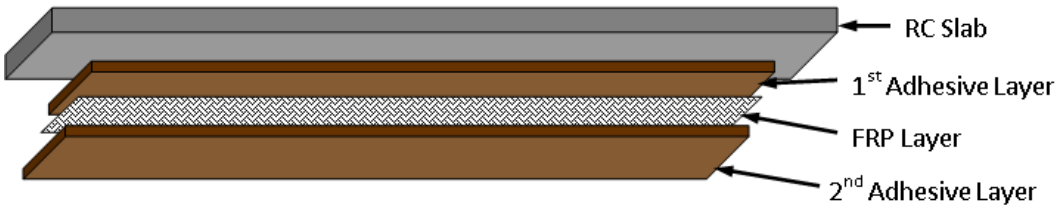

Figure 2: Layers of the Externally Bonded Technique

2.2.1 Failure Modes of Flexural Strengthened Members

There are three main failure modes associated with externally bonded FRP strengthening systems for reinforced concrete structures. These three failure modes are, (a) debonding of the FRP sheet/plate, (b) rupture of the FRP sheet/plate, or (c) crushing of the concrete after yielding of the reinforcing steel. The most desirable failure mode of these three is crushing of the concrete after yielding of the reinforcing bars. This failure mode evaluates the effectiveness of the FRP strengthening system. Failure due to debonding of the FRP material before crushing of the concrete indicates that the FRP system was not fully utilized. Failure due to rupture of the FRP material before yielding indicates that fiber reinforcement ratio is not large enough to utilize the full strength of the existing member. Rupture of the fibers occurs when the induced strain in the fibers due to the applied load exceeds the rupture strain in the FRP material. Concrete crushing occurs when the strain in the compression zone of the concrete exceeds the concrete crushing strain. Fiber rupture and the concrete crushing failure modes are fairly easy to predict using the material properties and by using a simple sectional analysis. The remaining discussion of this section will be devoted to the debonding failure mode in the strengthened reinforced concrete structure, which is more difficult to predict.

2.2.1.1 Parameters Affecting Type of Debonding

Premature debonding is one of the primary concerns for designers, partly due to the fact that it is not easy to predict. In a study by Nurbaiah et al. (2010), the beams that were reinforced using externally bonded FRP sheets all failed due to premature debonding of the FRP sheets before crushing of the concrete. Since the beams failed before crushing of the concrete, the FRP strengthening system was adequate to utilize the full strength of the member. There are several factors that influence the type of debonding that will occur in externally bonded systems. A study conducted by Kamel, Elwi, and Cheng (2006) state the following factors include, but are not limited to, the bond length, bond width, the stiffness of the bonded sheet, concrete strength, and the bond surface conditions. The authors also mention another very important parameter that they failed to look at in their study, and that is surface preparation. As mentioned in the introduction, surface preparation is often overlooked as an important parameter that could affect they type of failure mode that is observed from a strengthened specimen. Recent studies have shown that the effective bond length may be a more important factor in determining the bond strength of FRP sheet than bond width (Kamel, Elwi, & Cheng 2006). This effective bond length is influenced by the stiffness of the FRP sheet and the tensile strength of the concrete. The experimental research conducted by Li et al. (2006), the researchers found that the longer the FRP sheet, the greater the stresses are in the fibers along the sheets. This is due to the fact that more stresses are being transferred from the cracked concrete to the fibers over a greater distance (Li, et al. 2006). The bond strength of the FRP sheet to the concrete substrata decreases as the sheet width increases (Kamel, Elwi, & Cheng 2006). Kamel, Elwi, and Cheng (2006) determined that the stiffness of the bonded sheet is directly related to the sheet width rather than the bond. There are three main types of debonding, Intermediate Crack (IC) debonding, Critical Diagonal Crack (CDC) debonding, and Plate End (PE) debonding. The most prominent and frequently occurring in flexurally strengthened concrete structures is Intermediate Crack debonding.

2.2.1.2 IC Debonding

Intermediate Crack (IC) Debonding is one of the most common debonding failures for flexurally strengthened structures, and is also the type typically ignored by the designer

because of this (Faella, Martinelli, & Nigro 2010). IC debonding typically occurs in the shear zone of the structure, which is the zone of the structure that lies between the point of loading and the support. IC debonding occurs due to the combination of shear stresses and bending moment stresses present in this zone as shown in Figure 3.

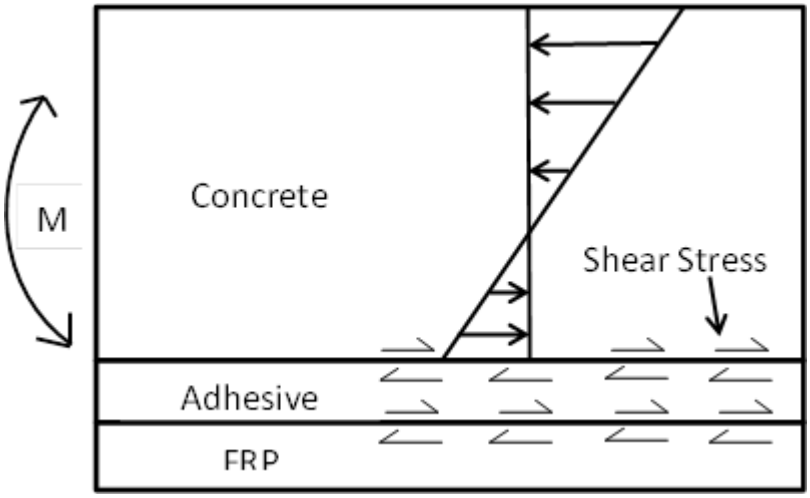

Figure 3: Stresses in System at Mid-Span

Understanding of IC debonding is extremely important since it governs the increase in moment capacity as well as the ductility of the reinforced concrete strengthened section. IC debonding occurs when flexural cracks in the shear zone produce a combination of shear stresses and bending moment stresses that exceed the bond strength of the adhesive attached to the concrete surface. These cracks propagate along the adhesive/concrete surface boundary towards the support, where the bending stresses are reduced. As these cracks propagate, more of the FRP debonding occurs between the concrete surface and the adhesive, and results in the reduction of the bonded length of the FRP. As the bonded length of the FRP decreases, the stresses in the remaining bonded FRP increases, leading to a premature failure of the strengthening system due to IC debonding. The IC debonding failure mechanism is shown in Figure 4.

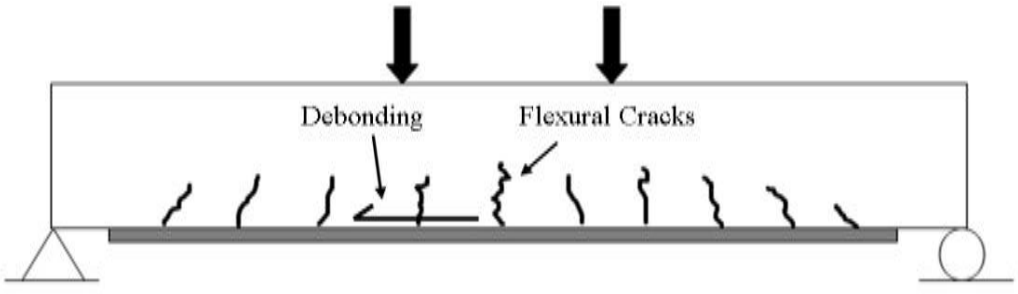

Figure 4: Intermediate Crack Debonding

2.2.1.3 Critical Diagonal Crack Debonding

According to research conducted by Oehlers and Seracino (2004) on strengthening of reinforced concrete specimens with FRP and then subjecting them to four-point bending, failure was often occurred due to Critical Diagonal Crack (CDC) debonding. This type of debonding occurs when a shear crack, whose apex is usually close to the point of loading where shear force and bending moment is highest, induces debonding of the FRP sheet due to the rigid body displacement induced by the formation of this crack. The reason that CDC debonding is rarely a problem in strengthened slabs is due to the fact that the shear resistance is normally large compared to the flexural capacity of the specimen. This shear resistance is attributed to the concrete. The shear force is directly transferred by the dowel action of the reinforcing bars and the passive aggregate interlock mechanism. This passive aggregate interlock is one important element that resists crack widening in reinforced slabs. Externally bonded FRP plates contribute to this resistance when a tensile force is developed in the plate which does not allow for these cracks to widening and become a critical diagonal crack. The CDC failure mechanism is shown in Figure 5.

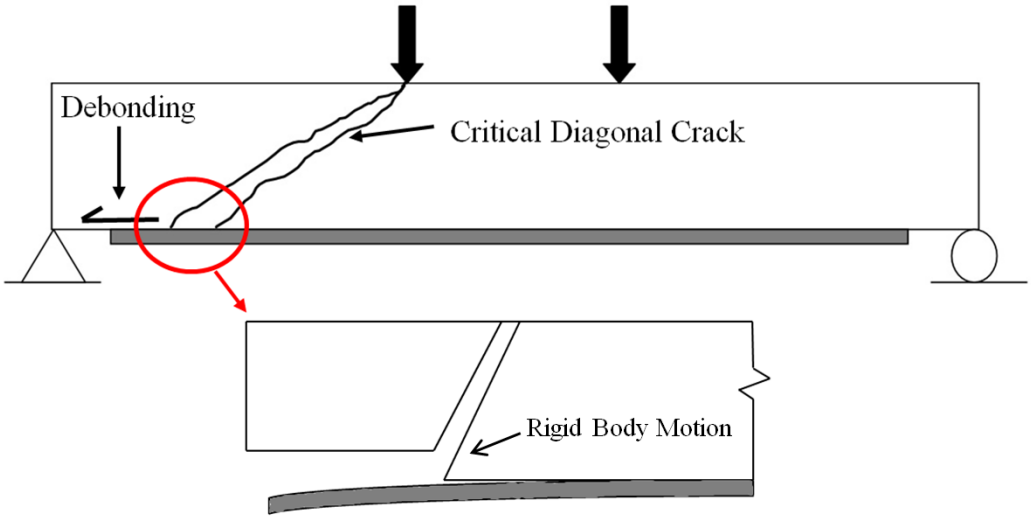

Figure 5: Critical Crack Debonding

2.2.1.4 Plate End Debonding

Another type of debonding failure that could occur for FRP strengthened structures is the Plate End (PE) debonding. Plate end debonding occurs when the interface shear stresses arising at the cutoff section, as a result of the abrupt change in the transverse section of the strengthened section, are greater than the bond strength at the end of the bonded FRP. Debonding of the plate from the end inwards occurs due to curvature of the beam while the plate tends to remain straight. This is opposite to the direction of debonding crack propagation for IC and CDC debonding. Plate end debonding is easier to predict in comparison to IC and CDC debonding because unlike IC and CDC debonding that occur in regions of ultimate failure and hence have nonlinear behavior, PE debonding occurs in regions with little to no flexural forces and have a linear elastic behavior, therefore a simple, linear elastic sectional analysis can be used in prediction. PE debonding can be easily prevented by terminating the reinforcement in regions where there is small curvature and flexural forces, typically observed near the supports. The PE failure mechanism is shown in Figure 6.

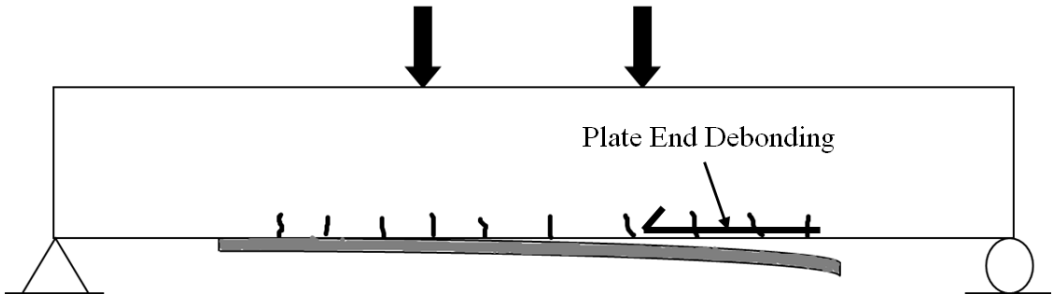

Figure 6: Plate End Debonding

2.2.2 Prediction

Premature debonding is quite challenging to predict due to the presence of various parameters that could affect the bond strength of the strengthening systems, including cracking of the concrete, yielding of the reinforcing steel, estimation of the bond strength between the adhesive and concrete, FRP reinforcement ratio, load distribution, and others (Faella, Martinelli, Nigro 2010). Several research programs have recently focused on predicting the various debonding failure modes, with the majority focusing on the IC debonding failure. In order to predict IC debonding, Mazzotti and Savoia (2009) introduced two main theories. The first of these theories involves calculating the theoretical strain in the FRP that is needed to debond the FRP, and the second involves calculating the required shear force that is needed to debond the FRP at the concrete/FRP interface (Mazzotti and Savoia 2009). Mazzotti and Savoia also used previously published models attempt to predict the strains of the FRP at debonding, however the previously published models under predict the strains in the FRP at IC debonding. In a study by Barros, Dias, and Lima (2006), the authors used ACI and *fib*, as well as the Italian design guideline, CNR, formulations to predict failure loads of strengthened concrete beams. Barros, Dias, and Lima (2006) found that these formulations gave inaccurate results for FRP plates and sheets. Faella, Martinelli, and Nigro (2010) agree that today's codes used by designers to predict IC debonding are not practical for designers so they introduced useful design equations to predict IC debonding. They developed two design equations which can be used to predict IC debonding. One of these design equations attempts to use observations and data from previous experimental programs to relate the onset of yielding of the reinforcing steel to the initiation of IC debonding. The

other design equation recalibrates a previously published equation, the CNR 2004 proposal, which estimates the available contribution of external composite reinforcement to the total bending resistance (Faella, Martinelli, & Nigro 2010). These researchers concluded that while at times these simplified equations were able to predict fairly accurately the strength at debonding, they recommend further research be undertaken to study all the parameters that could affect debonding (Faella, Martinelli, & Nigro 2010). ACI 440.2R-08 was used to predict the ultimate load carrying capacities of the strengthened slabs in the following experimental program. For externally bonded systems, ACI 440.2R-08 attempts to limit the strain level in the FRP at which debonding may occur, ε_{fd}, as defined in Eq. 1. A sectional analysis may be used with this equation to determine the predicted ultimate load carrying capacity of the strengthening system for those systems that use the externally bonded technique.

$$\epsilon_{fd} = 0.083\sqrt{\frac{f'_c}{(n * E_f * t_f)}} \leq 0.9\varepsilon_{fu}$$ where: ε_{fd} = debonding strain of FRP reinforcement, in./in ε_{fu} = design rupture strain of FRP reinforcement, in./in. f'_c = compressive strength of concrete, psi n = number of layers E_f = tensile modulus of elasticity of FRP, psi t_f = nominal thickness of one ply of FRP reinforcement, in	Eq. 1

2.2.3 Plates vs Sheets of FRP

FRP materials are commercially available in sheet or plate configuration for externally bonded systems. FRP sheets are very thin and usually cover the entire width of the specimen that needs to be strengthened. FRP sheets are produced as woven sheets, grids and as a plate.

Plates are usually thick and cover part or the full width of the specimen. A comparison can be is shown in Figure 7.

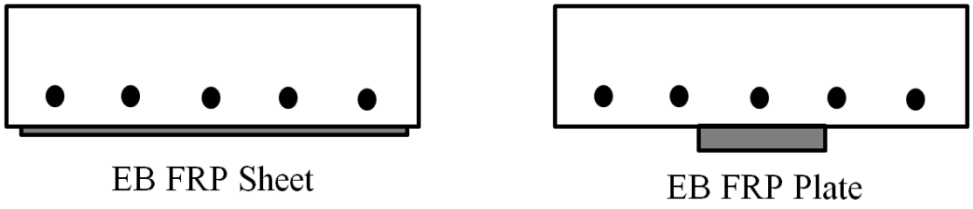

Figure 7: FRP Sheet and FRP Plate

Results from an experimental program conducted by Tann (2005) found that the premature debonding was the main cause of failure in slabs strengthened with FRP pultruted plates. Failure of slabs strengthened with FRP sheets was typically due to rupture of the sheet. This was also seen in an experimental program that used CFRP sheets to strengthen concrete beams (Spadea, Swamy, & Bencardino 2001) and one that strengthened concrete beams with either FRP plates or sheets (Barros, Dias, & Lima 2006). However, if the pultruted plates are placed side by side and cover most of the width of the specimen, the debonding that is associated with FRP plates could occur after crushing of concrete. This was reported based on the experimental program conducted by Alagusundaramoorthy, Harik, and Choo (2003). In this experimental program, beams were strengthened with either an FRP sheet or plate. It was observed that the FRP sheets failed due to rupture of the fibers, and the pultruted plates that were placed side by side in such a way that the plates covered two-thirds of the specimen failed due to concrete crushing with debonding of the FRP plates occurring after crushing of concrete (Alagusundaramoorthy, Harik, and Choo 2003). If FRP sheets have the same cross sectional area as an FRP plate, in terms of effectiveness, research has shown that FRP sheets are more effective than FRP plates because the sheet takes on the contour surface of the concrete surface that it is bonded too, causing the energy needed for fracture to be greater (Mazzotti and Savoia 2009). As the number of layers of FRP sheets is increased, the failure mode could change from rupture of the FRP to debonding (Barros, Dias, & Lima 2006). This is confirmed in other experimental programs (Li, et al. 2006).

2.2.4 Load Carrying Capacity of EB

Application of an externally bonded FRP strengthening system to a reinforced concrete structure, in general, increases the load carrying capacity. The percentage increase of the load carrying capacity depends on several factors. These factors includes the material properties of the FRP, the area of strengthening, the number of layers of FRP, use of either FRP plates or sheets, and the type of adhesive used. Alagusundaramoorthy, Harik, and Choo (2003) conducted an experimental program that involved strengthening beams with different combinations of FRP plates and fabrics. They presented several conclusions regarding some of the variables discussed above. Their conclusions included that increasing the width of the pultruted plates increases the load carrying capacity. Increasing the number of layers of FRP also increases the failure load, and the ultimate load is slightly higher than members strengthened with FRP sheets (Alagusundaramoorthy, Harik, & Choo 2003). The increase in the number of layers leading to the increase of the failure load is presented in other research findings (Barros, Dias, & Lima 2006 and Nurbaiah et al. 2010). In an experimental program where one of the parameters investigated was the affect the internal reinforcement ratio had on the failure load, it was concluded that use of small internal steel reinforcement ratio lead to effective use of EB FRP sheets (Ceroni 2010).

2.2.5 Ductility of EB

When a strengthening system is applied to any reinforced concrete structure, it typically increases the stiffness of the structure. Increase of the stiffness corresponds to greater stresses and strains experienced in the concrete and steel, as well as the strengthening system itself. These additional strains and stresses lead to a failure at a ductility that is much less than the unstrengthened specimen. Decrease of the ductility depends on many variables, such as material properties of the FRP, the area of strengthening, the number of layers of FRP, use of either FRP plates or sheets, and the type of adhesive used. In general, strengthening a structure with EB FRP sheets decreases the ductility of that structure (Nurbaiah et al. 2010). In the experimental program conducted by Tann (2005), when he compared slabs strengthened with FRP sheets to those strengthened with FRP plates, the ductility was decreased more for slabs strengthened with FRP plates in comparison to slabs

strengthened with FRP sheets (Tann 2005). However, if the pultruted plates are placed over most of the width of the specimen, the ductility of members strengthened with plates was almost identical in comparison to members strengthened with sheets (Alagusundaramoorthy, Harik, & Choo 2003). It should be noted that increasing the width of the FRP sheet or plate increases the loss of ductility. The same loss can be observed if the number of FRP layers increases (Alagusundaramoorthy, Harik, & Choo 2003). This is confirmed by other experimental programs (Barros, Dias, & Lima 2006 and Li, et al. 2006).

2.3 Near Surface Mounted (NSM) technique

Recent research in the strengthening field has focused on developing a new and more efficient application technique to use the FRP material for the strengthening of reinforced concrete structures. An emerging technique in the field of strengthening and repair of reinforced concrete structures is the application technique referred to as the near surface mounted (NSM) technique. This technique is also a multi-step process and begins with cutting grooves into the reinforced concrete structures. This is usually done with a diamond cutting saw. Research has shown that the groove size is typically 1.5 times the FRP bar diameter or 3mm larger than the height and thickness of the FRP strip (De Lorenzis & Teng 2007). An adhesive, usually a two-part epoxy or a cementitious material, is then used to coat the bottom and sides of the groove. A two-party epoxy has been the most common type of adhesive used due to its excellent tensile and shear strengths. With the demand identified by the industry to become environmentally friendly and more cost effective, cement paste or mortar has been used as the adhesive. Using cement paste or mortar lowers material cost, reduces environmental impact, allows good bonding to wet surfaces, and achieves better fire resistance (De Lorenzis & Teng 2007). The FRP material is then placed in the groove atop of the adhesive. Unlike the externally bonded technique, where most of the FRP material is either made into a sheet or plate, the FRP material is shaped into a bar or, more recently, a strip that can be placed into the groove. Typically, CFRP is used with the NSM method to strengthen RC structures, whereas GFRP is used with the NSM method to strengthen masonry and timber structures (De Lorenzis & Teng 2007). Once the FRP material has been

placed in the groove, an additional layer of the adhesive is then applied to the top of the FRP material and leveled with the surrounding concrete, therefore, a smooth surface can be achieved. An example of the Near Surface Mounted (NSM) technique is shown in Figure 8.

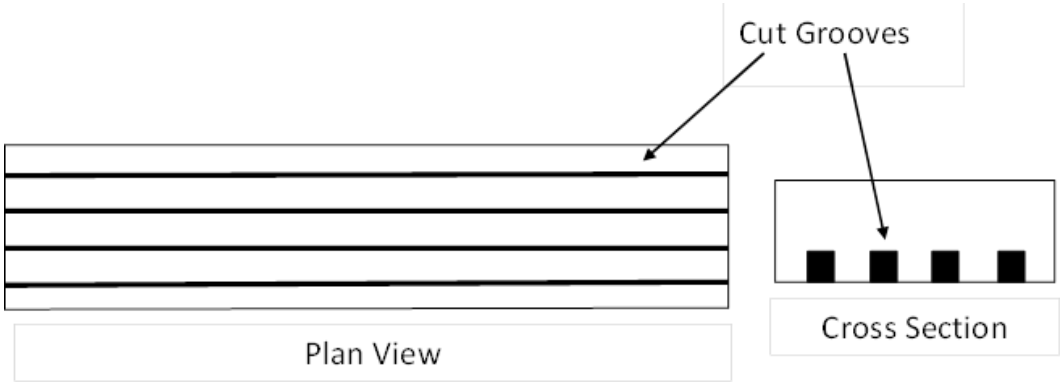

Figure 8: Near Surface Mounted Technique

2.3.1 Advantages of NSM vs. Externally Bonded System

There are several advantages to using the NSM mounted technique in comparison to the EB technique. One of the advantages is that the NSM technique reduces the possibility of debonding of FRP due to the techniques ability to allow for a better bond of the FRP and adhesive to the concrete due to the fact that there is more surface area of the FRP exposed to the bond between the adhesive and concrete (Ceroni 2010). This allows for a greater stress and correlating strain concentration in the FRP itself. This method allows for the development of higher strain in the FRP, making the strengthening system more likely to fail due to rupture of the FRP. Rupturing of the FRP is a more desirable failure mode than debonding of the FRP because if the FRP ruptures then that means that the FRP was fully utilized in the strengthening system. This is also reported in the summary of the work complied by De Lorenzis and Teng (2007) that show that NSM is more efficient that EB due to the fact that NSM debonded at a higher strain, and in most cases it did not debond at all. The possibility of debonding of the NSM technique is very low since the bars and strips used can be anchored to existing structures. Another advantage that NSM in comparison to EB is that unlike the externally bonded technique which requires extensive surface preparation to make sure all the concrete paste is removed and the surface is rough enough to allow for the

adhesive to form a strong bond with the concrete substrata, which can be a very expensive and time consuming process, the near surface mounted technique requires very little surface preparation. The only requirement for the surface preparation is cutting grooves into the concrete, which is a relatively simple process. FRP that is applied using the EB technique is exposed to corrosive environments as well as other potential harmful scenarios that include damage from accidental impact, mechanical damage, and fire (Palmieri, Matthys, & Taerwe 2010). By applying the NSM technique the risk associated with these potentially harmful scenarios is very unlikely. An additional advantage to using NSM in comparison to EB is that the FRP that can be used in the NSM technique can be more easily prestressed (De Lorenzis and Teng 2007). The NSM technique is also more aesthetically pleasing since the grooves are cut into the concrete surface and filled with FRP and adhesive typically leveled with the surface and does not alter the original elevation of the concrete. The grooves can then be painted in a way to completely hide the strengthening system. Using the EB technique, the system will become a visible system that cannot be easily concealed. When Barros, Dias, and Lima (2006) directly compared beams that were strengthened with the externally bonded technique to beams strengthened with the near surface mounted technique, they found that the failure modes were more favorable for the NSM technique than the EB technique and came to the conclusion that NSM is more efficient than the EB techniques. This was confirmed by an experimental program conducted in 2010 that compared reinforced concrete beams strengthened with the EB technique to those strengthened with the NSM technique (Ceroni 2010) and in another similar experimental program (Nurbaiah et al. 2010). It was reported that the measured ultimate loads for members strengthened by using NSM FPR bars were greater than the measured values for EB FRP sheets strengthening systems. There was also greater ductility for the NSM FRP bars than the EB FRP sheets and it was concluded that the NSM technique was the most effective way to strengthen structures in comparison to the EB technique (Nurbaiah et al. 2010).

2.3.2 Failure Modes

The failure modes that are witnessed using the Near Surface Mounted technique are similar to the ones witnessed for concrete structures strengthened using the externally bonded

technique. The main failure mode is directly related to bonding of the FRP bars or strips to the surrounding adhesive as shown in Figure 9.

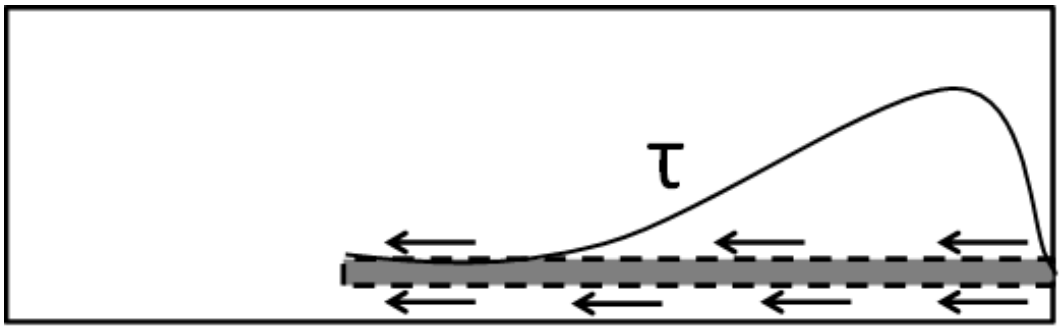

Figure 9: Bond Stresses in the Longitudinal Plane of NSM FRP

The main parameters that affect the bond behavior of NSM applications are also the surface preparation of the groves, material characteristics of the FRP, geometry of grooves, and epoxy cover thickness-to-bar diameter ratio (Ceroni 2010 and De Lorenzis & Teng 2007). This can been seen in a recently conducted program, where increasing the groove width from 1.5 times the diameter to 2 times the diameter enhanced the resistance to splitting of the epoxy. Therefore, it was recommend that when using a cement adhesive the groove size not be greater than 1.5 times the bar diameter used due to greater shrinkage of the cement adhesive (Soliman, El-Salakawy, & Benmokrane 2011). Also, when comparing the failure mode of NSM to EB, it should be noted that a development length exists instead of an effective bond length like for externally bonded systems. The development length is when the maximum stress of the bonded joint between the NSM bar and the concrete substrate is larger than the tensile strength of the FRP bar (De Lorenzis & Teng 2007). In an experimental program conducted by Teng et al. (2006) it was seen that the longer the bond length the less likely the failure will be controlled by debonding and separating of the concrete cover, and the more likely crushing of the concrete will occur. It has been recommended that the development length should not be less than 80 times the bar diameter to ensure proper bond strength and to limit the free-end slip (Hassan and Rizkalla 2004). Whether NSM FRP bars of NSM FRP strips are used, three failure modes can be observed, debonding, FRP rupture, or concrete crushing (De Lorenzis & Teng 2007). Since rupture of

the FRP and concrete crushing failure modes are fairly easy to predict using the material properties and a simple sectional analysis, the following section will discuss debonding failure as the most dominating failure mode for the strengthened reinforced concrete structure.

2.3.2.1 Debonding

There are three types of bond failure modes that a NSM FRP can experience in a pull-out test that can lead to failure due to the debonding of the strengthening system. These bond failures could occur at the bar-epoxy interface, at the epoxy-concrete interface, and/or splitting of the epoxy cover (De Lorenzis & Teng 2007) as shown in Figure 10.

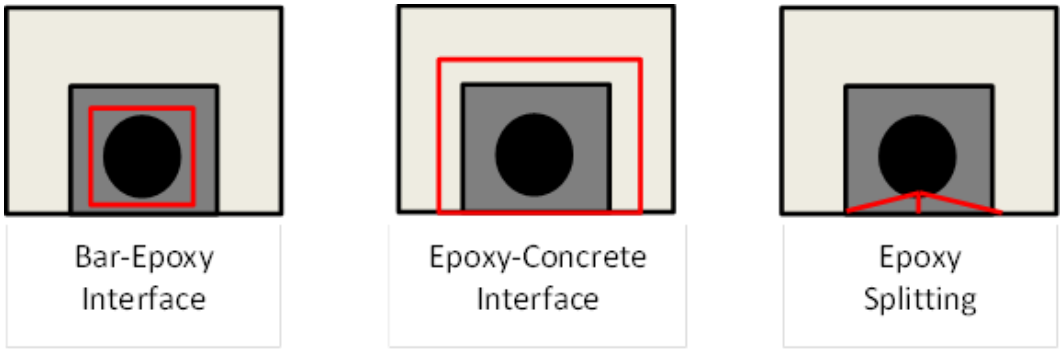

Figure 10: Typical Bond Failure Modes for Pull-Out Test

Some of these bond failure modes occurred using full scale testing of reinforced concrete structures in flexural bending. In the experimental program conducted by De Lorenzis and Teng (2007), there were two main types of failure modes, debonding and separation of the concrete cover. Two types of debonding were observed, bar-epoxy interfacial debonding and epoxy-concrete interfacial debonding. Four types of concrete cover separation were also observed, including bar end cover separation, localized cover separation, flexural crack-induced cover separation, and beam edge cover separation (De Lorenzis & Teng 2007). Failure due to debonding of the epoxy-concrete interface was observed in other experimental programs (Nurbaiah et al. 2010). In an experimental program conducted in 2006 by Barros, Dias, & Lima, the NSM FRP strip strengthened concrete beams failed after yielding of steel and due to delamination of concrete cover (Barros, Dias, & Lima 2006). The beams in the experimental program conducted by Ceroni for strengthened members with NSM bars, led to

a brittle failure due to the sudden detachment of the NSM bars and concrete cover (Ceroni 2010). This is slightly different than the debonding observed for concrete structures strengthened with NSM FRP strips. Failure of FRP NSM strips usually occurs at the strip-epoxy or epoxy-concrete interface. This is due to the greater bond strengths that can be achieved with NSM FRP strips than with NSM FRP bars or EB sheets/plates (Teng et al. 2006). This phenomenon has been reported by many other experimental programs. Palmieri, Matthys, and Taerwe conducted an experimental program that included beams that were strengthened with either NSM CFRP bars or CFRP strips. In their findings, these authors state that NSM CFRP strips failed due to debonding of the FRP by concrete cover separation below the steel reinforcement whereas the beam strengthened with the NSM FRP bars failed by splitting of epoxy cover followed by complete debonding of the reinforcing bar at the CFRP-epoxy interface (Palmieri, Matthys, & Taerwe 2010).

2.3.3 Prediction

As was the case for externally bonded technique, predicting the failure load and debonding of the near surface mounted technique is quite a challenge. However, predicting the failure load for NSM is slightly different from the prediction of the behavior for EB strengthening systems. This is because the most critical failure mode seems to be the concrete cover separation starting at the maximum moment region and not IC debonding as was the case for EB strengthened beams due to the fact that NSM allows for better anchorage of the fibers to the existing members (De Lorenzis & Teng 2007). Barros, Dias, and Lima attempted to predict failure loads of NSM FRP strips strengthened systems using ACI and *fib* along with the Italian design guideline, CNR. Both of these design guidelines gave inaccurate results (Barros, Dias, & Lima 2006). Another experimental program attempted to use ACI 440.2R-08 to predict the failure load of concrete beams strengthened with either NSM FRP strips or NSM FRP bars but were also not successful (Nguyen, Guadagnini, Pilakoutas, & Nam Le 2010). The authors gave several reasons for the differences between the measured and predicted values. One of the reasons is the development of an arch and/or a truss mechanism together with the formation of shear cracks may cause a redistribution of stress to the shear links and the tensile reinforcements. When the compressive zone becomes small, the arch

action is taken over by the truss mechanism. This change in stress distribution causes greater strain in the tensile bars and CFRP than predicted. As a result, the interfacial bond stresses in the FRP increases significantly in the area where the FRP ended. Also, the occurrence of shear cracks may cause a sudden increase of the stresses and strains in the reinforcement that could lead to premature debonding of the FRP (Nguyen, Guadagnini, Pilakoutas, & Nam Le 2010). There have been several studies that attempt to use the bond-slip curves from bond test and apply them to the models in an attempt to try to predict the failure loads of NSM strengthened systems. Teng et al. came to the conclusion that no simple or direct relationship exists between the debonding failure modes observed for large specimens to those observed in bond test (Teng et al. 2006). ACI 440.2R-08 was used to predict the ultimate load carrying capacities of the strengthened slabs in the following experimental program. For the near surface mounted systems, ACI 440.2R-08 attempts to limit the strain level in the FRP at which debonding may occur, ε_{fd}, as defined in Eq. 2. A sectional analysis may be used with this equation to determine the predicted ultimate load carrying capacity of the strengthening system for those that use the near surface mounted technique.

$\epsilon_{fd} = 0.7\varepsilon_{fu}$ where: ε_{fd} = debonding strain of FRP reinforcement, in./in. ε_{fu} = design rupture strain of FRP reinforcement, in./in.	Eq. 2

2.3.4 Bars vs Strips for NSM

When the near surface mounted technique was first introduced, the main type of FRP that was used was FRP bars. In recent years, FRP strips have been studied in an effort to create a more efficient strengthening system as shown in Figure 11. One of the main reasons is that NSM FRP strips have been shown to be the least prone to debonding when compared to CFRP bars. The two main reasons for this behavior are the fact that FRP strips maximize ratio of surface to cross-sectional areas, which minimizes bond stresses and the normal stresses that accompany the tangential bond stresses that act towards the thick lateral

concrete layer and therefore reduces the possibility of splitting failure (Teng et al. 2006). Use of the FRP strips maximizes the surface to cross-sectional area and therefore the strips can achieve a higher percentage of their rupture strain than NSM CFRP bars (Palmieri, Matthys, & Taerwe 2010). Barros, Dias and Lima compared strengthened concrete beams with NSM FRP strip or EB plate or sheet. They observed that the loss of ductility was significantly less for the NSM FRP strip in comparison to the EB systems (Barros, Dias, & Lima 2006). These finding were not duplicated in the experimental program conducted by Ceroni when she compared NSM FRP bars to EB sheets. Ceroni concluded that there was little difference in the loss of ductility between the NSM FRP bars and the EB sheets (Ceroni 2010). The main difference in terms of debonding between NSM bars and strips is that NSM bars tend to debond in the FRP-epoxy interface where NSM strips debond by concrete cover separation (Palmieri, Matthys, & Taerwe 2010).

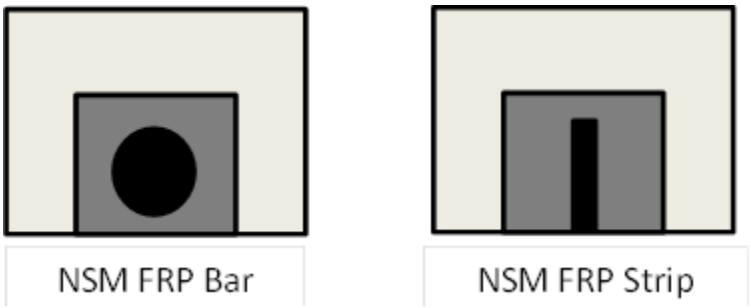

Figure 11: FRP Bars and FRP Strips

2.3.5 Load Carrying Capacity of NSM

The summary reported by De Lorenzis and Teng show that all beams strengthened by NSM led to an increase of the ultimate load carrying capacity and the load corresponding to yielding of the reinforcement, as well as the post-cracking stiffness (De Lorenzis & Teng 2007). As is the case for externally bonded strengthening systems, near surface mounted strengthening systems increases the cracking load, load at yielding of the reinforcing steel, and failure load of the reinforced concrete slab. In general, increasing the number of FRP strips or bars increases the failure load (Barros, Dias, & Lima 2006) (Nurbaiah et al. 2010). The same conclusion was supported by the experimental program conducted by Ceroni (Ceroni 2010). When NSM FRP strips are compared to EB reinforced beams with the same

FRP reinforcement ratio, the greatest increase in failure load is seen in NSM FRP strip strengthening system (Teng et al. 2006). A direct comparison of the increase in strength between NSM bars and strips was conducted and it was found that there was not a significant difference in the percent increase in load carrying capacity between the two types of fibers (Palmieri, Matthys, & Taerwe 2010).

2.3.6 Decrease Ductility

Decrease in ductility is common for externally bonded strengthening systems. The same behavior is also reported for members strengthened with near surface mounted technique. In a study by Barros, Dias, and Lima, they observed that increasing the number of near surface mounted FRP strips significantly decreases the ductility (Barros, Dias, & Lima 2006). The same conclusion was reported for NSM FRP bars (Nurbaiah 2010). However, researchers also concluded the loss of ductility was much less prominent when NSM FRP strips were compared to externally bonded systems (Barros, Dias, & Lima 2006). It was reported that the loss of ductility is about the same for both EB sheets and NSM bars (Ceroni 2010). It was reported that the use of NSM FRP bars caused a greater loss of ductility when compared to NSM FRP strips (Palmieri, Matthys, & Taerwe 2010).

2.4 Research Needs

While much research has been done to investigate both the NSM and EB strengthening systems, further research is needed to understand the phenomenon that causes premature failure of the strengthened systems. Due to the number of parameters that affect the failure modes of these strengthened reinforced concrete structures, more detailed analysis are required to study the effect of these parameters. Once these parameters are looked at more closely, better prediction models may be introduced to help predict the ultimate load carrying capacity of these FRP strengthened members. The equations and design principles that are used today do not provide accurate results when premature debonding occurs. Full understanding of the behavior will build more confidence in the use of FRP to strengthen concrete structures. Also, many of the equations and design principles today are calibrated using the results from externally bonded, epoxy, FRP plate or sheet strengthening systems.

These equations may not accurately predict the debonding of strengthening systems that use fiber grids or alternative adhesives such as cementitious materials. Further research should be done in order to accurately predict premature debonding of these alternative strengthening systems. The relationship between the measured bond for bond test specimens and debonding mechanisms for flexurally-strengthened beams needs to be clarified in order to predict possible premature debonding in many of these strengthened structures. Many of the experimental programs tested these strengthening systems under monotonic loading but did not consider cyclic loading. Therefore, it is recommended that effectiveness of these strengthening systems be determined for cyclic loading. There is also a need to explore the behavior of FRP strengthening systems to repair damaged structures. Many of the beams and slabs that have been strengthened and tested have been undamaged at the time of testing and therefore are not representative to field conditions. Further research is needed to examine the behavior of damaged structures repaired with these FRP strengthening systems. The same parameters considered for undamaged members strengthened with FRP systems should be considered for damaged structures repaired with FRP. The long term performance of these strengthening systems should also be determined with the use of fatigue testing and testing under environmental conditions. The research should also focus on development of design equations and recommendations for designers to use for FRP strengthening systems that are used to repair damaged structures in the field.

CHAPTER 3 - EXPERIMENTAL PROGRAM

The following chapter will describe the experimental program that was conducted at the Constructed Facilities Laboratory at North Carolina State University to study the effectiveness of different strengthening systems applied to reinforced concrete structures. The material properties of the concrete used in casting of the slabs, the steel that was used to reinforce the concrete slabs, and the fibers that were used to strengthen the reinforced concrete slabs will be described in detail. The standards that were used to obtain these materials properties will also be discussed. A portrayal of the two different application techniques that were used to strengthen the reinforced concrete slabs is also found in this chapter. The test setup along with the test instrumentation is also summarized in this chapter.

3.1 Material Properties

3.1.1 Concrete Properties

Portland cement (PC) concrete was used to cast the one-way slabs for both phases of the experimental program. The two phases of the experimental program were cast using different batches of Portland cement concrete. The Portland cement concrete was provided by a local ready mix company. The target 28-day compressive strength (f'c) of each of the batches was 5,000 psi using a 3/8" max size aggregate. A number of 4"x8" concrete cylinders and 6"x6"x18" prisms were made and tested from each batch so that the 28-day and day of testing compressive strength could be determined as well as the rupture strength of the Portland cement concrete. The 28-day 4"x8" cylinders were removed from their casing and moist cured in water saturate with calcium hydroxide as described in ASTM C31/C31M standard. They were then removed from the moist curing at 28 days and tested using the procedure outlined in ASTM C39/C39M standard. The cylinders that were designated to be used to determine the concrete strength of the slabs at day of testing were air cured next to the slab specimens so that they would subjected to the same curing conditions as the one-way slabs were. The cylinders were tested in a set of three and the average compressive strength was used as the compressive strength for that set. The typical test setup used for determining the compressive strength of the Portland cement is shown in Figure 12.

The 28 day strength, as well as the range of compressive strengths during testing of the one-way slabs for each batch are given in Table 1 for each cast.

Figure 12: Typical Compressive Strength Test Setup

Table 1: Compressive Strength of Portland cement Concrete

	28 day strength (f'c)	Range of strength during testing
Cast #1	4,520 psi	5,270 psi – 5,840 psi
Cast #2	5,710 psi	6,340 psi – 6,800 psi

The rupture strengths of the concrete batch were determined by constructing 6"x6"x18" prisms and then moist cured in water hydrated with calcium hydroxide as required in ASTM C31/C731M. Once these prisms cured for 28 days, they were tested using the ASTM C78/C78M testing protocol. A typical test set up is shown in Figure 13. A test set consisted

of three prisms for each batch, and the average rupture strengths of these three prisms were calculated and are given in Table 2 for each cast.

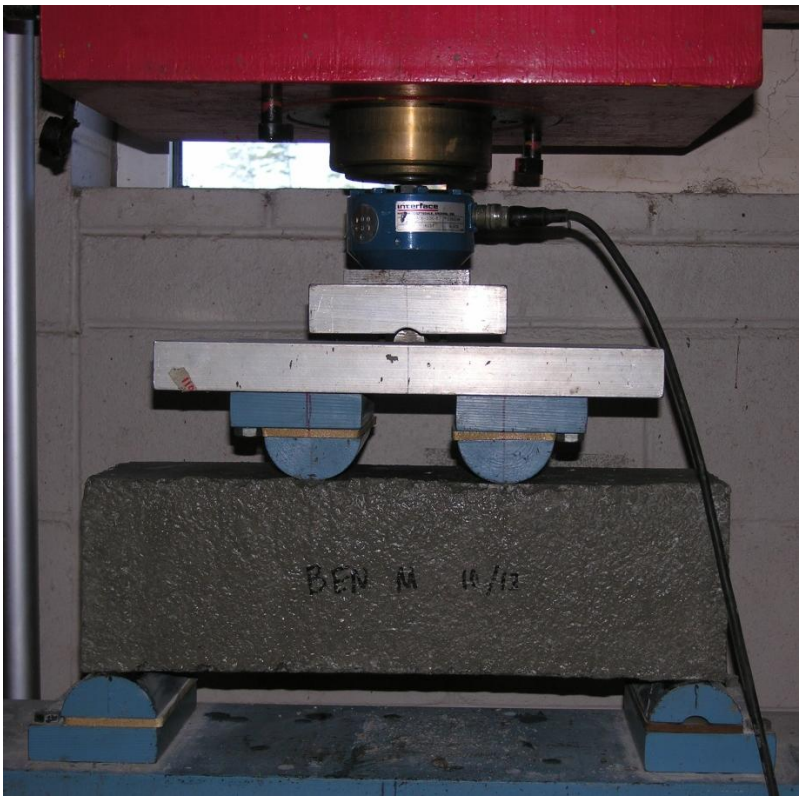

Figure 13: Typical Rupture Strength Test Setup

Table 2: Rupture Strength of Portland cement Concrete

	Rupture Strength (fr)
Cast #1	648 psi
Cast #2	717 psi

The elastic modulus of each of the batches was determined by using the 4”x8” cylinders. The cylinders were tested using the ASTM C469 testing protocol. A typical test set up is shown in Figure 13. A test set consisted of three cylinders for each batch, and the average elastic moduli of these three cylinders were calculated and are given in Table 3 for each cast.

Figure 14: Typical Elastic Modulus Test Setup

Table 3: Elastic Modulus of Portland cement Concrete

	Elastic Modulus E
Cast #1	4,350 ksi
Cast #2	4,690 ksi

3.1.2 Steel Reinforcement

The steel that was used to reinforce the concrete slabs was Grade A706 and was chosen due to the high quality control requirements and high ductility in comparison to the regular Grade 60 steel. The steel reinforcement was tested using an MTS machine prior to casting of the one-way slabs to determine the material properties. A typical tensile test set up is shown in Figure 15. The material properties that were investigated were the yielding stress and strain, as well as the elastic modulus. The strain was measured using a MTS extensometer with a gauge length of 2". The average stress-strain response of the steel is shown in Figure 16. Based on these results, the stress and strain at yielding of the steel was 70 ksi and 0.00255

in/in, respectively and the elastic modulus of the steel was 27,450 psi. The testing of the tensile properties of the steel rebar was performed according to ASTM A370 annex A9.

Figure 15: Typical Tensile Test Setup

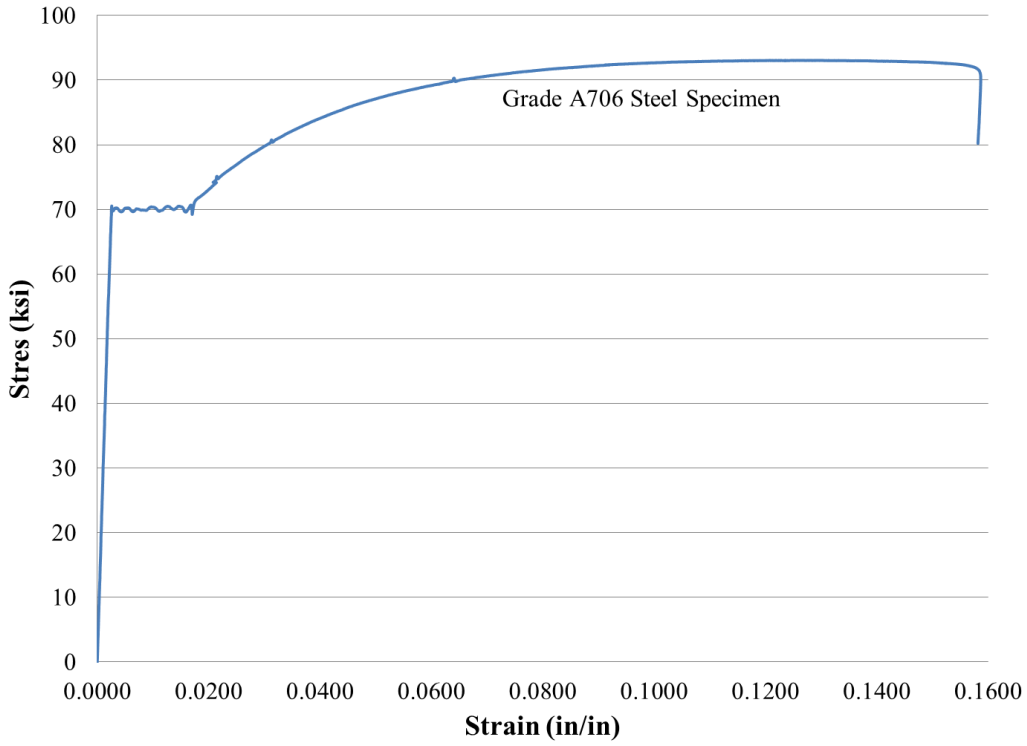

Figure 16: Grade A706 Steel-Stress Strain Properties

3.1.3 Fiber Reinforced Polymers (FRP)

There were a total of five different fibers that were used in the experimental program. They include a carbon strand sheet that was produced with either a high elastic modulus or high tensile strength, a carbon grid, and a glass grid that was produced with either a 0.25" grid spacing or a 1" grid spacing. The material testing was conducted using a MTS machine and an Optotrak system to measure the deformation of the FRP material as it was being subjected to a tensile test. A typical test set-up is shown in Figure 17. The Optotrak system is camera based system that uses a camera and computer to record the distance between special LED sensors that are attached to the FRP. The Optotrak camera system is shown in Figure 18. The recorded data can be used to calculate the strain in the fiber up to rupture. The cross sectional area of the FRP is measured and used to calculate the stress in the fiber. A stress-strain graph is then produced and the elastic modulus is calculated. A description of each fiber, as well as the material properties of each, is provided in the following sections.

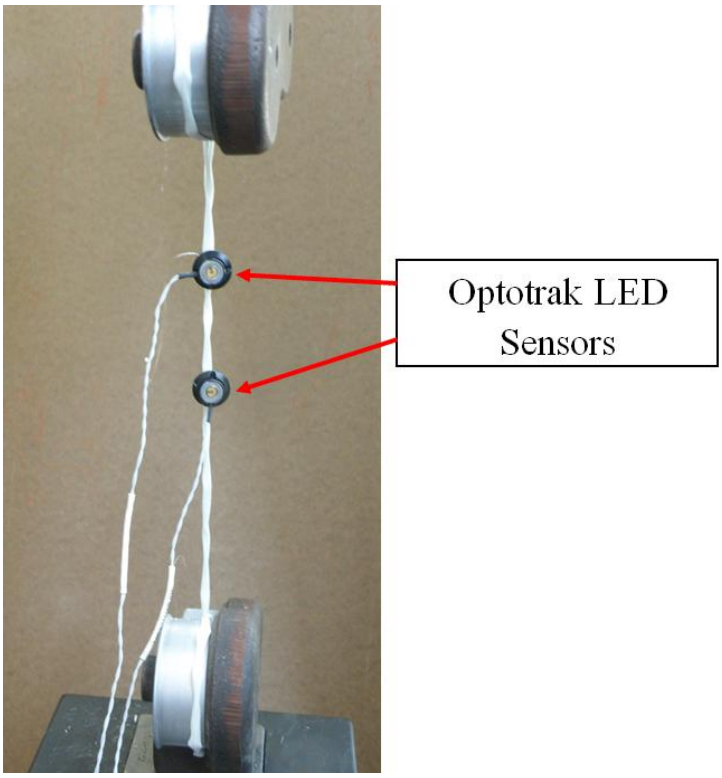

Figure 17: Typical Test Setup for FRP Material Tensile Test

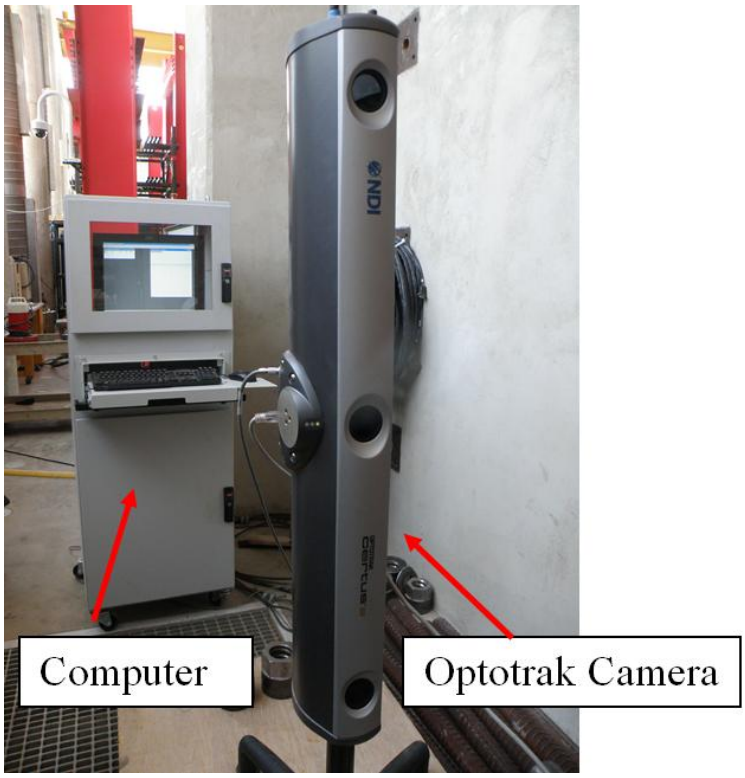

Figure 18: Optotrak Camera and Computer System

3.1.3.1 Glass Vinyl Coated Grid – ¼" grid spacing

The ¼" glass grid is made up of glass stows woven in both the longitudinal and transverse directions. This weave produces a grid spacing that is approximately ¼" square. This ¼" glass grid is shown in Figure 19. The glass stows are coated with a vinyl coating to improve handling of the sheets as well as to protect the fibers. However, this vinyl coating significantly reduces the bonding of the fibers to the adhesive, creating a weak bond at this interface. This weak bond interface is compensated by the mechanical interaction of the transverse stows and the friction forces that develop between the vinyl coating and the fibers and does not take advantage of the interaction between the fibers and the concrete substrata. The mechanical properties of the ¼" glass grid are given in Table 4. The cross sectional area was determined using a micrometer. The typical, measured stress-strain behavior for the ¼" glass grid is shown in Figure 20.

Figure 19: ¼" Glass Grid

Table 4: Mechanical Properties of the ¼" Glass Grid

Fiber Cross-Sectional Area	Rupture Load per Strand	Tensile Strength	Rupture Strain	Modulus of Elasticity
0.00164 in^2	110 lbs	69 ksi	0.0227 in/in	3,184 ksi

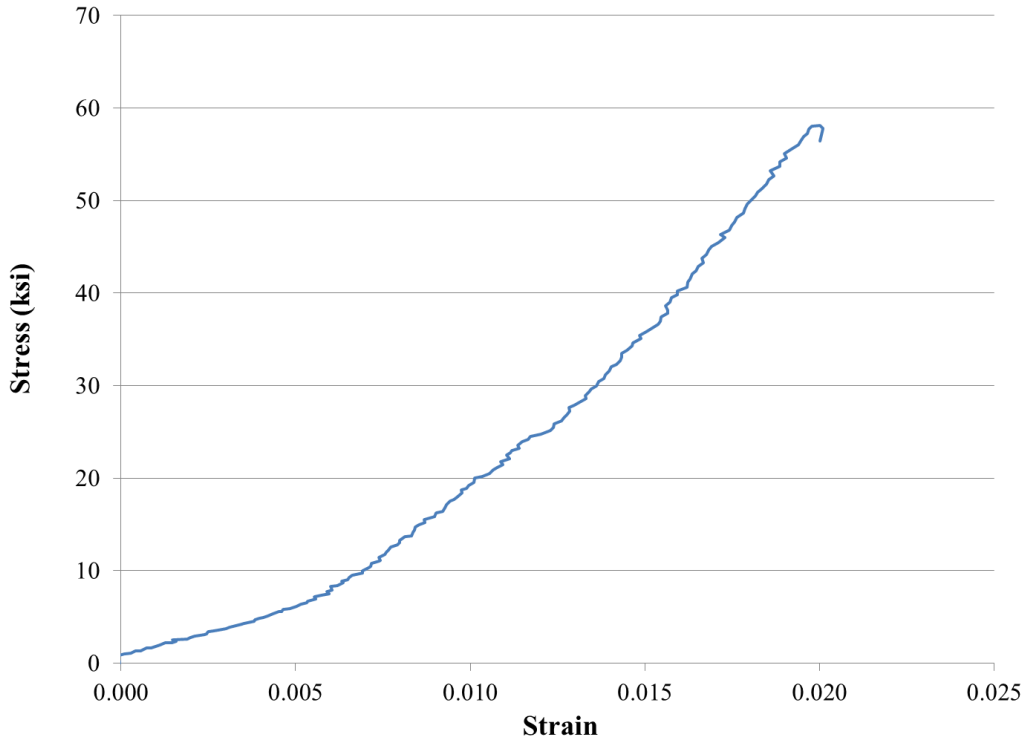

Figure 20: Typical Stress-Strain Curve for ¼" Glass Grid

3.1.3.2 Glass Vinyl Coated Grid – 1" spacing

The 1" glass grid is made up of glass stows woven in both the longitudinal and transverse directions. This 1" glass grid is similar to the ¼" glass grid but has a greater number of fibers per stow, increasing the rupture load per strand when compared to the ¼" glass grid. This weave produces a grid spacing that is approximately 1" square. This 1" glass grid is shown in Figure 21. The glass stows are coated with a vinyl coating to improve handling of the sheets as well as to protect the fibers. However, this vinyl coating significantly reduces the bonding of the fibers to the adhesive, creating a weak bond at this interface. This weak bond interface is compensated by the mechanical interaction of the transverse stows and the friction forces that develop between the vinyl coating and the fibers and does not take advantage of the interaction between the fibers and the concrete substrata. The transverse and longitudinal glass stows are connected with a small amount of adhesive, which is very weak and can be easily pulled apart. This may be the cause for the lower stiffness of the grid. The mechanical properties of the 1" glass grid are given in Table 5. The cross sectional

area was determined using a micrometer. The typical, measured stress-strain behavior for the 1" glass grid is shown in Figure 22.

Figure 21: 1" Glass Grid

Table 5: Mechanical Properties of the 1" Glass Grid

Fiber Cross-Sectional Area	Rupture Load per Strand	Tensile Strength	Rupture Strain	Modulus of Elasticity
0.00398 in^2	366 lbs	85 ksi	0.0133 in/in	3,996 ksi

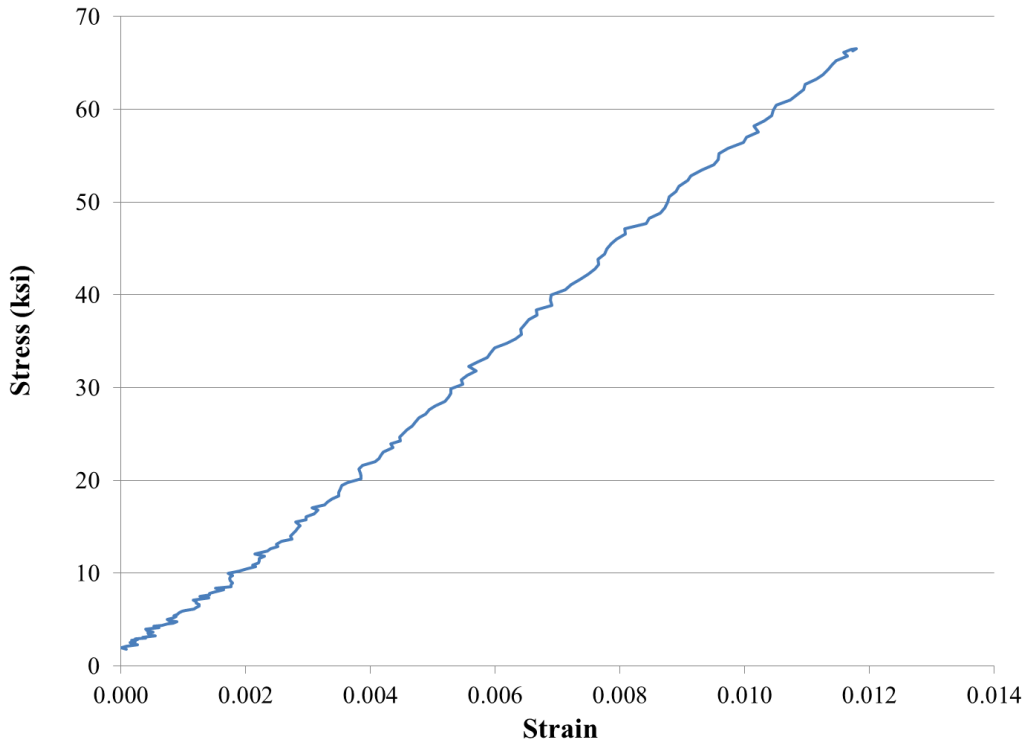

Figure 22: Typical Stress-Strain Curve for 1" Glass Grid

3.1.3.3 High Tensile Carbon Strand

The carbon fiber strands are produced using three different types of carbon fibers; high-modulus, intermediate modulus, and high-tensile strength. The high-tensile strength was chosen to be used in this experimental program due to its potential to greatly increase the load carrying capacity. The sheets are produced by tying together unidirectional carbon strands together. The strengthening system has a designated epoxy resin which has been proven to work well with the fibers. The sheets are also produced with different spacing between the unidirectional carbon strands. The center-line to center-line distance between the high-tensile carbon strands can range from 1.64 mm to 4.92 mm. The larger spacing between the carbon strands promotes the use of cementitious materials, like Grancrete, as the adhesive, which can increase the fire resistance of the strengthening system. The high-tensile strength carbon strand sheet was selected for this project due to their high rupture load per strand and high rupture strain. The high-tensile carbon strand sheet is shown in Figure 23.

The mechanical properties of the high-tensile carbon strand sheet are given in Table 6. The cross-sectional area was determined using a micrometer. The typical, measured stress strain behavior of the high tensile carbon strand is shown in Figure 24.

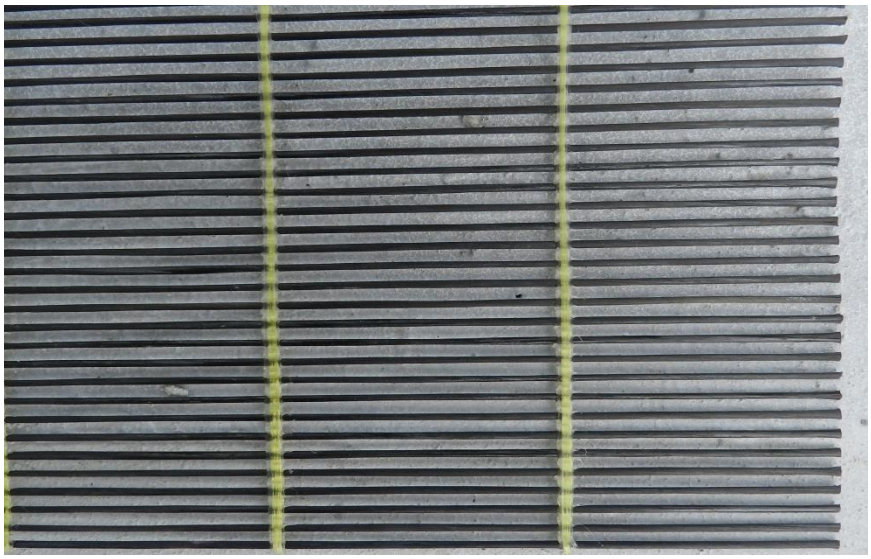

Figure 23: High Tensile Carbon Strand Sheet

Table 6: Mechanical Properties of the High-Tensile Strength Carbon Strands

Fiber Cross-Sectional Area	Rupture Load per Strand	Tensile Strength	Rupture Strain	Modulus of Elasticity
0.00165 in^2	547 lbs	332 ksi	0.0173 in/in	14,946 ksi

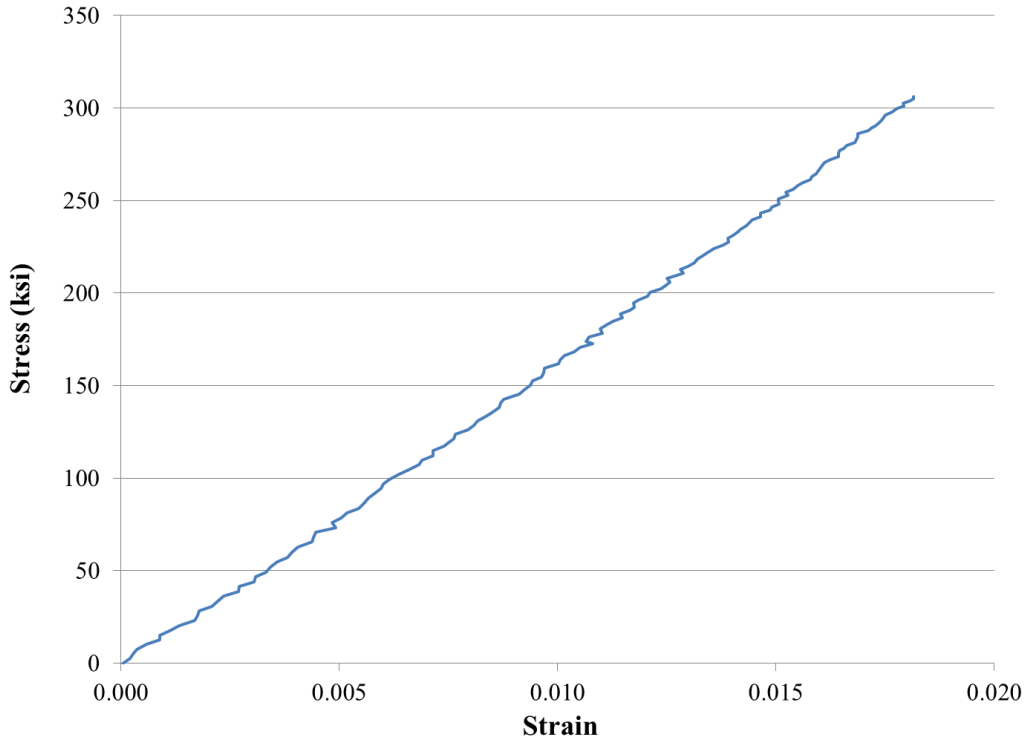

Figure 24: Typical Stress-Strain Curve for HT Carbon Strand

3.1.3.4 High Modulus Carbon Strand

The carbon fiber strands are produced using three different types of carbon fibers; high-modulus, intermediate modulus, and high-tensile strength. The high-modulus stand was chosen to be used in this experimental program due to its potential to greatly increase the load carrying capacity. The sheets are produced by tying together unidirectional carbon strands together. The strengthening system has a designated epoxy resin which has been proven to work well with the fibers. The sheets are also produced with different spacing between the unidirectional carbon strands. The center-line to center-line distance between the high-modulus carbon strands can range from 1.42 mm to 4.26 mm. The larger spacing between the carbon strands promotes the use of cementitious materials like Grancrete as the adhesive, which can increase the fire resistance of the strengthening system. The high-modulus strength carbon strand sheet was selected for this project due to the high stiffness of the carbon fibers. The high-modulus carbon strand sheet is shown in Figure 25. The

mechanical properties of the high-modulus carbon strand sheet are given in Table 7. The cross-sectional area was determined using a micrometer. The typical, measured stress strain behavior is shown in Figure 26.

Figure 25: High Modulus Carbon Strand Sheet

Table 7: Mechanical Properties of the High Modulus Carbon Strands

Fiber Cross-Sectional Area	Rupture Load per Strand	Tensile Strength	Rupture Strain	Modulus of Elasticity
0.00195 in^2	233 lbs	121 ksi	0.0038 in/in	31,273 ksi

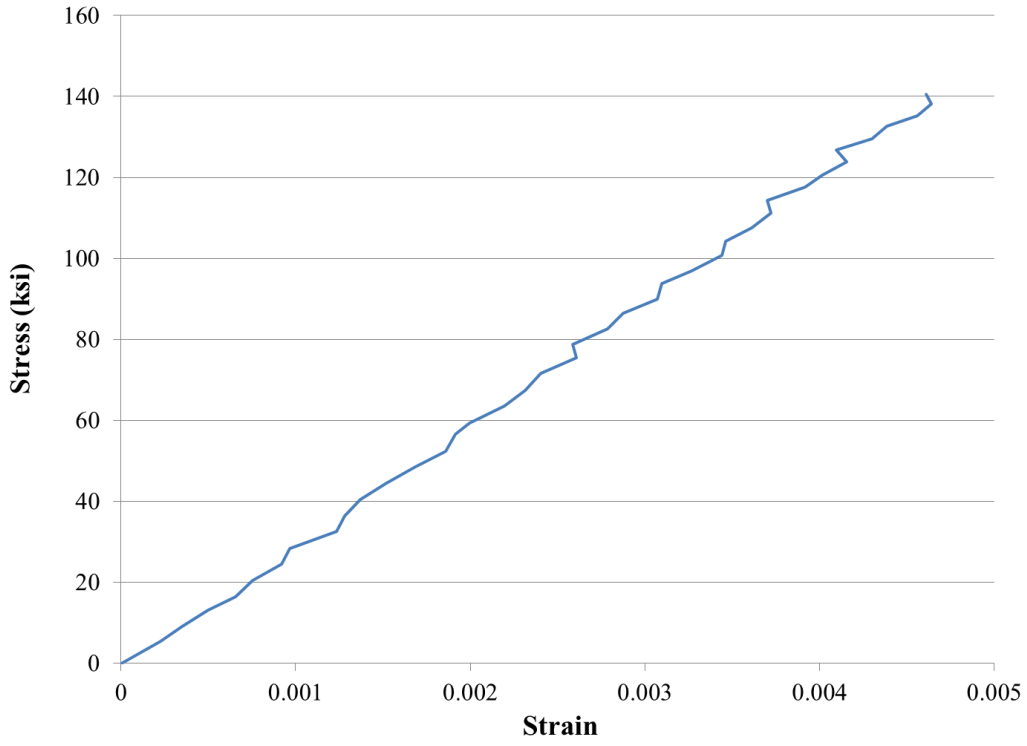

Figure 26: Typical Stress-Strain Curve for HM Carbon Strand

3.1.3.5 Carbon Grid

The carbon grid has both longitudinal and transverse stows that are made up of carbon fibers. These longitudinal and transverse stows are connected by weaving the fibers together. There is approximately double the amount of fibers in the longitudinal direction than the transverse direction as shown in Figure 27. This forms 9.5 mm x 19.5 mm grid spacing. The stows are then coated with an epoxy resin to increase the stiffness of the system as well as to make the carbon grid easier to handle. This coating could affect the bond of adhesives to the fibers due to possible slipping of the fibers in the adhesive. This possible slip could cause the stress to be transferred by frictional forces rather than by the fibers. The carbon grid is supplied with two adhesives, an epoxy resin and an experimental cementitious material, that work well with the fibers. The mechanical properties of the high-modulus carbon strand sheet are given in Table 8. The cross-sectional area was determined using a micrometer. The typical, measured stress strain behavior is shown in Figure 28.

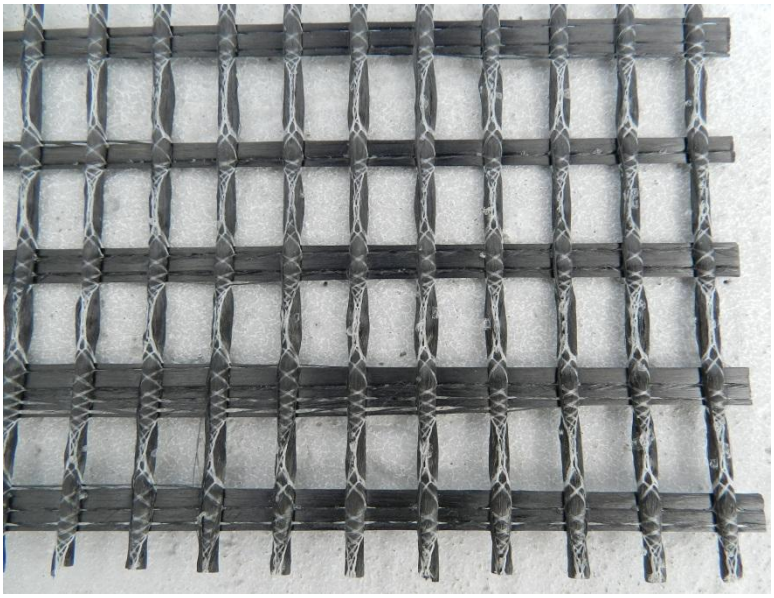

Figure 27: Carbon Grid

Table 8: Mechanical Properties of the Carbon Grid (Longitudinal Direction)

Fiber Cross-Sectional Area	Rupture Load per Strand	Tensile Strength	Rupture Strain	Modulus of Elasticity
0.006 in^2	654 lbs	109 ksi	0.0143 in/in	9,366 ksi

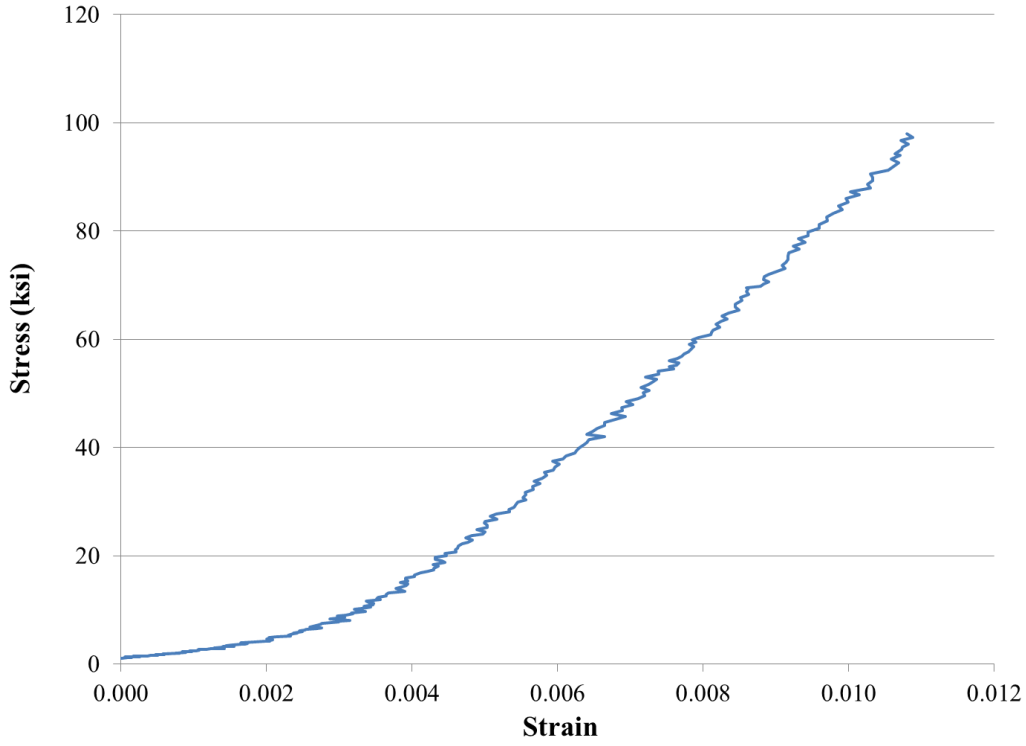

Figure 28: Typical Stress-Strain Curve for Carbon Grid

3.2 Test Specimens

The overall experimental program consisted of sixteen reinforced concrete slabs cast using two different batches. The testing was performed in two phases. Phase I consisted of a total of nine reinforced concrete slabs and Phase II consisted of a total of seven reinforced concrete slabs. The overall dimensions of a typical reinforced slab is 11'x2'x6" as shown in Figure 29. Each slab was reinforced with five longitudinal #4 steel bars spaced at five inches center to center and eight transverse #4 steel bars spaced at eighteen inches center to center.

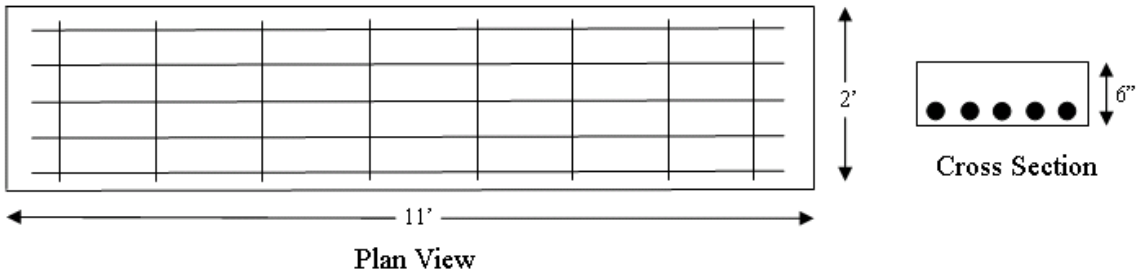

Figure 29: Slab Dimensions

All of the slabs tested in Phase I were cast from the same batch, as were the slabs tested in Phase II. Different types of FRP strengthening systems were used for fourteen of the slabs. Two slabs were left unstrengthened, one in each phase, and were used as the control specimens to evaluate the effectiveness of the strengthening systems. Details of the FRP strengthening systems used for the Phase I slabs are given in Table 9 and the FRP strengthening systems used for the Phase II slabs are given in Table 10. A guide to reading these tables is found below.

First Column: The first column in these tables provides the mark number of each slab tested. The mark number was selected based on the type of fiber and adhesive used, as well as the application method used for the strengthening system and the spacing between the fibers. A description of the typical mark is illustrated in Figure 30.

Second Column: The second column in these tables identifies the type of fibers that were used in the strengthening systems. There are three different types of fibers that were explored in Phase I. They include the carbon fiber strand sheet, the high modulus and high tensile strength, the carbon grid, and the glass grid. For Phase II, only one type of fiber was investigated, and that was the carbon strand sheet, both the high modulus and the high tensile strength.

Third Column: The third column in these tables identifies the type of adhesives used. Three types of adhesives were investigated in this Phase I, two cementitious materials, Grancrete PCW and Tyfo C-Matrix, and one epoxy, Tyfo TC. In Phase II, two different adhesives were studied, the cementitious material known as Grancrete PCW and an epoxy. Grancrete PCW is a cementitious material that, when combined with water, forms a binding agent that is

rapid setting, develops high-early bond strength, and has enhanced durability. Grancrete PCW also has excellent fire and heat resistance when compared to epoxy. There are several different types of Grancrete, and the one used in this experimental program is commercially known as Grancrete PCW. Throughout this thesis, Grancrete PCW will be referred to as Grancrete for simplicity.

Fourth Column: The fourth column in these tables refers to the method used to apply the FRP strengthening systems. All the strengthened systems used in Phase I used the externally bonded (EB) application technique. In Phase II, both the externally bonded and near surface mounted (NSM) were investigated.

Fifth Column: The fifth column in these tables identifies the spacing between the longitudinal fibers in each strengthening system. The Carbon Strand Sheet was manufactured with three alternative spacing distances between fibers, referred in this experimental program as Type 1, 3, and 4. In Phase I, Type 1 sheets were investigate which had a center-line to center-line spacing of 1.64 mm for the high tensile sheet and 1.42 mm for the high modulus sheet. In Phase II, Type 3 sheets were investigated which had a center-line to center-line spacing of 3.28 mm for the high tensile sheet and 2.84 mm for the high modulus sheet. The Carbon Grid has a spacing of 9.5 mm center to center of the longitudinal fibers and a 19.5 mm center to center spacing of the transverse strands. The Glass Grid has two different grid spacing, a 0.25" (6.35 mm) grid spacing and a 1" (25.4 mm) grid spacing.

Sixth Column: The sixth column references the number of specimens that were tested in the different phases of the experimental program.

Table 9: Testing Plan for Phase I

Phase I					
Name	**Fiber Details**	**Adhesive**	**Application**	**Spacing**	**No. of Specimens**
Control	None	None	N/A	N/A	1
HT-G-E-1	High Tensile Carbon Strand	Grancrete	Externally Bonded (EB)	Type 1	1
HM-G-E-1	High Modulus Carbon Strand	Grancrete	EB	Type 1	1
C-C-E	Carbon Grid	Cementitious Material (Tyfo C-Matrix)	EB	9.5mm x 19.5mm Grid	2
C-E-E	Carbon Grid	Epoxy (Tyfo TC)	EB	9.5mm x 19.5mm Grid	1
C-G-E	Carbon Grid	Grancrete	EB	9.5mm x 19.5mm Grid	1
G-G-E-0.25in	Glass Grid	Grancrete	EB	0.25” Grid	1
G-G-E-1in	Glass Grid	Grancrete	EB	1.0” Grid	1

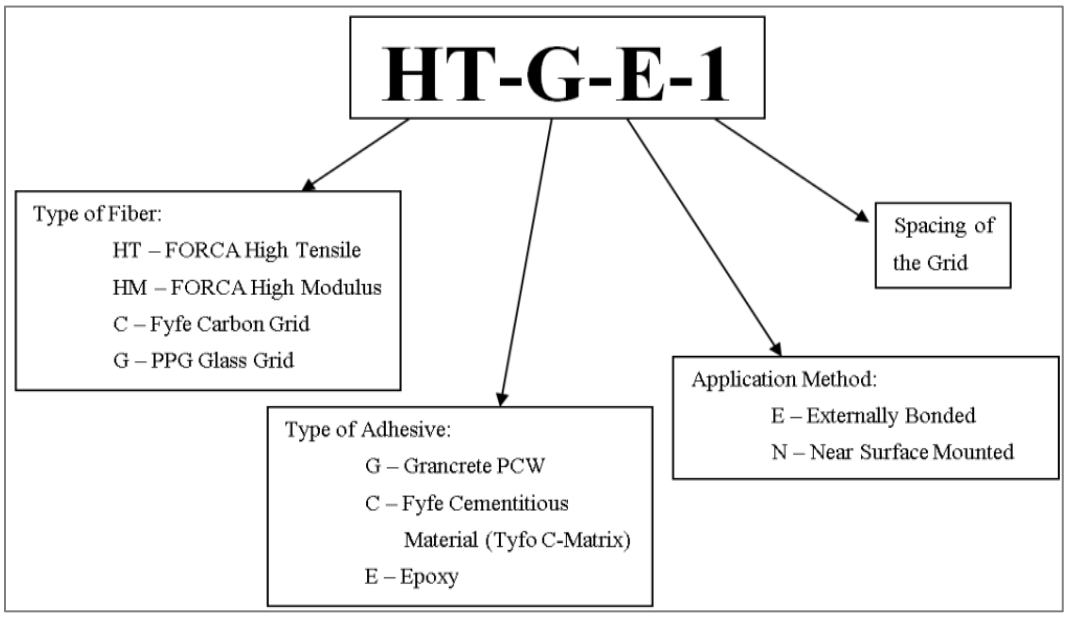

Figure 30 : Mark Guide for Phase I

Table 10: Testing Plan for Phase II

Phase II					
Name	**Fiber Details**	**Adhesive**	**Application**	**Spacing**	**No. of Specimens**
Control	None	None	N/A	N/A	1
HM-E-E-3	High Modulus Carbon Strand	Epoxy	Externally Bonded (EB)	Type 3	1
HM-G-E-3	High Modulus Carbon Strand	Grancrete	EB	Type 3	1
HM-G-N-3	High Modulus Carbon Strand	Grancrete	Near Surface Mounted (NSM)	Type 3	1
HT-E-E-3	High Tensile Carbon Strand	Epoxy	EB	Type 3	1
HT-G-E-3	High Tensile Carbon Strand	Grancrete	EB	Type 3	1
HT-G-N-3	High Tensile Carbon Strand	Grancrete	NSM	Type 3	1

3.3 Application Technique

Two application techniques will be explored in this experimental program. These two application techniques are the externally bonded technique and the near surface bonded technique. The externally bonded technique is the more extensively researched and used of the two but the near surface mounted has gained popularity in recent years due to research that suggest it is a more efficient system than the externally bonded technique. The two techniques are described in the following sections.

3.3.1 Externally Bonded Application Technique

The externally bonded technique (EB) is the older of the two application techniques. It was first used with steel plates to strengthen reinforced concrete structures. Either epoxy or cementitious materials may be used with this technique. This technique typically involves bonding the FRP to the exposed face of the concrete surface with an adhesive. The strengthening system can then be painted in order to try to minimize any aesthetic complications that may arise. In this experimental study, the externally bonded technique

was used with the cementitious adhesives as well as the epoxy adhesive as shown in Figure 31 and Figure 32. For this application, the slab was flipped up-side-down in order to expose the tension face for strengthening. A bottom layer of adhesive was then applied to the concrete surface. Once this layer was applied, the fibers were placed on top of the adhesive and pressed into the adhesive to ensure the fibers would be completely encased in the adhesive. A top layer was used to coat the fibers and to form the level surface of the strengthening system.

Figure 31: Using Cementitious Adhesive in the Externally Bonded Technique

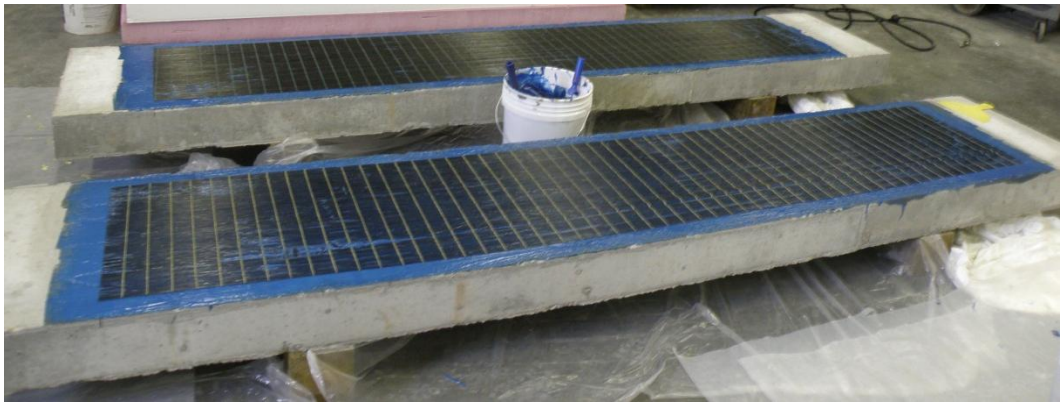

Figure 32: Using Epoxy in the Externally Bonded Technique

3.3.2 Near Surface Mounted Technique

The near surface mounted technique (NSM) is an innovative application technique that has been proven to be more effective that the externally bonded technique. The technique usually involves cutting grooves into the reinforced concrete structure and then bonding the FRP into these grooves with either a cementitious or epoxy adhesive. Since the FRP strengthening system is cut into the grooves, there are fewer complications aesthetically than the externally bonded technique. In this experimental program, the near surface mounted technique is used with the cementitious material so a direct comparison can be made with the externally bonded technique that uses the same cementitious adhesive. The first step of the near surface mounted technique was to cut grooves in the slabs with a concrete skill saw as shown in Figure 33. Next the strengthening system was applied. This was done in several phases. The first phase included applying a bottom layer of adhesive into the grooves. This layer was spread out along the bottom and sides of the groove to ensure that the entire groove was coated with the adhesive. After this the carbon strand sheet, which had been cut into four even bundles, was impregnated with the adhesive, rolled into circular bundles, and then placed into the grooves. A top layer of the adhesive was then applied and leveled with the existing concrete surface to from a level surface. The applications of the strengthening system are shown in Figure 34, Figure 35, and Figure 36.

Figure 33: Cutting Grooves for NSM technique

Figure 34: FRP Bundle in Groove before Adhesive is Applied

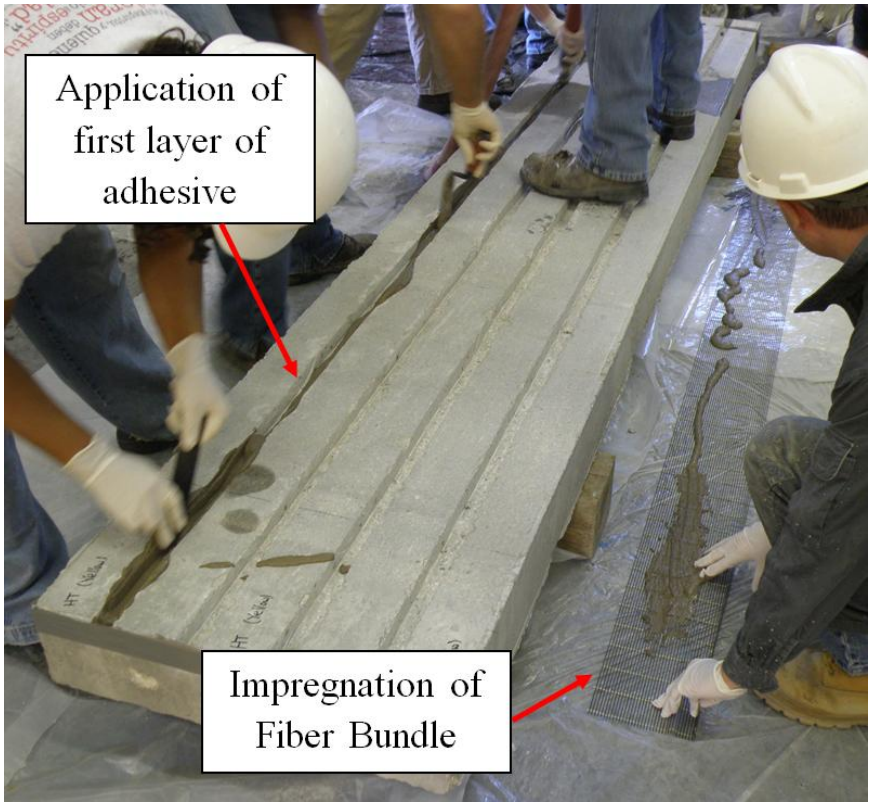

Figure 35: Impregnation of Fiber Bundle

Figure 36: Cementitious Adhesive being applied to NSM Groove

3.4 Test Setup

The flexural response of each slab was examined using a four-point loading configuration. A schematic of the test setup is shown in Figure 37. The test setup is shown in Figure 38. The slab was simply supported with a roller and pin configuration that provided a 10’ clear span. A 55-kip MTS hydraulic actuator was used to apply the load to the slab which was tested up to failure. A spreader beam was used to distribute the load from the actuator to two HSS steel beams that produced two point loads that were 2’ apart and distributed over the entire width of the slab. The load was applied at a controlled rate of 0.10 in/min until failure occurred.

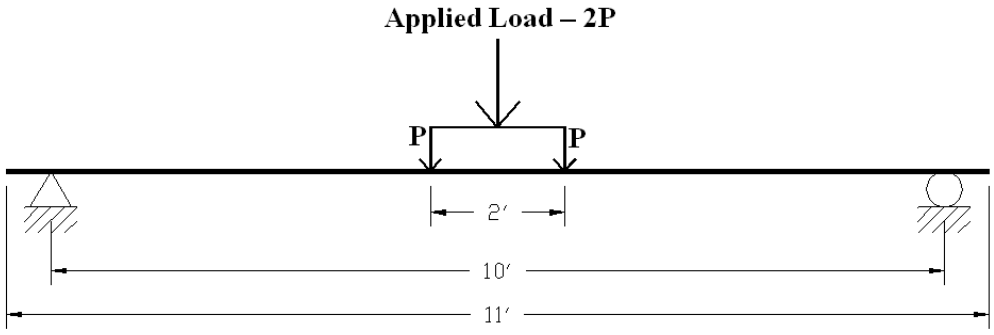

Figure 37: Test Setup Schematic

Figure 38: Test Set-Up

3.5 Test Instrumentation

A total of seven measurements were recorded during testing. A schematic of the instrumentation is shown in Figure 39. The load was measured using a load cell attached to the actuator. Vertical displacements of the slabs were measured at two locations at the mid-span of the slab using two 12" string potentiometers. Two sting potentiometers located at midspan were placed four inches apart along the widths of the specimen for redundancy and to capture any torsion. A total of four 200 mm pi gauges were located at the mid-span of the slab, two at the top surface and two at the bottom surface, spaced 6 inches apart. These pi gauges were used to measure strain at the top and bottom surface of the slab at mid-span and used to determine the strain profile for each slab under different stages of loading.

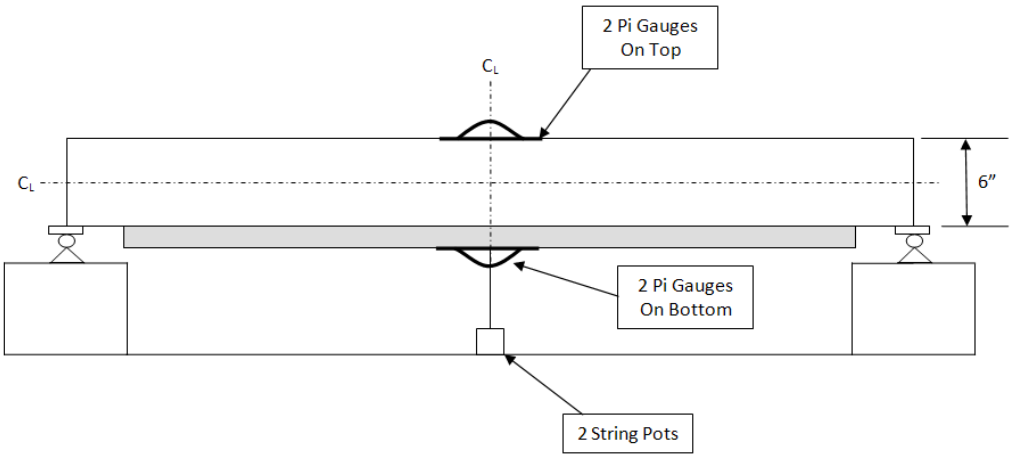

Figure 39 : Test Instrumentation

CHAPTER 4 - TESTS RESULTS AND DISCUSSION

The following chapter describes test results of the two phases of the experimental program. The criterions that were used to evaluate the effectiveness of the strengthening systems are described followed by examining the measured data and observed behavior of the strengthened slabs in the first phase. Test results were examined to determine the strengthening systems that will be used in the second phase of the experimental program. Test results of Phase II are also presented and discussed to determine the most effective strengthening system.

4.1 Phase I of the Experimental Program

4.1.1 Testing Criteria

The two criteria used to evaluate the flexural performance of the different FRP strengthened slabs were the measured maximum load and the ductility at failure. Ductility of the slabs was determined based on the type of failure that was observed. If concrete crushing was observed to be the source of failure, the ductility was determined by comparing the mid-span deflection at failure due to crushing of the concrete within the compression zone, $\Delta_{Failure}$, to mid-span deflection at yielding of the steel reinforcement $\Delta_{Yielding}$. A schematic of this approach is shown in Figure 40.

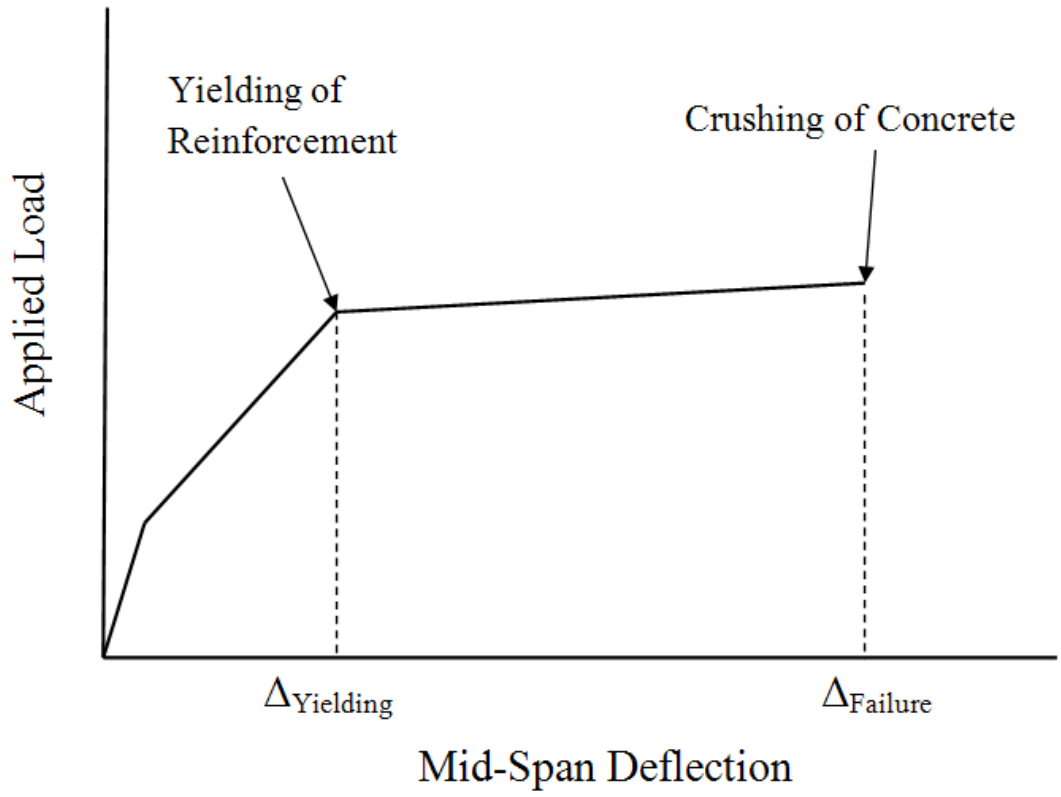

Figure 40: Schematic of Ductility Calculation for Concrete Crushing

If failure of the strengthening system by either rupture or debonding of the fibers after yielding of the reinforcing steel was observed to be the source of failure, ductility was determined by comparing the deflections at failure, which is typically due to failure of the FRP strengthening system, $\Delta_{FRP\ Failure}$, to the deflection at yielding of the steel reinforcement, $\Delta_{Yielding}$. A schematic of this scenario for failure of the strengthening system after yielding of the reinforcement is shown in Figure 41. If failure of the FRP strengthening system by either rupture or debonding of the FRP occurred before yielding of the steel reinforcement, the failure is consider brittle and the ductility is less than unity. This type of failure is not desirable.

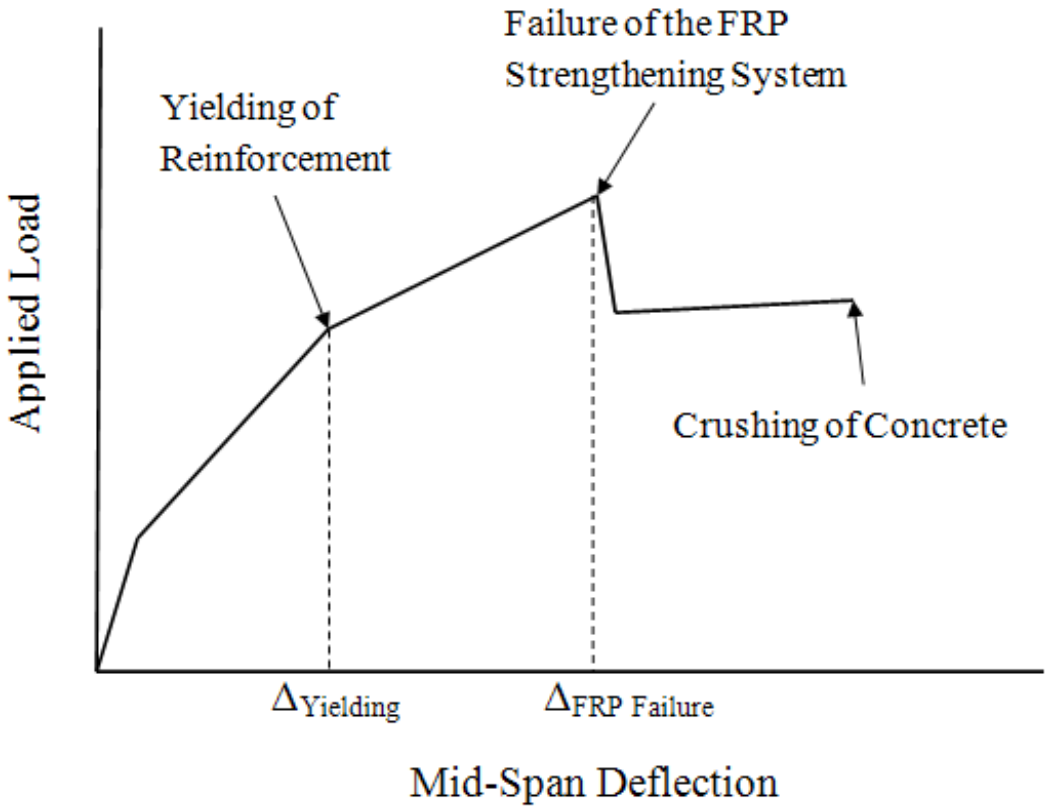

Figure 41: Schematic of Ductility Calculation for FRP Rupture or Debonding

4.1.2 Control Unstrengthened Slab

The control slab was reinforced with the same steel reinforcement and was cast using the same concrete batch as the other slabs in Phase I. The control specimen failed as expected due to crushing of concrete in the compression zone in the maximum moment region. The load–deflection behavior of the control specimen is shown in Figure 42. The behavior was linear up to the initiation of the first crack which occurred at load level of 3000 lbs. The behavior after cracking was non-linear up to yielding of the reinforcing steel at a load level of 12,767 lbs followed by a significant decrease of the stiffness up to failure due to crushing of the concrete at a load level of 14,678 lbs. Comparing the deflection at failure of 5.60 inches to the deflection at yielding of 1.00 inches, the ductility of the control specimen is estimated to be 5.60. The deflected shape of the control slab at failure is shown in Figure 43 and the crack pattern is shown in Figure 44. The failure was very ductile as evident by the large

defection and the propagation of a significant number of cracks before failure. Test results are given in detail in Appendix A.1.

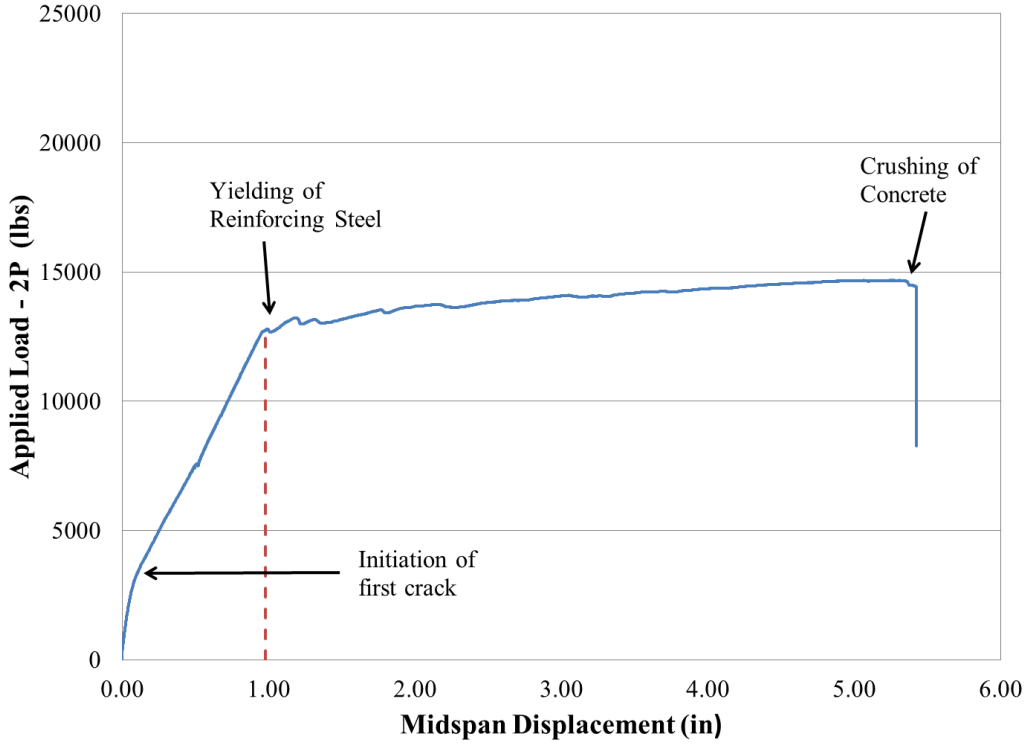

Figure 42 : Load-Deflection Behavior of Control Specimen

Figure 43: Deflected Shape of the Control Slab at Failure

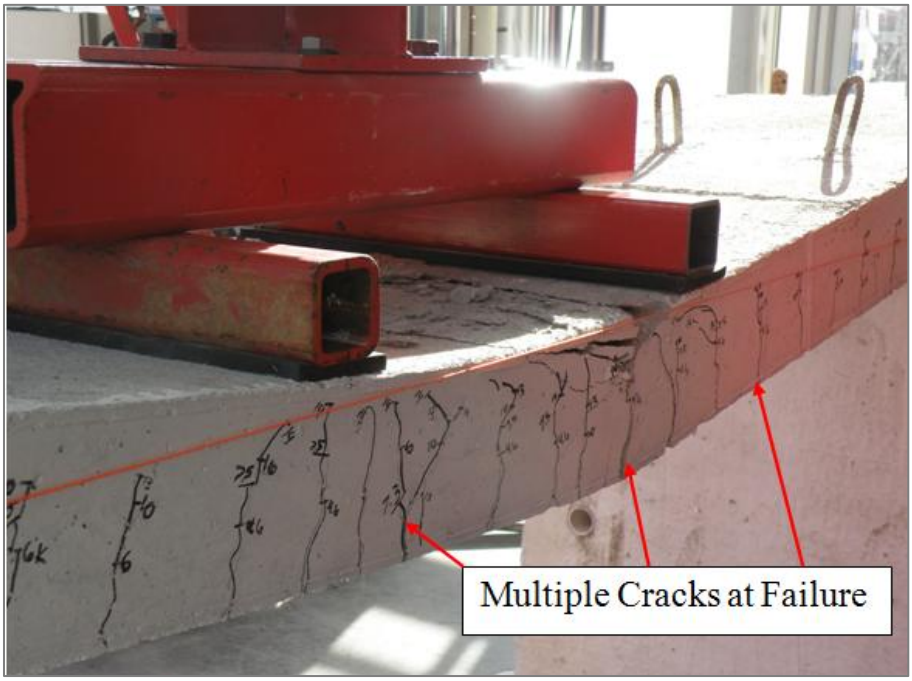

Figure 44: Crack Pattern of Control Slab at Failure

4.1.3 Slabs Strengthened with Carbon Strand

Two of the slabs were strengthened with the CFRP Strand. The spacing between the strands was 1.64 mm for the high tensile CFRP and 1.42 mm for the high modulus CFRP. This small spacing between the strands is designated as Type 1 as given in Table 9. The fiber reinforcement ratio of the High Tensile Carbon Strand was 0.43% compared to fiber reinforcement ratio of the High Modulus Carbon Strand of 0.57%. This was due to a manufacturing process. Therefore, while the effectiveness of the High Tensile and High Modulus strengthening systems will be compared, these comparisons will be made with the understanding that the fiber reinforcement ratio is slightly different for each strengthening system. Test results indicate that the strengthening system increased the load to initiate cracking and the ultimate load carrying capacity when compared to the control specimen as shown in Figure 45. However, the measured strain indicates that the reinforcing steel did not yield before failure of the strengthening system as discussed in section A.2 and A.3. Therefore, the failure was sudden and occurred within the shear span of the slab.

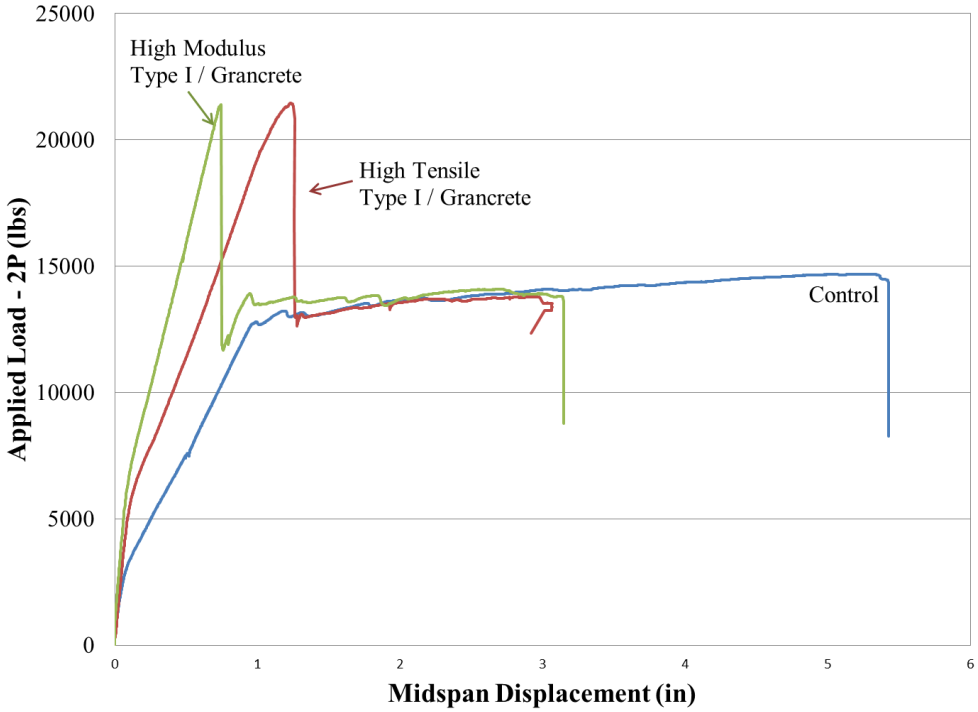

Figure 45: Load-Deflection Behavior of Type 1 Carbon Strand Specimens

Failure of the strengthening system was due to debonding of the sheet within the shear span as shown clearly in Figure 46. The shear span is defined as the length of the slab between the support and the point of load application. It was observed that once both of the high strength and high modulus Carbon Strand Sheet – Type 1 strengthening systems failed, the slabs behaved as the control specimen until failure due to crushing of concrete as shown in Figure 45. A typical pattern of this crack propagation after debonding of the Carbon Strand Sheet is shown in Figure 47. Test results indicate that using high modulus carbon strands, as expected, increases the stiffness of the strengthened slab as shown in Figure 45. Both slabs strengthened with high modulus and high tensile carbon strands achieved the same increase in ultimate load carrying capacity since the failure for both of these slabs was due to delaminating of the fibers and did not fully utilize the characteristics of the fibers.

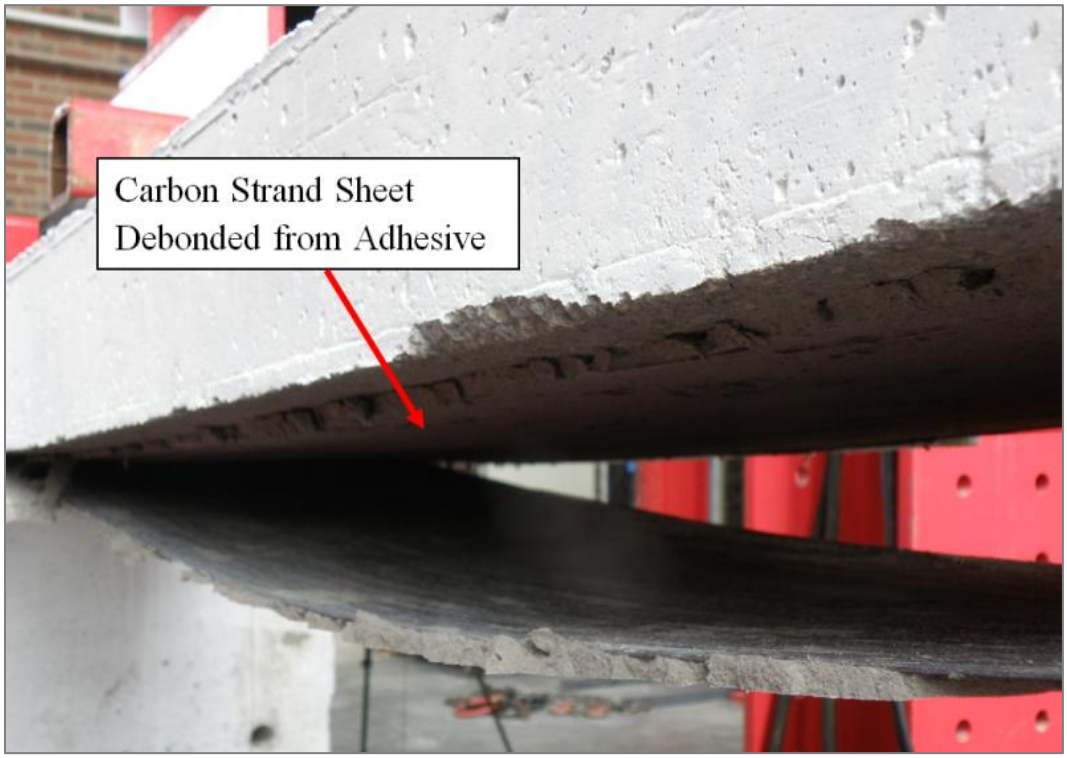

Figure 46 : Typical Failure of Carbon Strand Sheet – Type 1 Sheet

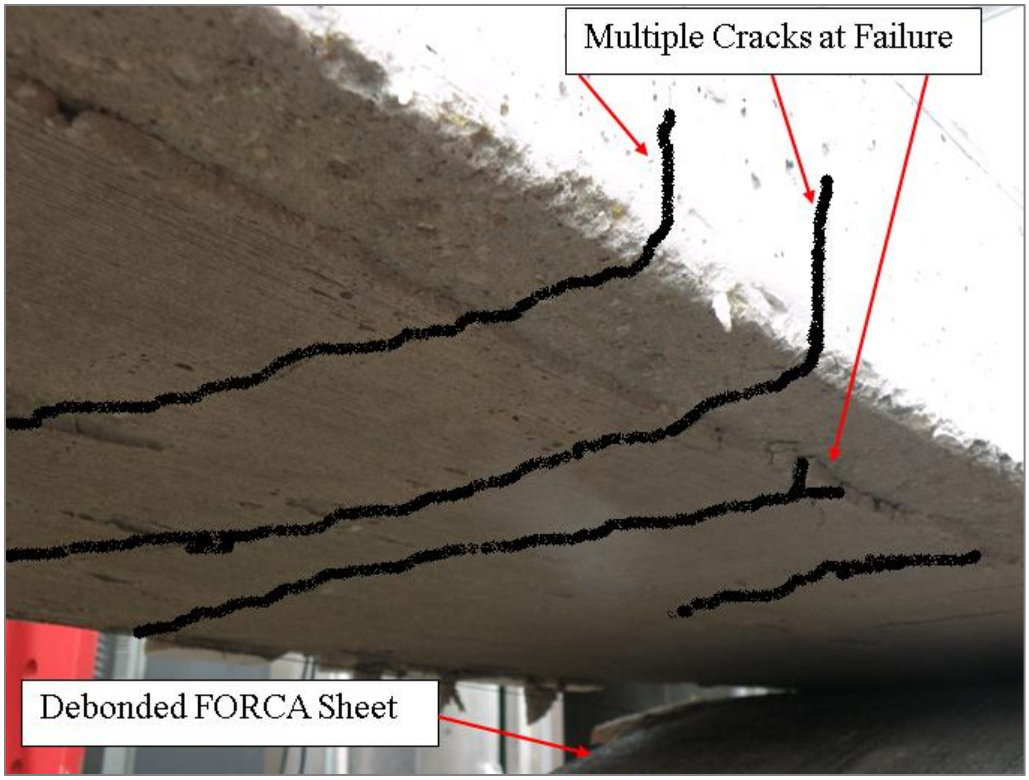

Figure 47 : Crack Propagation through Adhesive after Carbon Strand Sheet Debonding

Test results indicate that the slabs strengthened with the Carbon Strand Sheet – Type 1 failed in a brittle nature. The results suggest that the reinforcement ratio used for strengthening the slab was large and did not allow yielding of the longitudinal bars, therefore, the failure was brittle. Use of carbon strands significantly increased the load required to cause cracking of the slab as shown in Figure 45. Pull-off tests were performed to determine the bond strength of the FRP strengthening system and all results indicate that the bond strength of the system with the Type 1 carbon strands is less than the 200 psi as required by ACI 440.2R-08. Test results are given in detail in A.2 and A.3. Test results suggest that the spacing between the strands was small and did not allow full bonding of the strand sheet to the concrete substrata, and therefore, it is recommended that a larger spacing between the strands be used for future testing.

4.1.4 Slabs Strengthened with Glass Grid

Two slabs that were strengthened with Glass Grid were tested in Phase I. Test results indicate that the Glass Grid strengthening system increased the load required to initiate cracking and yield of the reinforcement when compared to the control slab. However, it did not increase the ultimate load carrying capacity when compared to the control specimen as shown in Figure 48. It was also observed that once the Glass Grid strengthening system failed, the slab followed the same behavior of the control specimen until failure occurred due to crushing of concrete as also shown in Figure 48. The behavior of the strengthened slab under the load was characterized by significant cracking and propagation of these cracks. This behavior can be characterized as a ductile failure. The typical crack pattern and crack propagation observed are shown in Figure 49. Test results also indicate reduction of the ductility for all tested slabs strengthened with the Glass Grid in comparison to the control slab. Test results suggest also that the reinforcement ratio used was insufficient to increase the overall load carrying capacity. Failure of the strengthening system was due to Intermediate Crack (IC) debonding as expected for most of the externally bonded sheets. Inspection of the test specimen after failure showed that the glass grid had debonded and ruptured in the region of maximum moment. Pull-off test were performed and the results indicate that the bond strength for the 1 inch grid was adequate to meet the ACI 440.2R-08 requirement of 200 psi whereas the bond strength for the 0.25 inch grid was not due to the small opening between the strands. Test results are given in detail in A.5 and A.6.

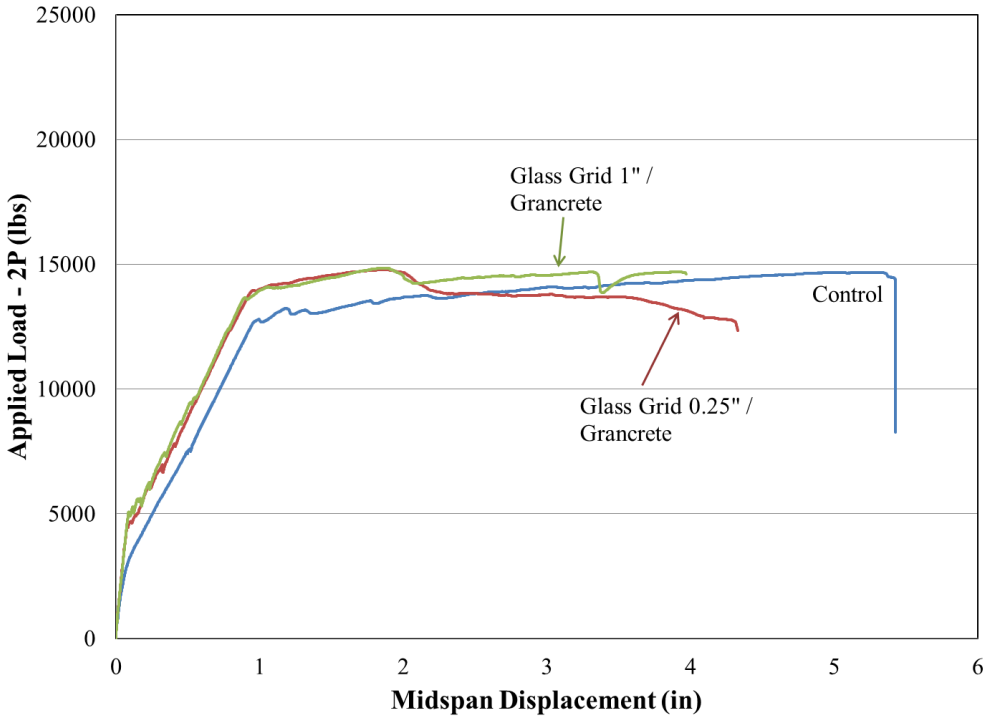

Figure 48: Load-Deflection Behavior of Glass Grid Specimens

Figure 49: Typical Failure of Glass Grid Strengthened Specimens

4.1.5 Slabs Strengthened with Carbon Grid

Four slabs that were strengthened using the 9.5 mm x 19.5 mm Carbon Grid were tested in Phase I. The two cementitious adhesives used were Grancrete and a cementitious bonding matrix known as Tyfo C-Matrix. The behavior was also compared to the slabs strengthened using CFRP grid and epoxy. Test results indicate in general that the Carbon Grid increased the load required to initiate cracking and yielding of the reinforcement and ultimate load carrying capacity, for all types of adhesives used, when compared to the control slab. The load-deflection behavior was linear up to the initiation of the first crack at a load level ranging from 3,620 lbs to 4,970 lbs which was higher than the control slab. Initiation of the cracks reduces the stiffness and the behavior was non-linear up to yield of the longitudinal bars evident by the significant loss of the stiffness as shown in Figure 50. Once the strengthening system failed, it was observed that the strengthened slab followed the same behavior of the control specimen until failure due to crushing of concrete in the compression zone using Grancrete and the cementitious material, Tyfo C-Matrix. The uniform crack pattern observed for these three slabs after failure is shown in Figure 51. The results of the two slabs, C-C-E-A and C-C-E-B that were strengthened with the Carbon grid and the cementitious material, Tyfo C-Matrix, are shown in Figure 50. The average of the two slabs matched very closely to the slab strengthened with the Carbon Grid and Grancrete as shown in Figure 50. Inspection of the test specimens after failure showed that the carbon grid had debonded, and in the cases when Grancrete was used as the adhesive, ruptured, in the region of maximum moment. Failure due to debonding of the fibers was also confirmed with pull off tests detailed in section A.6, A.7, and A.8. Pull off tests are used to determine the bond strength of an FRP strengthening system. The tensile strength of carbon grid and cementitious material strengthening systems were less than the 200 psi as recommended by ACI 440.2R-08 as shown in section A.6, A.7, and A.8.

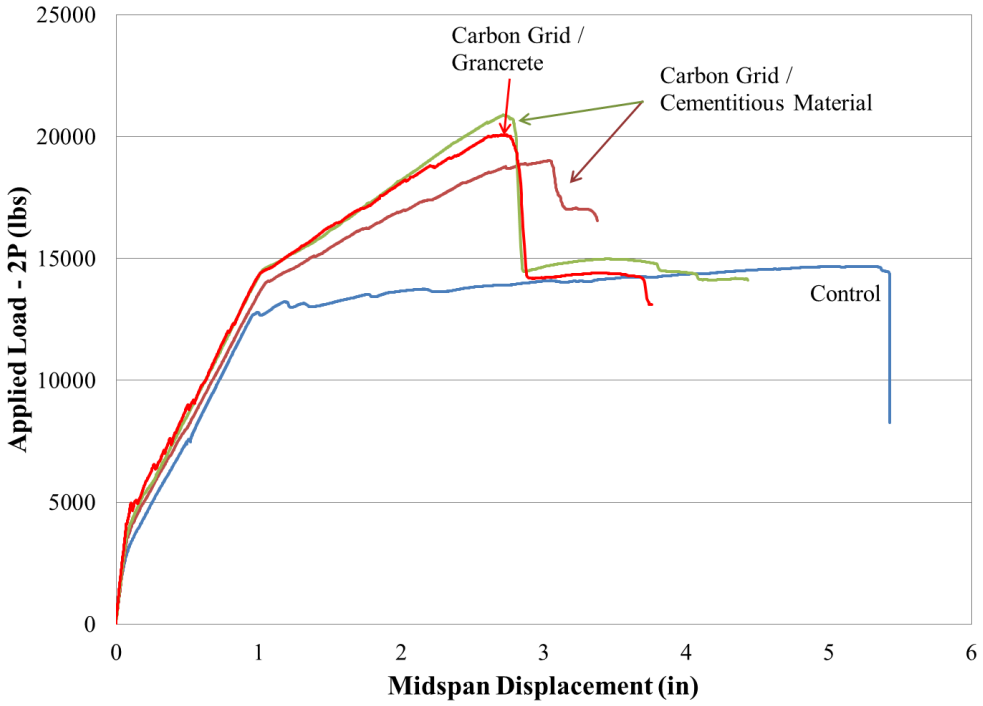

Figure 50: Behavior of slabs strengthened with Carbon Grid and Cementitious Materials

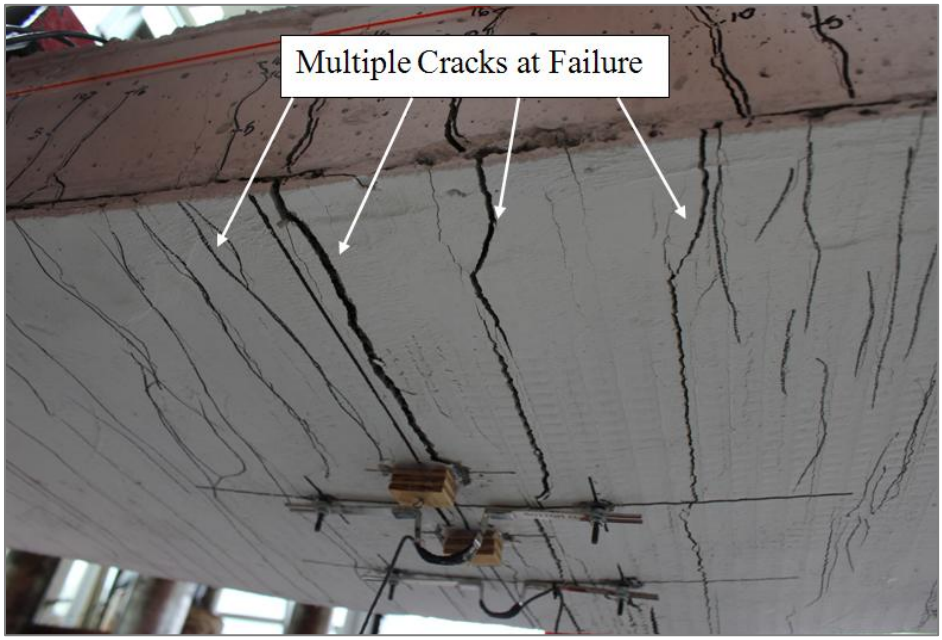

Figure 51 : Typical Failure slabs strengthened with Grancrete or Tyfo C-Matrix

The slab strengthened with the Carbon Grid and Tyfo TC epoxy as the adhesive, C-E-E, did not follow the same behavior after failure of the strengthening system. The behavior of this slab compared to the control slab can be seen in Figure 52. This was due to the fact that the failure was sudden and brittle in nature due to the formation of a single crack instead of several cracks observed for the slabs strengthened with Grancrete or the cementitious bonding matrix. Cracking of this slab was characterized by a single, wide crack as shown in Figure 53 for the slab strengthened with the Carbon Grid and epoxy adhesive.

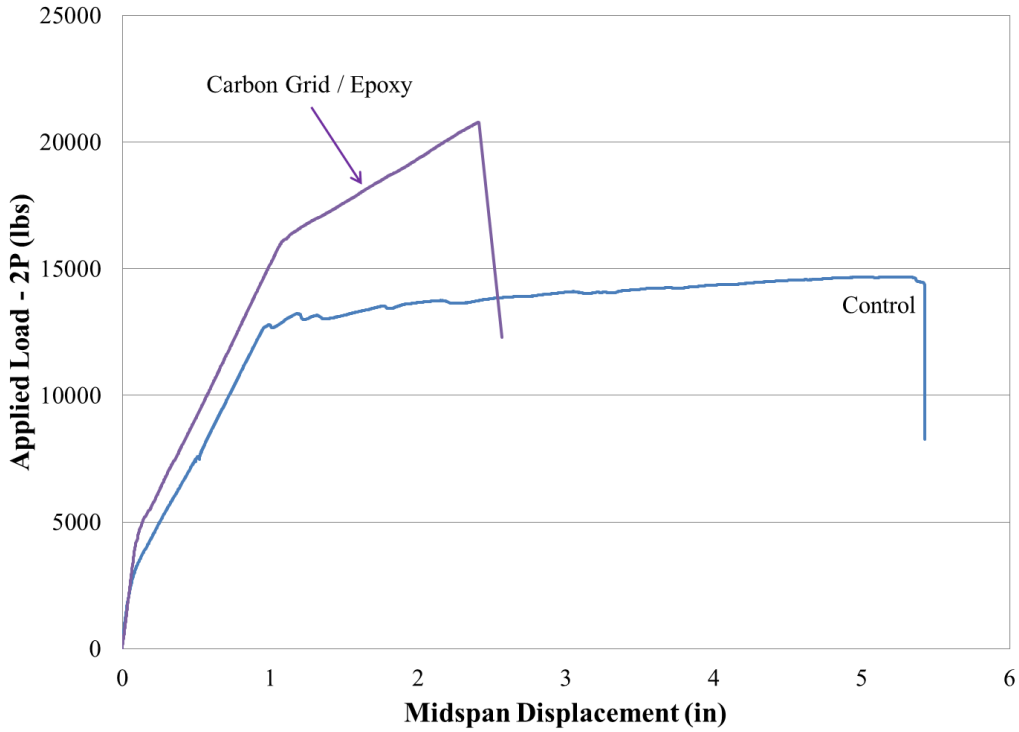

Figure 52: Behavior of Slab strengthened with Tyfo TC epoxy

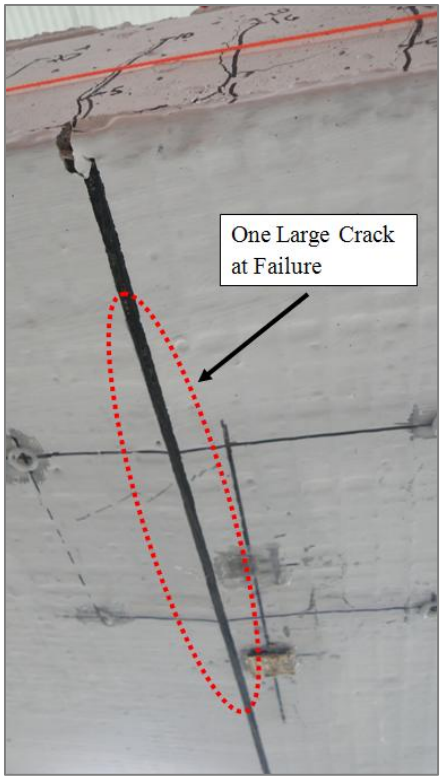

Figure 53 : Typical Failure of Epoxy Specimen

Use of the Carbon Grid with Grancrete and the cementitious material, Tyfo C-Matrix, allowed uniform distribution of the cracks which propagated through the adhesive material and the concrete thickness of the slab as shown in Figure 51. This behavior allowed for a more ductile failure mode in comparison to the epoxy adhesive. Test results indicate a decrease in the overall ductility at failure for all tested strengthened slabs. The behavior of the four slabs strengthened with the Carbon Grid system and various adhesives, compared with the control specimen, is shown in Figure 54. Figure 54 shows that slabs strengthened with the cementitious material, Tyfo C-Matrix, and Grancrete had a greater overall ductility than the slab strengthened with Tyfo TC epoxy adhesive, which is consistent with the observed evenly distributed cracks in the slabs strengthened with the cementitious materials. Failure of the slabs reinforced with the Carbon Grid was due to debonding of the strengthened layer at the maximum moment region. This failure is known as IC debonding, which is typical for slabs externally bonded with FRP Sheets. The water/material ratio of the

cementitious material, Tyfo C-Matrix, provided by the manufacturing company may not be adequate to achieve the full bond characteristics of the material. This is discussed in detail in A.7 and A.8. Pull-off tests were performed and the results indicate that the bond strength of the strengthening systems that used the cementitious materials as the adhesive is less than the 200 psi required by ACI 440.2R-08. When epoxy was used as the adhesive, the bond strength met the ACI 440.2R-08 requirement of 200 psi. Test results are given in detail in A.6, A.7, A.8, and A.9. Based on the test results, it is recommended to increase the spacing of the grid for future testing to increase the bond strength between the fibers and the concrete substrata. It is also recommended that the water/material ratio of the cementitious material provided be adjusted to increase the workability and set time of the adhesive.

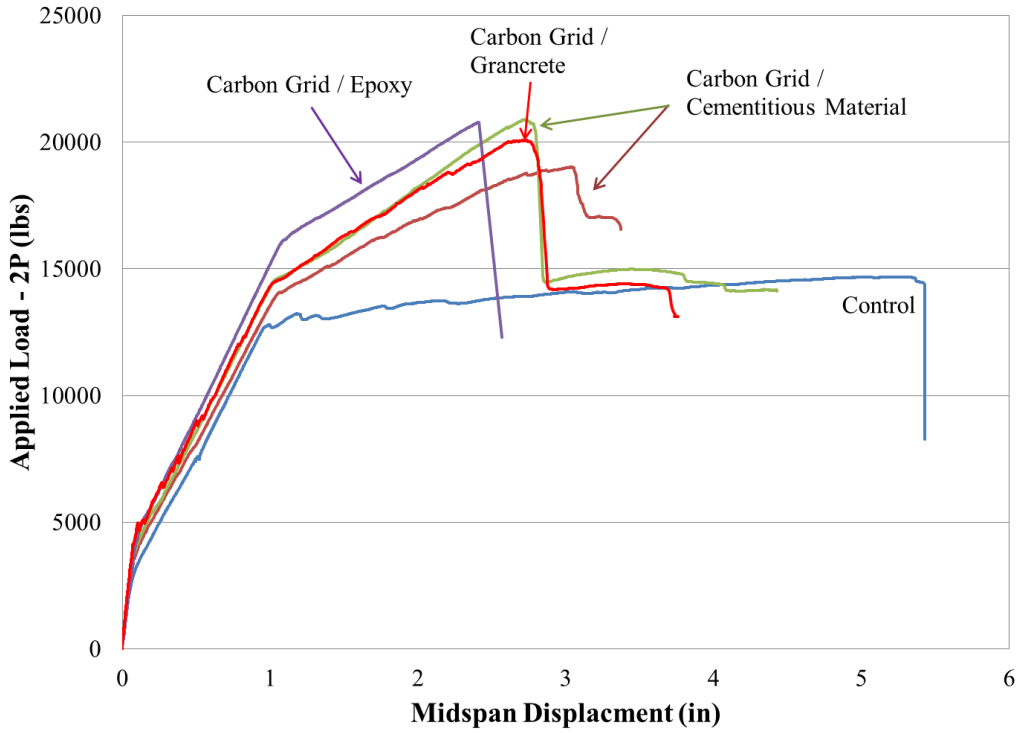

Figure 54: Load-Deflection Behavior of Carbon Grid Specimens

4.1.6 Predictions

ACI 440.2R-08 was used to predict the ultimate load carrying capacity of the FRP strengthened slabs. ACI 440.2R-08 recommends limiting the strain in the FRP to either the calculated debonding strain, ε_{fd}, or 90% of the published rupture strain, $0.9\varepsilon_{fu}$, whichever is less. The debonding strain equation is found in section 2.2.2 and was used in a sectional analysis to predict the ultimate load carrying capacity of the FRP strengthened slabs. It should be noted that the debonding equation recommended by ACI 440.2R-08 was formulated and calibrated for FRP strengthening systems that used FRP sheets or plates with epoxy adhesive. Since all the strengthening systems used in this experimental program were used either FRP grids, strands and used a cementitious material as the adhesive, ACI 440.2R-08 may not accurately predict the debonding strain of the strengthening system. Further research must be done in order to accurately predict debonding strains for strengthening systems that use alternative types of FRP and adhesives. Taking this into account, the ACI 440.2R-08 predicted values, along with the measured experimental values for each strengthened slab are shown in Figure 55.

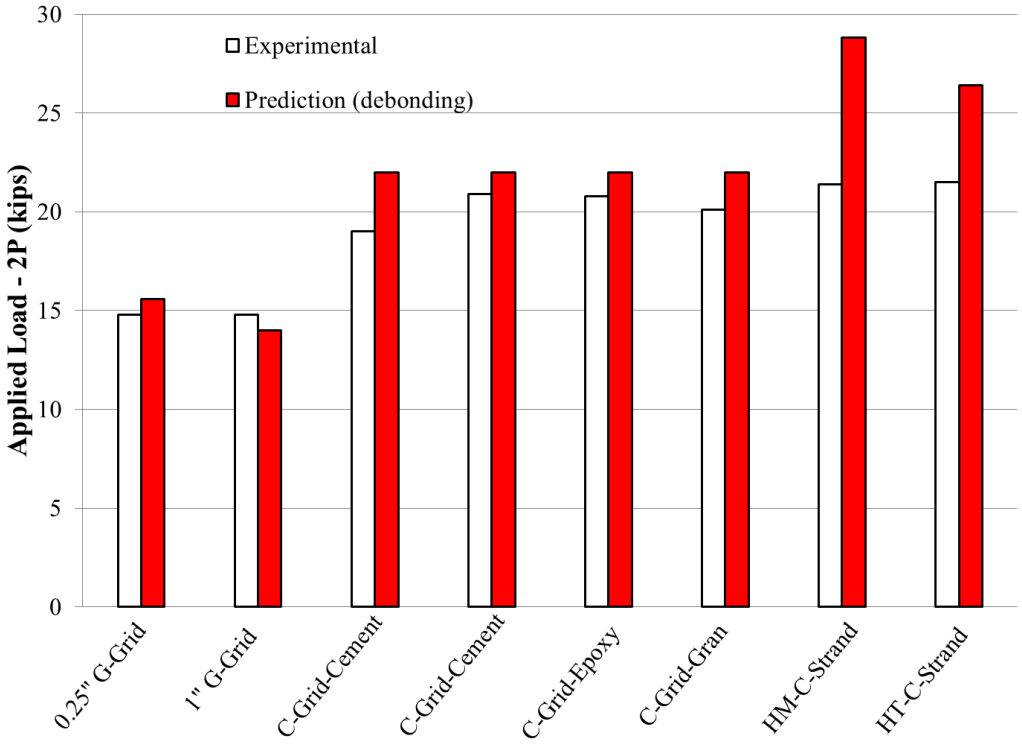

Figure 55: Phase I Predictions vs. Experimental Results

This figure shows that, in general, ACI 440.2R-08 over-predicts the ultimate load carrying capacity of the strengthened systems. Premature debonding of the strengthening systems for the slabs in Phase I of the experimental program was the main failure mechanism. Premature debonding is not a desirable failure mechanism because it prevents the full utilization of the strengthening system. Figure 55 also shows that the strain causing debonding proposed by ACI 440.2R-08 is not adequate to predict the ultimate load carrying capacity when debonding is the failure mechanism since it was mainly calibrated for sheets and epoxy system rather than the configuration of the fiber used and the cementitious material tested in this experimental program. Further research must be done in order to accurately predict debonding strains for strengthening systems that use alternative types of FRP and adhesives.

4.1.7 Overall Evaluation of Phase I

All of the strengthened specimens were able to increase the cracking load capacity and all but the slabs strengthened with ¼" and 1" glass grid were able to increase the ultimate load

carrying capacity when compared to the control specimen as shown in Figure 56. Figure 56 also provides evidence that the high modulus carbon strand and the high tensile carbon strand sheet increased the load to initiate cracking of the concrete and ultimate load carrying capacity the most in comparison to the other fibers tested in Phase I. This was expected due to the high tensile strength and elastic modulus of the carbon strands when compared to the other fibers.

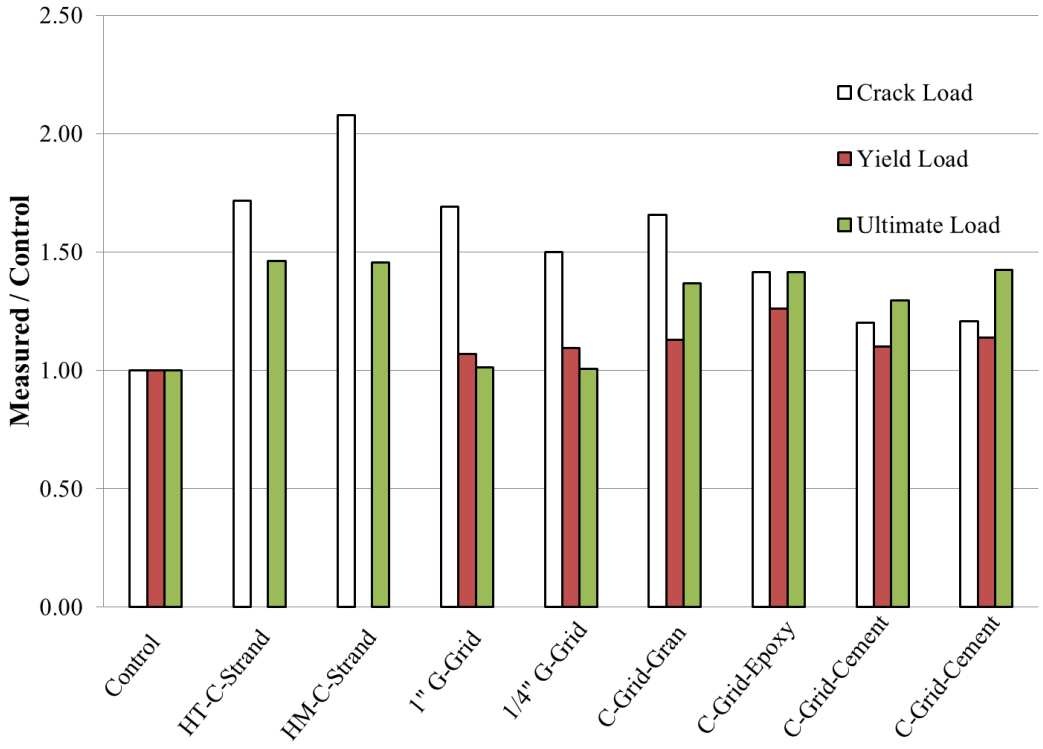

Figure 56: Load Stages of Phase I slabs

As expected, all of the strengthened specimens caused a decrease of the ductility of the specimen when compared to the control specimen as shown in Figure 57. The figure indicates that the carbon grid decreased ductility the least when compared to the ¼" and 1" glass grid. The reduction in ductility by using the carbon grid cannot be compared to the reduction in ductility when using the carbon strands because the slabs that were strengthened using the carbon strands failed in a brittle manner.

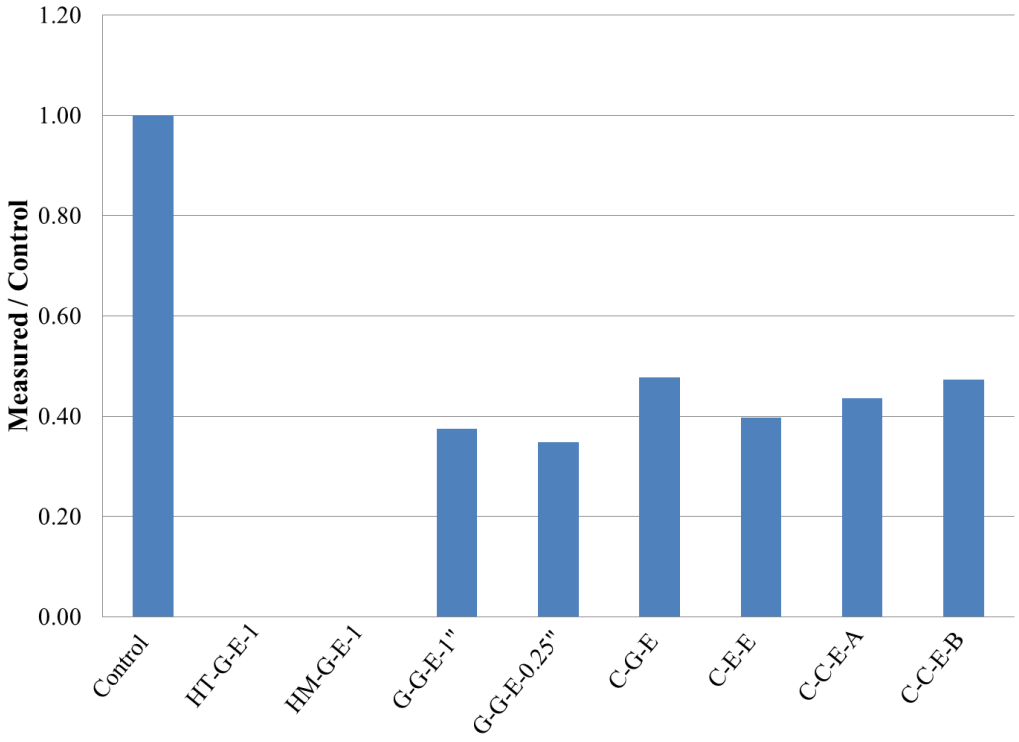

Figure 57: Ductility of Phase I Slabs

Test results of the first phase of the experimental program provided the knowledge to formulate the second phase of the experimental program. Findings of the first phase provided clear understanding of the effect of type of fiber, type of adhesive, and fiber reinforcement ratio. Discussion of each of these parameters is presented in the following sections.

4.1.7.1 Type of Fiber

A total of three different types of fiber types were studied in Phase I. They included the carbon fiber strands, both high modulus and high tensile, carbon fiber grid, and glass fiber grid, both the ¼" and 1" grid spacing. The two criteria used to evaluate the flexural performance of the different types of fibers were the measured maximum load and the ductility at failure. A comparison of the load-deflection behavior is shown in Figure 58. The figure indicates that the carbon strands strengthening system with Grancrete provided the optimum increase of the load to initiate cracking of the concrete and ultimate load carrying

capacity in comparison to all other fibers. Use of the carbon grid increased the strength almost in the same order as the carbon strands; however, the carbon grid provided some ductility before failure. Debonding of the carbon strands due to the small spacing between the strands did not allow for the cementitious material to penetrate between the strands and form a strong and complete bond between the fibers, adhesive, and concrete surface. Both the high modulus and high tensile carbon fibers have a greater tensile strength and elastic modulus when compared to the other fibers as given in Table 11. This could be possible if a strong bond was achieved between the adhesive, fibers, and concrete surface. It was also observed that the slabs strengthened with the carbon grid and the cementitious materials failed due to IC debonding due to the small openings produced by the manufacturing process. The manufacturing of the carbon grid could not be altered to allow for a larger opening of the grid. Therefore, it was decided to use the carbon strands with a greater spacing between the strands for the second phase of the experimental program.

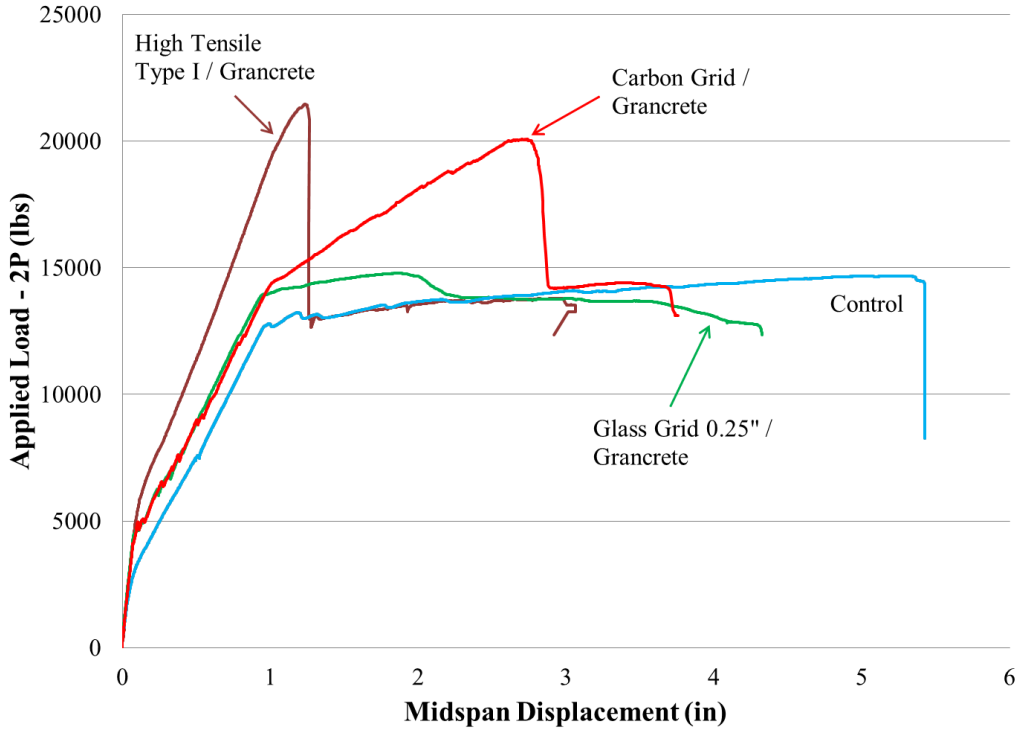

Figure 58: Specimens from Phase I comparing different types of fibers

Table 11: Material Properties of Fibers used in Phase I

Type of Fiber	Tensile Strength (ksi)	Elastic Modulus (ksi)
High Tensile Carbon Strand	333	14,946
High Modulus Carbon Strand	120	31,273
Carbon Grid	109	9,366
1/4" Glass Grid	69	3,184
1" Glass Grid	85	1,595

4.1.7.2 Type of Adhesive

A total of three different adhesives were investigated in Phase I. They included two different cementitious materials, Grancrete and Tyfo C-Matrix, and the typical epoxy adhesive. Since the carbon grid was used with all three of the adhesives, the load-deflection behavior of the

specimens that used the carbon grid fiber is shown in Figure 59. The figure indicates that the cementitious materials increased the ultimate load carrying capacity as much as when the epoxy was used. However, test results also indicate that the slabs that used the cementitious materials achieved a greater ductility than the slab strengthened with the epoxy adhesive. This behavior was expected since the cementitious material is not as stiff as the epoxy which allows for a uniform distribution of cracks before failure. The epoxy does not allow for propagation of flexural cracks whereas the cementitious materials allow for flexural cracks to propagate. This propagation of flexural cracks leads to a reduction of the stiffness and increase in ductility in comparison to the epoxy. Based on test results of the first phase, it was decided to further explore the behavior of the cementitious material in the second phase of the experimental program. The two cementitious materials, Grancrete and Tyfo C-Matrix, increased in ultimate load carrying capacity and achieved similar ductility before failure. As discussed before, the use of Tyfo C-Matrix was difficult and produced undesirable failure modes. One of the slabs strengthened with Tyfo C-Matrix failed due to debonding of the strengthening system and the layer of the Tyfo C-Matrix peeled away from the fibers in the shear zone in the second slab. Peeling of the adhesive layer was not observed when using Grancrete. Therefore, it was decided to expand the use of Grancrete adhesive in Phase II of the experimental program.

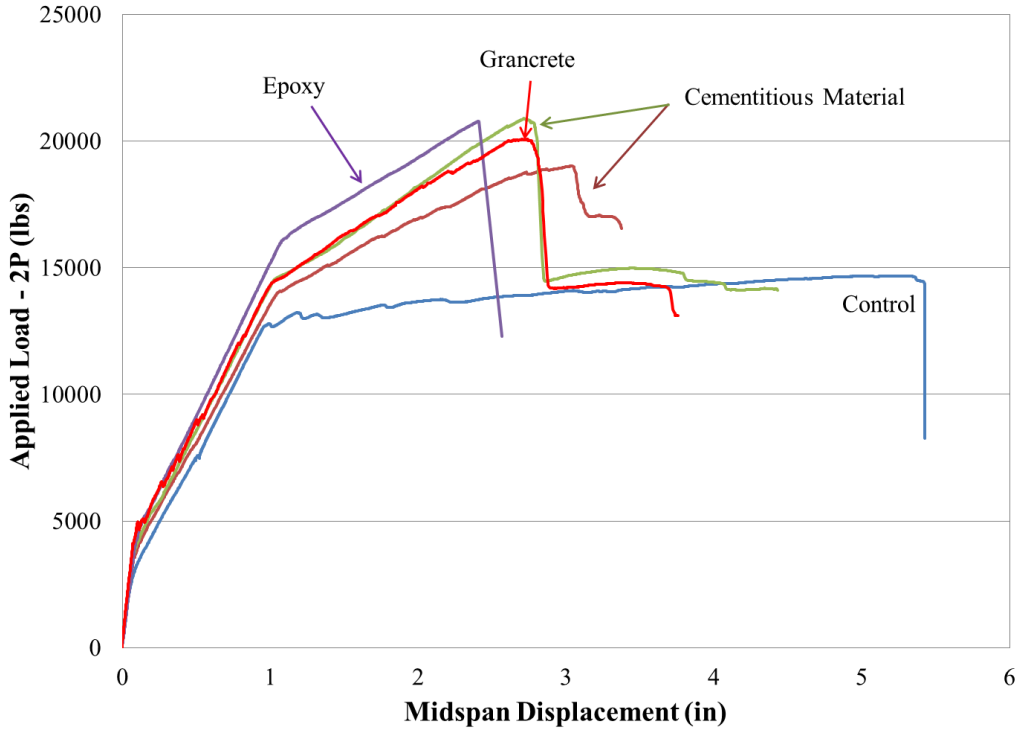

Figure 59: Specimens from Phase I comparing different adhesives

4.1.7.3 Fiber Reinforcement Ratio

A total of four different fiber reinforcement ratios were investigated in Phase I. The spacing between the fibers was considered as a possible parameter that affects the failure modes of the strengthened systems. The fiber reinforcement ratios for all the strengthened slabs, as well as the percent increase in ultimate load carrying capacity, are shown in Table 12. This table indicates that the as the fiber reinforcement ratio increases, the ultimate load carrying capacity reaches a limit. This is evident by the fact that increasing the fiber reinforcement ratio from 0.28% to 0.43% or 0.57% which is almost double, did not increase the load carrying capacity. This suggests that the optimum fiber reinforcement ratio is less than 0.30% and any increase of the fiber reinforcement ratio after this will have minimal effect on the load carrying capacity. Therefore, it was decided to keep the fiber reinforcement ratio less than 0.30% for Phase II of the experimental program.

Table 12: Effect of the Fiber Reinforcement Ratio on Load Carrying Capacity

Slab ID	Number of Longitudinal Fibers	Area of Fiber (in^2)	Fiber Reinforcement Ratio (%)	Increase in Load (%)
Control	---	---	---	0
HT-G-E-1	309	0.00165	0.43	46
HM-G-E-1	352	0.00194	0.57	46
G-G-E-1in	24	0.00398	0.08	1
G-G-E-0.25in	96	0.00164	0.13	1
C-G-E	57	0.00599	0.28	37
C-E-E	57	0.00599	0.28	42
C-C-E-A	57	0.00599	0.28	30
C-C-E-B	57	0.00599	0.28	42

The spacing of fibers was also closely looked at during Phase I of the experimental program. The spacing between the fibers is very important because if the spacing between the fibers is not sufficient for the cementitious material to penetrate between the fibers then a strong bond will not be achieved. Weak bond leads to a premature failure due to debonding of the strengthening system. The bond strength for each of the strengthened slabs was determined using a standard pull off test. Results of the pull off test of specimens that used cementitious materials as the adhesive are shown in Figure 60. The figure indicates that the spacing between fibers is a critical parameter that must be considered when using cementitious materials. Increasing the spacing between the fibers should increase the bond strength. The failure of the pull off test with small spacing were typically at the fiber/adhesive bond layer as described in detail in APPENDIX A. The 1" glass grid did not fail at this bond layer, but rather in the adhesive bond layer. This indicates that the bond spacing was large enough to form a strong bond at the fiber/adhesive bond layer. Therefore, it was recommended that the spacing between the fibers be increased for the carbon grid, the carbon strand, and the ¼" glass grid.

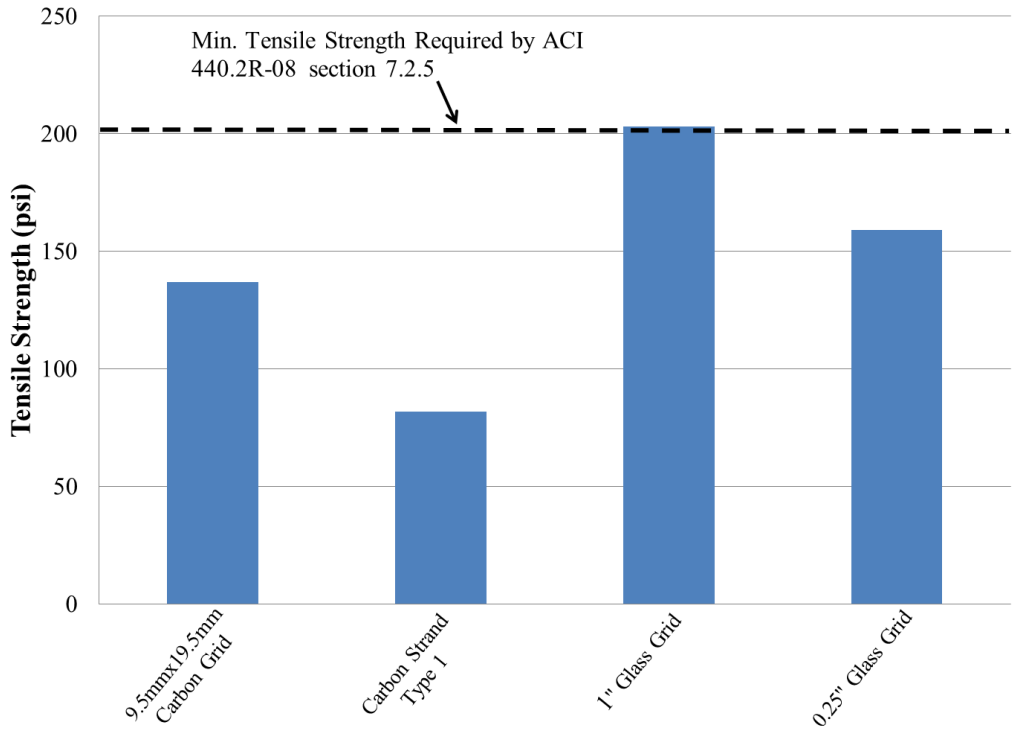

Figure 60: Effect on Spacing between Fibers on Bond Strength

4.1.7.4 Recommendations for Phase II

The three parameters that were closely investigated in Phase I were type of fiber, type of adhesive, and fiber reinforcement ratio which is affected by the spacing between the fibers. From the test results from Phase I, it was decided to use the High Tensile and High Modulus Carbon Strand due to their high tensile strength and elastic modulus that allows the fibers to have the greatest potential to increase the load to initiate cracking of the concrete and the ultimate load carrying capacity. It was also decided that the cementitious material known as Grancrete be used as the adhesive. This cementitious material was chosen since it forms a strong between the fibers and the concrete surface while still allowing the strengthened system to fail in a ductile manner. The epoxy has a greater tendency to form a very stiff system that can cause the strengthening system to fail in a very brittle manner. The test results from Phase I also showed that the spacing between fibers for the carbon strand sheet

needs to be increased. It was therefore decided to replace the Type 1 carbon strand sheet with Type 3 carbon strand sheet, which has double the spacing between fibers as Type I.

4.2 Phase II

4.2.1 Testing Criteria

Based on results of Phase I, it was decided to use the high modulus and high tensile carbon strand sheets due to their potential of greatly increasing the ultimate load carrying capacity. It was decided to use Grancrete as an adhesive to compare the behavior with the traditional epoxy. The second phase explored also the near surface mounted technique to compare the behavior to the externally bonded technique. The two criteria used to evaluate the flexural performance of the different FRP strengthened slabs were the measured maximum load and the ductility at failure. Ductility of the slabs was determined based on the type of failure that was observed for that specimen. A detailed description on how the ductility of the slabs was calculated is shown in section 4.1.1.

4.2.2 Control Unstrengthened Slab

The control slab was reinforced with the same steel reinforcement and was cast using the same concrete batch as the other slabs in Phase II. The control specimen failed as expected due to crushing of concrete in the compression zone in the maximum moment region. The load –deflection behavior of the control specimen is shown in Figure 42. The behavior was linear up to the initiation of the first crack which occurred at load level of 3000 lbs. The behavior after cracking was non-linear up to yielding of the reinforcing steel at a load level of 12,814 lbs followed by a significant decrease of the stiffness up to failure due to crushing of the concrete at a load level of 13,751 lbs. Comparing the deflection at failure of 4.35 inches to the deflection at yielding of 1.10 inches, the ductility of the control specimen is estimated to be 3.95. The deflected shape of the control slab at failure is shown in Figure 43 and the crack pattern is shown in Figure 44. The failure was very ductile as evident by the large defection and the propagation of a significant number of cracks before failure. Test results are given in detail in A.10.

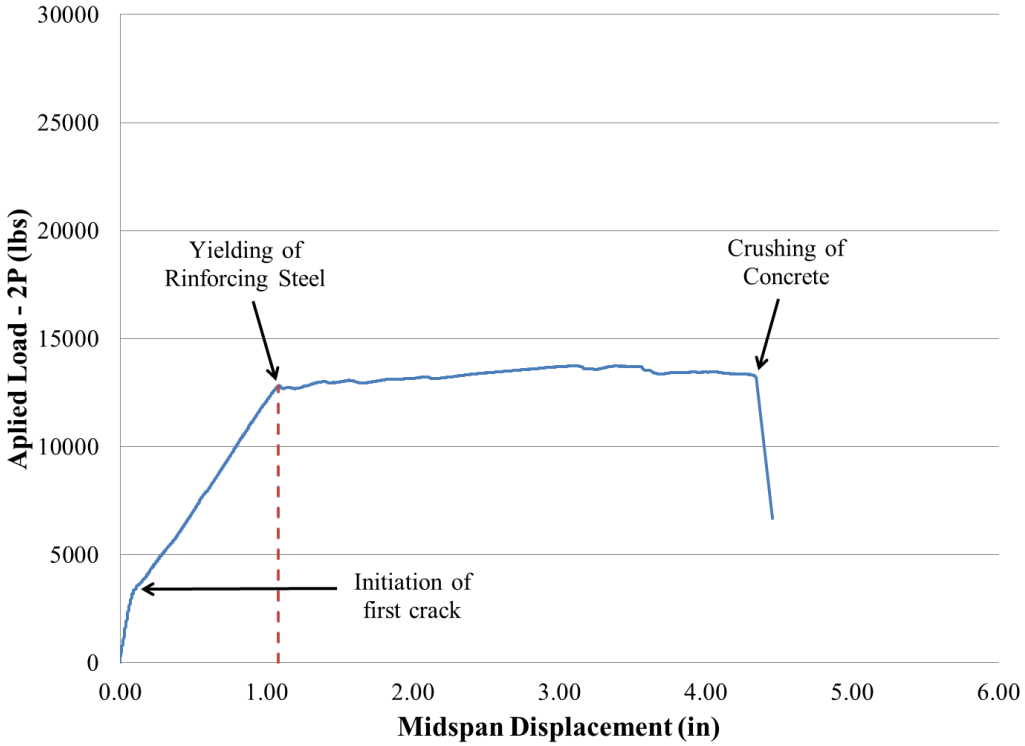

Figure 61 : Load-Deflection Behavior of Control Specimen

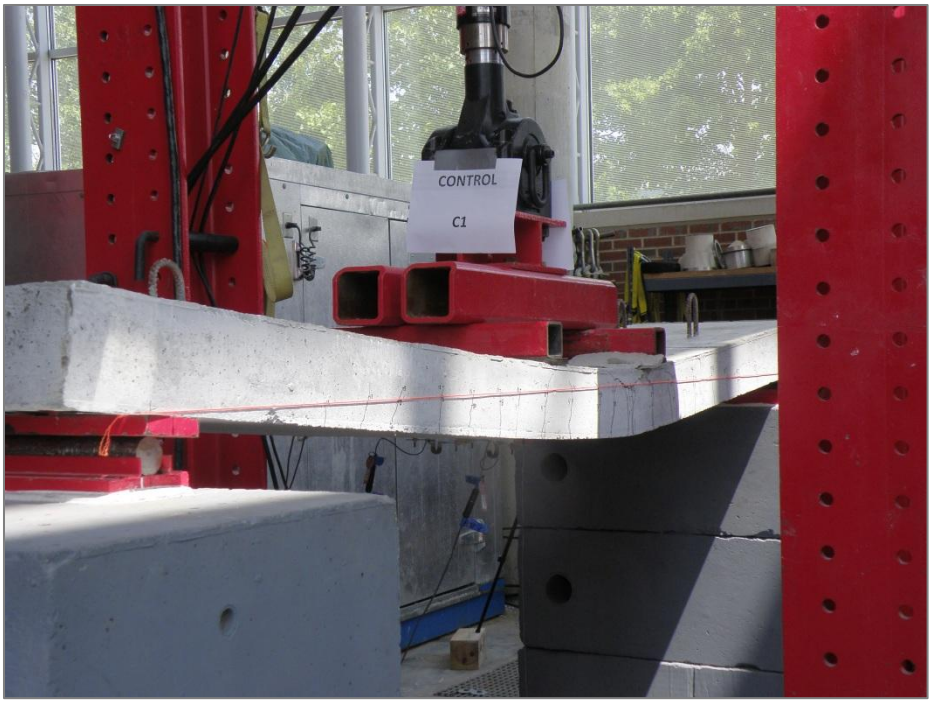

Figure 62: Deflected Shape of the Control Slab at Failure

Figure 63: Crack Pattern of Control Slab at Failure

4.2.3 Slabs Strengthened with High Modulus Carbon Strands

Three of the slabs were strengthened with the High Modulus Carbon Strand sheet system with spacing of 2.84 mm between the strands. These sheets of strands are designated by Type 3 as given in Table 10 in section 3.2. Two of the slabs were strengthened using the externally bonded technique and the third was strengthened using the near surface mounted technique. Test results indicate that all the strengthening systems increased the load required to initiate cracking and the ultimate load carrying capacity when compared to the control specimen as shown in Figure 64. Test results indicate that using high modulus carbon strands, as expected, increases the stiffness of the strengthened slab as shown in Figure 64. However, the measured strain indicates that the reinforcing steel did not yield before failure of the strengthening system as discussed in section A.11, A.12, and A.13.

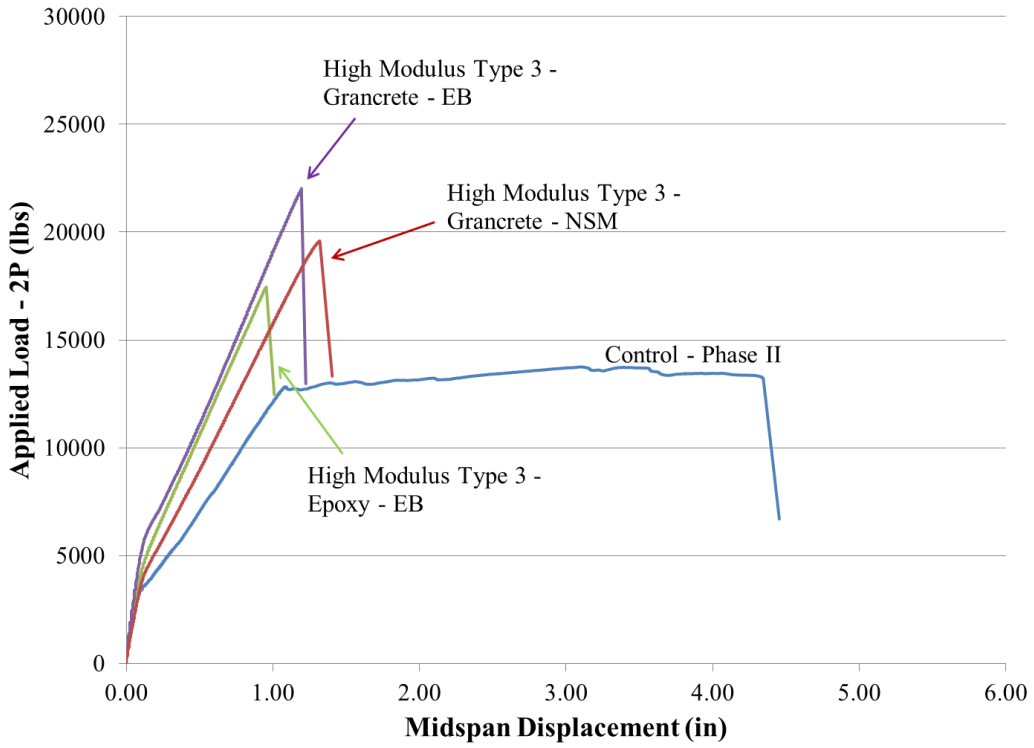

Figure 64: Load-Deflection Behavior of High Modulus Carbon Strand Specimens

The failure of the slabs strengthened with the High Modulus Carbon Strand – Type 3 was sudden and occurred within the region of maximum moment as shown in Figure 65. Failure of the strengthening system was due to rupture of the carbon fibers within the region of maximum moment. This was true of both the externally bonded systems and the near surface mounted system.

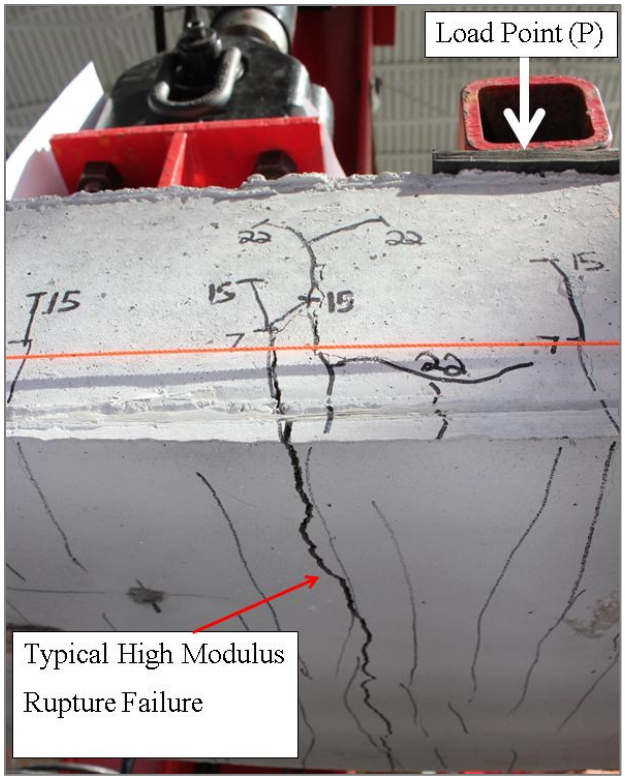

Figure 65 : Typical Failure of FORCA High Modulus Sheet

When comparing the two slabs that used the externally bonded technique, the strengthened slab that used the cementitious material achieved a higher ultimate load carrying capacity in comparison to the strengthened slab with epoxy adhesive shown in Figure 64. This behavior suggests that the cementitious material allows for the formation of uniform cracks which propagate through the strengthening system where as the epoxy allows for the formation of one major crack. The flexural cracks tend to form and widen in the maximum moment region. Increase in the number of flexural cracks in the maximum moment region leads to a more even distribution of the high strains in the FRP carbon strands. The formation of one

major crack for the epoxy adhesive causes a high strain concentration at the location of this crack and leads to earlier rupture of these fibers. Early rupture of fibers led to a lowered measured ultimate load carrying capacity as shown in Figure 64 in comparison to the cementitious material strengthening systems. Measurement of higher ultimate load carrying capacity of the cementitious material externally bonded system may also be due to possible slipping of the fibers at the two ends of the cracks due to the weaker bond strength of the cementitious material in comparison to epoxy, therefore reducing the strain concentration at the cracks. When comparing the slabs that used the cementitious material as the adhesive, the strengthened slab that used the externally bonded technique achieved a slightly higher load carrying capacity than the strengthened slab that used the near surface mounted technique as shown in Figure 64. When comparing the two slabs that were strengthened using Grancrete but used either the externally bonded technique or the near surface mounted technique, it is observed in Figure 64 that the externally bonded technique achieved a slightly greater ultimate load carrying capacity when compared to the near surface mounted technique. The results suggest that the externally bonded technique has a greater moment carrying capacity than the near surface mounted technique because the lever arm is longer for the externally bonded technique than the near surface mounted technique as shown in Figure 66. This greater moment capacity of the section corresponds to an increase in load carrying capacity.

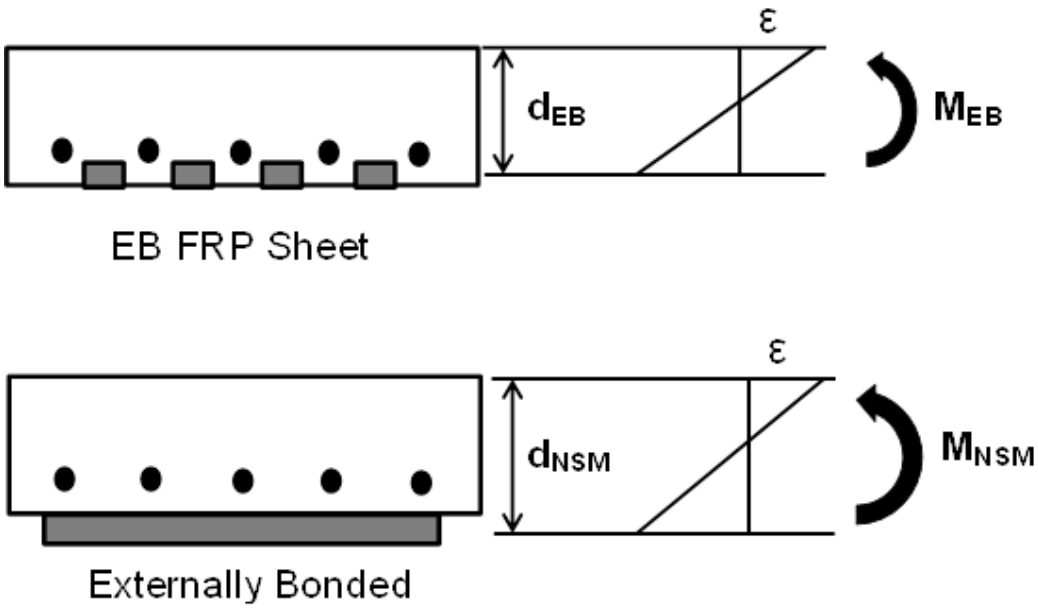

Figure 66: Lever arm distance for EB and NSM applications

Test results indicate that the slabs strengthened with the Carbon Strand Sheet – Type 3 failed also in a brittle nature. The results suggest that the reinforcement ratio used for strengthening the slab was large and did not allow yielding of the longitudinal bars, therefore, the failure was brittle. Use of the carbon strand strands significantly increased the load required to cause cracking of the slab as shown in Figure 64. Pull-off tests were performed on the specimens that were strengthened using the externally bonded technique and all results indicate that the bond strength of the system with the Type 3 carbon strands is more than the 200 psi required by ACI. Test results are given in detail in section A.11 and A.12. Test results suggest that the spacing between the strands was large enough to allow for full bonding of the sheet to the concrete substrata.

4.2.4 Slabs Strengthened with High Tensile Carbon Strand

Three of the slabs were strengthened with the High Tensile Carbon Strand sheet system with spacing of 3.28 mm between the strands. These sheets of strands are designated by Type 3 as given in Table 9 in section 3.2. Test results indicate that the High Tensile Carbon Strand strengthening system increased the load required to initiate cracking, yielding of the

reinforcement and the ultimate load when compared to the control specimen as shown in Figure 67. All the strengthened slabs achieved about the same ultimate load carrying capacity which is to be expected because the failure mode for all the strengthened beams was crushing of the concrete in the maximum compression zone. The strengthened system that used epoxy as the adhesive achieved the greatest increase in load carrying capacity because it formed the stiffest system while still failing due to crushing of concrete. Test results also indicate a slight loss in ductility for all tested slabs strengthened with the High Tensile Carbon Strands. Test results suggest that the reinforcement ratio used was large enough to increase the overall load carrying capacity.

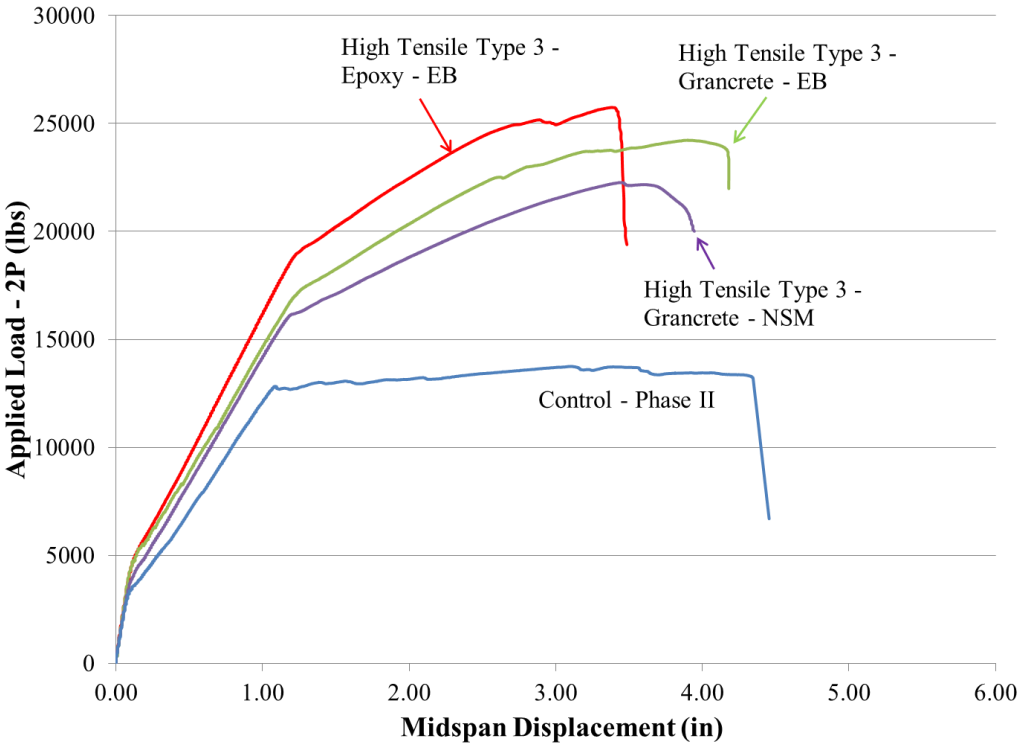

Figure 67: Load-Deflection Behavior of High Tensile Carbon Strand Specimens

The behavior of the strengthened slab under the load was characterized by significant cracking and propagation of these cracks as shown in Figure 68. This behavior was considered to be ductile. The typical crack pattern and crack propagation observed are

shown in Figure 68. Failure of all of the strengthening systems strengthened with the High Tensile – Type 3 Carbon Strand was due to crushing of the concrete as shown in Figure 68.

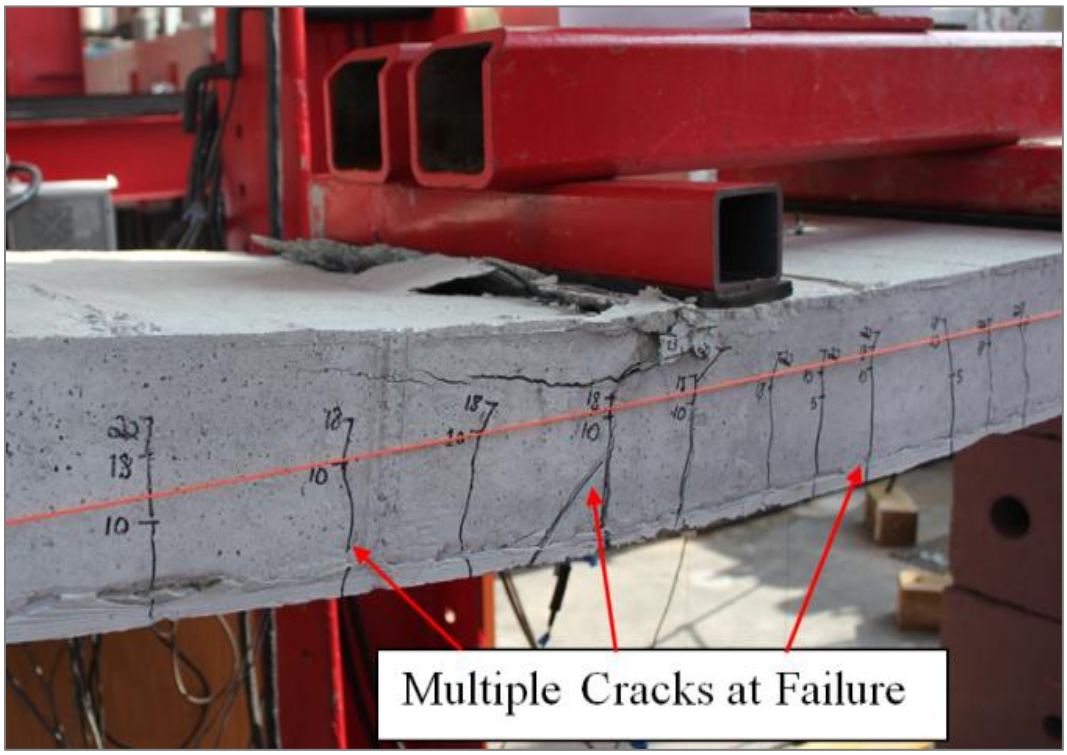

Figure 68: Typical Failure of High Tensile Sheet

Inspection of the test specimen after failure showed that the carbon strands did not rupture in the region of maximum moment. As expected, the slabs that were strengthened using the cementitious material achieved a higher ductility than the slab strengthened with epoxy. This is due to the formation of a greater number of flexural cracks that propagate through the cementitious material and the concrete thickness as shown in Figure 68. These flexural cracks dissipate the stresses on the fibers and move them away from the maximum moment region and towards the shear zone, allowing for a greater ductility. Also as expected the use of epoxy as the adhesive created a stiffer system than the slabs strengthened with the cementitious materials, which lead to a greater increase in the ultimate load carrying capacity as shown in Figure 68. When comparing the slabs that used the cementitious material as the adhesive, the strengthened slab that used the externally bonded technique achieved a slightly higher load carrying capacity than the strengthened slab that used the near surface mounted

technique. An explanation for this is that the externally bonded technique has a greater moment carrying capacity than the near surface mounted technique because the lever arm is longer for the externally bonded technique than the near surface mounted technique as shown in Figure 66. Pull-off test were performed on the slabs that were strengthened using the externally bonded technique and the results indicate that the bond strength for the Type 3 sheet was adequate to meet the ACI 440.2R-08 requirement of 200 psi. Test results are given in detail in A.14 and A.15. Test results show that the High Tensile Carbon Strand Sheet – Type 3 used with a cementitious bonding material and using either an externally bonded or near surface mounted application technique produces a very desirable strengthening system. It produces a strengthening system that increases the cracking, yield, and ultimate load carrying capacity. The failure is ductile, with the prominent failure mode due to crushing of concrete in the maximum compressive zone. The Type 3 spacing allows the cementitious material to penetrate between the strands and form a very strong bond between the fibers, adhesive, and concrete surface as shown in all of the pull off test that meet the ACI 440.2R-08 requirement of 200 psi.

4.2.5 Predictions

ACI 440.2R-08 was used to predict the ultimate load carrying capacity of the externally bonded FRP strengthened slabs. ACI 440.2R-08 recommends limiting the strain in the FRP to either the calculated debonding strain, ε_{fd}, or 90% of the published rupture strain, $0.9\varepsilon_{fu}$, whichever is less. ACI 440.2R-08 was also used to predict the ultimate load carrying capacity of the near surface mounted FRP strengthened slabs. ACI 440.2R-08 recommends limiting the strain in near surface mounted FRP by the calculated debonding strain, ε_{fd}. The debonding strain equation is found in section 2.2.2 and 2.3.3 and was used in a sectional analysis to predict the ultimate load carrying capacity of the externally bonded and near surface mounted FRP strengthened slabs. The predicted values for debonding and capacity design, along with the measured experimental values for each strengthened slab, are shown in Figure 69.

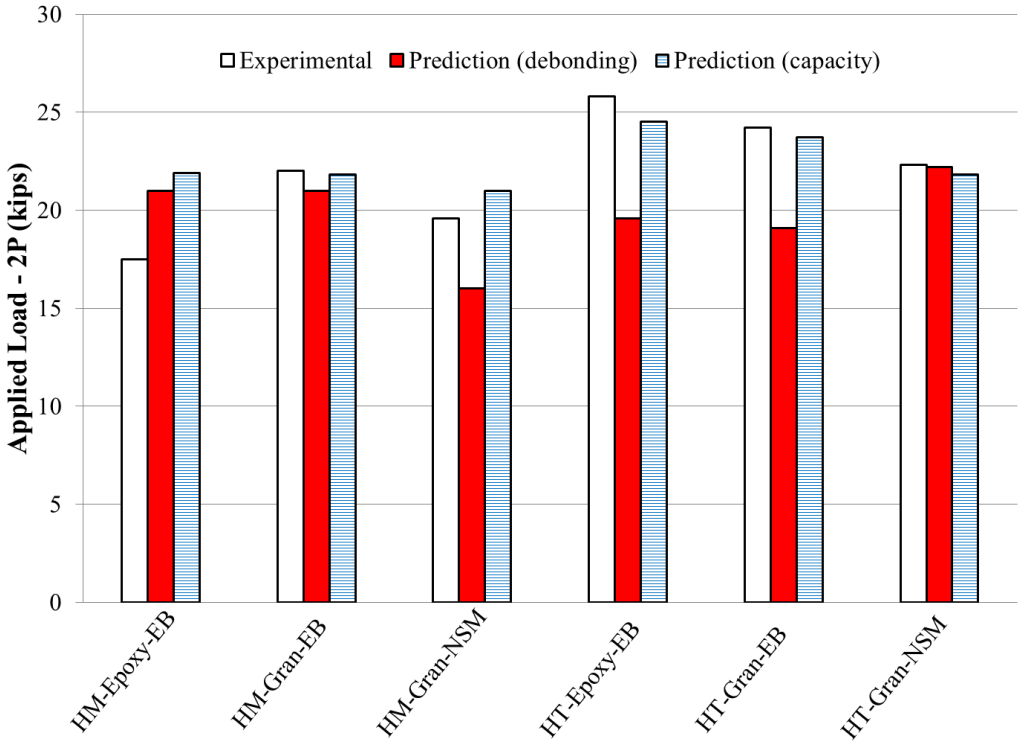

Figure 69: Phase II Predictions vs. Experimental Results

The slabs strengthened with the High Tensile Carbon Strands all failed due to crushing of the concrete in the region of maximum moment and the slabs strengthened with the High Modulus Carbon Strands all failed due to rupture of the fibers. Figure 69 shows that, in general, ACI 440.2R-08 does a fairly good job predicting the ultimate load carrying capacity when the failure is capacity controlled. Capacity controlled means that the slab failed either by concrete crushing at a compressive strain of 0.003 in/in or fiber rupture. This is to be expected if the material properties are known and used in prediction of the ultimate load carrying capacity.

4.2.6 Overall Evaluation of Phase II

All of the strengthened specimens were able to increase the load to initiate cracking of the concrete and the ultimate load carrying capacity when compared to the control specimen as shown in Figure 70. This was expected due to the high tensile strength and elastic modulus of the carbon strands.

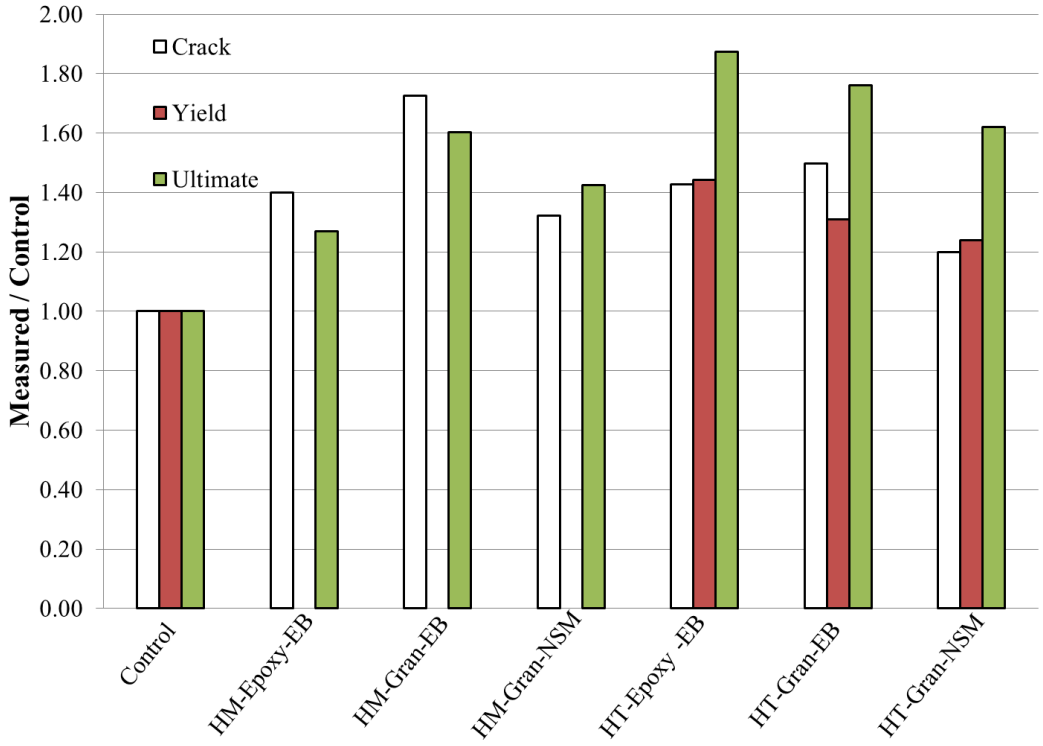

Figure 70: Load Stages of Phase II slabs

As expected, all of the strengthened specimens caused a decrease of the ductility of the specimen when compared to the control specimen as shown in Figure 71. The reduction in ductility by using the High Tensile Carbon Strand – Type 3 cannot be compared to the reduction in ductility when using the High Modulus Carbon Strand – Type 3 because the slabs that were strengthened using the High Modulus Carbon Strands failed in a brittle manner.

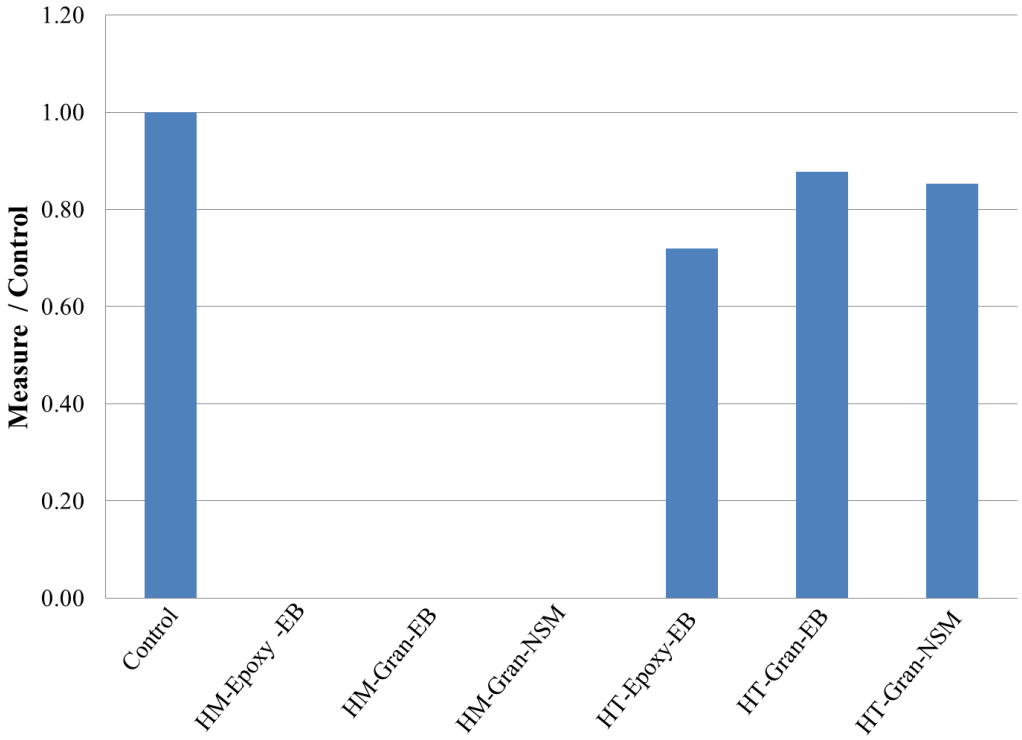

Figure 71: Ductility of Phase II Slabs

Test results of the second phase of the experimental program provided the knowledge to formulate conclusions regarding the High Tensile and High Modulus Carbon Strand Sheets. Findings of the second phase provided clear understanding of the effect of type of fiber, type of adhesive, fiber reinforcement ratio, and application technique. Discussion of each of these parameters is presented in the following sections.

4.2.6.1 Type of Fiber

Both the High Modulus and High Tensile Carbon Strands were explored in Phase II. The two criteria used to evaluate the flexure performance of the different types of fibers were the measured maximum load and the ductility at failure. A comparison of the load-deflection behavior is shown in Figure 72. The figure indicates that the High Tensile Carbon Strands strengthening system provided the greatest increase of the ultimate load carrying capacity in comparison to High Modulus Carbon Strand. The High Modulus Carbon Strand strengthening system increased the load to initiate cracking of the concrete more when

compared to the High Tensile Carbon Strand which was expected due to its high modulus when compared to the High Tensile Carbon Strand. Use of the High Tensile carbon strand provided some ductility before failure, whereas the High Modulus carbon strand did not because it failed in a brittle manner. It was therefore recommended that the High Tensile Carbon Strand be used in order to ensure an increase in load carrying capacity and some ductility at failure.

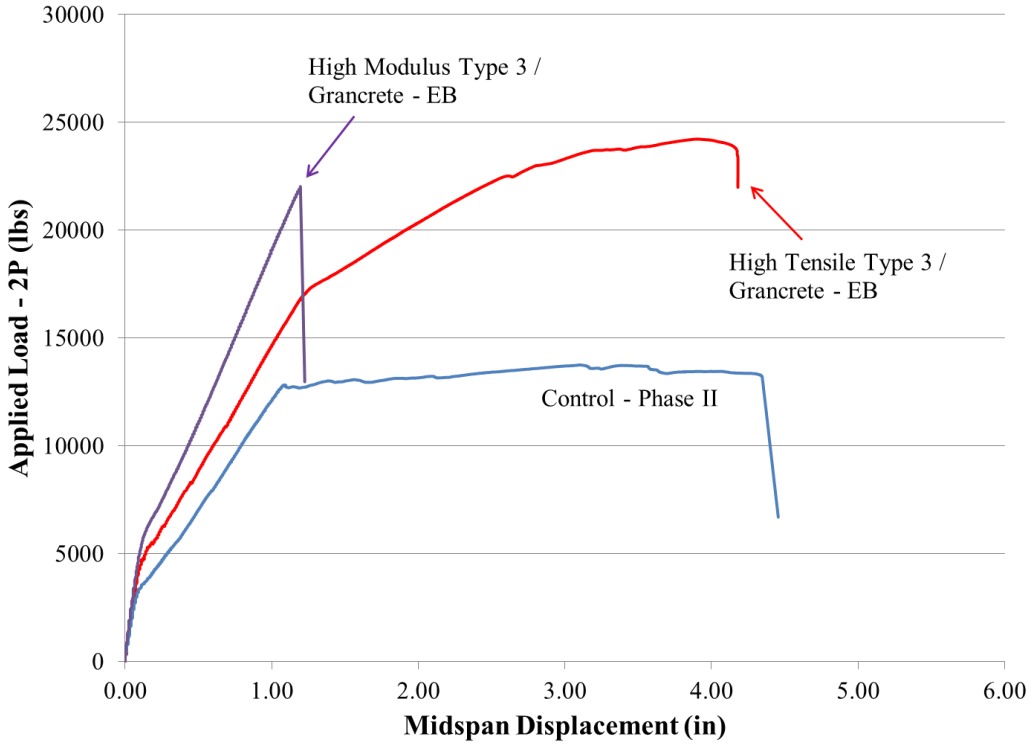

Figure 72: Specimens from Phase II comparing different types of fibers

4.2.6.2 Type of Adhesive

Two different adhesives were investigated in Phase II. They included Grancrete and a typical epoxy adhesive. Since the High Tensile carbon strand was used with all of the adhesives, the load-deflection behavior of the specimens that used the High Tensile carbon strand is shown in Figure 73. The figure indicates that Grancrete increased the ultimate load carrying capacity approximately as much as when the epoxy was used. However, test results indicate that the slabs that used Grancrete achieved a greater ductility that the slab

strengthened with the epoxy adhesive. This behavior was expected since the Grancrete is not as stiff as the epoxy which allowed a uniform distribution of cracks before failure. The epoxy does not allow for propagation of flexural cracks whereas the cementitious materials allow for flexural cracks to propagate. This propagation of flexural cracks leads to a reduction of the stiffness and increase in ductility in comparison to the epoxy. Another advantage of using Grancrete over the epoxy is the increase in fire resistance. In event of a high temperature situation, epoxy tends to soften and the bond between it and the concrete substrata weakens at temperatures around 200 °F. This could lead to failure due to deboning of the strengthening system. Grancrete can resist temperatures ups to 2,100 °F, which is much higher when compared to the epoxy system.

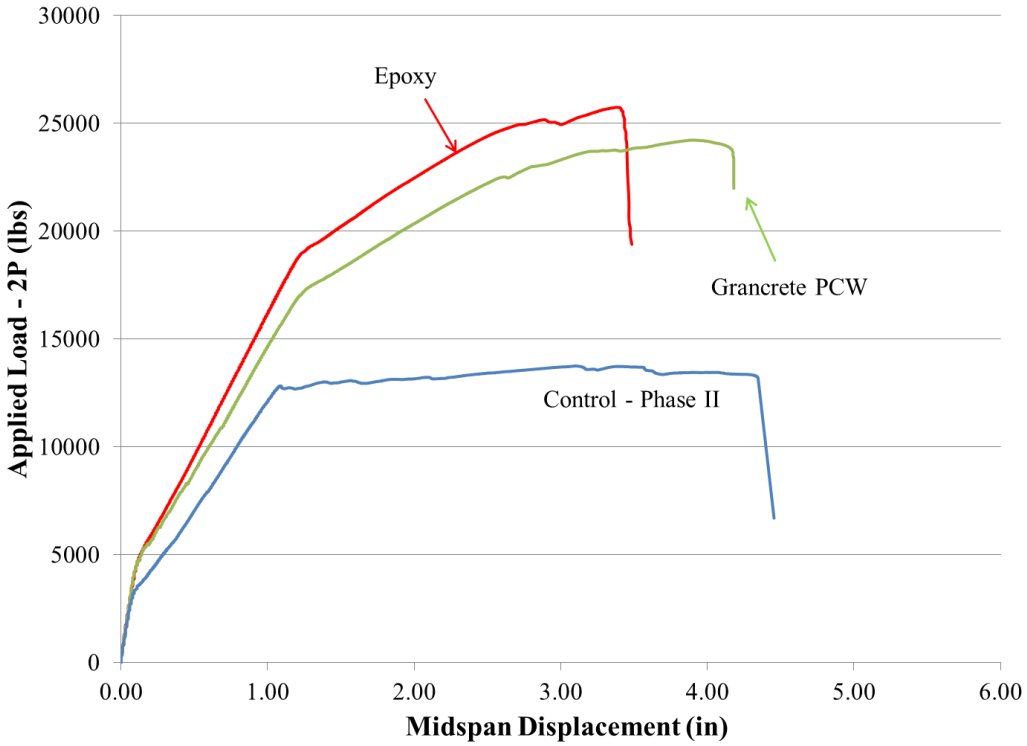

Figure 73: Specimens from Phase II comparing different adhesives

4.2.6.3 Fiber Reinforcement Ratio

The Type 3 Carbon Strand Sheet was explored in Phase II. The spacing between the fibers was considered as a possible parameter that affects the failure modes of the strengthened

systems. The fiber reinforcement ratio for all the strengthened slabs, as well as the percent increase in ultimate load carrying capacity is shown in Table 13. This table indicates that the optimum fiber reinforcement ratio is between 0.20% and 0.30%

Table 13: Effect of the Fiber Reinforcement Ratio on Load Carrying Capacity

Slab ID	Number of Longitudinal Fibers	Area of Fiber (in^2)	Fiber Reinforcement Ratio	Increase in Load (%)
Control	---	---	---	0
HT-E-E-3	154	0.00165	0.21	87
HT-G-E-3				76
HT-G-NSM-3				62
HM-E-E-3	178	0.00194	0.29	27
HM-G-E-3				60
HM-G-NSM-3				42

The spacing of fibers was also closely looked at during Phase II of the experimental program. The spacing between the fibers is very important because if the spacing between the fibers is not sufficient for the cementitious material to penetrate between the fibers and achieve the proper bond. Weak bond leads to a premature failure due to debonding of the strengthening system. The bond strength for each of the strengthened slabs was determined using a standard pull off test. Results of the pull off test of specimens that were strengthened with the externally bonded technique are shown in Figure 74. This figure indicates that the Type 3 spacing for both the High Tensile and High Modulus was large enough to allow for full penetration of the cementitious material. This is confirmed as the fibers for the near surface mounted and the externally bonded were exposed as shown in Figure 75 and Figure 76, respectively. It was therefore recommend that the Type 3 spacing be used for both the High Tensile and High Modulus Carbon Strand.

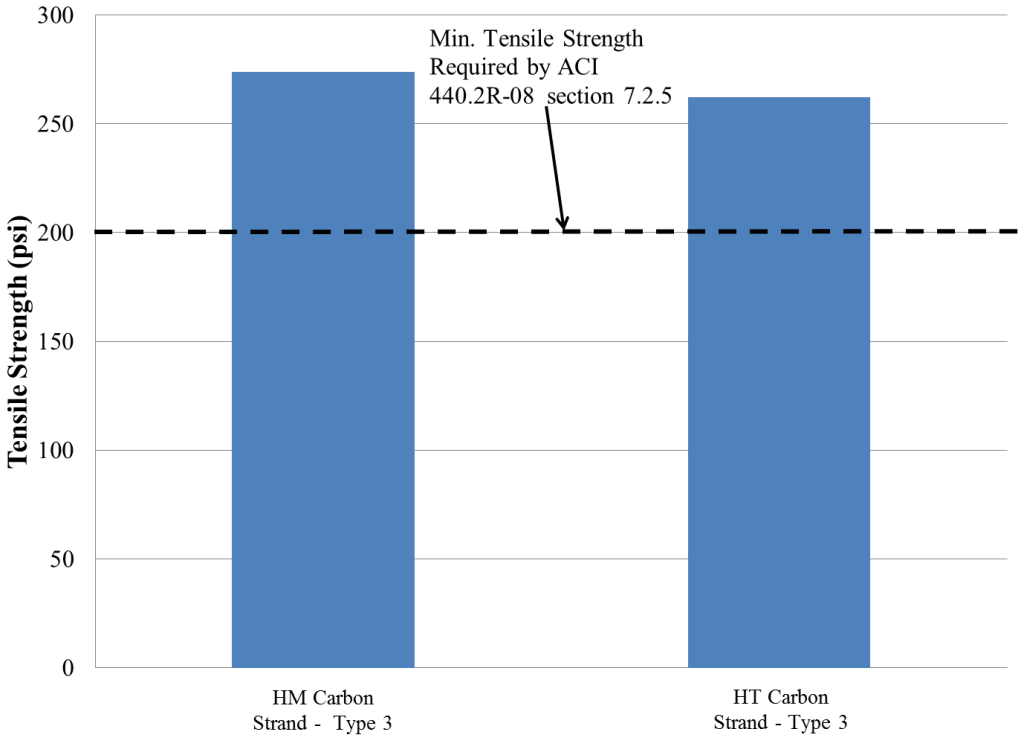

Figure 74: Effect on Spacing between Fibers on Bond Strength

Figure 75: Exposed NSM Carbon Strand Fibers

Figure 76: Exposed EB Carbon Strand Fibers

4.2.6.4 Application Technique

Two application techniques were used in Phase II of the experimental program, the externally bonded technique and the near surface mounted technique. It was observed that the externally bonded technique achieved a slightly greater load carrying capacity when compared to the near surface mounted technique as shown in Figure 77. This is because the lever arm is longer for the externally bonded technique than the near surface mounted technique. The figure also indicates that the ductility is approximately the same when comparing the externally bonded technique and the near surface mounted technique. When using the High Modulus Carbon Strand and Grancrete adhesive strengthening system, the same failure mode was observed for the externally bonded system and the near surface mounted system. The same behavior was observed for the High Tensile and Grancrete adhesive strengthening system. Therefore, no recommendations can be made on what type of application technique should be used.

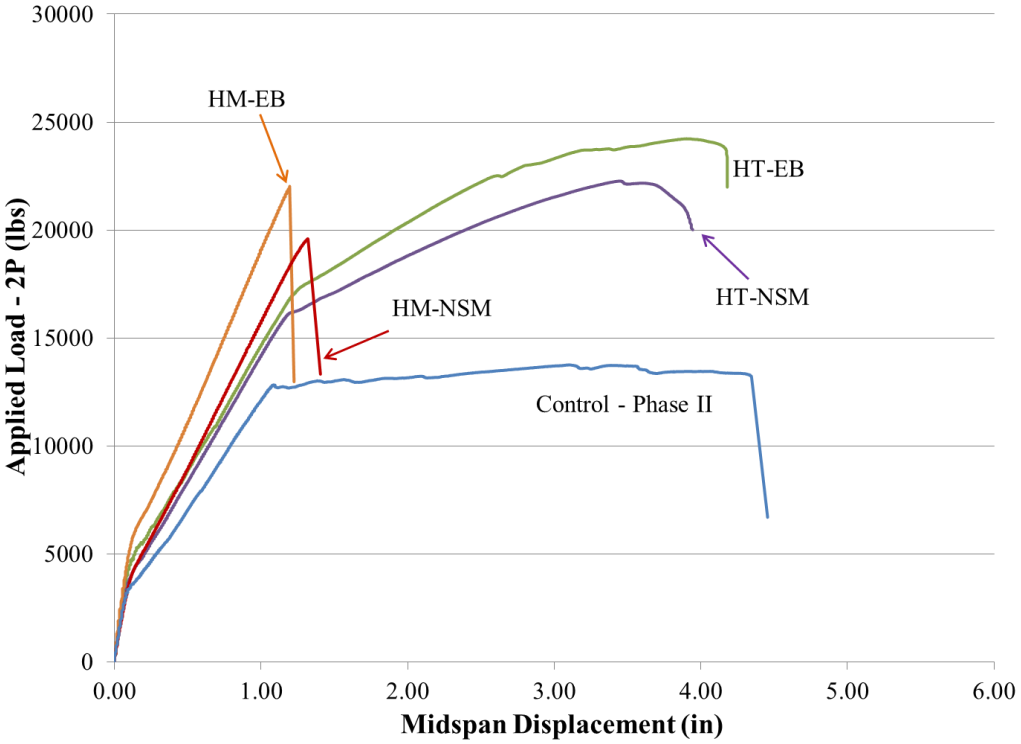

Figure 77: Specimens for Phase II Comparing Application Technique

CHAPTER 5 - SUMMARY AND CONCLUSIONS

This chapter summarizes and discusses the measured results and observed behavior of Phase I and II of the experimental program. The two criterion, increase in load carrying capacity and reduction in ductility will be discussed for each of these phases. Based on analysis of the test results a recommendation is provided regarding the four parameters considered in this study including the type of fiber, type of adhesive, fiber reinforcement ratio, and application technique. The needs for further research will also be presented, with several recommendations on the direction of the future research.

5.1 Summary of Phase I

The first phase of the experimental program includes testing of eight reinforced concrete slabs strengthened with various types of fibers and adhesives. The testing included also one unstrengthened reinforced concrete slab which was used as the control specimen to determine the effectiveness of the strengthening system. Four slabs were strengthened with a Carbon Grid, two slabs were strengthened with a Carbon Strand, and two slabs were strengthened using a Glass Grid. Three different adhesives were investigated, Grancrete, a cementitious material, with commercial name Tyfo C-Matrix, and an epoxy. All of the strengthened slabs with these FRP systems show an increase in the measured cracking load, yield load, and ultimate load carrying capacity when compared to the control specimen. In general, it was found that strengthening the slab with a FRP strengthening system increases the ultimate load carrying capacity and reduces the overall ductility. A summary of these results are given in Table 14.

Table 14: Test Results of Phase I

Specimen	Ultimate Load (lbs)	Load Increase (%)	Ductility	Reduction in Ductility (%)
Control	14,678	0	5.60	0
HT-G-E-1	21,461	46	BRITTLE	---
HM-G-E-1	21,386	46	BRITTLE	---
G-G-E-1in	14,849	1	2.10	63
G-G-E-0.25in	14,785	1	1.94	65
C-G-E	20,085	37	2.68	52
C-E-E	20,780	42	2.22	60
C-C-E-A	19,012	30	2.44	56
C-C-E-B	20,895	42	2.65	53

Test results indicate that using carbon fibers lead to a significant increase in the ultimate load carrying capacity ranging between 30% – 46%. However, the increase in the ultimate load carrying capacity was limited to less than 1% when using the glass grids. The behavior is highly dependent on the bond characteristics of the adhesive material used to bond the FRP grid to the concrete substrata. Test results suggest that this bond is highly dependent on the spacing of the grid or the spacing between the strands. It is observed that using small spacing between the strands did not allow enough penetration of the cementitious material between the strands and therefore reduces the bond strength. Reduction of the bond strength introduces a significant change of the mode of failure and could cause a shift from the typical IC failure mechanism to debonding and failure within the shear span for the carbon strands with small spacing. It was also observed that that all strengthened slabs experienced a decrease in ductility. Decrease of ductility is due to the reduction of the number and depth of cracks before failure in comparison to the unstrengthened slab. Use of the strengthening systems delayed the yielding of the reinforcement and therefore increases the load required for yielding. The increase of the ultimate load carrying capacity is highly dependent on the FRP reinforcement ratio and the bond characteristics of the adhesive materials. Figure 78 shows the load deflection behavior of all the tested specimens compared to the control specimen. As stated above, this figure clearly shows that small spacing between strands significantly reduces the bond strength between the fibers and concrete substrata and

therefore causes premature failure before yielding of the reinforcement. This figure also suggests that using carbon fibers significantly increases the load carrying capacity. When epoxy is used as the adhesive in the strengthening system, the bond strength is much higher and therefore does not allow initiation of many cracks in comparison to the cementitious materials, and therefore the failure is less ductile.

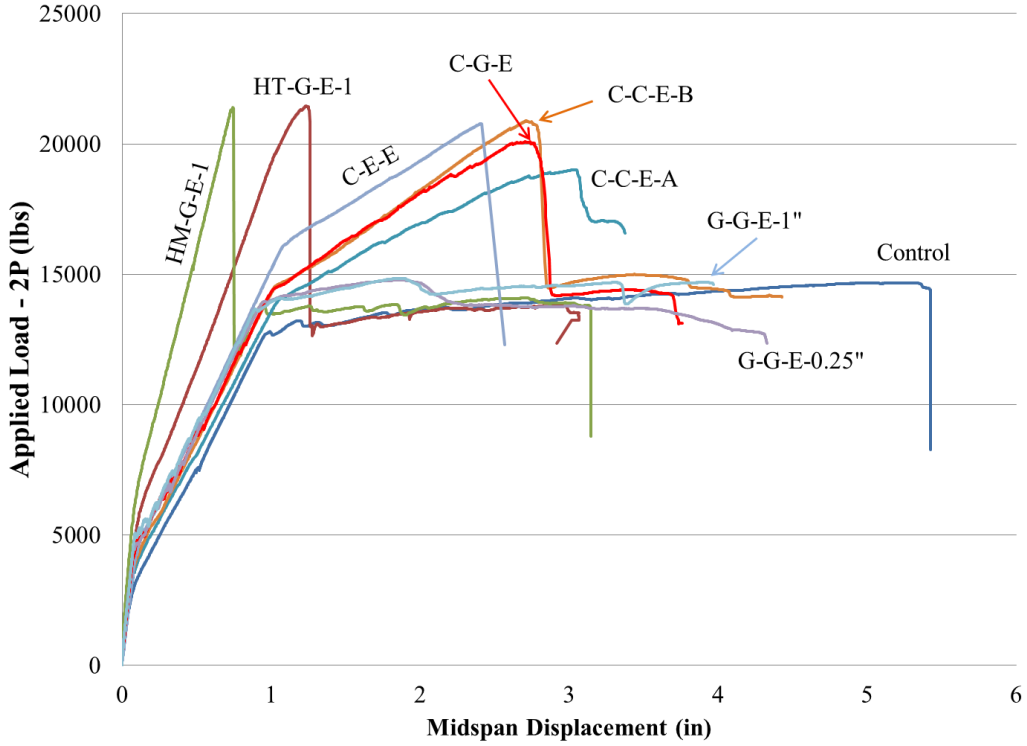

Figure 78 : Load-Deflection Behavior of all Tested Specimens in Phase I

5.2 Summary of Phase II

The second phase of the experimental program includes testing of six reinforced concrete slabs strengthened with various types of fibers and adhesives. The testing also included one unstrengthened reinforced concrete slab which was used as the control specimen to determine the effectiveness of the strengthening system to increase the load carrying capacity. Three slabs each were strengthened with a High Tensile and High Modulus Carbon Strand. Two different adhesives were investigated, Grancrete and an epoxy. All of the strengthened slabs with these FRP systems show an increase in the measured cracking load and ultimate load

carrying capacity when compared to the control specimen. In general, it was found that strengthening the slab with a FRP strengthening system increases the ultimate load carrying capacity and reduces the overall ductility. A summary of these results are given in Table 14.

Table 15: Test Results of Phase II

Specimen	Ultimate Load (lbs)	Load Increase (%)	Ductility	Reduction in Ductility (%)
Control	13,751	0	3.97	0
HM-E-E-3	17,457	27	BRITTLE	---
HM-G-E-3	22,026	60	BRITTLE	---
HM-G-N-3	19,589	42	BRITTLE	---
HT-E-E-3	25,749	87	2.86	-28
HT-G-E-3	24,226	76	3.48	-12
HT-G-N-3	22,268	62	3.39	-15

Test results indicate that using carbon fibers lead to a significant increase in the ultimate load carrying capacity ranging between 27% – 87%. The behavior is highly dependent on the bond characteristics of the adhesive material used to bond the FRP grid to the concrete sub-strata. Test results suggest that this bond is highly dependent on the spacing between the strands. It is observed that using larger spacing between the strands than used in Phase I allows enough penetration of the cementitious material between the strands and therefore increases the bond strength. Increase of the bond strength introduces a significant change of the mode of failure and could cause a shift from the typical IC failure mechanism to one where concrete crushing controls. It was also observed that all strengthened slabs experienced a decrease in ductility. Decrease of ductility is due to the reduction of the number and depth of cracks before failure in comparison to the unstrengthened slab. From Table 14, it can be seen that the loss in ductility is comparable for both the externally bonded technique and the near surface mounted technique. Use of the High Tensile strengthening systems delayed the yielding of the reinforcement and therefore increased the load required for yielding. The increase of the ultimate load carrying capacity is highly dependent on the FRP reinforcement ratio and the bond characteristics of the adhesive materials. Figure 79 shows the load deflection behavior of all the tested specimens compared to the control

specimen. This figure also suggests that using carbon fibers significantly increases the load carrying capacity. When epoxy is used as the adhesive in the strengthening system, the bond strength is much higher and therefore does not allow initiation of many cracks in comparison to the cementitious materials, and therefore the failure is less ductile as seen in Figure 79. This figure also shows that the behavior of the strengthening system is highly dependent on the type of fiber used. If the fiber has a very high elastic modulus, it usually means that the fiber also has a low rupture strain when compared to fibers that do not have such a high elastic modulus. This low rupture strain can be reached quickly in these stiff systems, causing a failure of the strengthening system due to fiber rupture.

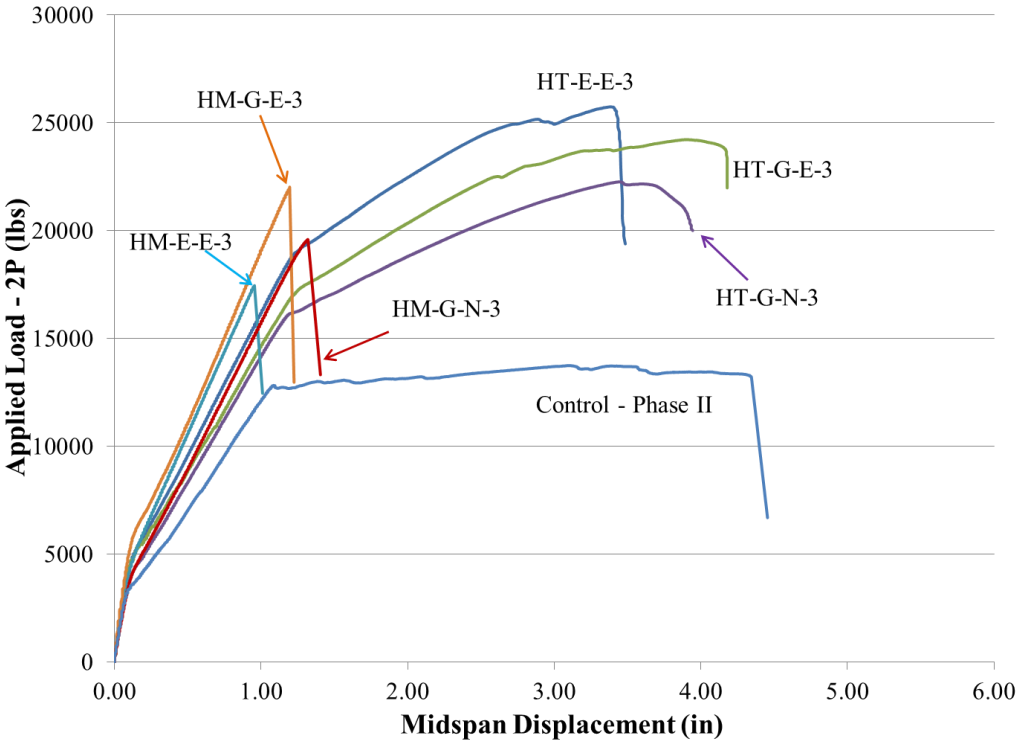

Figure 79 : Load-Deflection Behavior of all Tested Specimens in Phase II

5.3 General Conclusions

After completing both phases of the experimental program and investigating the acquired data, several conclusions have been made about the four parameters that were investigated in this experimental program. The four parameters were type of fiber used, type of adhesive

used, application technique used, and the fiber reinforcement ratio. The general conclusions that can be drawn in regards to these parameters are as follows.

5.3.1 Type of Fiber

A total of three different fibers were investigated, two different carbon strand, a carbon grid and two different glass grids. Test results obtained from Phase I and Phase II indicate that strengthening systems that use carbon fibers in the strengthening system provided the highest load carrying capacity. Use of the glass fibers barley increased the ultimate load carrying capacity, while the carbon fibers were able to increase the ultimate load carrying capacity between 27% – 87%. The elastic modulus must be considered as well. Low elastic modulus of the fibers did not allow for an increase ultimate load carrying capacity, where as a very high elastic modulus leads to a brittle failure of the strengthening system. Therefore, it was concluded that the High-Tensile Carbon Strand be recommended to be used in strengthening systems.

5.3.2 Type of Adhesive

A total of four different adhesives were investigated, two cementitious materials and two epoxies. From the results obtained from Phase I and Phase II, it has been concluded that strengthening systems that use a cementitious material, in particular Grancrete, allow for a more ductile system when compared to an epoxy strengthening system. Strengthening systems that use an epoxy adhesive form a very stiff system, which reduces ductility and leads to a brittle failure of the strengthening slab. Cementitious materials allow for flexural cracks to propagate and widen, leading to a relatively ductile system. When only the adhesive is the parameter, it was shown that a higher reduction in ductility in the range of 28% when epoxy was used in comparison to the cementitious material which varied from 12% to 15%. The Tyfo C-Matrix was not chosen due to concerns that the water/cement ratio may not be adequate to achieve the full bond characteristics of the material.

5.3.3 Application Technique

Two different application techniques were investigated. Test results indicate that the near surface mounted strengthening systems provided a comparable result to those that use the

externally bonded technique. Both the externally bonded technique and the near surface mounted technique have comparable increase in ultimate load carrying capacity and reduction of the ductility.

5.3.4 Fiber Reinforcement Ratio

From the results obtained from Phase I and Phase II, it has been concluded that strengthening systems that use a fiber reinforcement ratio between 0.20% and 0.30% provided the optimum increase in the load carrying capacity. There will be negligible increase in ultimate load carrying capacity if the fiber reinforcement ratio is greater than this. The spacing between fibers is also an important factor. If a grid is used with a cementitious material, the grid must be large enough to allow for the cementitious material to fully penetrate between the fibers of the grid. A grid with an opening greater than 0.25" square (6.35 mm square) is recommended. If a sheet of fibers is used, spacing between the fibers must be large enough for the cementitious material to fully encase the fibers. A spacing of at least 2.84 mm or larger is recommended.

5.4 Future Work

Based on the experimental data and conclusions drawn from this experimental program, the following topics are recommended for future research.

1. Additional testing be conducted on the optimal strengthening system that was chosen in this experimental program, the High Tensile Carbon Strand Sheet – Type 3 with Grancrete used as the adhesive and either the externally bonded or near surface mounted technique be used as the application technique.
2. Additional combinations of fibers and adhesives to be used with the near surface mounted technique so it can be more thoroughly compared with the externally bonded technique.
3. Study the effect of different environmental conditions has on the proposed strengthening system.
4. Determine what effect that time dependent factors, like creep and shrinkage, have on the strengthening systems.

5. Investigate how this strengthening system may be used to increase the shear strength of reinforced concrete structures.
6. Explore several additional fundamental characteristics of the strengthening system. These additional characteristics include bond length, number of layers, and different types of surface preparations.
7. Perform additional testing to establish enough data that would be statistically significant to designers.

REFERENCES

ACI Committee 440. *Guide for the Design and Construction of Externally Bonded FRP Systems for Strengthening Concrete Structures*. ACI 440.2R-08 Vol. Farmington Hills, MI: American Concrete Institute, 2008.

Alagusundaramoorthy, P., I. E. Harik, and C. C. Choo. "Flexural Behavior of R/C Beams Strengthened with Carbon Fiber Reinforced Polymer Sheets Or Fabric." *Journal of Composites for Construction* 7.4 (2003): 292-301.

Barros, J. A. O., S. J. E. Dias, and J. L. T. Lima. "Efficacy of CFRP-Based Techniques for the Flexural and Shear Strengthening of Concrete Beams." *Cement and Concrete Composites* 29.3 (2007): 203-17.

Ceroni, F. "Experimental Performances of RC Beams Strengthened with FRP Materials." *Construction and Building Materials* 24.9 (2010): 1547-59.

De Lorenzis, L., and J. G. Teng. "Near-Surface Mounted FRP Reinforcement: An Emerging Technique for Strengthening Structures." *Composites Part B: Engineering* 38.2 (2007): 119-43.

Faella, Ciro, Enzo Martinelli, and Emidio Nigro. "A Simplified Design Formula for Intermediate Debonding Failure in RC Beams Externally Strengthened by FRP". 3rd fib International Congress. 05/29/2010 - 06/02/2010, Washington D.C., United States.

Hassan, Tarek K., and Sami H. Rizkalla. "Bond Mechanism of Near-Surface-Mounted Fiber-Reinforced Polymer Bars for Flexural Strengthening of Concrete Structures." *ACI Structural Journal* 101.6 (2004): 830-9.

Kamel, Ayman S., Alaa E. Elwi, and Roger J. J. Cheng. "Experimental Study on the Behavior of Carbon Fiber Reinforced Polymer Sheets Bonded to Concrete." *Canadian Journal of Civil Engineering* 33.11 (2006): 1438-49.

Li, L. J., et al. "An Experimental and Numerical Study of the Effect of Thickness and Length of CFRP on Performance of Repaired Reinforced Concrete Beams." *Construction and Building Materials* 20.10 (2006): 901-9.

Mazzotti, C., and M. Savoia. "Experimental Tests on Intermediate Crack Debonding Failure in FRP - Strengthened RC Beams." Advances in Structural Engineering 12.5 (2009): 701-13.

Nguyen, Van Hien, et al. "Failure of Beams Retrofitted with Near Surface Mounted FRP Reinforcement: Experimental Work". 3rd fib International Congress. 05/29/2010 - 06/02/2010, Washington D.C., United States.

Nurbaiah, M. N., et al. "Flexural Behaviour of RC Beams Strengthened with Externally Bonded (EB) FRP Sheets Or Near Surface Mounted (NSM) FRP Rods Method". 2010 International Conference on Science and Social Research, CSSR 2010, December 5, 2010 - December 7. 2010,

Oehlers, D. J., and R. Seracino. Design of FRP and Steel Plated Structures. 1st ed. Elsevier Science, 2004.

Palmieri, Aniello, Stijn Matthys, and Luc Taerwe. "Strengthening with Near Surface Mounted Reinforcement: Structural and Fire Behavior". 3rd fib International Congress. 05/29/2010 - 06/02010, Washington D.C., United States.

Soliman, Shehab M., Ehab El-Salakawy, and Brahim Benmokrane. "Bond Performance of Near-Surface-Mounted FRP Bars." *Journal of Composites for Construction* 15.1 (2011): 103-11.

Spadea, G., R. N. Swamy, and F. Bencardino. "Strength and Ductility of RC Beams Repaired with Bonded CFRP Laminates." *Journal of Bridge Engineering* 6.5 (2001): 349-55.

Tann, D. B. "Determination of Ductility and Deformability Indices for FRP Strengthened RC Slabs." Proceedings of the international conference held at the University of Dundee, Scotland, UK (2005): 311-20.

Teng, J. G., et al. "Debonding Failures of RC Beams Strengthened with Near Surface Mounted CFRP Strips." *Journal of Composites for Construction* 10.2 (2006): 92-105.

APPENDICES

APPENDIX A

This appendix describes in detail the measured data and observed behavior of the slabs used to conduct Phase I and Phase II of the experimental program. Each specimen was given a unique strengthening ID, which is used to describe the type of fiber, type of adhesive, fiber reinforcement ratio and application technique used to strengthen the slabs. The IDs of the specimens, as well as the description of each, are shown in Table A-1 and Table A-2.

Table A-1: Phase I ID Descriptions

Phase I	
Specimen ID	*Description*
Control	Unstrengthened reinforced concrete slab
HM-G-E-1	Slab Strengthened with High Modulus Type 1 Carbon Strands and Grancrete Adhesive using the Externally Bonded technique
HT-G-E-1	Slab Strengthened with High Tensile Type 1 Carbon Strands and Grancrete Adhesive using the Externally Bonded technique
G-G-E-1”	Slab Strengthened with 1” Glass Fiber Grid and Grancrete Adhesive using the Externally Bonded technique
G-G-E-0.25”	Slab Strengthened with 0.25” Glass Fiber Grid and Grancrete Adhesive using the Externally Bonded technique
C-G-E	Slab Strengthened with Carbon Grid and Grancrete Adhesive using the Externally Bonded technique
C-C-E-A	Slab Strengthened with Carbon Grid and Cementitious Bonding Matrix (Tyfo C-Matrix) adhesive using the Externally Bonded technique
C-C-E-B	Slab Strengthened with Carbon Grid and Cementitious Bonding Matrix (Tyfo C-Matrix) adhesive using the Externally Bonded technique
C-E-E	Slab Strengthened with Carbon Grid and Epoxy adhesive using the Externally Bonded technique

Table A-2: Phase II ID Descriptions

Phase II	
Specimen ID	*Description*
Control	Unstrengthened reinforced concrete slab
HM-E-E-3	Slab Strengthened with High Modulus Type 3 Carbon Strands and Epoxy using the Externally Bonded technique
HM-G-E-3	Slab Strengthened with High Modulus Type 3 Carbon Strands and Grancrete Adhesive using the Externally Bonded technique
HM-G-N-3	Slab Strengthened with High Modulus Type 3 Carbon Strands and Grancrete Adhesive using the Near Surface Mounted technique
HT-E-E-3	Slab Strengthened with High Tensile Type 3 Carbon Strands and Epoxy using the Externally Bonded technique
HT-G-E-3	Slab Strengthened with High Tensile Type 3 Carbon Strands and Grancrete Adhesive using the Externally Bonded technique
HT-G-N-3	Slab Strengthened with High Tensile Type 3 Carbon Strands and Grancrete Adhesive using the Near Surface Mounted technique

A.1 Control – Phase I

The unstrengthened control specimen tested in Phase I was used as a benchmark to measure the effectiveness of the various FRP strengthened slabs explored in Phase I. The control specimen, as well as the strengthened slabs, was subjected to a four-point bending test as shown in Figure A-1.

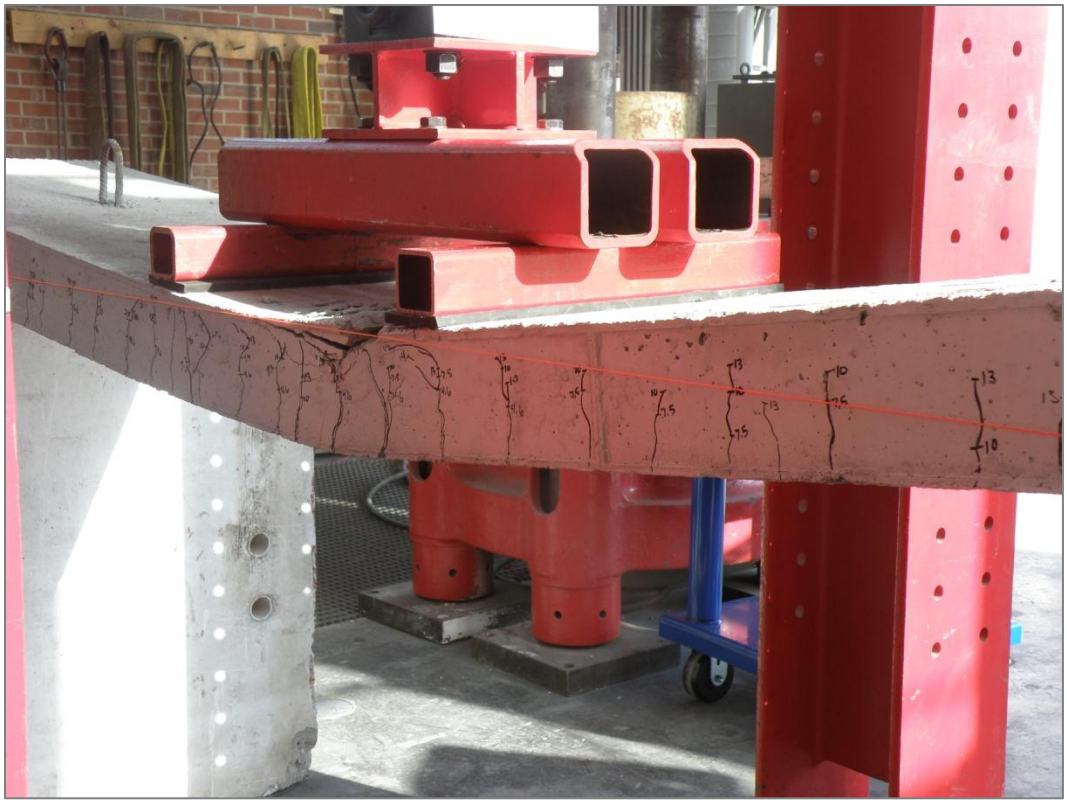

Figure A-1: Control Specimen – Phase I under four-point bending

A.1.1 Load Displacement

The Load-Displacement behavior of the control slab is shown in Figure A-2. Failure of the slab was due to crushing of the concrete in the maximum moment zone. The measured maximum load carrying capacity was 14,678 lbs and the maximum mid-span deflection was 5.51 inches. The behavior consists of three distinct linear behaviors as shown in Figure A-2. Initially a linear behavior up to the initiation of the first crack is observed. This is followed by a semi-nonlinear behavior up to yielding of the steel reinforcement. This is followed by significant reduction of the stiffness up the failure due to crushing of the concrete in the

compression zone. The measured load of the control specimen at first crack was 3000 lbs, the load at yielding was 12,767 lbs, and the slab failed at a load of 14,678 lbs. The ductility of the control specimen based on comparing the deflection at failure to the deflection at yielding of the reinforcement was 5.60.

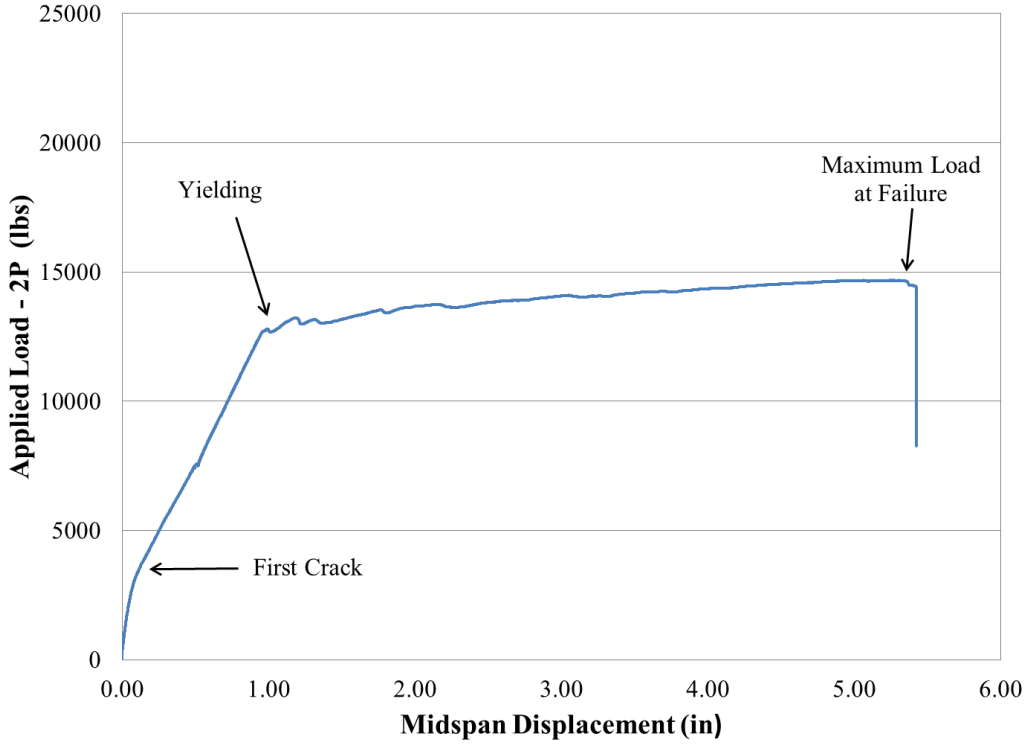

Figure A-2: Load-Deflection Behavior of Control Specimen – Phase I

A.1.2 Load Strain

The measured Load-Strain relationship of the top surface and bottom surface of the concrete for the control slab is shown in Figure A-3. The measured concrete strain represents the average strain within the gauge length of the pi gauges. Test results indicate that the maximum measured concrete strain in compression was 0.0067. The figure indicates also that all the reinforcement is yielded before failure.

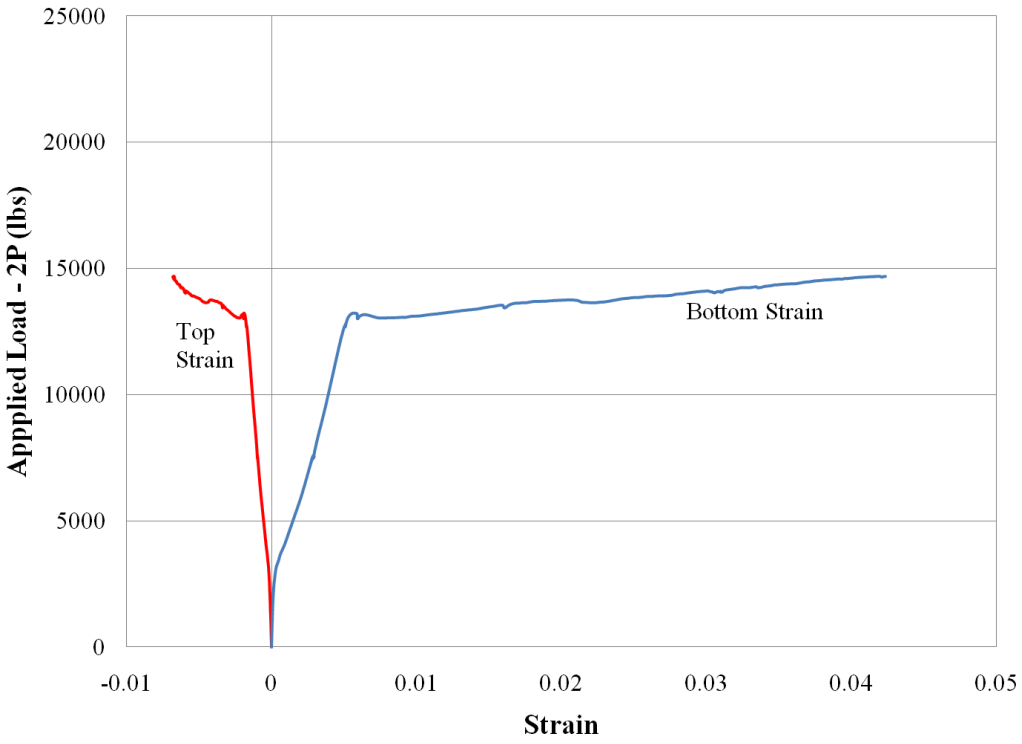

Figure A-3: Strain Measurement of Concrete for Control Specimen – Phase

A.2 HM-G-E-1 Specimen

This slab was strengthened with an externally bonded High Modulus Carbon Strand Sheet – Type I, commercially referred to as FORCA Carbon Strands, and bonded with Grancrete PCW. This specimen was subject to a four-point bending test as shown in Figure A-4.

Figure A-4: HM-G-E-1 specimen under four-point bending

A.2.1 Load Displacement

The measured Load-Displacement behavior of the strengthened slab is shown in Figure A-5. This behavior shows a sudden drop in load due to failure of the strengthened system due to debonding of the strengthening system. The measured maximum load carrying capacity was 21,286 lbs, compared to a measured value of 14,678 for the control slab. Deflection at mid-span was 0.75 inches at failure of the strengthening system and 3.23 inches at failure due to crushing of the concrete. This behavior suggests that failure of the strengthening system occurred before yielding of the steel reinforcement of the slab. This was evident by continuous increase of the load carrying capacity before ultimate failure due to crushing of

the concrete in the maximum compression zone after the strengthening system had failed. Since failure of the strengthened system occurred before yielding of the steel bars, the ductility was less than unity and the failure was brittle and sudden. This was due to the use of a high FRP reinforcement ratio, small spacing between carbon strands, and the high elastic modulus, characteristic of the Carbon FRP Strands. The measured cracking load was 6,230 lbs in comparison to 3000 lbs measured for the control slab.

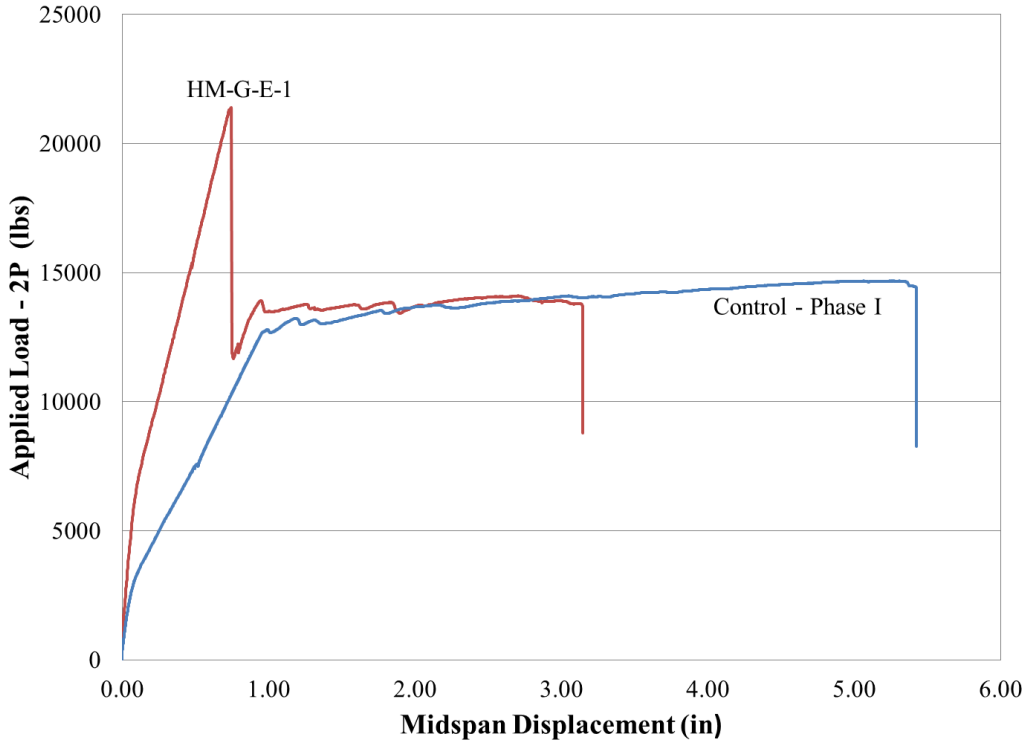

Figure A-5: Load- Deflection Behavior of HM-G-E-1 specimen

A.2.2 Load Strain

The measured Load-Strain of the top concrete surface of the slab and the bottom surface of the FRP strengthening system is shown in Figure A-6. The measured concrete strain represents the average strain within the gauge length of the pi gauges. Test results indicate that the maximum measured concrete strain in compression was 0.0096. The figure also indicates that the steel reinforcement had not completely yielded before failure. Test results indicate that this slab did not reach the full potential of the high modulus carbon strands since

the failure was due to debonding of the fiber within the shear span without utilizing the full rupture strength of the fiber.

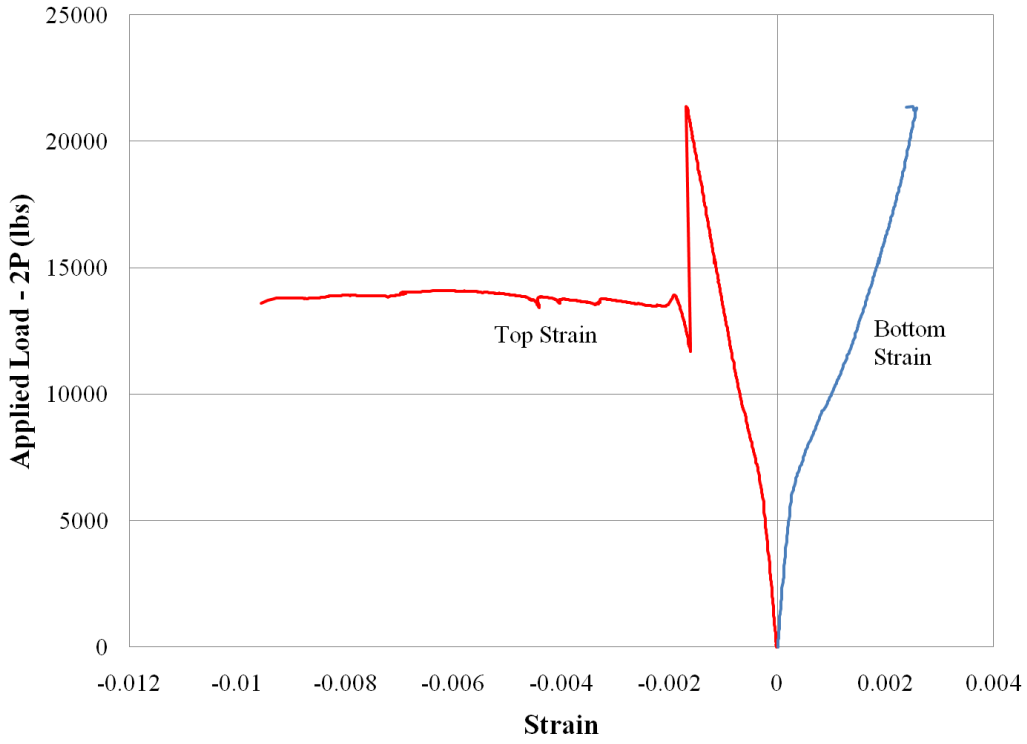

Figure A-6: Strain Measurement for HM-G-E-1 specimen

A.2.3 Inspection of Failure

Failure of the strengthening system was sudden and occurred within the shear span of the slab. The shear span is defined as the length of the slab between the support and the points of load application. Failure of the strengthening system was due to debonding of the sheet within the shear span of the slab. This failure is shown in Figure A-7. Once failure of the strengthening system occurred, the specimen followed the same behavior of the control specimen until overall failure due to crushing of concrete, as shown in Figure A-5. Inspection of the test specimen after failure showed that the FORCA carbon strand sheet had debonded from the slab along most of the span length. It was also observed that very little adhesive penetrated the FORCA carbon strands to the concrete sub-strata. Penetration of the

adhesive through the carbon strands to the sub-strata is needed so that a strong bond can be achieved.

Figure A-7: Debonding within the shear span of the FORCA Carbon Sheet – Type I

A.2.4 Pull Offs

Pull-off tests were conducted in areas of the slab that were away from the region of maximum moment and therefore considered undisturbed by the test to evaluate the tensile strength of the strengthening system. Results of the four pull-off tests performed on the specimen are presented in Figure A-8. The figure indicates that none of the four pull-off tests performed satisfied the ACI requirement for a desirable bond strength of 200 psi. All four of the pull-off tests failed in the bond layer between the Grancrete PCW paste and the fibers, indicating a weak bond was formed at this bond layer. The results indicate that the Type 1 spacing of the FORCA carbon strand sheet is too small to allow penetration of the Grancrete PCW between the stands and the concrete sub-strata and therefore did not provide the required bond characteristics for the strengthened system.

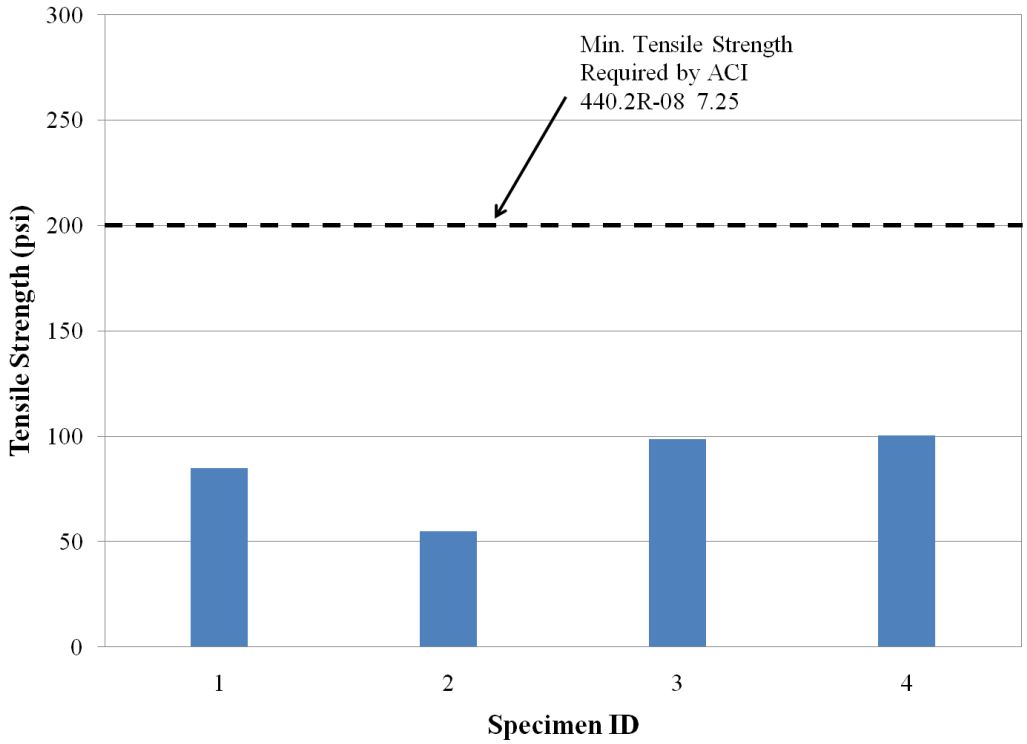

Figure A-8: Pull-Off Test Results for HM-G-E-1 specimen

A.2.5 Summary of Test Results

It was observed that the load carrying capacity was increased by 37% when compared to the unstrengthened control specimen. There was no measured ductility due to the sudden and brittle failure of the strengthening system before yielding of the reinforcement. The failure occurred due to debonding of the FRP Sheet within the shear span caused by the small spacing between the fibers not allowing for penetration of the Grancrete PCW through the fibers to concrete sub-strata. Since the bond strength did not meet the tensile bond strength required by ACI due to this small spacing, it is recommended that larger spacing between carbon strands be used in future testing.

A.3 HT-G-E-1 Specimen

This slab was strengthened with an externally bonded High Tensile Carbon Strand Sheet – Type I, commercially referred to as FORCA Carbon Strands, and was bonded with Grancrete PCW. This specimen was subject to a four-point bending test and is shown in Figure A-9.

Figure A-9: HT-G-E-1 specimen under four-point bending

A.3.1 Load Displacement

The measured Load-Displacement behavior of the strengthened slab is shown in Figure A-10. This behavior shows a sudden drop in load once the FORCA carbon sheet had debonded. The maximum load carrying capacity was 21,461 lbs, compared to a measured value of 14,678 for the control slab. Deflection at mid-span was 1.23 inches at failure of the strengthening system and 3.07 inches at failure due to crushing of the concrete. This behavior suggests that failure of the strengthening system occurred before yielding of the steel reinforcement of the slab. This was evident by continuous increase of the load carrying capacity before ultimate failure due to crushing of the concrete in the maximum compression

zone after the strengthening system had failed. Since failure of the strengthened system occurred before yielding of the steel bars, the ductility was less than unity and the failure was brittle and sudden. This was due to the use of a high FRP reinforcement ratio, small spacing between carbon strands, and the high tensile FRP. The cracking load was 5,145 lbs in comparison to 3000 lbs measured for the control slab.

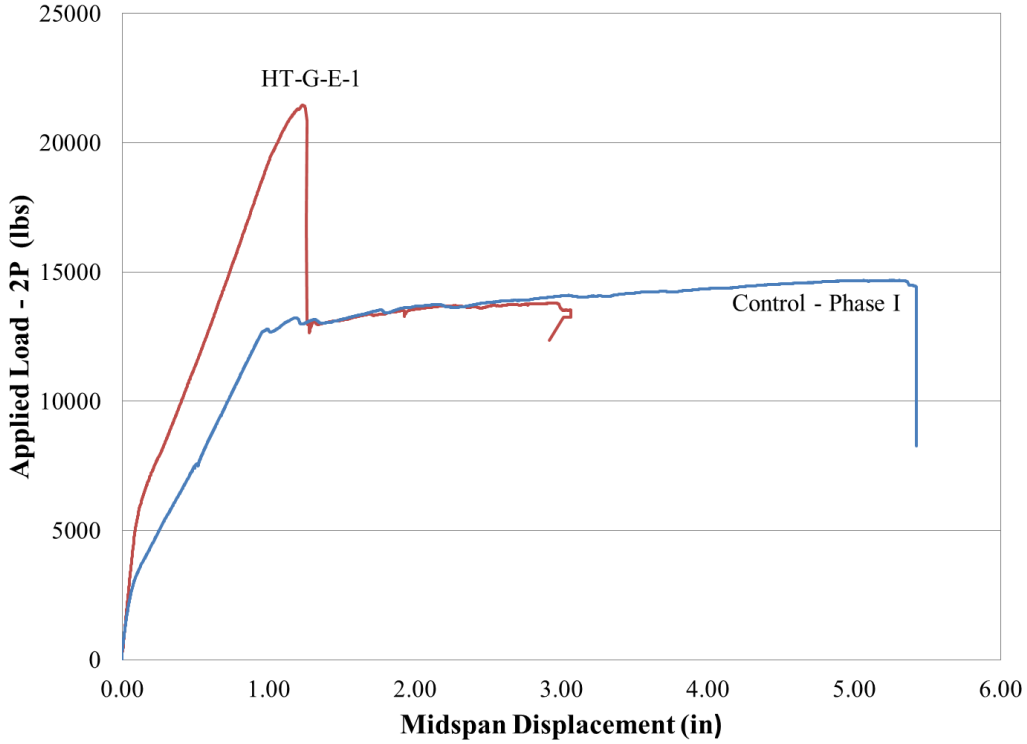

Figure A-10: Load- Deflection Behavior of HT-G-E-1 specimen

A.3.2 Load Strain

The measured Load-Strain of the top concrete surface of the slab and the bottom surface of the FRP strengthening system is shown in Figure A-11. Test results indicate that the maximum measured concrete strain in compression was 0.0088. The figure also indicates that the steel reinforcement had not completely yielded before failure. Test results indicate that this slab did not reach the full potential of the high tensile carbon strands since the failure was due to debonding of the fiber within the shear span without utilizing the full rupture strength of the fiber.

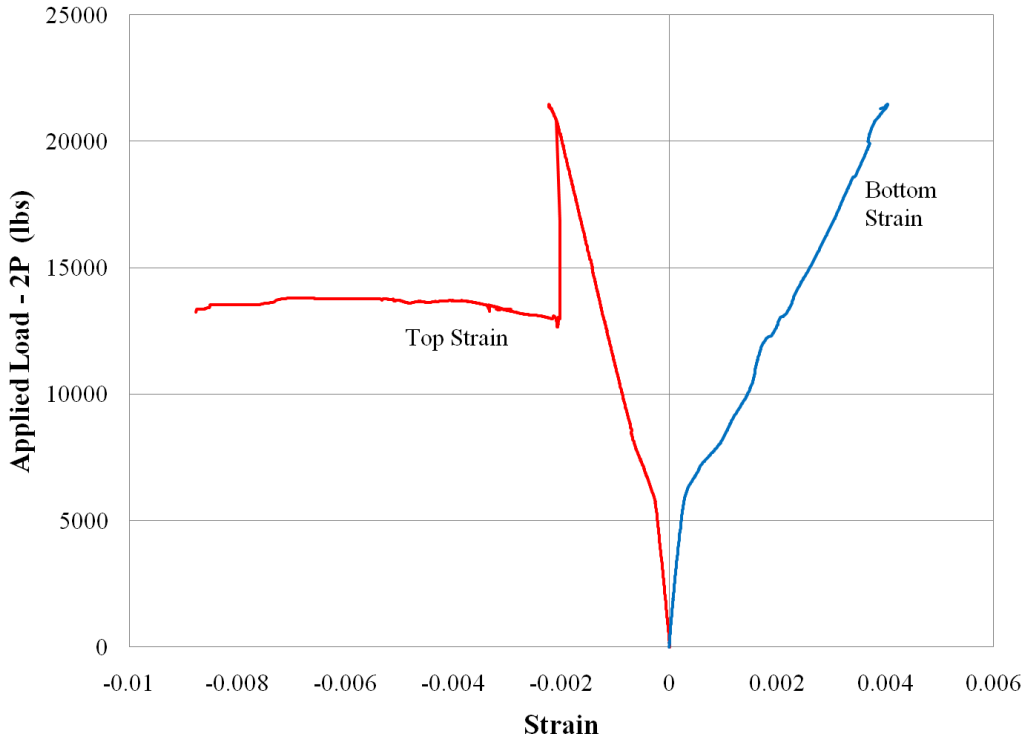

Figure A-11: Strain Measurement for HT-G-E-1 specimen

A.3.3 Inspection of Failure

Failure of the strengthening system was sudden and occurred within the shear span of the slab. Failure of the strengthening system was due to debonding of the sheet within the shear span of the slab. This failure is shown in Figure A-12. Once failure of the strengthening system occurred, the specimen followed the same behavior of the control specimen overall until failure due to crushing of concrete, as shown in Figure A-10. Inspection of the test specimen after failure showed that the FORCA carbon strand sheet had debonded from the slab along most of the span length. It was also observed that very little adhesive penetrated through the FORCA carbon strands causing a weak bond to form below and above the strands. Penetration of the adhesive through the carbon strands to the sub-strata is needed so that a strong bond can be achieved.

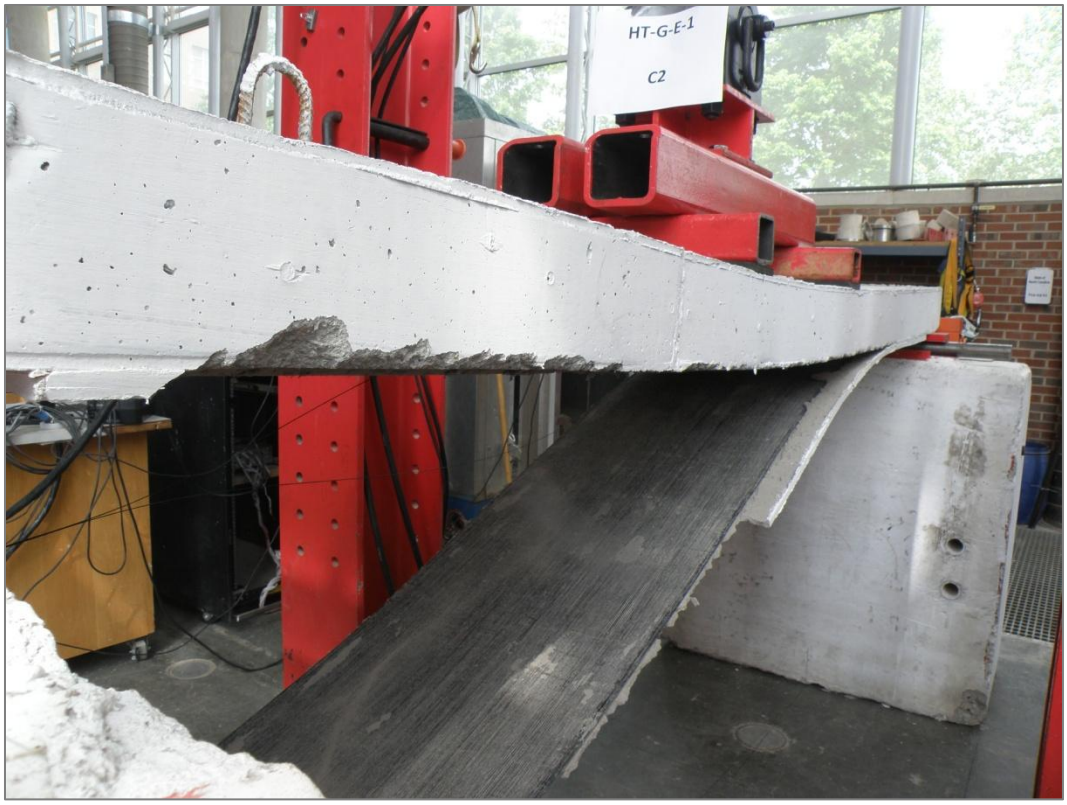

Figure A-12: Debonding within the shear span of the FORCA Carbon Sheet – Type I

A.3.4 Pull Offs

Results of the four pull-off tests performed on the specimen are presented Figure A-13. The figure indicates that none of the four pull-off tests performed satisfied the ACI requirement for a desirable bond strength of 200 psi. All four of the pull-off tests failed in the bond layer between the Grancrete PCW paste and the fibers, indicating a weak bond was formed at this bond layer. The results indicate that the Type 1 spacing of the FORCA carbon strand sheet is too small to allow penetration of the Grancrete PCW between the stands to the concrete sub-strata and therefore did not provide the required bond characteristics for strengthened system.

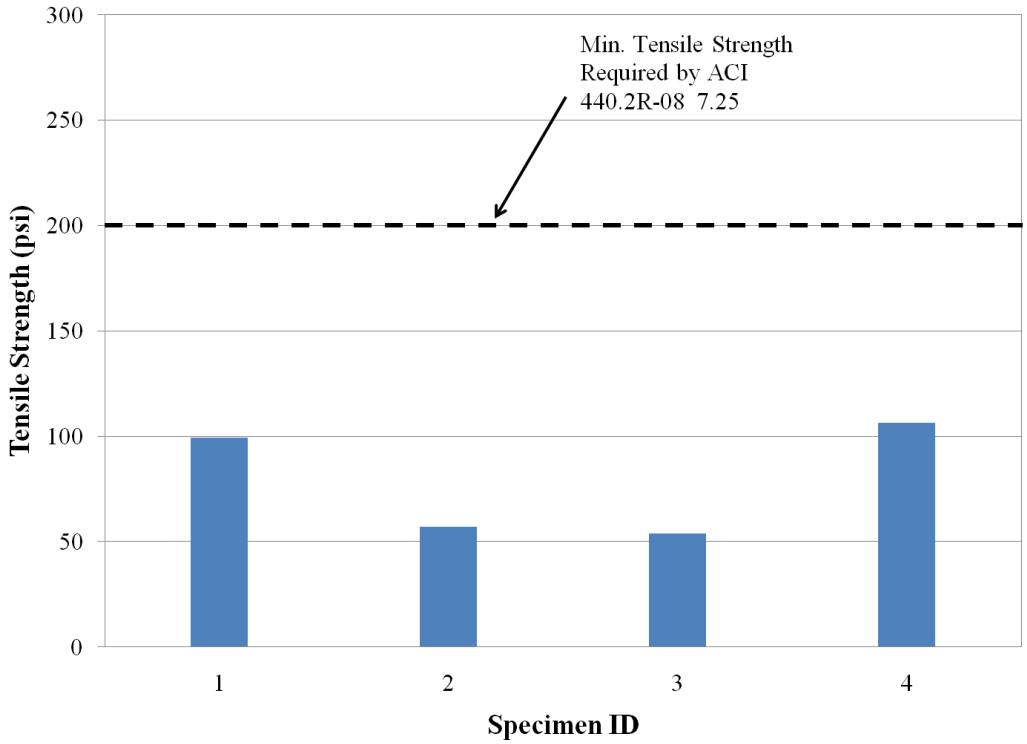

Figure A-13: Pull-Off Test Results for HT-G-E-1 specimen

A.3.5 Summary of Test Results

It was observed that the system increased the load carrying capacity by 38% in comparison to the unstrengthened control specimen. There was no measured ductility due to the sudden and brittle failure of the strengthening system before yielding of the reinforcement. The failure occurred due to debonding of the sheet within the shear span and was caused by the small spacing between the fibers not allowing for penetration of the Grancrete PCW through the fibers to the concrete sub-strata. Since the bond strength did not meet the tensile bond strength required by ACI due to this small spacing, it is recommended that larger spacing between carbon strands be used in future testing.

A.4 G-G-E-1” Specimen

This slab was strengthened with an externally bonded glass fiber grid with a 1” grid spacing, provided by PPG Company, and was bonded with Grancrete PCW. This specimen was subject to a four-point bending test and is shown in Figure A-14.

Figure A-14: G-G-E-1” specimen under four-point bending

A.4.1 Load Displacement

The measured Load-Displacement behavior of the strengthened slab is shown in Figure A-15. From this figure it can be seen that the maximum load carrying capacity was 14,849 lbs, compared to a measured value of 14,678 for the control slab. Deflection at mid-span was 1.87 inches at failure of the strengthening system and 4.13 inches at failure of the slab due to crushing of the concrete. The behavior consists of four distinct linear behaviors as shown in Figure A-15. Initially a linear behavior up to the initiation of the first crack is observed. This is followed by a semi-nonlinear behavior up to yielding of the steel reinforcement. After yielding there was significant reduction in stiffness up to failure of the strengthening

system due to rupture and debonding of the strengthening system accompanied by a sudden drop in load and finally overall failure due to crushing of the concrete in the maximum compression zone. The cracking load and yielding load of the strengthened specimen was 5,076 lbs and 13,652 lbs, compared to 3,000 lbs and 12,767 lbs for the control slab, respectively. The ductility of the strengthened specimen was 2.10 and was determined by comparing the deflections at failure to the deflection at yielding of the steel reinforcement. This behavior shows a sudden drop in load due to failure of the strengthening system by debonding and rupturing of the glass fibers. This failure is known as IC debonding of the strengthening system which is typical for externally bonded applications. Once failure of the strengthening system occurred, the specimen followed the same behavior of the control specimen until failure due to crushing of concrete.

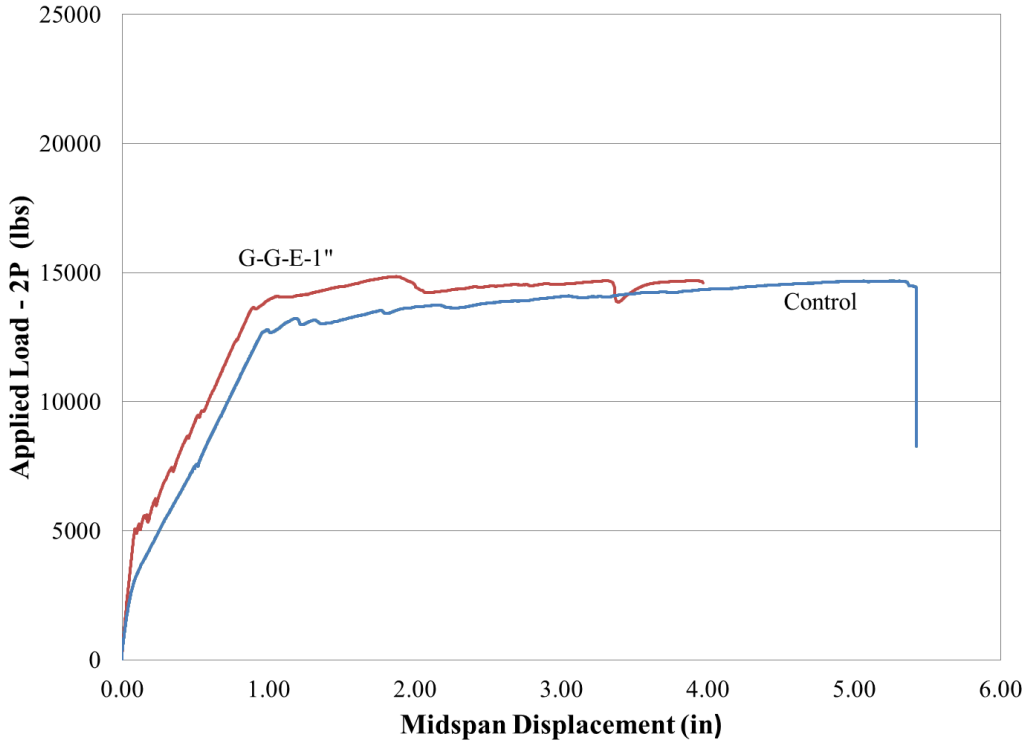

Figure A-15: Load- Deflection Behavior of G-G-E-1" specimen

A.4.2 Load Strain

The measured Load-Strain of the top concrete surface of the slab and the bottom surface of the FRP strengthening system is shown in Figure A-16. Test results indicate that the maximum measured concrete strain in compression was 0.005. The figure indicates also that all the steel reinforcement had yielded before failure.

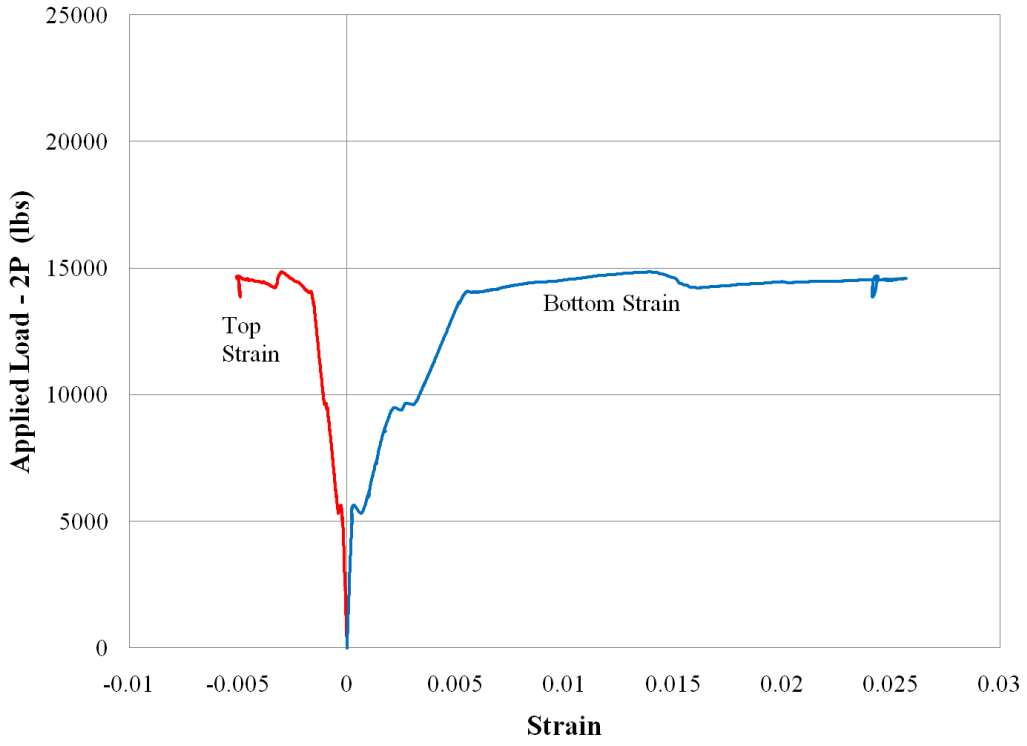

Figure A-16: Strain Measurement for G-G-E-1" specimen

A.4.3 Inspection of Failure

Inspection of the test specimen after failure showed that the 1 inch glass grid had debonded and ruptured in the region of maximum moment region. It was also observed that very large crack widths had formed in the region of maximum moment, where failure occurred. The widths of some of these cracks were 4-5mm. Figure A-17 shows the debonded and ruptured grid once the slab had been turned over for inspection of the fibers. It should be noted that the glass grid achieved a very good bond by using the Grancrete PCW, evident by rupture of the fibers that were observed during the inspection process as shown Figure A-17.

Figure A-17: Ruptured and Debonded Fibers from G-G-E-1" specimen

A.4.4 Pull Offs

Results of the three pull-off tests performed on the specimen are presented in Figure A-18. The figure indicates that all of the three pull-off tests performed approximately satisfied the ACI requirement for a desirable bond strength of 200 psi. All three of the pull-off tests failed in the Grancrete PCW paste bond layer, indicating that the weakest part of the bond was in the Grancrete PCW bond layer. The results may indicate that the grid spacing is large enough to allow for the adhesive material to form a good bond between the fibers and the concrete surface.

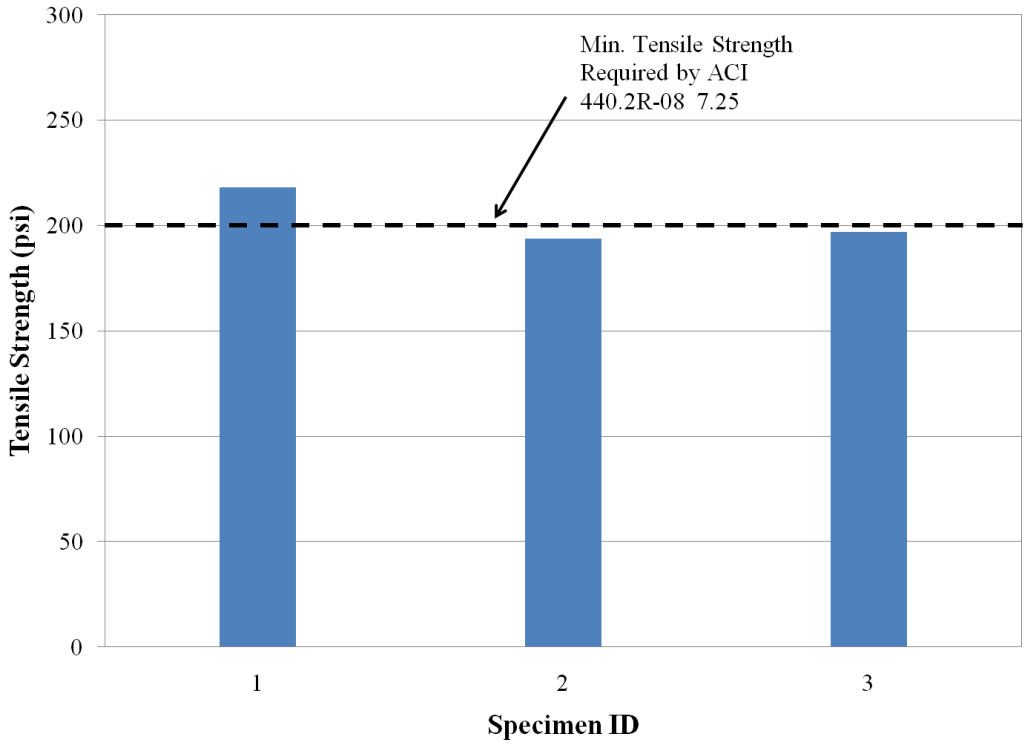

Figure A-18: Pull-Off Test Results for G-G-E-1" specimen

A.4.5 Summary of Test Results

It was observed that the load carrying capacity is increased by less than 1% when compared to the unstrengthened control specimen. Test results suggest that the reinforcement ratio used was small and not capable to increase the overall load carrying capacity of the slab. The ductility was decreased by 63%. The failure was due to IC debonding and was caused by the debonding and rupturing the glass grid in the maximum moment region. It is recommended to increase the reinforcement ratio for future testing to increase the ultimate load carrying capacity of the slab.

A.5 G-G-E-0.25” Specimen

This slab was strengthened with an externally bonded glass fiber grid with a 0.25” grid spacing, provided by PPG Company, and was bonded with Grancrete PCW. This specimen was subject to a four-point bending test and is shown in Figure A-19.

Figure A-19: G-G-E-0.25” specimen under four-point bending

A.5.1 Load Displacement

The measured Load-Displacement behavior of the strengthened slab is shown in Figure A-20. From this figure it can be seen that the maximum load carrying capacity was 14,785 lbs, compared to a measured value of 14,678 for the control slab. Deflection at mid-span was 1.85 inches at failure of the strengthening system and 4.35 inches at failure of the slab due to crushing of the concrete. The behavior consists of four distinct linear behaviors as shown in Figure A-20. Initially a linear behavior up to the initiation of the first crack is observed. This is followed by a semi-nonlinear behavior up to yielding of the steel reinforcement. After yielding there was significant reduction in stiffness up to failure of the strengthening

system due to rupture and debonding of the strengthening system accompanied by a sudden drop in load and finally overall failure due to crushing of the concrete in the maximum compression zone. The cracking load and yield load of the strengthened specimen was 4,494 lbs and 13,951 lbs, compared to 3,000 lbs and 12,767 lbs for the control slab, respectively. The ductility of the strengthened specimen was 1.94 and was determined based on the comparing the mid-span deflection at failure of the strengthened system to the mid-span deflection at yielding of the longitudinal reinforcing bars. The slab failed by IC debonding of the strengthening system which is typical for externally bonded applications. Once failure of the strengthening system occurred, the specimen followed the same behavior of the control specimen until failure due to crushing of concrete.

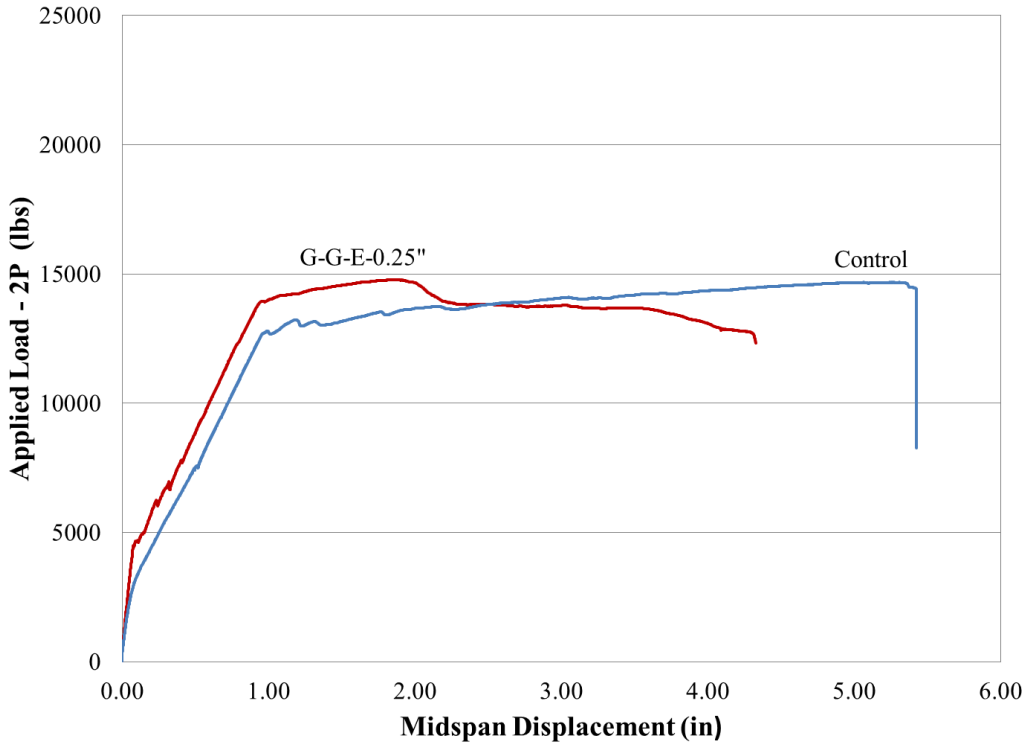

Figure A-20: Load- Deflection Behavior of G-G-E-0.25" specimen

A.5.2 Load Strain

The measured Load-Strain of the top concrete surface of the slab and the bottom surface of the FRP strengthening system is shown in Figure A-21. Test results indicate that the maximum measured concrete strain in compression was 0.0033. The figure indicates also that all the steel reinforcements had yielded before failure.

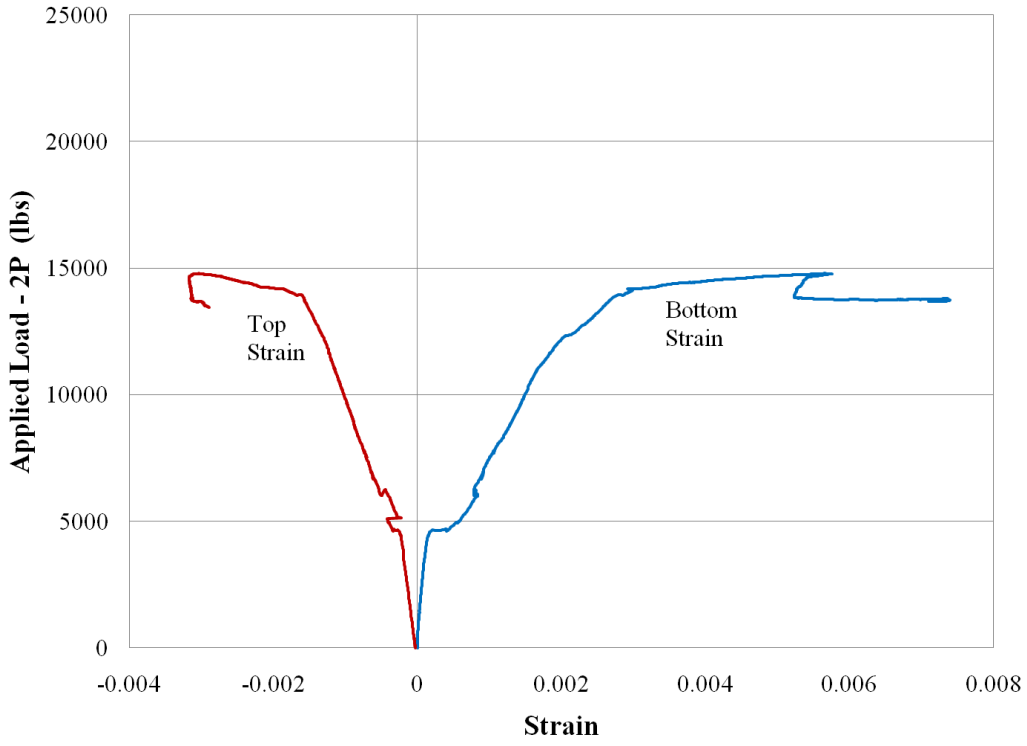

Figure A-21: Strain Measurement for G-G-E-0.25" specimen

A.5.3 Inspection of Failure

Inspection of the test specimen after failure showed that the 0.25" glass grid had debonded and ruptured in the region of maximum moment region. It was also observed that a very large crack had formed in the region of maximum moment, where failure occurred. Figure A-22 shows the debonded and ruptured grid once the slab had been turned over for inspection of the fibers. It should be noted that the glass grid achieved a very good bond by using the Grancrete PCW, evident by rupture of the fibers that were observed during the inspection process as shown in Figure A-22.

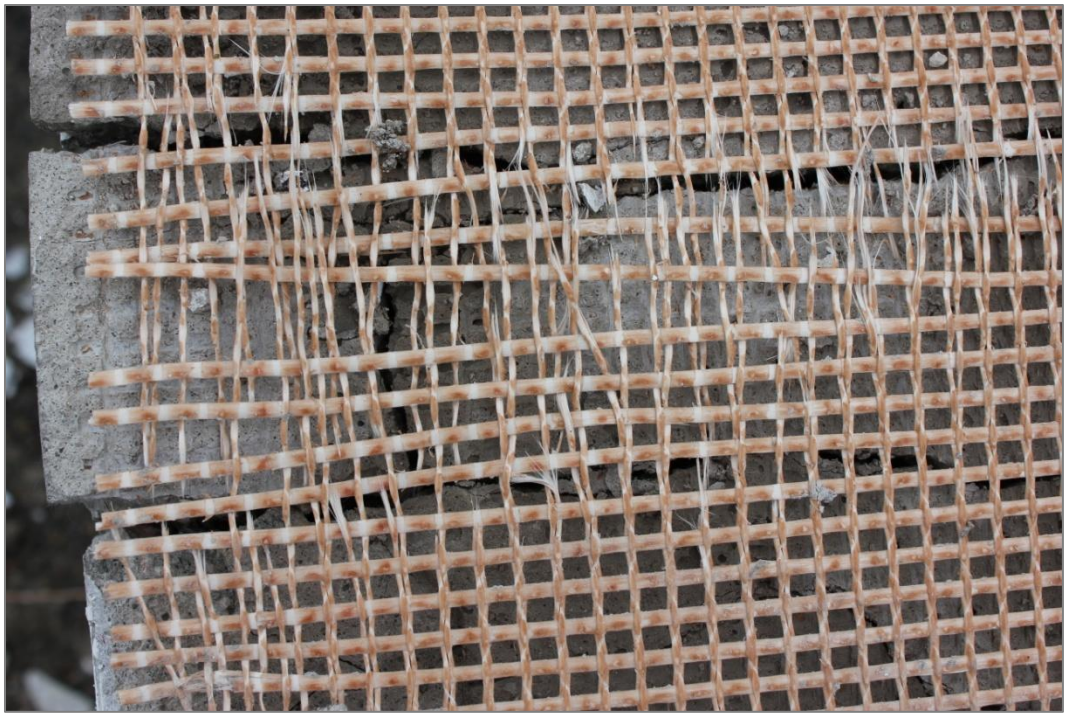

Figure A-22: Ruptured and Debonded fibers of G-G-E-0.25" specimen

A.5.4 Pull Offs

Results of the four pull-off tests performed on the specimen are presented in Figure A-23. The figure indicates that four pull-off tests performed did not quite satisfy the ACI requirement for a desirable bond strength of 200 psi. Three of the pull-off tests failed in the bond layer between the Grancrete PCW paste and the fibers, indicating a weak bond of the glass grid to the concrete sub-strata. The other pull-off test failed in the bond layer between the Grancrete PCW paste and the concrete slab. The results may indicate that the grid spacing is too small to allow penetration of the Grancrete PCW between the fibers of the grid and the concrete sub-strata and therefore did not provide adequate bond characteristics for the strengthened system.

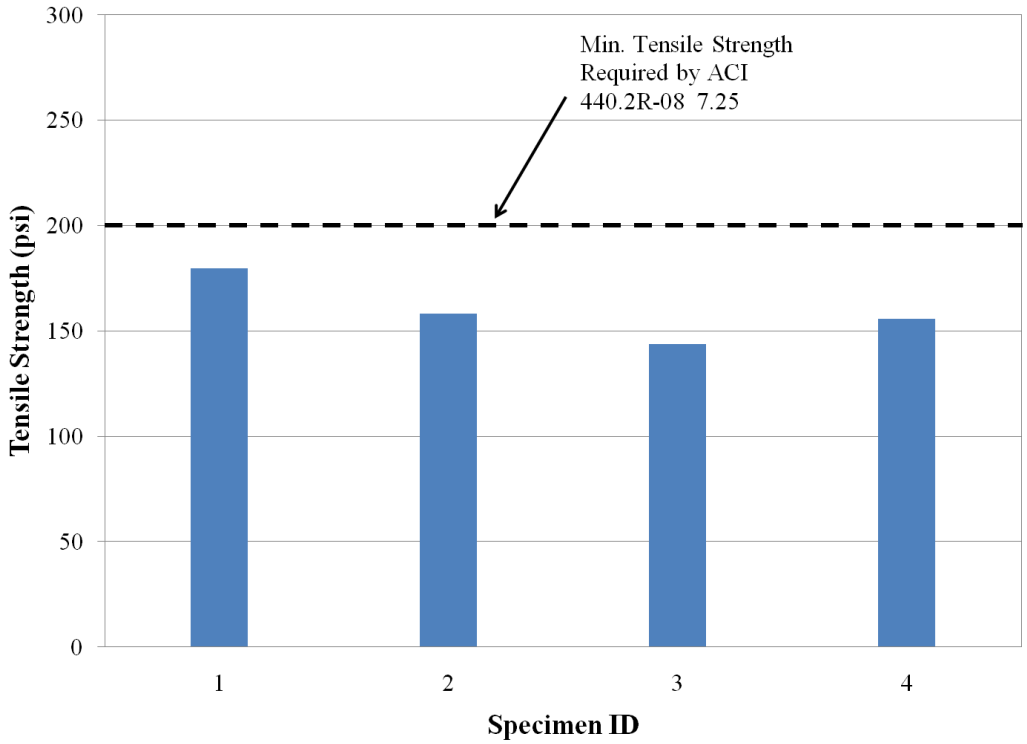

Figure A-23: Pull-Off Test Results for G-G-E-0.25" specimen

A.5.5 Summary of Test Results

It was observed that the load carrying capacity was increased by less than 1% when compared to the unstrengthened control specimen. Test results suggest that the reinforcement ratio used was small and not capable to increase the overall load carrying capacity of the slab. The ductility was decreased by 65%. The failure was due to IC debonding and was caused by the debonding and rupturing the glass grid in the maximum moment region. The bond strength did not quite satisfy the tensile bond strength required by ACI due to the small spacing of the grid. It is recommended that the grid spacing be increased for future testing to increase the bond strength between the fibers and the concrete sub-strata.

A.6 C-G-E Specimen

This slab was strengthened with an externally bonded carbon fiber grid, provided by Fyfe Company, which has a spacing of 9.5mm center to center of the longitudinal fibers and a 19.5mm center to center spacing of the transverse strands and was bonded with Grancrete PCW. This specimen was subject to a four-point bending test and is shown in Figure A-24.

Figure A-24: C-G-E specimen under four-point bending

A.6.1 Load Displacment

The measured Load-Displacement behavior of the strengthened slab is shown in Figure A-25. From this figure it can be seen that the maximum load carrying capacity was 20,085 lbs, compared to a measured value of 14,678 for the control slab. Deflection at mid-span was 2.71 inches at failure of the strengthening system and 4.05 inches at failure due to crushing of the concrete. The behavior consists of four distinct linear behaviors as shown Figure A-25. Initially a linear behavior up to the initiation of the first crack is observed. This is followed by a semi-nonlinear behavior up to yielding of the steel reinforcement. After yielding, there

was a significant reduction of the overall stiffness up to failure of the strengthening system due to rupture and debonding of the strengthening system where then a sudden drop in load is observed. After failure of the strengthening system the slab follows the behavior of the control slab up to the up to failure due to crushing of the concrete in the maximum compression zone. The cracking load and yielding load of the strengthened slab was 4,970 lbs and 14,400 lbs, compared to 3,000 lbs and 12,767 lbs for the control slab, respectively. The ductility of the strengthened specimen was 2.68 and was determined based on the comparing the mid-span deflection at failure of the strengthened slab to the mid-span deflection at yielding of the longitudinal reinforcement. Figure A-25 shows a sudden drop in load due to debonding and rupture of the fibers. This failure is characterized as IC debonding and is typical for externally bonded FRP. Once failure of the strengthening system occurred, the specimen followed the same behavior of the control specimen until failure due to crushing of concrete.

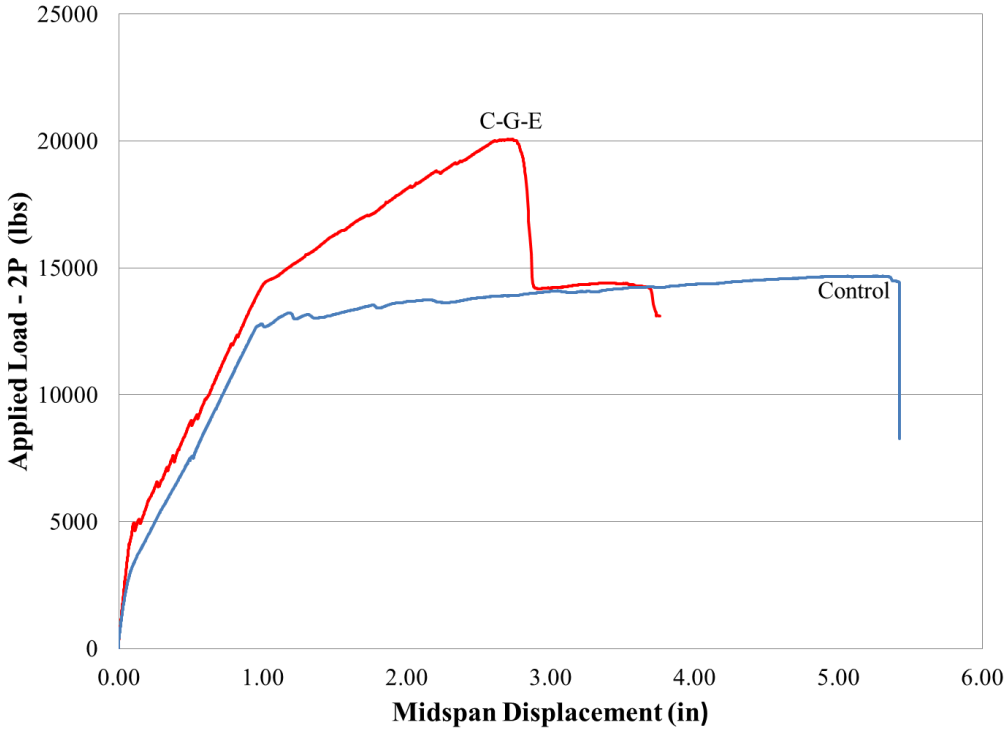

Figure A-25: Load- Deflection Behavior of C-G-E specimen

A.6.2 Load Strain

The measured Load-Strain of the top concrete surface of the slab and the bottom surface of the FRP strengthening system is shown in Figure A-26. Test results indicate that the maximum measured concrete strain in compression was 0.0089. The figure indicates also that all the steel reinforcements had yielded before failure.

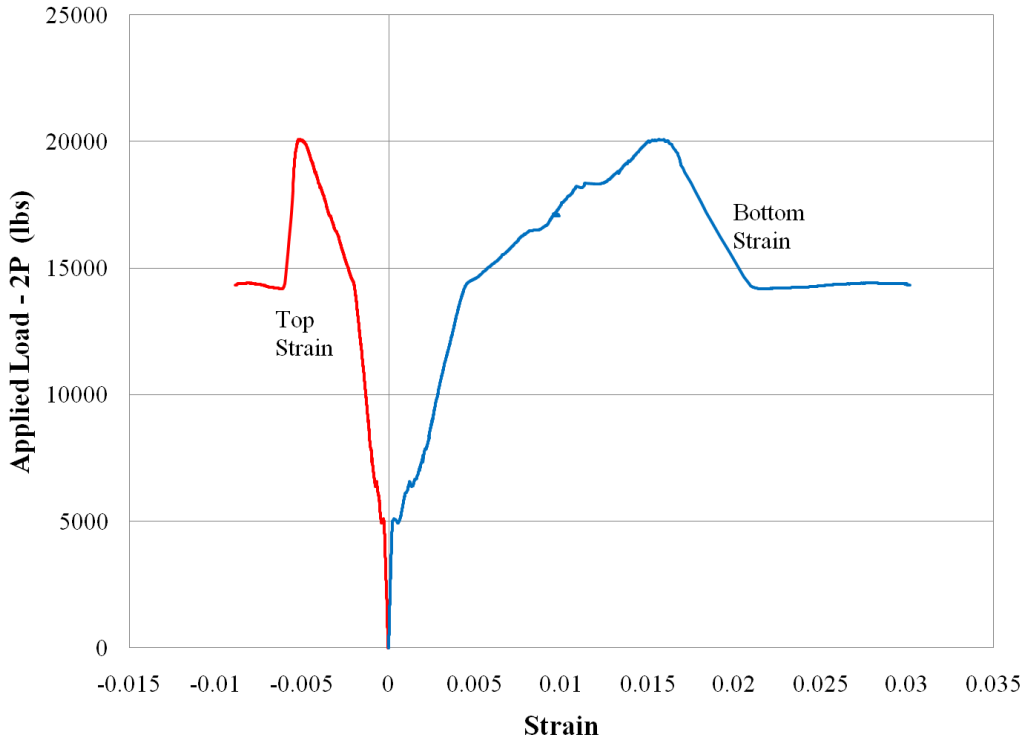

Figure A-26: Strain Measurement for C-G-E specimen

A.6.3 Inspection of Failure

Inspection of the test specimen after failure showed that the carbon grid had debonded and ruptured in the region of maximum moment. Figure A-27 shows the debonded and ruptured grid when the slab had been turned over for inspection. It was also noted that the fibers were still bonded to the bottom layer of Grancrete PCW after the top layer of the adhesive was removed for inspection of the fibers.

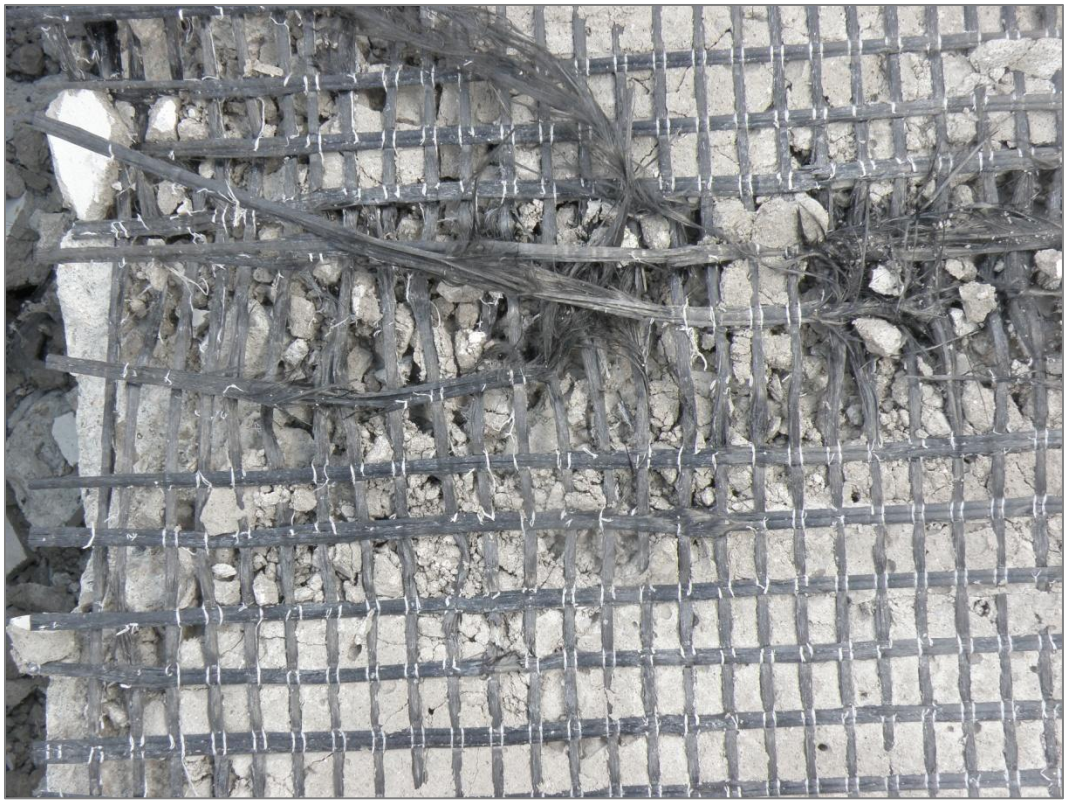

Figure A-27: Ruptured and Debonded Fibers of C-G-E specimen

A.6.4 Pull Offs

Results of the four pull-off tests performed on the specimen are presented in Figure: A-28. The figure indicates the measured bond strength does not quite satisfy the ACI requirement for a desirable bond strength of 200 psi. All of the pull-off tests failed in the bond layer between the Grancrete PCW paste and the fibers, indicating a weak bond characteristic of the bonded layer. The results may indicate that the grid spacing is too small to allow penetration of the Grancrete PCW between the fibers of the grid and the concrete sub-strata and therefore did not provide the required bond characteristics for the strengthened system.

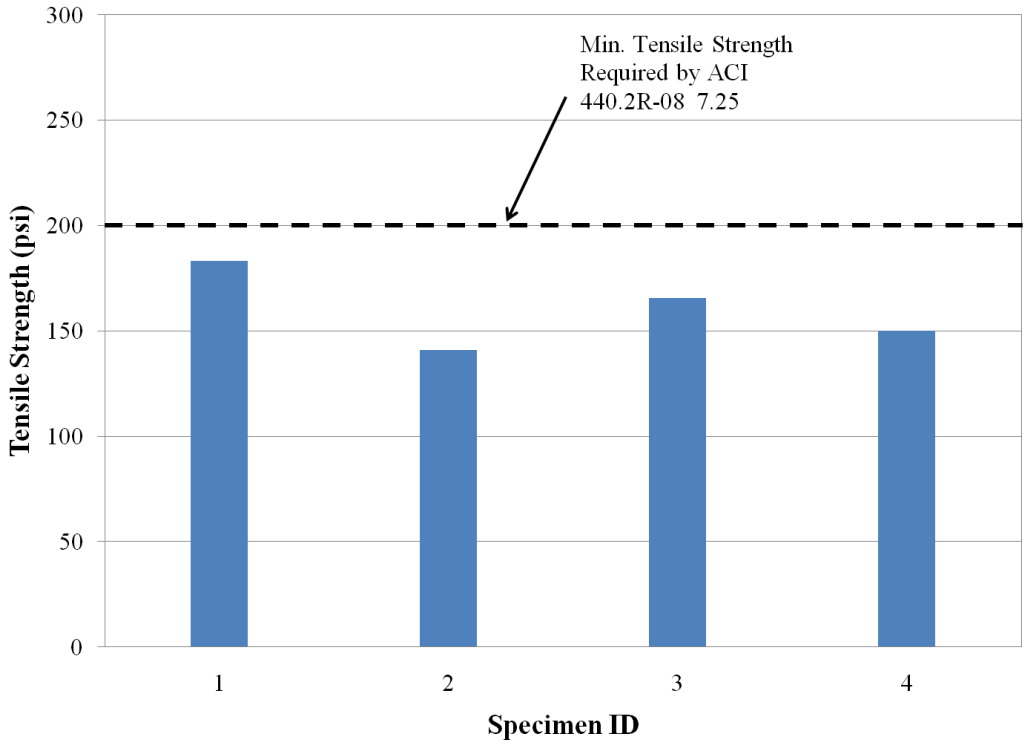

Figure: A-28: Pull-Off Test Results for C-G-E specimen

A.6.5 Summary of Test Results

The measured load carrying capacity was 31% higher than the unstrengthened control specimen. Test results suggest that the reinforcement ratio used was large enough to increase the overall load carrying capacity of the slab. The ductility was decreased by 52%, and the failure occurred due to IC debonding and was caused by the debonding and rupturing the carbon grid in the maximum moment region. Based on these results, it is recommended to increase the spacing of the grid for future testing to increase the bond strength between the fibers and the concrete sub-strata.

A.7 C-C-E-A Specimen

This slab was strengthened with an externally bonded carbon fiber grid, provided by the Fyfe Company, that has a spacing of 9.5mm center to center of the longitudinal fibers and a 19.5mm center to center spacing of the transverse strands and bonded with a cementitious material provided by the Fyfe Company, commercially referred to as Tyfo C-Matrix. This specimen was subject to a four-point bending test as is shown in Figure A-29.

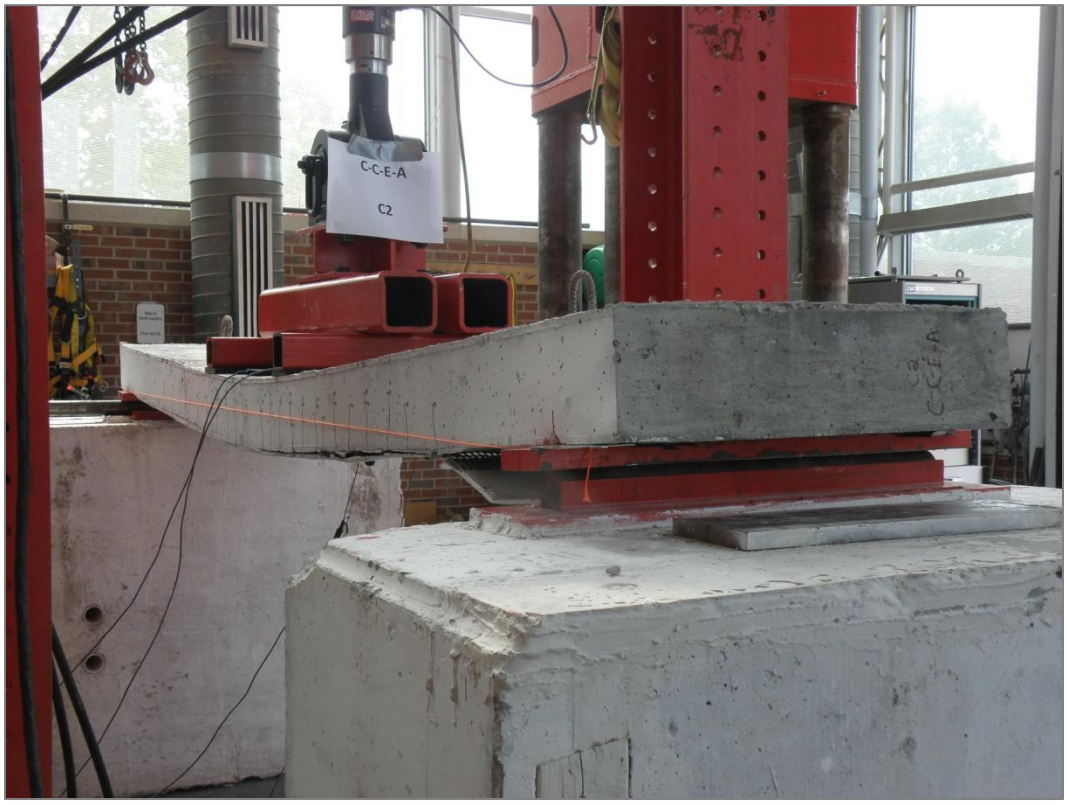

Figure A-29: C-C-E-A specimen under four-point bending

A.7.1 Load Displacement

The measured Load-Displacement behavior of the strengthened slab is shown Figure A-30. From this figure it can be seen that the maximum load carrying capacity was 19,012 lbs, compared to a measured value of 14,678 for the control slab. Deflection at mid-span was 2.59 inches at failure of the strengthening system and 3.49 inches at failure due to crushing of the concrete. The behavior consists of four distinct linear behaviors as shown in Figure A-30. Initially a linear behavior up to the initiation of the first crack is observed. This is

followed by a semi-nonlinear behavior up to yielding of the steel reinforcement and the failure occurred due to debonding of the strengthening system accompanied by a sudden drop of the load as shown in Figure A-30. The cracking load and yielding load were 3,604 lbs and 14,470 lbs, compared to 3,000 lbs and 12,767 lbs measured for the control slab, respectively. The ductility of the strengthened specimen was 2.44 and was determined based on the comparing the mid-span deflection at failure of the strengthened system to the mid-span deflection at yielding of the longitudinal reinforcements.

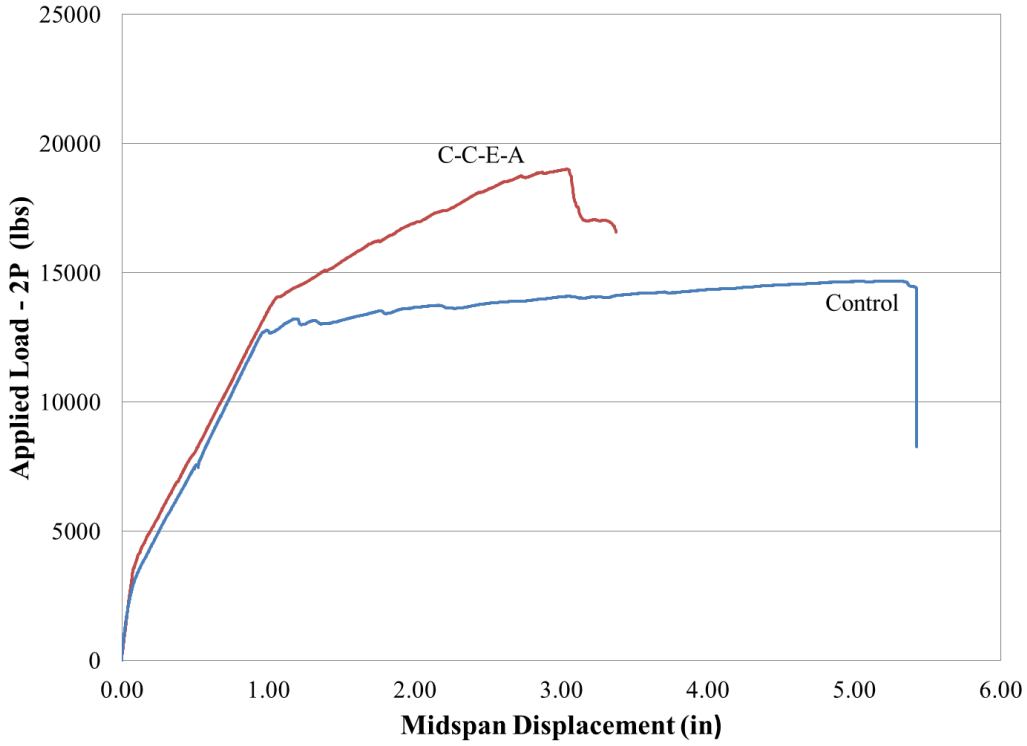

Figure A-30: Load- Deflection Behavior of C-C-E-A specimen

Failure of the strengthening system occurred due to debonding of the strengthening system as shown in Figure A-31. One unique event that was observed was that the overlaying layer of cementitious material on the fibers crushed in the shear zone of the strengthening system. This is shown in Figure A-32. The failure due to debonding was characterized also by crushing of the cementitious material as shown in Figure A-32 and may suggest that the recommended water/material ratio of the cementitious material may not be adequate to

achieve the full bond characteristics of the material. The behavior suggests that there is a need to adjust the water/material ratio. It was also very dry during application and hardened in a very short time.

Figure A-31: Debonding of C-C-E-A specimen

Figure A-32: Crushed Overlaying Layer of Cementitious Material of C-C-E-A specimen

A.7.2 Load Strain

The measured Load-Strain of the top concrete surface of the slab and the bottom surface of the FRP strengthening system is shown in Figure A-33. Test results indicate that the maximum measured concrete strain in compression was 0.0099. The figure indicates also that all the steel reinforcements had yielded before failure.

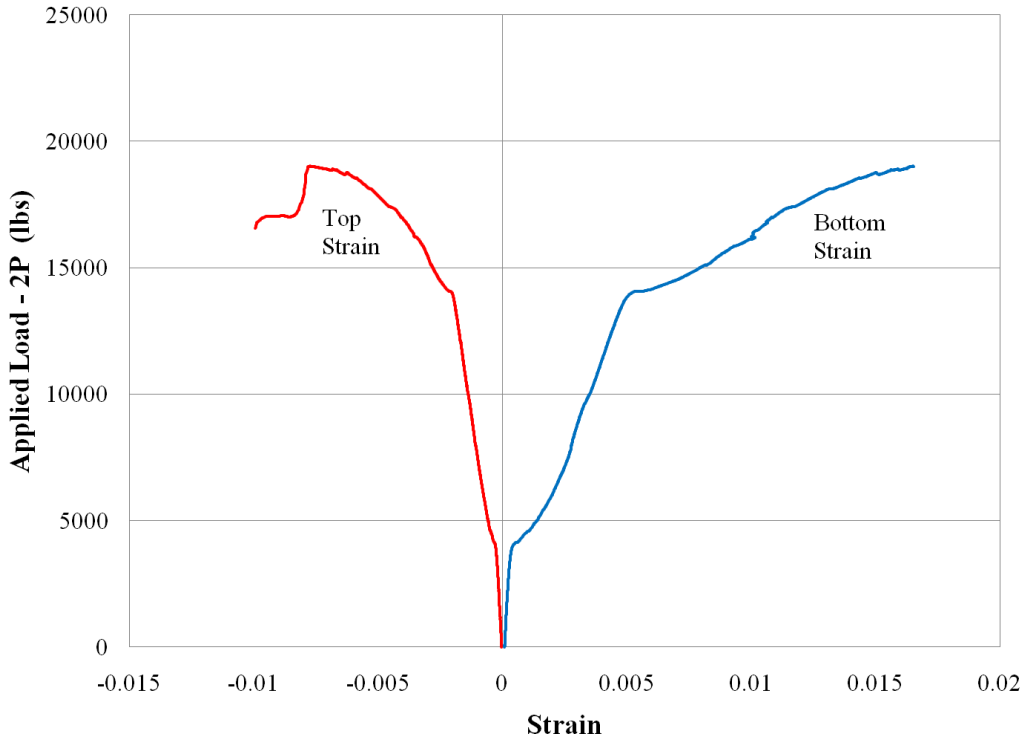

Figure A-33: Strain Measurement for C-C-E-A specimen

A.7.3 Inspection of Failure

Inspection of the test specimen after failure showed that the carbon grid was debonded without rupture of the fibers in the region of maximum moment region. Figure A-34 shows that the debonded grid when the slab had been turned over for inspection of the fibers.

Figure A-34: Debonded fibers in region of maximum moment of C-C-E-A specimen

A.7.4 Pull Offs

Results of the three pull-off tests performed on the specimen are presented in Figure A-35. The figure indicates that the three pull-off tests performed did not quite satisfy the ACI requirement for a desirable bond strength of 200 psi. Failure of the pull-off tests occurred at the interface of the Tyfo C-Matrix material and the fibers, reflecting weak bond characteristics of the material to the carbon grid. Test results indicate also that the grid spacing is not large enough to allow penetration of the Tyfo C-Matrix material between the fibers of the grid and the concrete sub-strata and therefore did not provide the significant bond for the strengthened system.

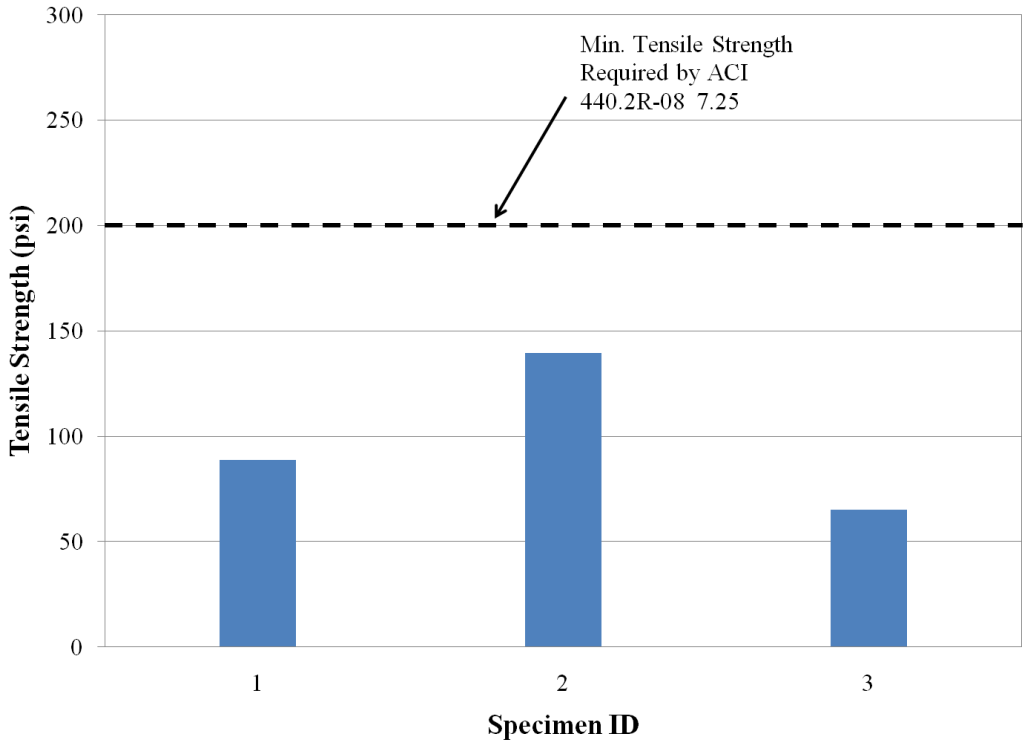

Figure A-35: Pull-Off Test Results for C-C-E-A specimen

A.7.5 Summary of Test Results

The measured load carrying capacity was increased by 26% in comparison to the unstrengthened control specimen. Test results suggest that the reinforcement ratio used was significant to increase the overall load carrying capacity of the slab. The ductility was decreased by 56% and the initial failure of the strengthening system was debonding of the carbon grid in the maximum moment region. The final failure was end anchorage debonding and was caused by the debonding of the strengthening system at the end of the slab near the support. Based on these results, it is recommended to increase the spacing of the grid for future testing to increase the bond strength between the fibers and the concrete sub-strata. It is also recommended that the mix design of the cementitious material be altered to allow for a more workable and stronger bonding adhesive.

A.8 C-C-E-B Specimen

This slab was strengthened with an externally bonded carbon fiber grid, provided by the Fyfe Company, that has a spacing of 9.5mm center to center of the longitudinal fibers and a 19.5mm center to center spacing of the transverse strands and bonded with a cementitious material provided by the Fyfe Company, commercially referred to as Tyfo C-Matrix. This specimen was subject to a four-point bending test and is shown Figure A-36.

Figure A-36: C-C-E-B specimen under four-point bending

A.8.1 Load Displacement

The measured Load-Displacement behavior of the strengthened slab is shown Figure A-37. From this figure it can be seen that the maximum load carrying capacity was 20,895 lbs, compared to a measured value of 14,678 for the control slab. Deflection at mid-span was 2.72 inches at failure of the strengthening system and 4.43 inches at failure due to crushing of the concrete. The behavior consists of four distinct linear behaviors as shown in Figure A-37. Initially a linear behavior up to the initiation of the first crack is observed. This is

followed by a semi-nonlinear behavior up to yielding of the steel reinforcement and the failure occurred due to debonding of the strengthening system accompanied by a sudden drop of the load as shown in Figure A-37. The cracking load and yielding load were 3,620 lbs and 14,531 lbs, compared to 3,000 lbs and 12,767 lbs measured for the control slab, respectively. The ductility of the strengthened specimen was 2.65 and was determined based on the comparing the mid-span deflection at failure of the strengthened system to the mid-span deflection at yielding of the longitudinal reinforcement. This figure shows a sudden drop in load due to debonding of the fibers. Once failure of the strengthening system occurred, the specimen followed the same behavior of the control specimen until failure due to crushing of concrete.

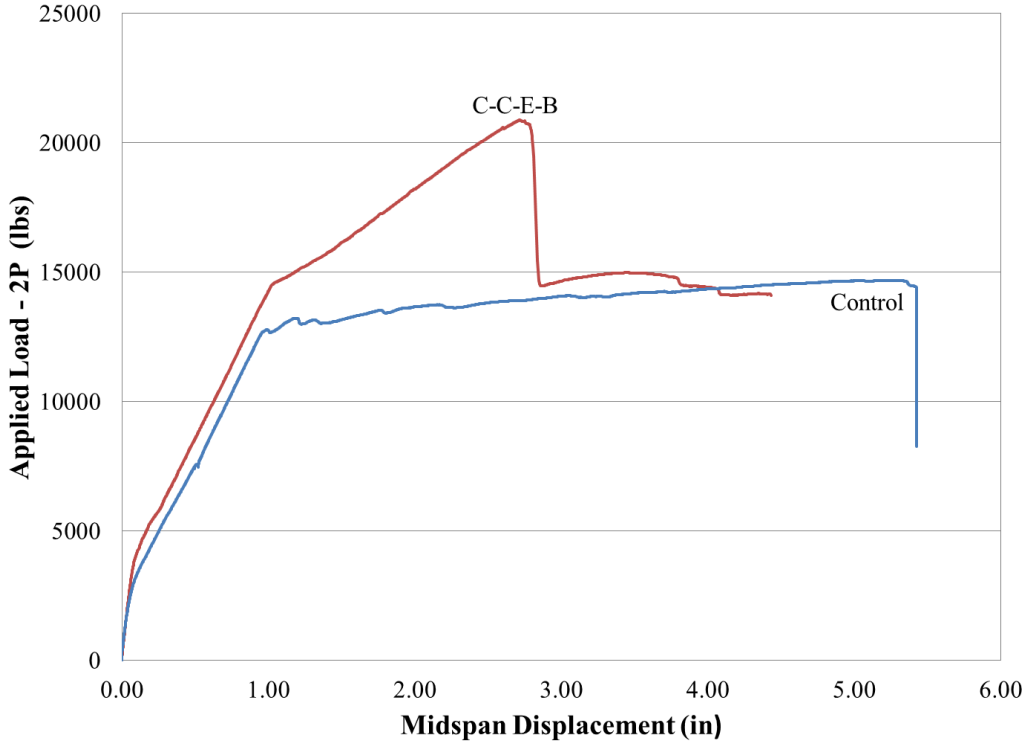

Figure A-37: Load- Deflection Behavior of C-C-E-B specimen

A.8.2 Load Strain

The measured Load-Strain of the top concrete surface of the slab and the bottom surface of the FRP strengthening system is shown in Figure A-38. Test results indicate that the maximum measured concrete strain in compression was 0.0099. The figure indicates also that all the steel reinforcements had yielded before failure.

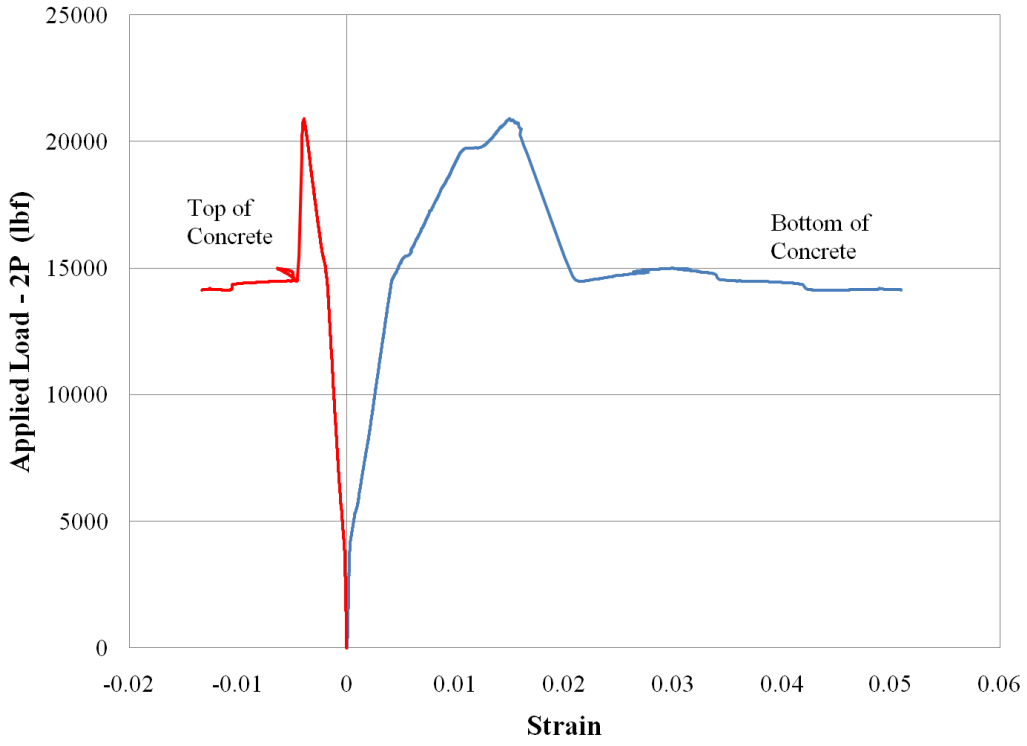

Figure A-38: Strain Measurement for C-C-E-B specimen

A.8.3 Inspection of Failure

Inspection of the test specimen after failure showed that the carbon grid was debonded without rupture of the fibers in the region of maximum moment. Figure A-39 shows the debonded grid when the slab had been turned over for inspection of the fibers. It should be noted that the top layer of adhesive on the fibers was very thin, and therefore it was difficult to remove during the inspection. The fibers were not ruptured during the testing of the specimen, and the failure occurred mainly due to debonding of the strengthening system.

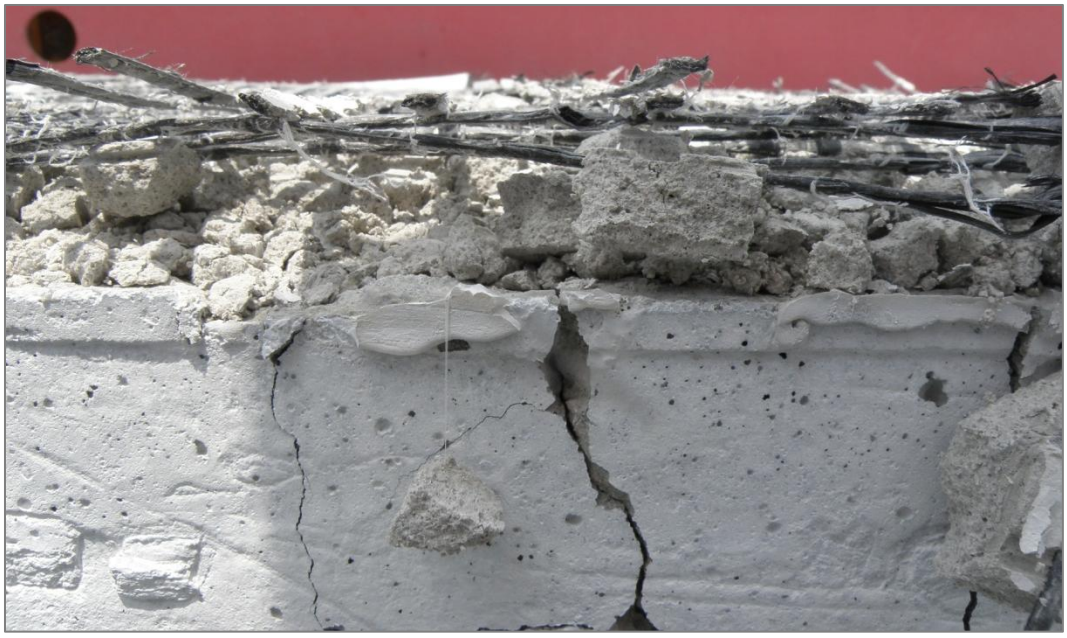

Figure A-39: Debonded fibers of C-C-E-B specimen

A.8.4 Pull Offs

Results of the three pull-off tests performed on the specimen are presented in Figure A-40. The figure indicates that the three pull-off tests performed did not quite satisfy the ACI requirement for a desirable bond strength of 200 psi. Failure of the pull off tests occurred at the interface of the Tyfo C-Matrix material and the fibers, reflecting weak bond characteristics of the material to the carbon grid. Test results indicate also that the grid spacing is not large enough to allow penetration of the Tyfo C-Matrix material between the fibers of the grid and the concrete sub-strata and therefore did not provide the significant bond for the strengthened system.

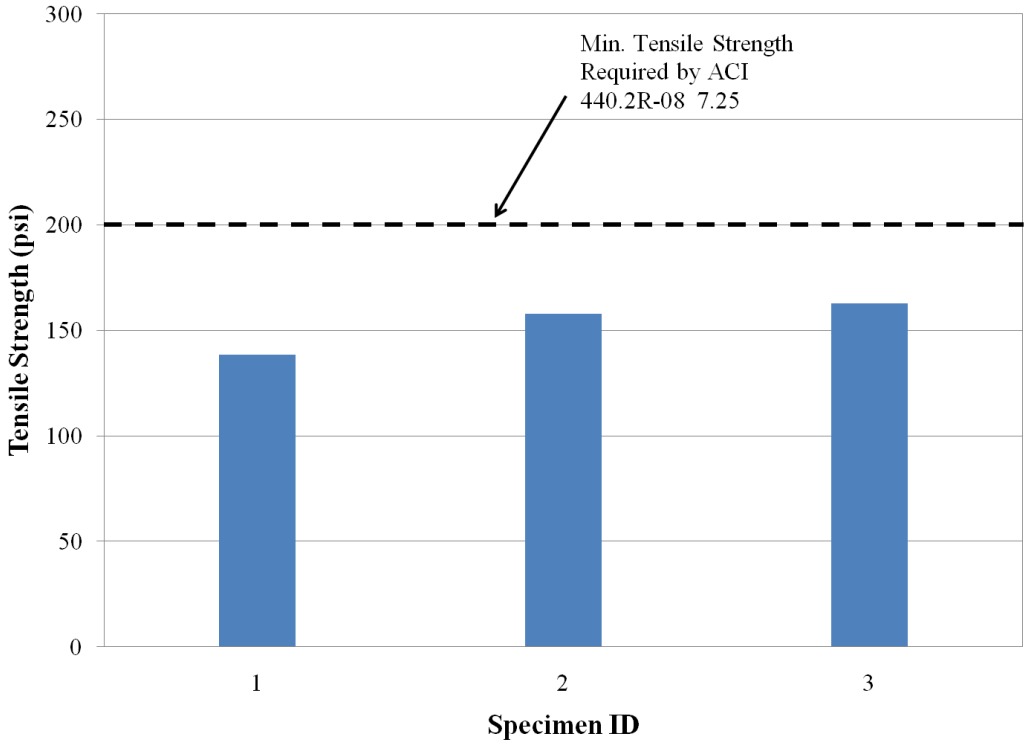

Figure A-40: Pull-Off Test Results for C-C-E-B specimen

A.8.5 Summary of Test Results

Test results reflect an increase the load carrying capacity by 35% in comparison to the unstrengthened control specimen. Test results suggest that the FRP reinforcement ratio used was sufficient to increase the overall load carrying capacity of the slab. The ductility was decreased by 53%. The failure of the strengthening system was debonding of the carbon grid in the maximum moment region, which is known as IC debonding. It is recommended that the grid spacing be increased for future testing to increase the bond strength between the fibers and the concrete sub-strata. It is also recommended that the mix design of the cementitious material be altered to allow for a more workability and better bond characteristics.

A.9 C-E-E Specimen

This slab was strengthened with an externally bonded carbon fiber grid, provided by the Fyfe Company that has a spacing of 9.5mm center to center of the longitudinal fibers and a 19.5mm center to center spacing between the transverse strands and was bonded with an epoxy adhesive, commercially known as Tyfo TC, provided by the Fyfe Company. This specimen was subject to a four-point bending test as shown in Figure A-41.

Figure A-41: C-E-E specimen under four-point bending

A.9.1 Load Displacement

The measured Load-Displacement behavior of the strengthened slab is shown in Figure A-42. Test results indicate that the maximum load carrying capacity was 20,780 lbs, in comparison to a measured value of 14,678 for the control slab. Deflection at mid-span was 2.41 inches at failure of the strengthening system. The behavior consists of three distinct linear behaviors as shown in Figure A-42. Initially a linear behavior up to the initiation of the first crack is observed. This is followed by a linear behavior up to yielding of the

reinforcement and then a sudden drop in load due to failure which occurred due to rupture of the fibers. The cracking load and yielding load was 4,245 lbs and 16,102 lbs, in comparison to 3,000 lbs and 12,767 lbs measured for the control slab, respectively. It should be noted that the load at yielding was much higher than the load at yielding for the other slabs that were strengthened by the same fiber but bonded by the cementitious adhesives. Ductility of the strengthened specimen was 2.22 and was determined based on the comparing the mid-span deflection at failure of the strengthened system to the mid-span deflection at yielding of the longitudinal reinforcements. Figure A-42 shows a sudden drop in load and consequential failure of the strengthened slab due to a sudden rupture of the strengthening system. The failure shown in Figure A-43 indicates formation of one single large width crack which is believed to be the main reason for rupture of the fibers.

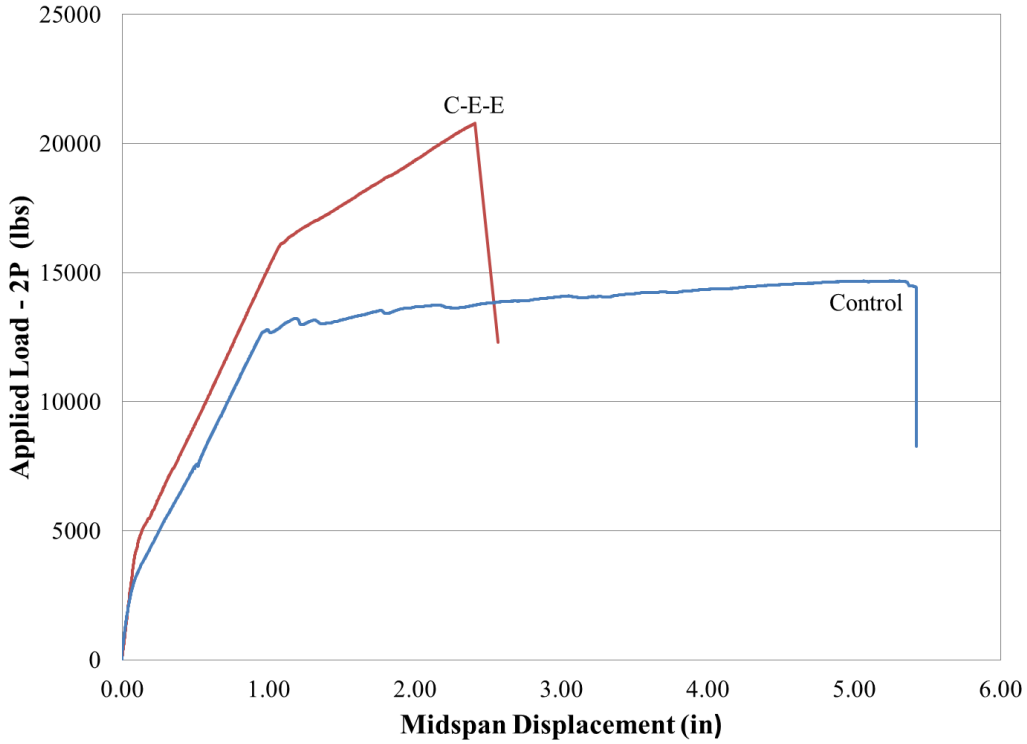

Figure A-42: Load- Deflection Behavior of C-E-E specimen

Figure A-43: Sudden Rupture of Epoxy Strengthening System on C-E-E specimen

A.9.2 Load Strain

The measured Load-Strain of the top concrete surface of the slab and the bottom surface of the FRP strengthening system is shown in Figure A-44. Test results indicate that the maximum measured concrete strain in compression was 0.0077. The figure indicates also that all the steel reinforcements had yielded before failure.

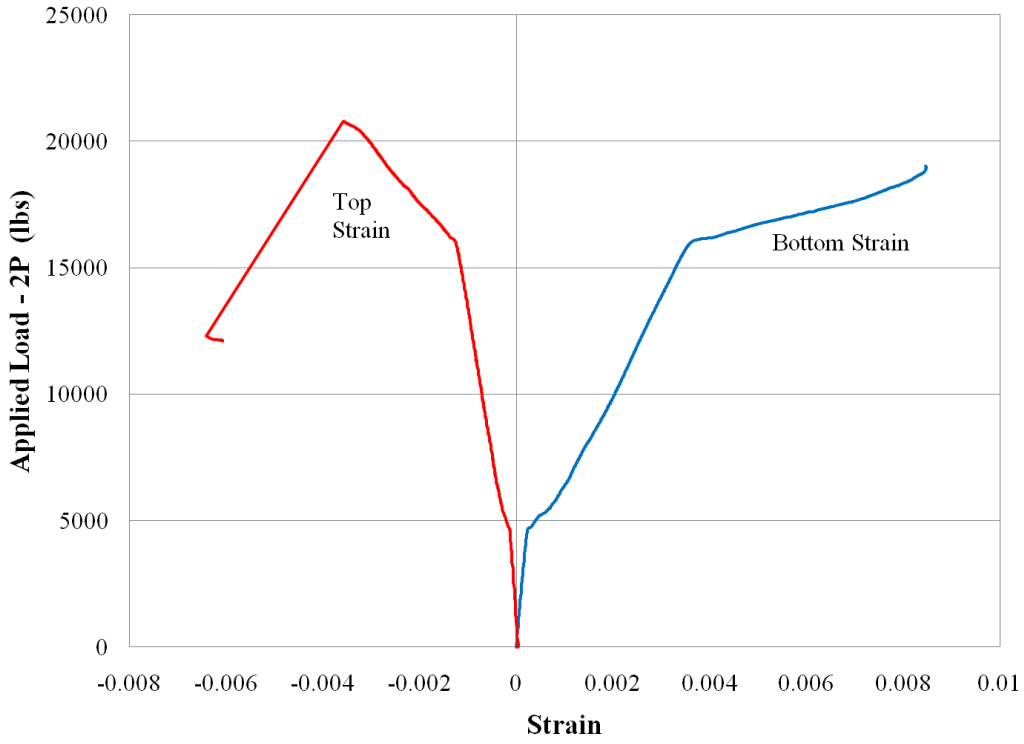

Figure A-44: Strain Measurement for C-E-E specimen

A.9.3 Inspection of Failure

Inspection of the test specimen after failure showed that the carbon grid was ruptured in the region of maximum moment when the strengthened slab had failed and formed a large crack at the center of the slab. Figure A-45 shows the ruptured fibers when the slab was turned over for inspection.

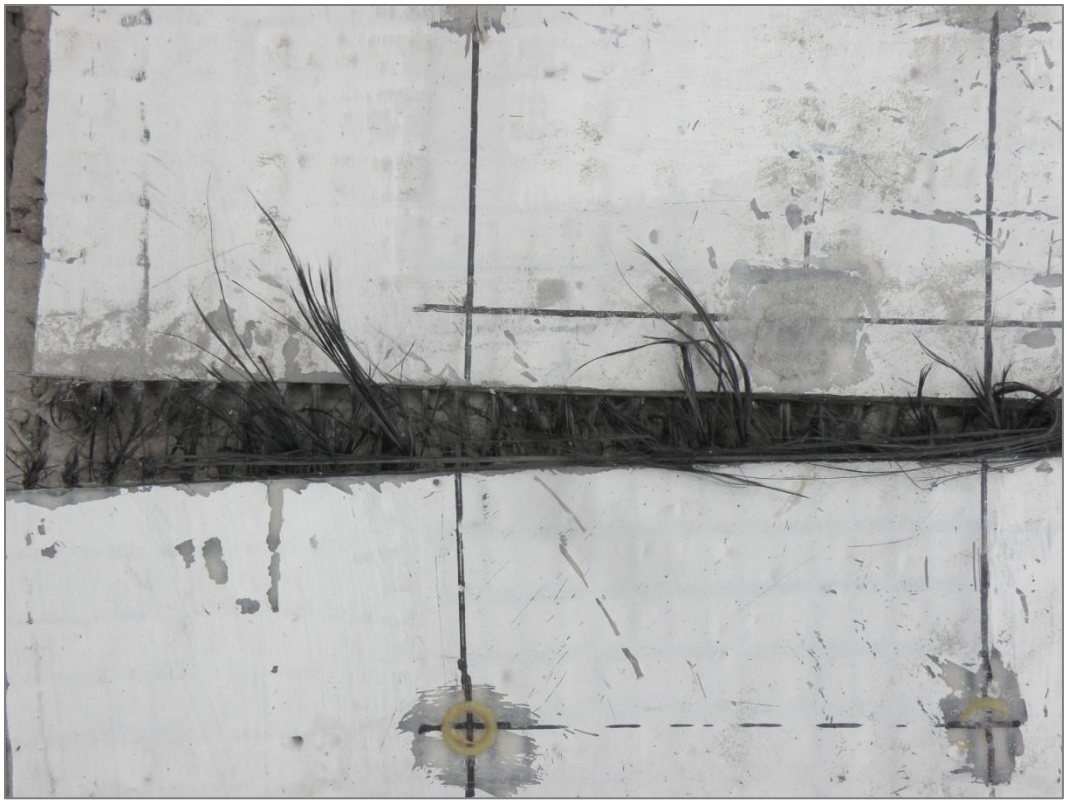

Figure A-45: Ruptured Fibers of C-E-E specimen

A.9.4 Pull Offs

Results of the three pull-off tests performed on the specimen are presented in Figure A-46. The figure indicates that all of the three pull-off tests performed satisfied the ACI requirement for a desirable bond strength of 200 psi. All of the pull-off tests failed in the concrete substrata, indicating a strong bond between the epoxy and concrete. The results may indicate that the using epoxy instead of cementitious material as the adhesive for this type of grid spacing forms a better bond between the fibers and the concrete sub-strata.

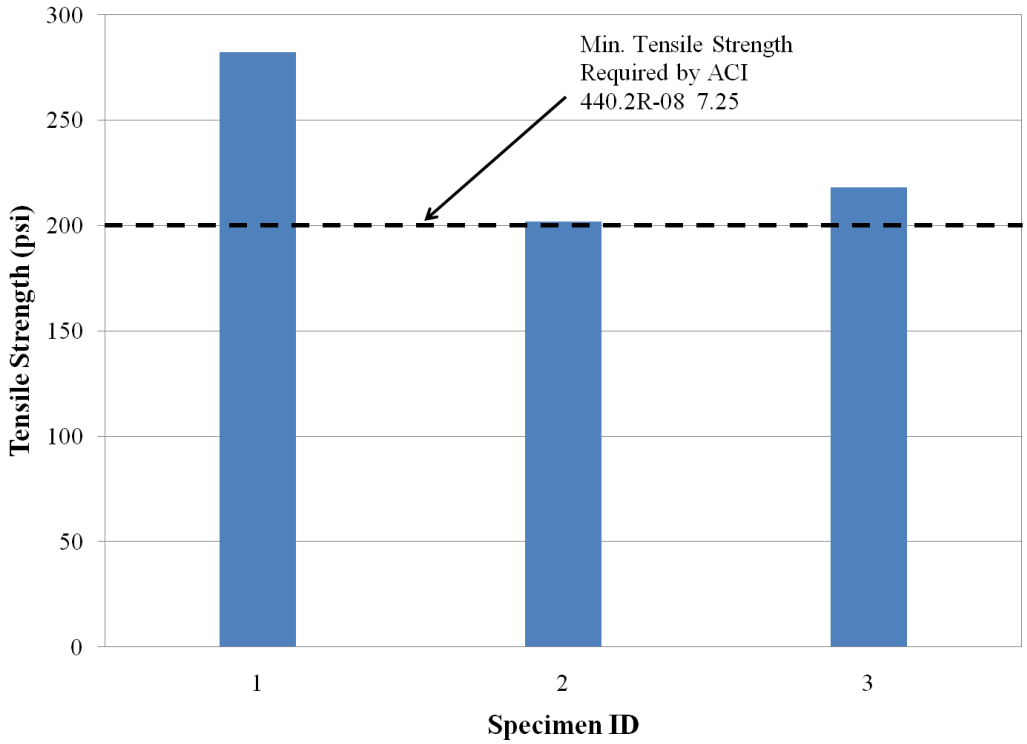

Figure A-46: Pull-Off Test Results for C-E-E specimen

A.9.5 Summary of Test Results

Test results indicate that the load carrying capacity was increased by 34% when compared to the unstrengthened control specimen. Test results suggest that the reinforcement ratio used was large enough to increase the overall load carrying capacity of the slab. The ductility was decreased by 60%. The failure of the strengthening system was due to rupture of the carbon grid in the maximum moment region. This formed a much stronger bond than using the cementitious adhesives. Since failure of the strengthening was very sudden and did not allow for the formation and prorogation of flexural cracks similar to the cementitious adhesives, it is concluded that the behavior of the carbon grid fiber with the cementitious materials described is more desirable due to the enhanced ductility which can be achieved.

A.10 Control – Phase II

The unstrengthened control specimen tested in Phase II was used as a benchmark to measure the effectiveness of the various FRP strengthened slabs explored in Phase II. The control specimen, as well as the strengthened slabs, was subjected to a four-point bending test as shown in Figure A-47.

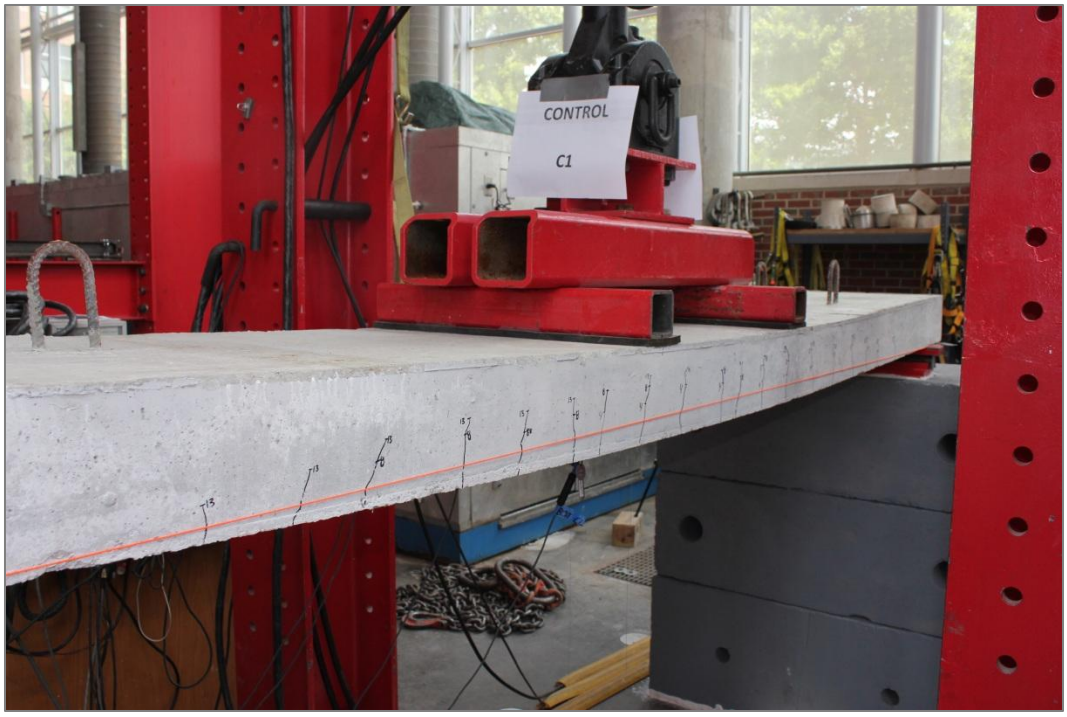

Figure A-47: Control Specimen – Phase II under four-point bending

A.10.1 Load Displacement

The Load-Displacement behavior of the control slab is shown in Figure A-48. Failure of the slab was due to crushing of the concrete in the maximum moment zone. The measured maximum load carrying capacity was 13,751 lbs and the maximum mid-span deflection was 4.35 inches. The behavior consists of three distinct linear behaviors as shown in Figure A-48. Initially a linear behavior up to the initiation of the first crack is observed. This is followed by a semi-nonlinear behavior up to yielding of the steel reinforcement. This is followed by significant reduction of the stiffness up the failure due to crushing of the concrete in the compression zone. The measured load of the control specimen at first crack

was 3000 lbs, the load at yielding was 12,814 lbs, and the slab failed at a load of 13,751 lbs. The ductility of the control specimen based on comparing the deflection at failure to the deflection at yielding of the reinforcement was 3.97.

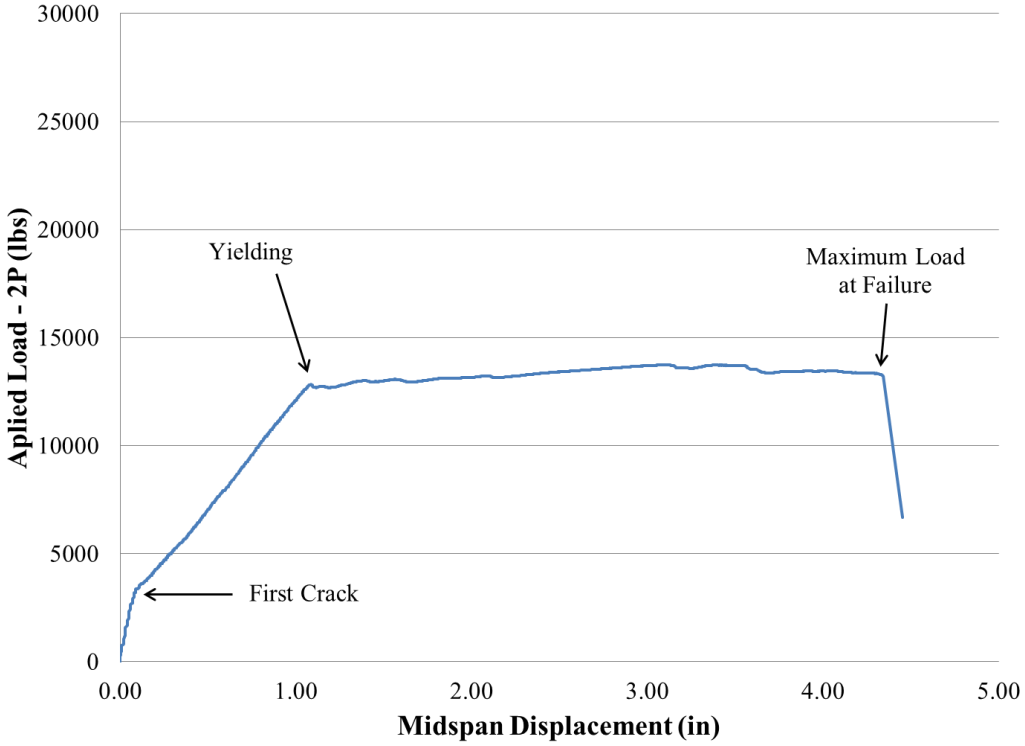

Figure A-48: Load-Deflection Behavior of Control Specimen – Phase II

A.10.2 Load Strain

The measured Load-Strain relationship of the top surface and bottom surface of the concrete for the control slab is shown in Figure A-49. The measured concrete strain represents the average strain within the gauge length of the pi gauges. Test results indicate that the maximum measured concrete strain in compression was 0.0066. The figure indicates also that all the reinforcement is yielded before failure.

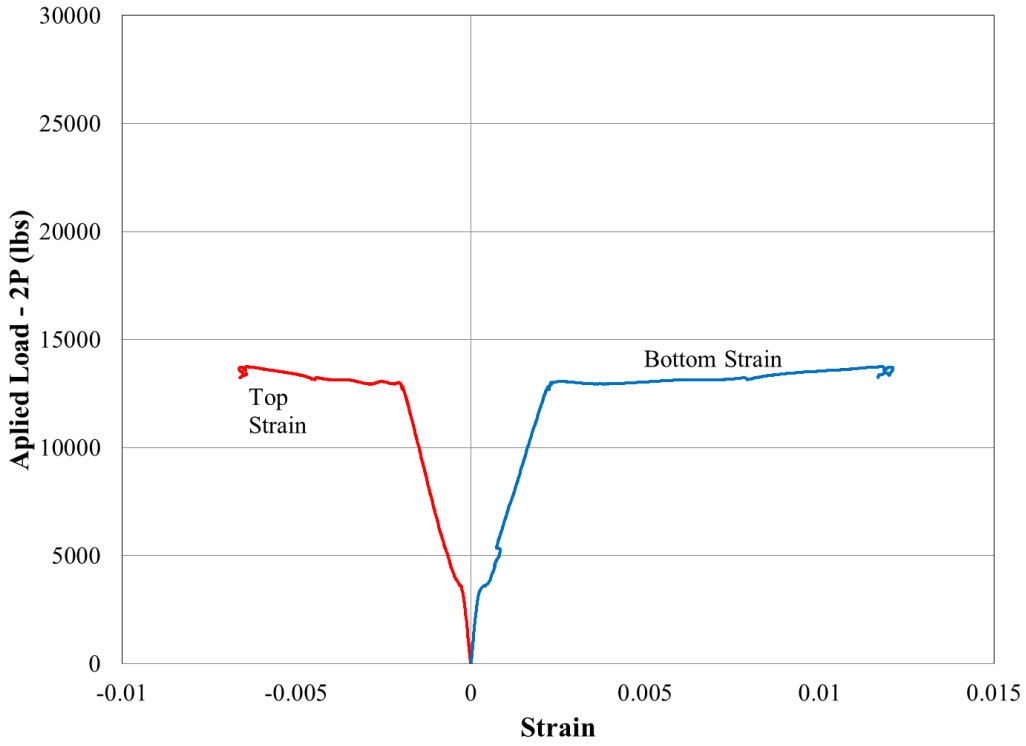

Figure A-49: Strain Measurement of Concrete for Control Specimen – Phase II

A.11 HM-E-E-3 Specimen

This slab was strengthened with an externally bonded High Modulus Carbon Strand Sheet – Type 3, commercially referred to as FORCA Carbon Strands, and bonded with an epoxy supplied by Nippon Steel Company using the externally bonded technique. This specimen was subject to a four-point bending test as shown in Figure A-50.

Figure A-50: HM-E-E-3 specimen under four-point bending

A.11.1 Load Displacement

The measured Load-Displacement behavior of the strengthened slab is shown in Figure A-51. This behavior shows a sudden drop in load due to failure of the strengthened system due to rupture of the fibers. The measured maximum load carrying capacity was 17,457 lbs, compared to a measured value of 13,751 for the control slab. Deflection at mid-span was 0.96 inches at failure of the strengthening system. This behavior suggests that failure of the strengthening system occurred before yielding of the steel reinforcement of the slab. Since failure of the strengthened system occurred before yielding of the steel bars, the ductility was less than unity and the failure was brittle and sudden. This was due to the use of a high FRP

reinforcement ratio and the high elastic modulus, characteristic of the Carbon FRP Strands. The measured cracking load was 4,201 lbs in comparison to 3000 lbs measured for the control slab.

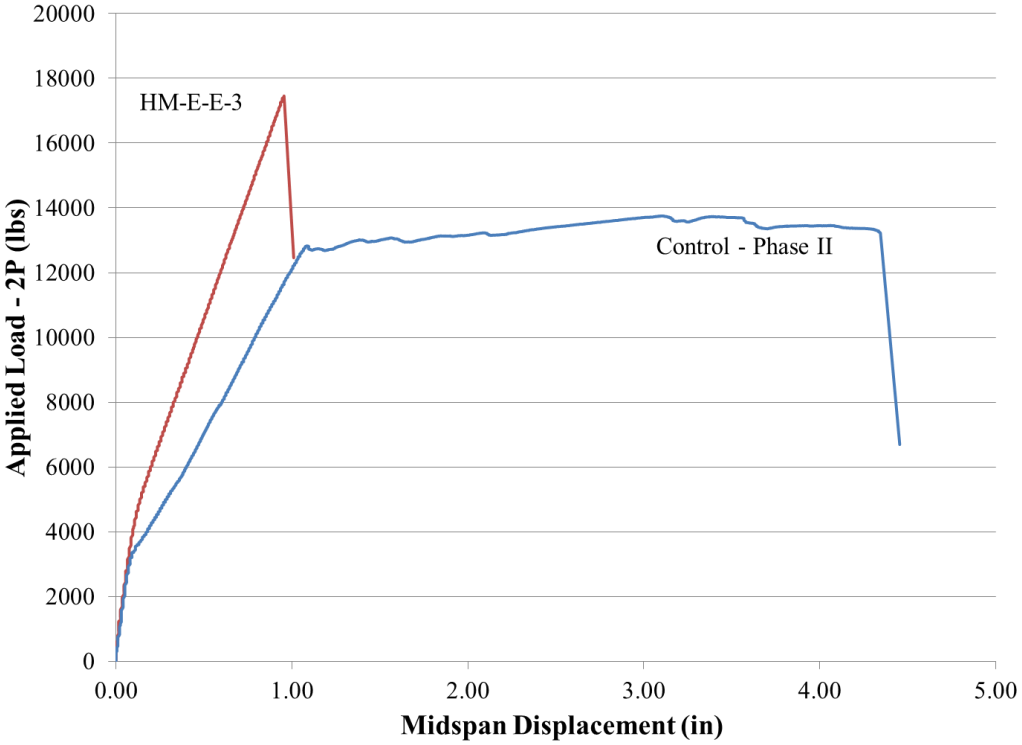

Figure A-51: Load- Deflection Behavior of HM-E-E-3 specimen

A.11.2 Load Strain

The measured Load-Strain of the top concrete surface of the slab and the bottom surface of the FRP strengthening system is shown in Figure A-52. Test results indicate that the maximum measured concrete strain in compression was 0.0021. The figure also indicates that the steel reinforcement had not completely yielded before failure and that the fibers ruptured at a strain of 0.0036, which was approximately the rupture strain measured using the witness panels.

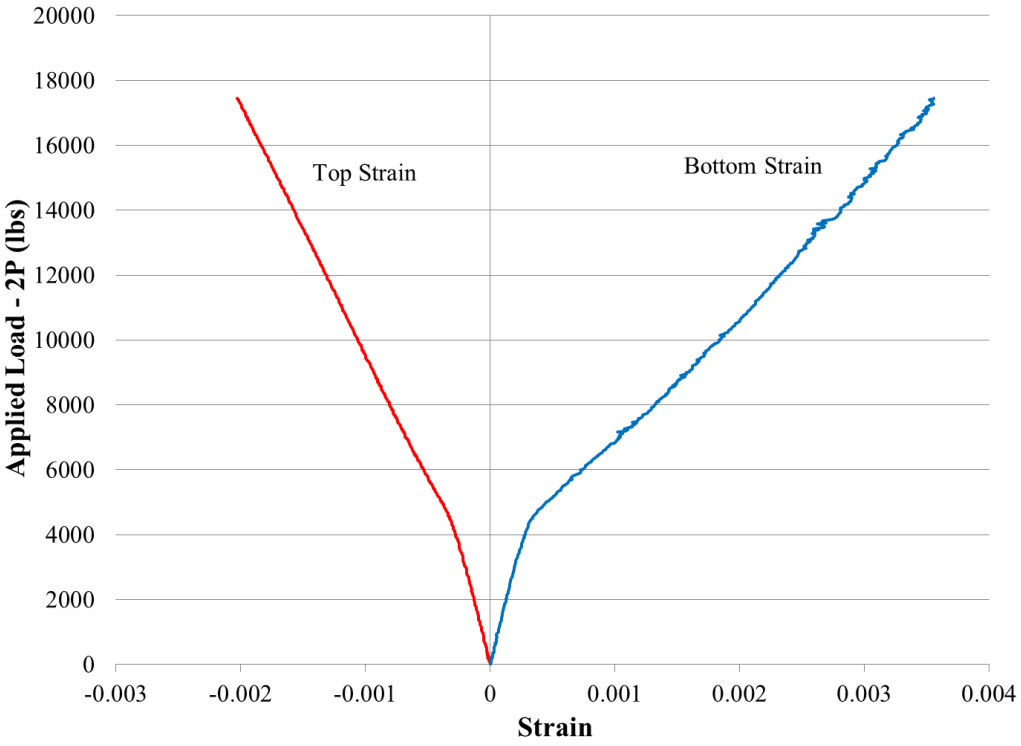

Figure A-52: Strain Measurement for HM-E-E-3 specimen

A.11.3 Inspection of Failure

Failure of the strengthening system was sudden and occurred within the maximum moment region of the slab. Failure of the strengthening system was due to rupture of the fiber within the maximum moment region of the slab. This failure is shown Figure A-53. Inspection of the test specimen after failure showed that the FORCA carbon strand sheet had ruptured. The ruptured fibers are shown in Figure A-54.

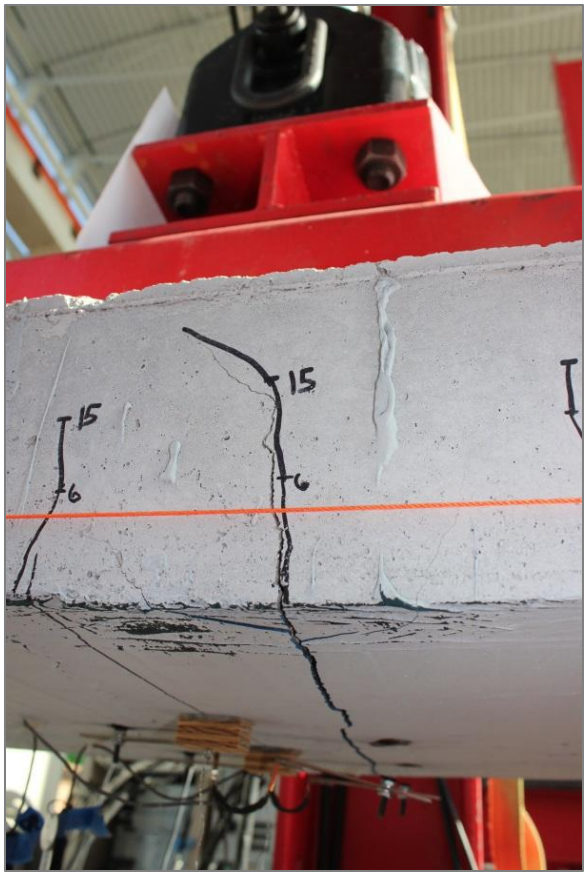

Figure A-53: Rupture of the of the FORCA High Modulus Carbon Sheet – Type 3

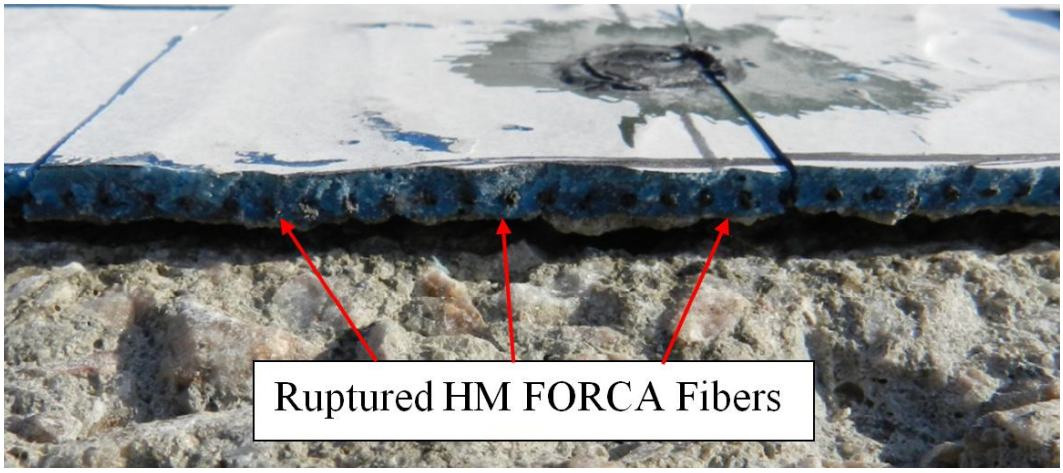

Figure A-54: Ruptured High Modulus Fibers upon Inspection

A.11.4 Pull Offs

Pull-off tests were conducted in areas of the slab that were away from the region of maximum moment and therefore considered undisturbed by the test to evaluate the bond strength of the strengthening system. Results of the four pull-off tests performed on the specimen are presented in Figure A-55. The figure indicates that all of the four pull-off tests performed satisfied the ACI requirement for a desirable bond strength of 200 psi. All of the pull-off tests failed in the concrete substrata, indicating a strong bond between the epoxy and concrete.

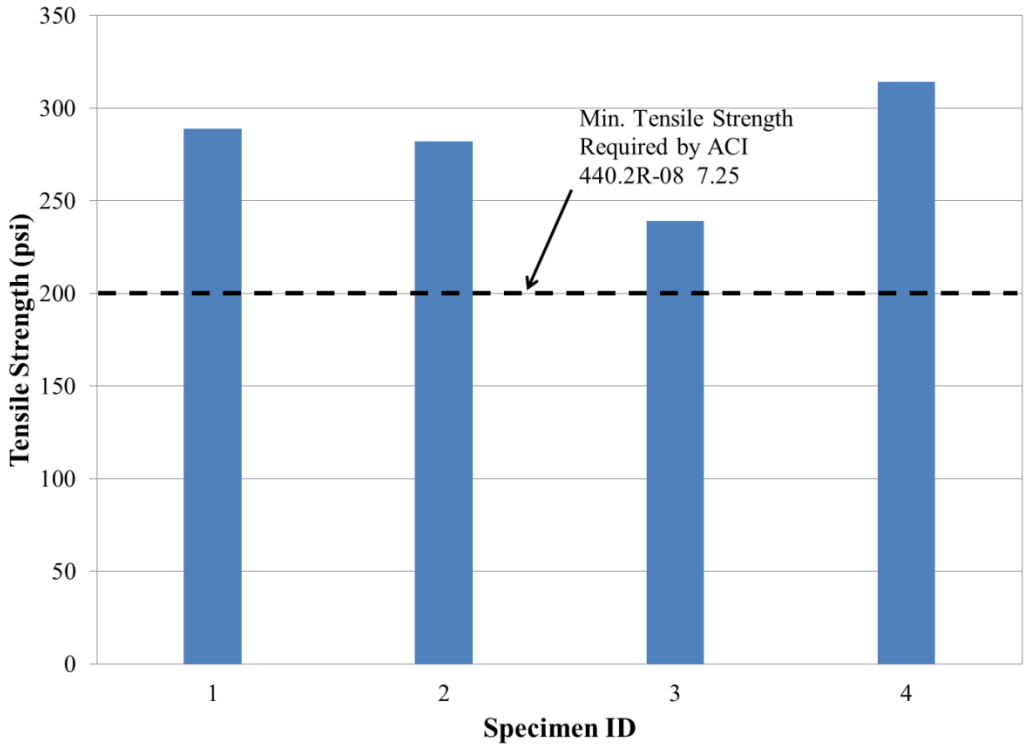

Figure A-55: Pull-Off Test Results for HM-E-E-3 specimen

A.11.5 Summary of Test Results

It was observed that the load carrying capacity was increased by 27% when compared to the unstrengthened control specimen. There was no measured ductility due to the sudden and brittle failure of the strengthening system before yielding of the reinforcement. The failure occurred due to rupture of the FRP Sheet within the maximum moment region caused by the

small rupture strain of the High Modulus fibers. The strengthening system did not allow the slab to be fully utilized due to failure of the slab before yielding of the reinforcing steel. It is recommended that fibers with a higher rupture strain be used to strengthen reinforced concrete structures to help prevent failure due to rupture of the fibers before yielding of the steel reinforcement.

A.12 HM-G-E-3 Specimen

This slab was strengthened with an externally bonded High Modulus Carbon Strand Sheet – Type 3, commercially referred to as FORCA Carbon Strands, and bonded with Grancrete PCW using the externally bonded application. This specimen was subject to a four-point bending test as shown in Figure A-56.

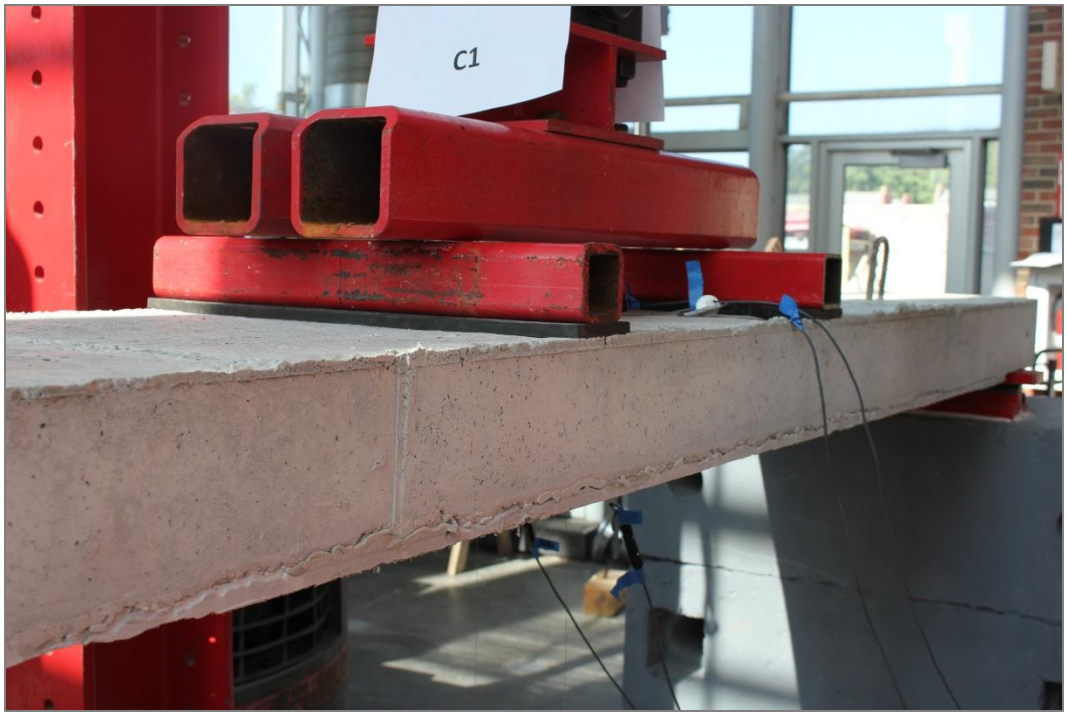

Figure A-56: HM-G-E-3 specimen under four-point bending

A.12.1 Load Displacement

The measured Load-Displacement behavior of the strengthened slab is shown in Figure A-57. This behavior shows a sudden drop in load due to failure of the strengthened system due to rupture of the fibers. The measured maximum load carrying capacity was 22,026 lbs, compared to a measured value of 13,751 for the control slab. Deflection at mid-span was 1.20 inches at failure of the strengthening system. This behavior suggests that failure of the strengthening system occurred before yielding of the steel reinforcement of the slab. Since failure of the strengthened system occurred before yielding of the steel bars, the ductility was less than unity and the failure was brittle and sudden. This was due to the use of a high FRP

reinforcement ratio and the high elastic modulus, characteristic of the Carbon FRP Strands. The measured cracking load was 5,178 lbs in comparison to 3000 lbs measured for the control slab.

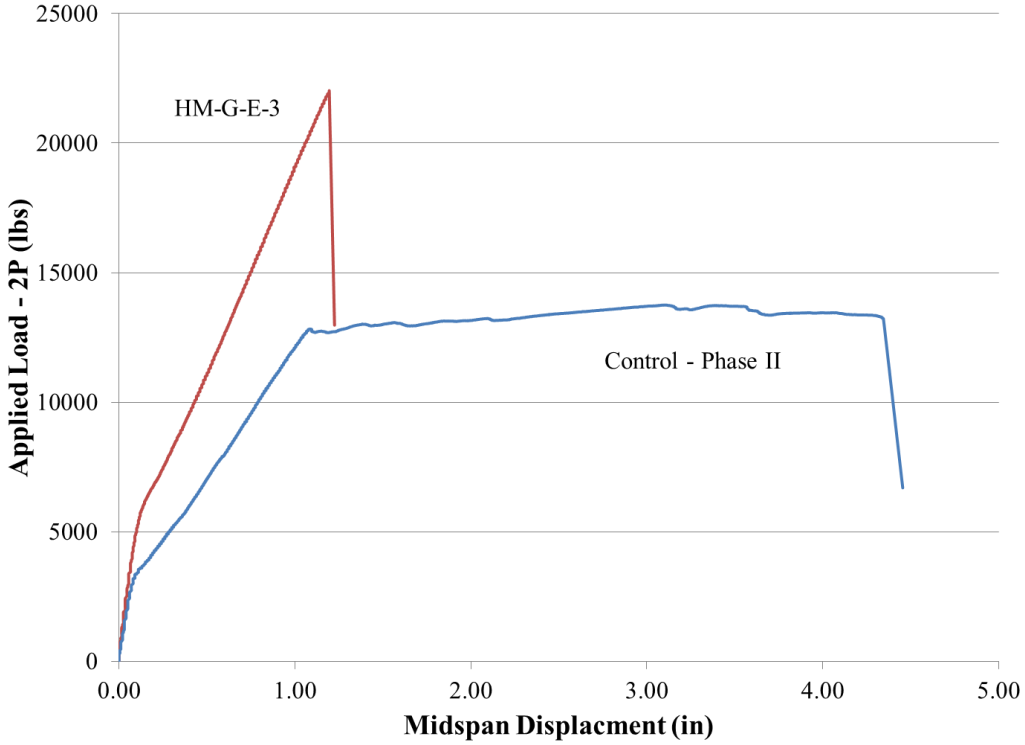

Figure A-57: Load- Deflection Behavior of HM-G-E-3 specimen

A.12.2 Load Strain

The measured Load-Strain is shown in Figure A-58. Test results indicate that the maximum measured concrete strain in compression was 0.00225. The figure also indicates that the steel reinforcement had not completely yielded before failure. This figure also indicates that the measured strain in the FRP was greater than the rupture strain that was measured using the witness panels. There are several theories for why this is. The first the measured strain in the FRP may not be actual "strain" in the carbon strands. The reason for that is the Grancrete PCW allows for flexural cracks to propagate from the sides of the slab along the bottom of the strengthening system. These flexural propagate and widen, causing these crack widths to be include in the gauge length of the PI gauges, and therefore the measured strain may be

greater than the actual strain in the carbon strands. The measured strain must be greater than the actual strain because according to Figure A-58, the reinforcing steel should have yielded due to the fact that the strain was greater than the yield strain of the reinforcing steel but it did not. A related theory is that these propagating cracks produce a strain concentration in the fibers, which may cause discrepancies between the measured strain and the actual strain.

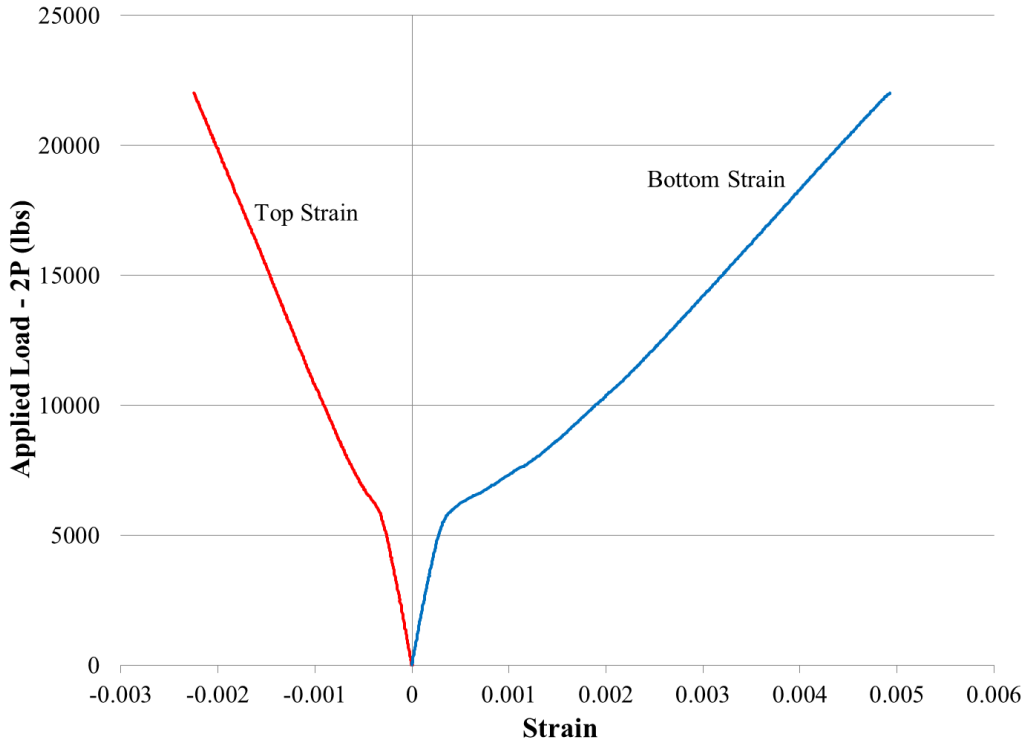

Figure A-58: Strain Measurement for HM-G-E-3 specimen

A.12.3 Inspection of Failure

Failure of the strengthening system was sudden and occurred within the maximum moment region of the slab. Failure of the strengthening system was due to rupture of the fiber within the maximum moment region of the slab. This failure is shown in Figure A-59. Inspection of the test specimen after failure showed that the FORCA carbon strand sheet had ruptured. The ruptured fibers are shown in Figure A-60.

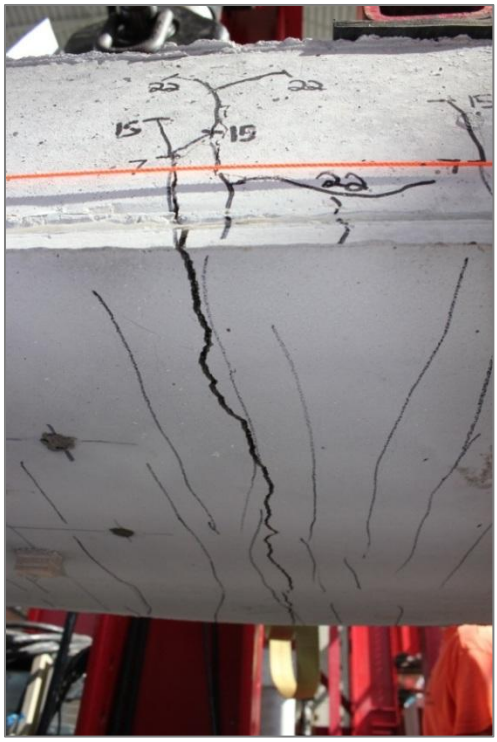

Figure A-59: Rupture of the of the FORCA High Modulus Carbon Sheet – Type 3

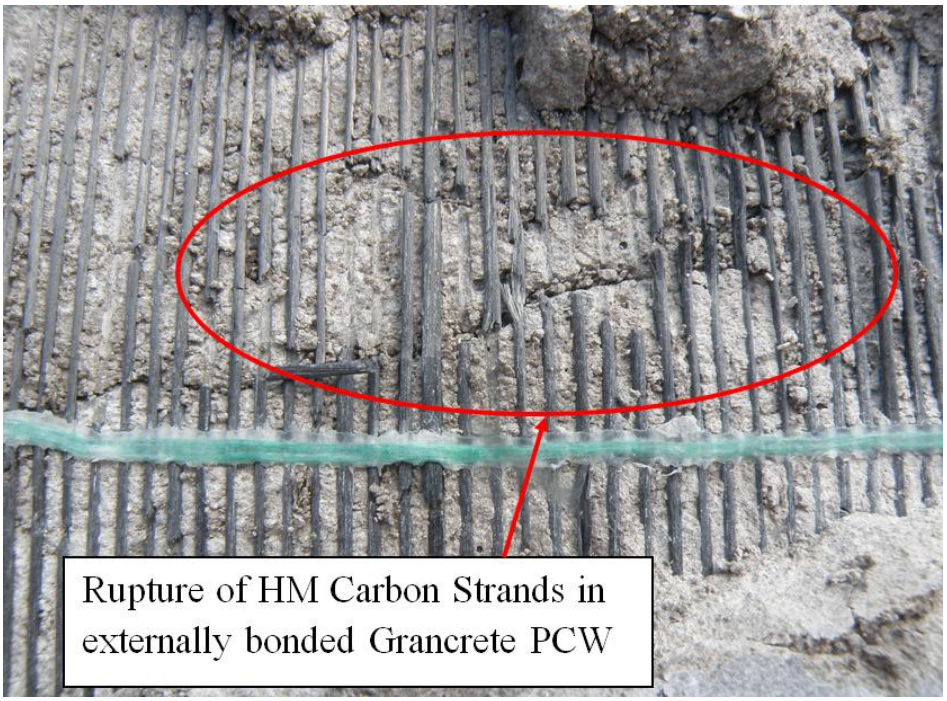

Figure A-60: Ruptured High Modulus Fibers upon Inspection

A.12.4 Pull Offs

Results of the three pull-off tests performed on the specimen are presented in Figure A-61. The figure indicates that all of the three pull-off tests performed satisfied the ACI requirement for a desirable bond strength of 200 psi. Two of the pull-off tests failed in the at the Grancrete / Fiber interface while the other failed in the concrete substrata.

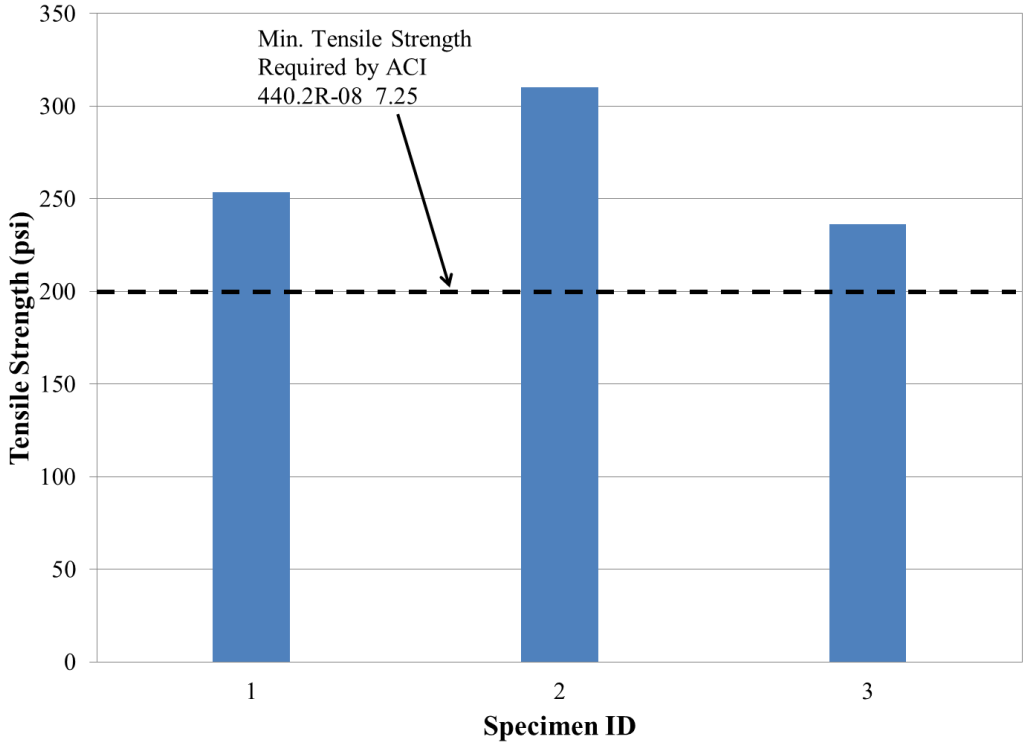

Figure A-61: Pull-Off Test Results for HM-G-E-3 specimen

A.12.5 Summary of Test Results

It was observed that the load carrying capacity was increased by 60% when compared to the unstrengthened control specimen. There was no measured ductility due to the sudden and brittle failure of the strengthening system before yielding of the reinforcement. The failure occurred due to rupture of the FRP Sheet within the maximum moment region caused by the small rupture strain of the High Modulus fibers. The strengthening system did not allow the slab to be fully utilized due to failure of the slab before yielding of the reinforcing steel. It is recommended that fibers with a higher rupture strain be used to strengthen reinforced

concrete structures to help prevent failure due to rupture of the fibers before yielding of the steel reinforcement.

A.13 HM-G-N-3 Specimen

This slab was strengthened with High Modulus Carbon Strand Sheet – Type 3, commercially referred to as FORCA Carbon Strands, and bonded with Grancrete PCW using the near surface mounted application. This specimen was subject to a four-point bending test as shown in Figure A-62.

Figure A-62: HM-G-N-3 specimen under four-point bending

A.13.1 Load Displacement

The measured Load-Displacement behavior of the strengthened slab is shown in Figure A-63. This behavior shows a sudden drop in load due to failure of the strengthened system due to rupture of the fibers. The measured maximum load carrying capacity was 19,589 lbs, compared to a measured value of 13,751 for the control slab. Deflection at mid-span was 1.32 inches at failure of the strengthening system. This behavior suggests that failure of the strengthening system occurred before yielding of the steel reinforcement of the slab. Since failure of the strengthened system occurred before yielding of the steel bars, the ductility was less than unity and the failure was brittle and sudden. This was due to the use of a high FRP

reinforcement ratio and the high elastic modulus, characteristic of the Carbon FRP Strands. The measured cracking load was 3,963 lbs in comparison to 3000 lbs measured for the control slab.

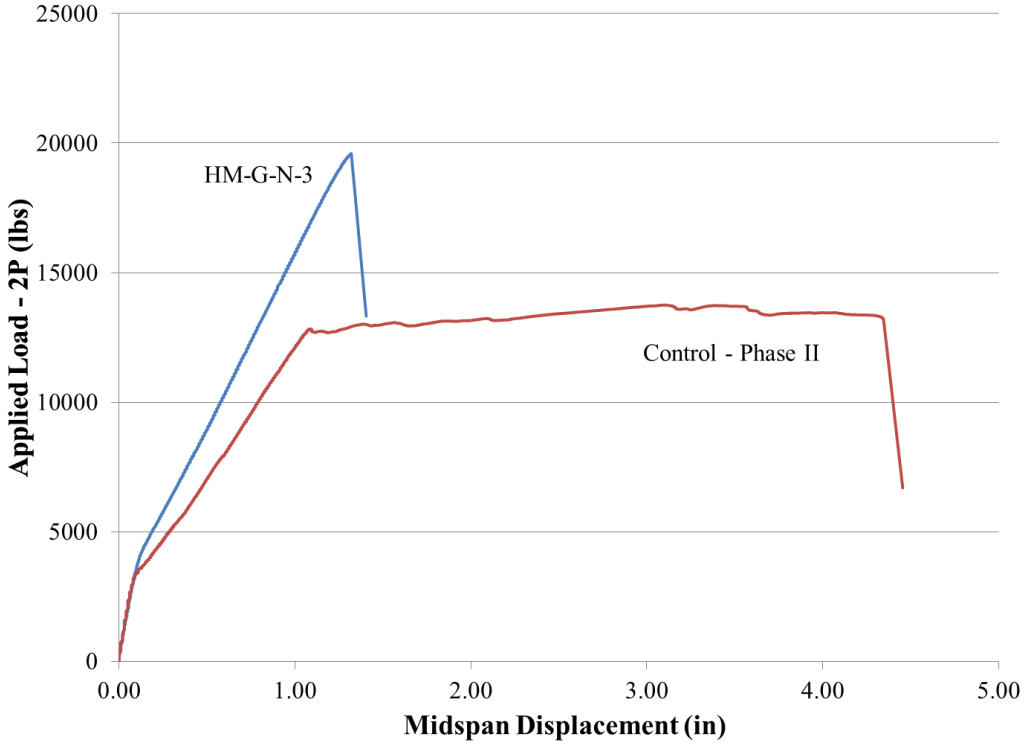

Figure A-63: Load- Deflection Behavior of HM-N-G-3 specimen

A.13.2 Load Strain

The measured Load-Strain of the top concrete surface of the slab and the bottom surface of the FRP strengthening system is shown in Figure A-64. Test results indicate that the maximum measured concrete strain in compression was 0.00258. The figure also indicates that the steel reinforcement had not completely yielded before failure. This figure also shows that the measured strain on the bottom of the slab in the maximum moment region is approximately the same in both the concrete and the Grancrete PCW adhesive that was used in the NSM grooves. This figure also indicates that the measured strain in the FRP was greater than the rupture strain that was measured using the witness panels. There are several theories for why this is. The first the measured strain in the FRP may not be actual "strain"

in the carbon strands. The reason for that is the Grancrete PCW allows for flexural cracks to propagate from the sides of the slab along the bottom of the strengthening system. These flexural propagate and widen, causing these crack widths to be include in the gauge length of the PI gauges, and therefore the measured strain may be greater than the actual strain in the carbon strands. The measured strain must be greater than the actual strain because according to Figure A-64, the reinforcing steel should have yielded due to the fact that the strain was greater than the yield strain of the reinforcing steel but it did not. A related theory is that these propagating cracks produce a strain concentration in the fibers, which may cause discrepancies between the measured strain and the actual strain.

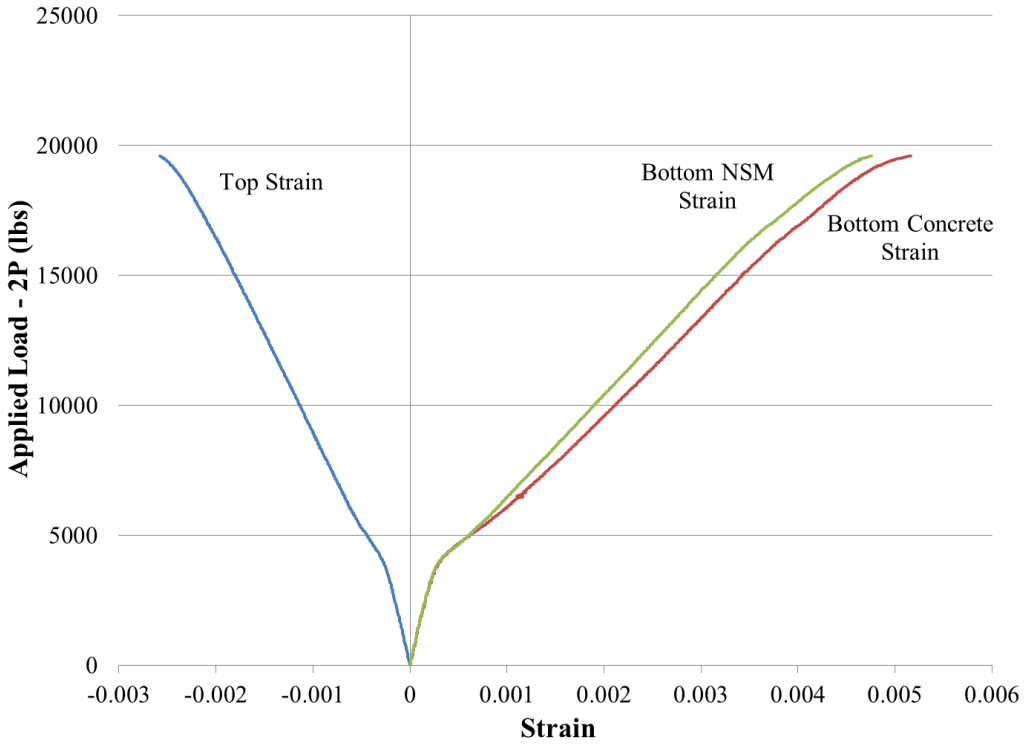

Figure A-64: Strain Measurement for HM-G-N-3 specimen

A.13.3 Inspection of Failure

Failure of the strengthening system was sudden and occurred within the maximum moment region of the slab. Failure of the strengthening system was due to rupture of the fiber within the maximum moment region of the slab. This failure is shown Figure A-65. Inspection of

the test specimen after failure showed that the FORCA carbon strand sheet had ruptured. The ruptured fibers are shown in Figure A-66. It was also observed that the adhesive was able to complete surround the bundle of carbon strands as shown in Figure A-67. This is very important because in order to achieve a strong bond, the adhesive must be able to completely surround the FRP carbon strand bundle so that a cohesive layer of adhesive may be achieved throughout the NSM groove. Failure of the adhesive to complete incase the FRP can lead to bond problems which can lead to premature debonding failures.

Figure A-65: Rupture of the of the FORCA High Modulus Carbon Sheet – Type 3

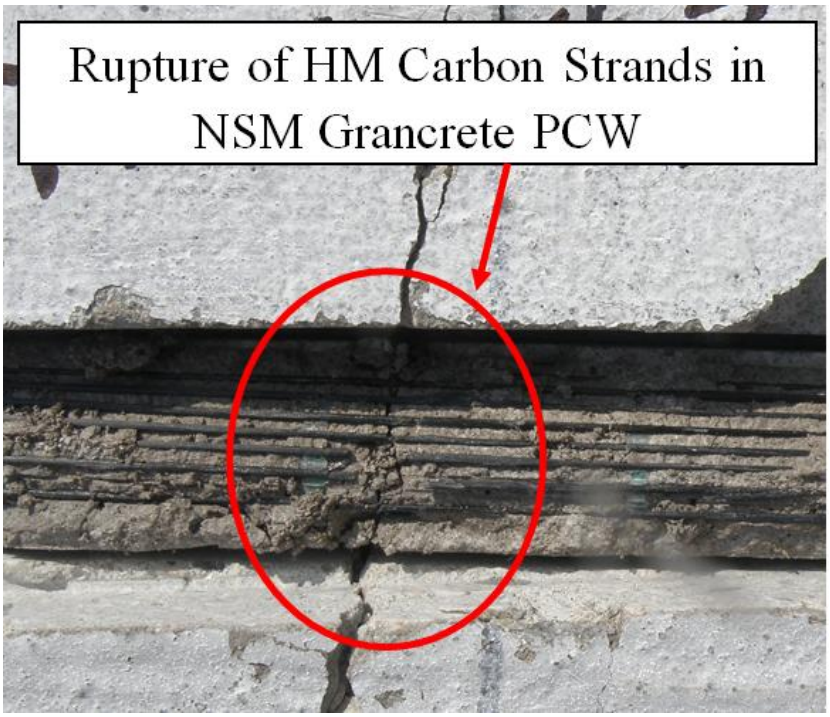

Figure A-66: Ruptured High Modulus Fibers upon Inspection

Figure A-67: Total Encasement of FRP Bundle by Grancrete

A.13.4 Pull Offs

Pull-off tests were not conducted on this specimen because the grooves were not large enough to fit the pull-off disk on the grooves.

A.13.5 Summary of Test Results

It was observed that the load carrying capacity was increased by 42% when compared to the unstrengthened control specimen. There was no measured ductility due to the sudden and brittle failure of the strengthening system before yielding of the reinforcement. During the testing, it was observed that the flexural cracks were not propagating through the Gracrete PCW in the NSM grooves as quickly as they were propagating through the concrete on the bottom the slab. The reason for this is that the Grancrete PCW/Carbon fiber system is a much stiffer system than the concrete surrounding it. This results in a greater tensile strength in the grooves, which resists cracking of the system. This delay in cracking of the NSM grooves can be seen in Figure A-68. The failure occurred due to rupture of the FRP Sheet within the maximum moment region caused by the small rupture strain of the High Modulus fibers. The strengthening system did not allow the slab to be fully utilized due to failure of the slab before yielding of the reinforcing steel. It is recommended that fibers with a higher rupture strain be used to strengthen reinforced concrete structures to help prevent failure due to rupture of the fibers before yielding of the steel reinforcement.

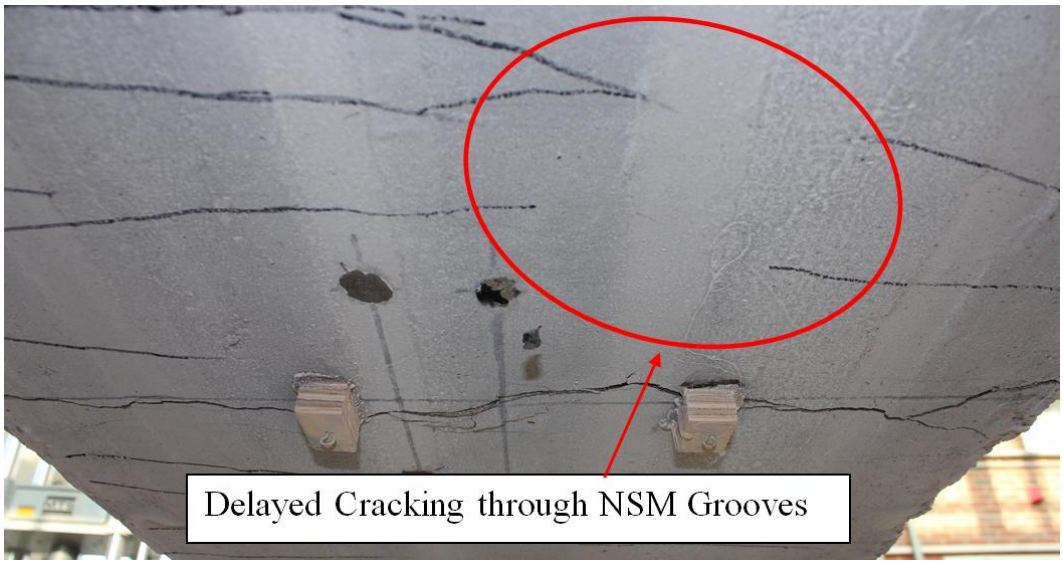

Figure A-68: Delayed Cracking through NSM Grooves

A.14 HT-E-E-3 Specimen

This slab was strengthened with a High Tensile Carbon Strand with a Type 3 spacing and epoxy supplied by the Nippon Steel Company using the externally bonded technique. This specimen was subject to a four-point bending test and is shown in Figure A-69.

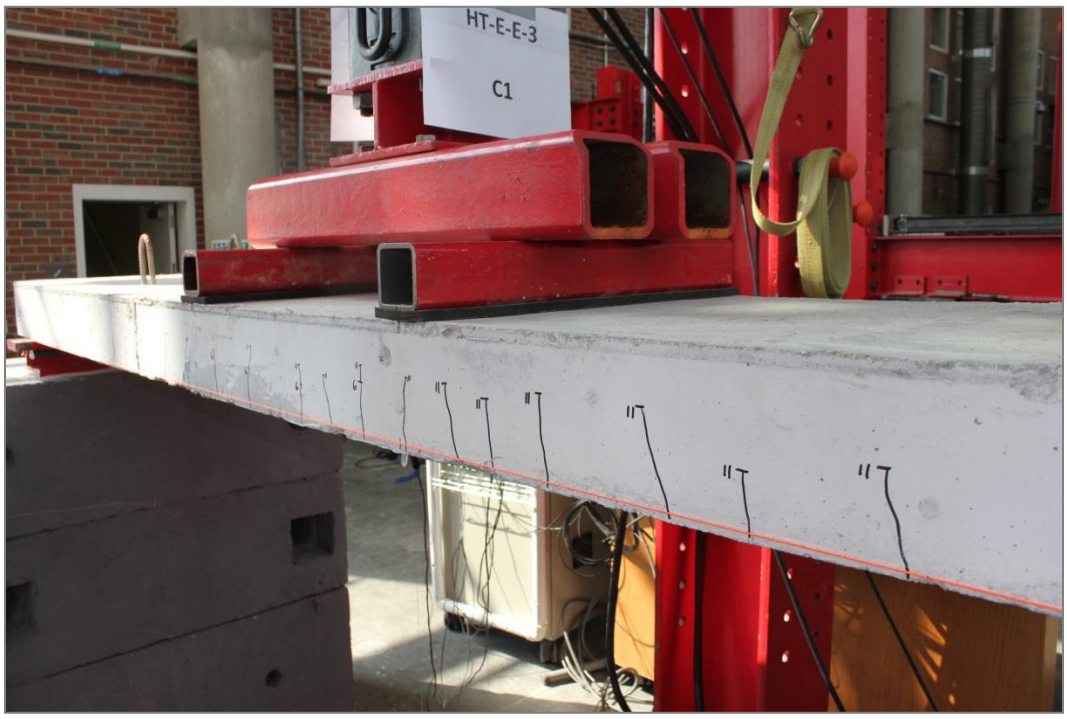

Figure A-69: HT-E-E-3 specimen under four-point bending

A.14.1 Load Displacement

The measured Load-Displacement behavior of the strengthened slab is shown in Figure A-70. From this figure it can be seen that the maximum load carrying capacity was 25,749 lbs, compared to a measured value of 13,751 for the control slab. Deflection at mid-span was 3.39 inches at failure of the slab due to crushing of the concrete followed by debonding of the strengthening system. The behavior consists of three distinct linear behaviors as shown in Figure A-70. Initially a linear behavior up to the initiation of the first crack is observed. This is followed by a semi-nonlinear behavior up to yielding of the steel reinforcement. After yielding there was reduction in stiffness up to failure due to crushing of the concrete in the maximum compression zone. The cracking load and yielding load of the strengthened

specimen was 4,284 lbs and 18,492 lbs, compared to 3,000 lbs and 12,814 lbs for the control slab, respectively. The ductility of the strengthened specimen was 2.86 and was determined by comparing the deflection at failure to the deflection at yielding of the steel reinforcement

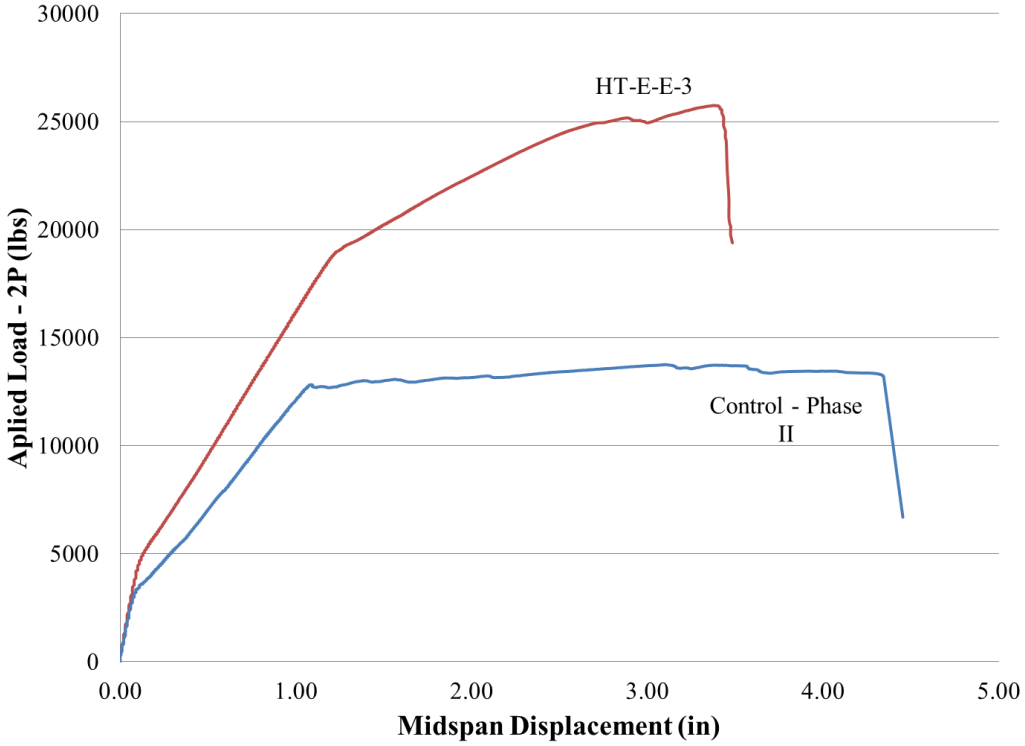

Figure A-70: Load-Deflection Behavior of HT-E-E-3 specimen

It was observed that the failure of the slab occurred at two different times. The first time it was observed that there was a failure it was observed that the concrete in the compression zone had crushed and there was a drop in load as seen in Figure A-70. The concrete crushing is shown in Figure A-71.

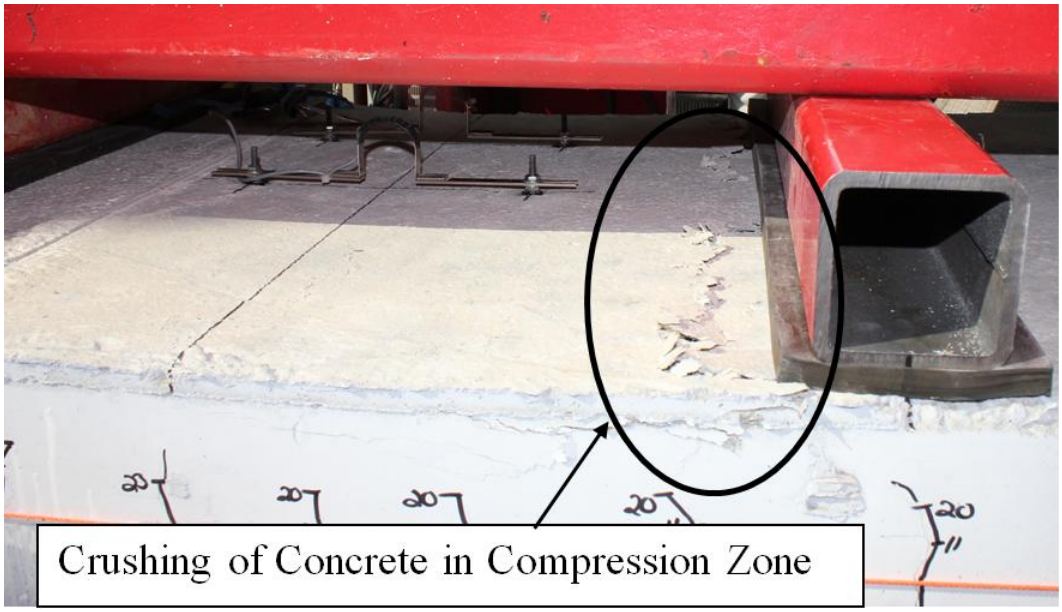

Figure A-71: Failure due to Crushing of Concrete in specimen HT-E-E-3

The second failure occurred when the strengthening system debonded from the slab. This was followed by a significant decrease in load as seen in Figure A-70. The debonding failure can be seen in Figure 80.

Figure 80: Failure due Debonding of Fibers in specimen HT-E-E-3

A.14.2 Load Strain

The measured Load-Strain of the top concrete surface of the slab and the bottom surface of the FRP strengthening system is shown in Figure A-72. Test results indicate that the maximum measured concrete strain in compression was 0.0065. The figure indicates also that all the steel reinforcement had yielded before failure.

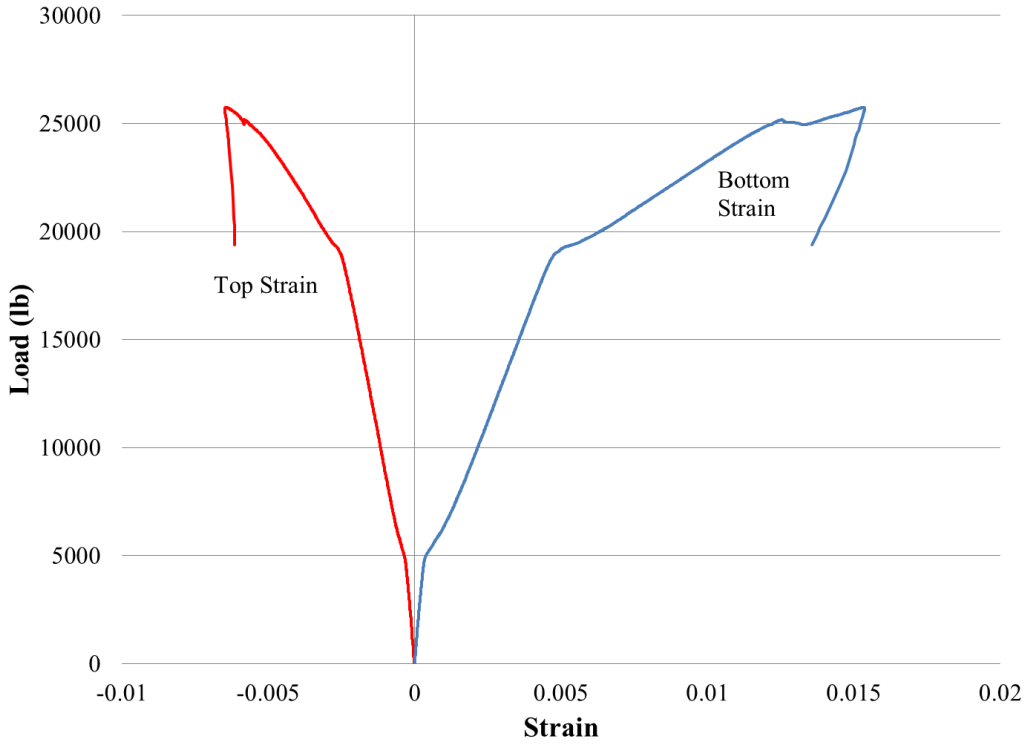

Figure A-72: Strain Measurement for HT-E-E-3 specimen

A.14.3 Inspection of Failure

Inspection of the test specimen after failure showed that the High Tensile Carbon Strand Sheet had debonded from one support to the maximum moment region. It was also observed that many flexural cracks had formed in the region of maximum moment, where debonding occurred after crushing of the concrete. Figure A-73 shows the debonded carbon strand sheet once the slab had been turned over for inspection of the fibers. It should be noted that the High Tensile Carbon Grid Strand Sheet-Type 3 achieved a very good bond when using the epoxy as the adhesive as evident by concrete cover that peeled away with the strengthening system when the system debonded as shown in Figure A-73 that shows the exposed reinforcing steel of the specimen.

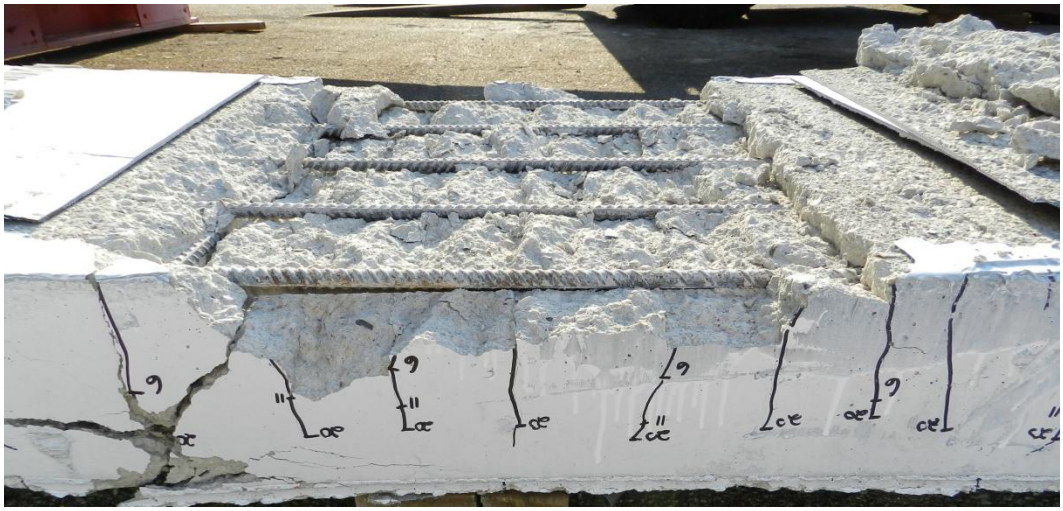

Figure A-73: Debonded Fibers from HT-E-E-3 specimen

A.14.4 Pull Offs

Results of the four pull-off tests performed on the specimen are presented in Figure A-74. The figure indicates that all of the four pull-off tests performed satisfied the ACI requirement for a desirable bond strength of 200 psi. All four of the pull-off tests failed in the in the concrete substrata, indicating that there was a strong bond between the strengthening system and the concrete surface. The results may indicate that the grid spacing is large enough to allow for the adhesive material to form a good bond between the fibers and the concrete surface.

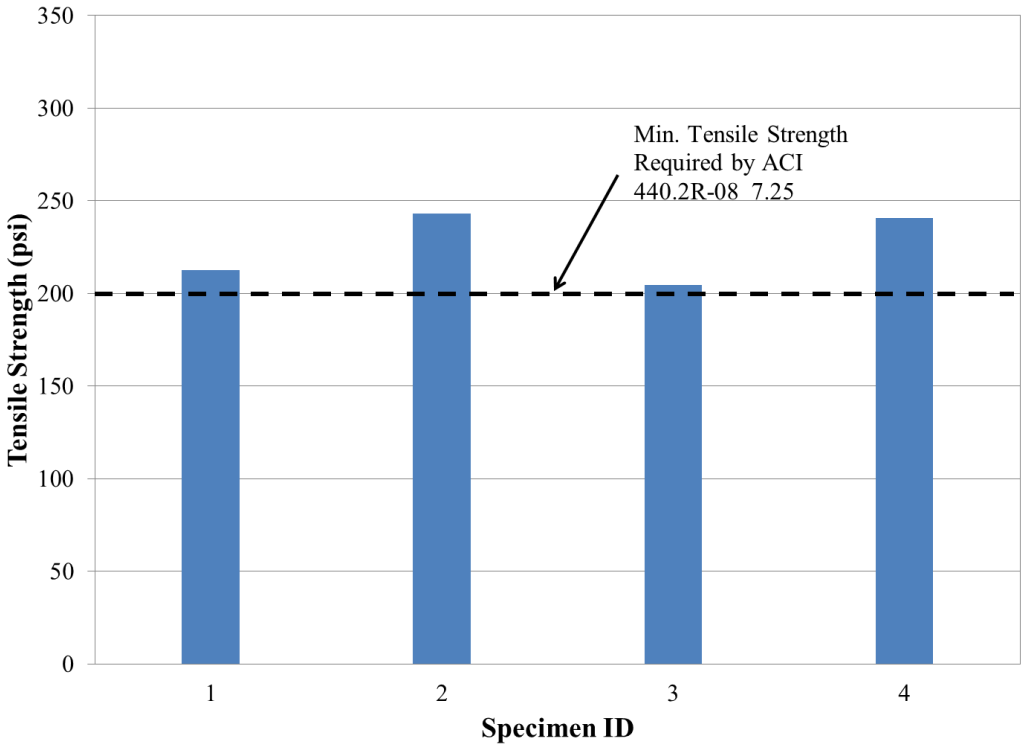

Figure A-74: Pull-Off Test Results for HT-E-E-3 specimen

A.14.5 Summary of Test Results

It was observed that the load carrying capacity is increased 87% when compared to the unstrengthened control specimen. Test results suggest that the reinforcement ratio used was capable to increase the overall load carrying capacity of the slab. The ductility was decreased by 28%. The failure was due to crushing of concrete in the maximum compression zone followed by debonding of the strengthening system. This strengthening system was fully utilized because the strengthening system debonded after failure due to concrete crushing, indicating that this is a very good system.

A.15 HT-G-E-3 Specimen

This slab was strengthened with a High Tensile Carbon Strand with a Type 3 spacing and Grancrete PCW using the externally bonded technique. This specimen was subject to a four-point bending test and is shown in Figure A-75.

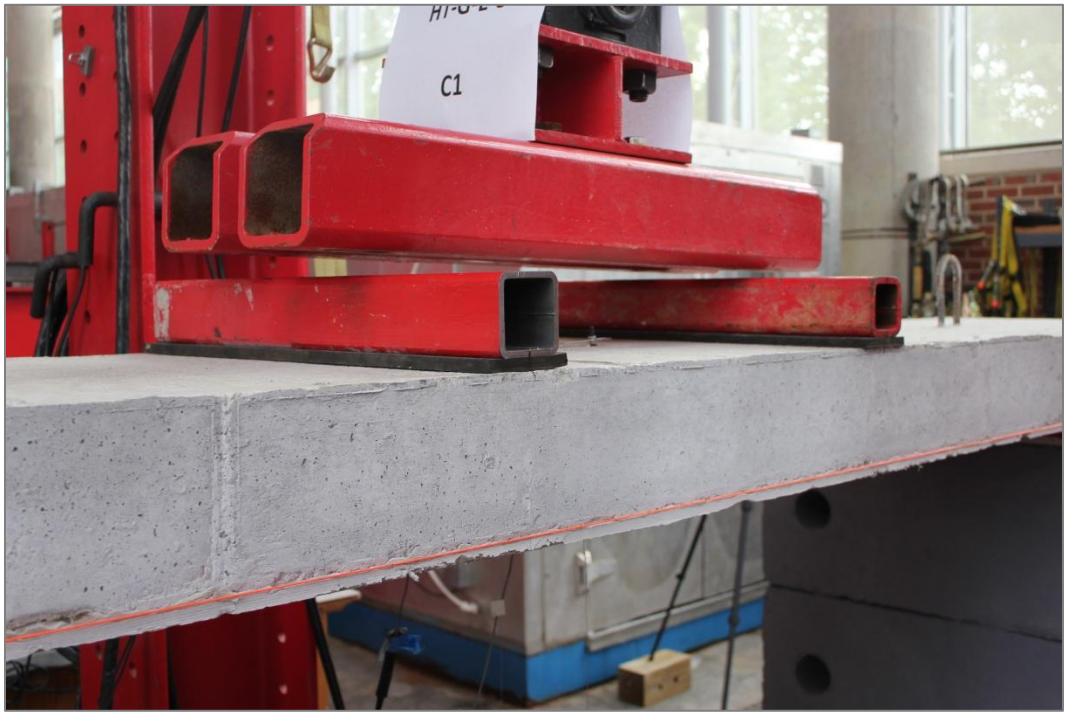

Figure A-75: HT-G-E-3 specimen under four-point bending

A.15.1 Load Displacement

The measured Load-Displacement behavior of the strengthened slab is shown in Figure A-76. From this figure it can be seen that the maximum load carrying capacity was 24,226 lbs, compared to a measured value of 13,751 for the control slab. Deflection at mid-span was 4.19 inches at failure of the slab due to crushing of the concrete in the maximum compression zone. The behavior consists of three distinct linear behaviors as shown in Figure A-76. Initially a linear behavior up to the initiation of the first crack is observed. This is followed by a semi-nonlinear behavior up to yielding of the steel reinforcement. After yielding there was reduction in stiffness up to failure due to crushing of the concrete in the maximum compression zone. The cracking load and yielding load of the strengthened

specimen was 4,495 lbs and 16,770 lbs, compared to 3,000 lbs and 12,814 lbs for the control slab, respectively. The ductility of the strengthened specimen was 3.48 and was determined by comparing the deflection at failure to the deflection at yielding of the steel reinforcement

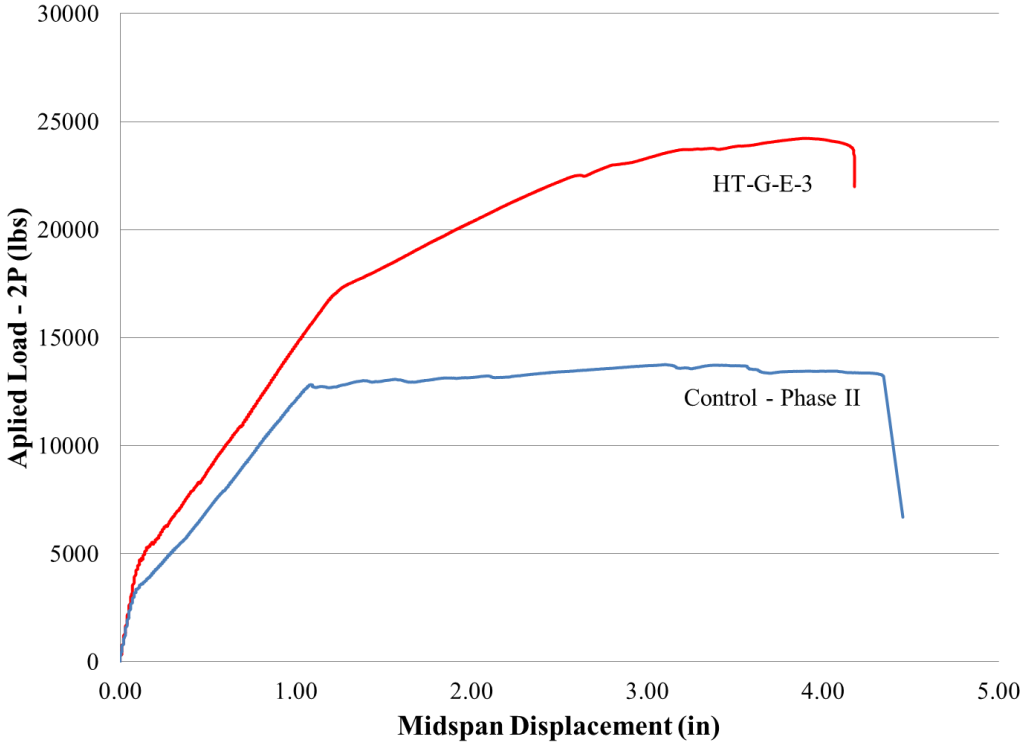

Figure A-76: Load- Deflection Behavior of HT-G-E-3 specimen

A.15.2 Load Strain

The measured Load-Strain of the top concrete surface of the slab and the bottom surface of the FRP strengthening system is shown in Figure A-77. Test results indicate that the maximum measured concrete strain in compression was 0.004. The figure indicates also that all the steel reinforcement had yielded before failure.

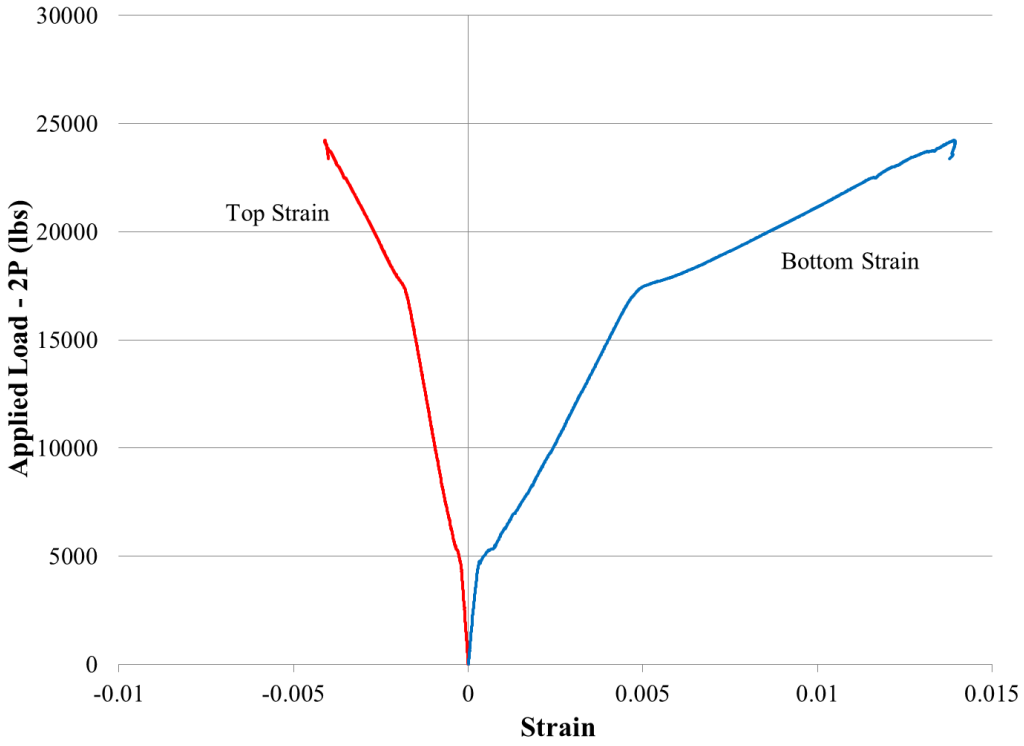

Figure A-77: Strain Measurement for HT-G-E-3 specimen

A.15.3 Inspection of Failure

Inspection of the test specimen after failure showed that the High Tensile Carbon Strand Sheet had not debonded and that failure was due to concrete crushing. It should be noted that the High Tensile Carbon Grid Strand Sheet-Type 3 achieved a very good bond when using Grancrete PCW as the adhesive as shown in Figure A-78 that shows the fibers had not debonded and that the Grancrete PCW had complete penetrated between the High Tensile Type 3 Carbon Strands. This penetration is important because it give a cohesive layer of adhesive and bond between the top layer of Grancrete PCW and the concrete surface.

Figure A-78: Grancrete penetrating between the Type 3 Carbon Strands

A.15.4 Pull Offs

Results of the three pull-off tests performed on the specimen are presented in Figure A-79. The figure indicates that all three of the pull-off tests performed satisfied the ACI requirement for a desirable bond strength of 200 psi. One of the pull offs failed at the Grancrete/Fiber interface, another in the concrete substrata, and the other at the epoxy/Grancrete interface. The results may indicate that the grid spacing is large enough to allow for the adhesive material to form a good bond between the fibers and the concrete surface.

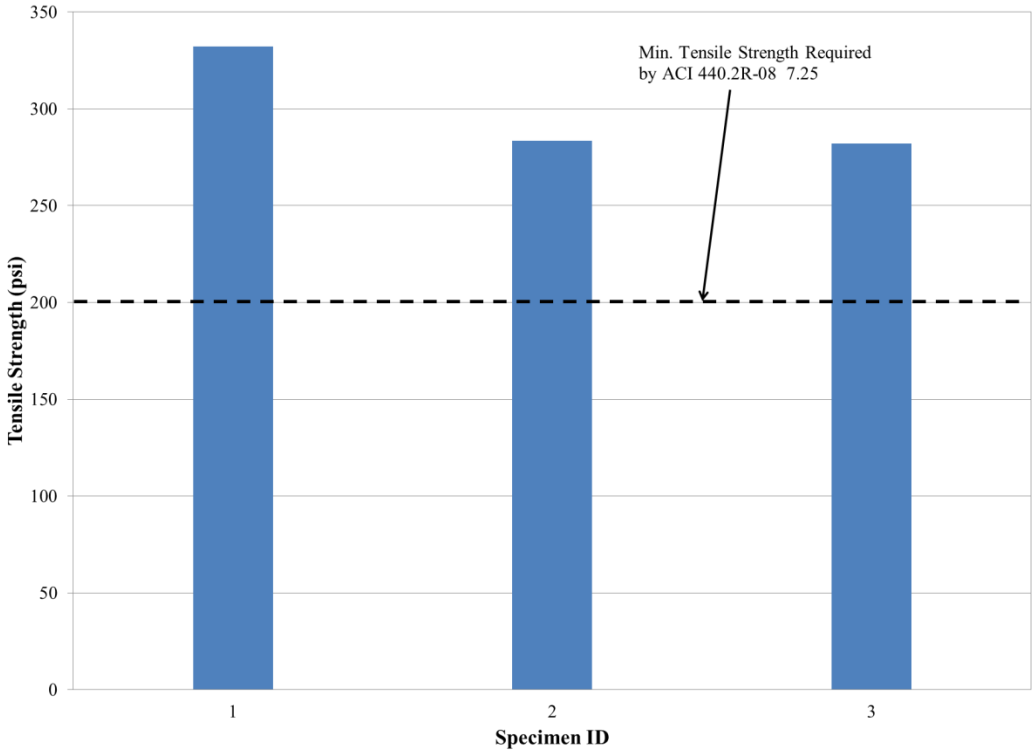

Figure A-79: Pull-Off Test Results for HT-G-E-3 specimen

A.15.5 Summary of Test Results

It was observed that the load carrying capacity is increased 76% when compared to the unstrengthened control specimen. Test results suggest that the reinforcement ratio used was capable to increase the overall load carrying capacity of the slab. The ductility was decreased by 12%. The failure was due to crushing of concrete in the maximum compression zone. This strengthening system was fully utilized because failure due to concrete crushing, indicating that this is a very good system. It should also be noted that increasing the spacing between the carbon fiber strands from a Type I to a Type 3 allowed for the cementitious material to form a better bond between the fibers, adhesive, and concrete surface, thus more fully utilizing the strengthening system. This system was also very ductile, with only a small decrease in ductility when compared to the control specimen.

A.16 HT-G-N-3 Specimen

This slab was strengthened with a High Tensile Carbon Strand with Type 3 spacing and Grancrete PCW using the near surface mounted technique. This specimen was subject to a four-point bending test and is shown in Figure A-80.

Figure A-80: HT-G-N-3 specimen under four-point bending

A.16.1 Load Displacement

The measured Load-Displacement behavior of the strengthened slab is shown in Figure A-81. From this figure it can be seen that the maximum load carrying capacity was 22,268 lbs, compared to a measured value of 13,751 for the control slab. Deflection at mid-span was 3.95 inches at failure of the slab due to crushing of the concrete in the maximum compression zone. The behavior consists of three distinct linear behaviors as shown in Figure A-81. Initially a linear behavior up to the initiation of the first crack is observed. This is followed by a semi-nonlinear behavior up to yielding of the steel reinforcement. After yielding there was reduction in stiffness up to failure due to crushing of the concrete in the maximum compression zone. The cracking load and yielding load of the strengthened

specimen was 3,595 lbs and 15,866 lbs, compared to 3,000 lbs and 12,814 lbs for the control slab, respectively. The ductility of the strengthened specimen was 3.39 and was determined by comparing the deflection at failure to the deflection at yielding of the steel reinforcement

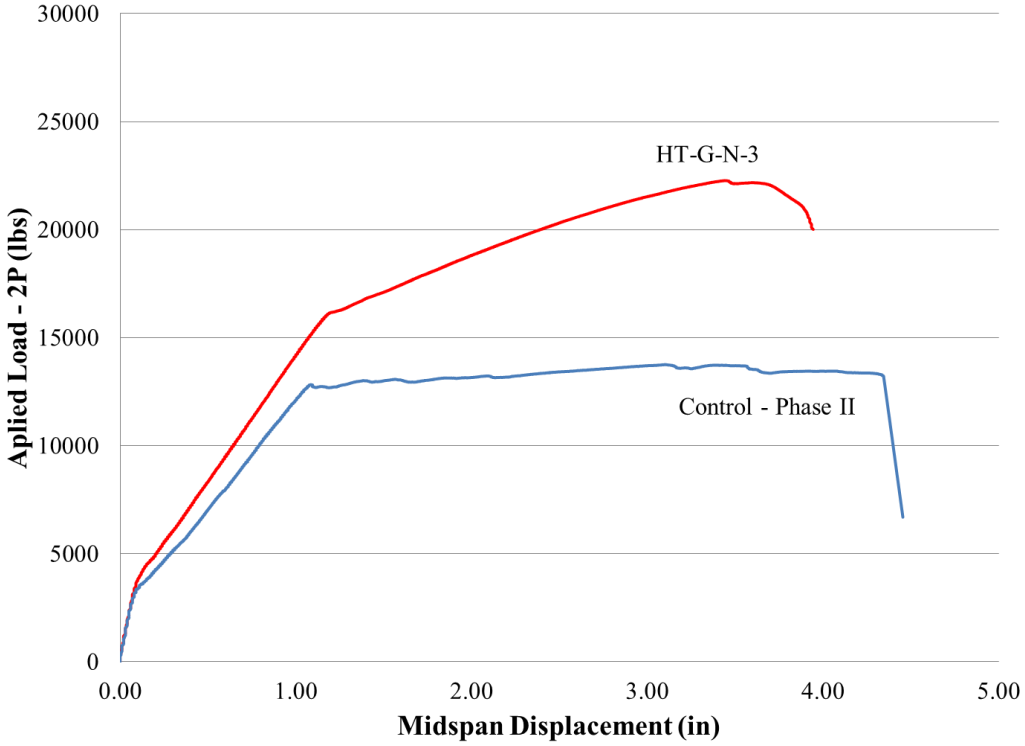

Figure A-81: Load- Deflection Behavior of HT-G-N-3 specimen

A.16.2 Load Strain

The measured Load-Strain of the top concrete surface of the slab and the bottom surface of the FRP strengthening system is shown in Figure A-82. Test results indicate that the maximum measured concrete strain in compression was 0.0068. The figure indicates also that all the steel reinforcement had yielded before failure. This figure also shows that the measured strain on the bottom of the slab in the maximum moment region is approximately the same in both the concrete and the Grancrete PCW adhesive that was used in the NSM grooves.

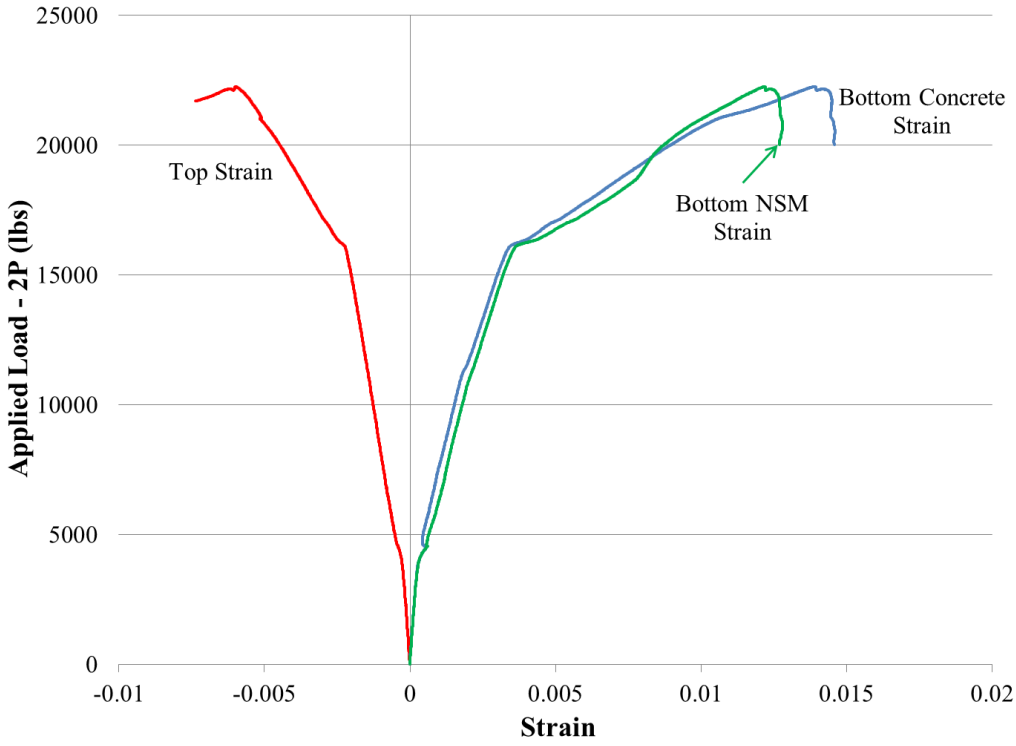

Figure A-82: Strain Measurement for HT-G-N-3 specimen

A.16.3 Inspection of Failure

Inspection of the test specimen after failure showed that the High Tensile Carbon Strand Sheet had not debonded and that failure was due to concrete crushing. It should be noted that the High Tensile Carbon Grid Strand Sheet-Type 3 achieved a very good bond when using Grancrete PCW as the adhesive as shown in Figure A-83 that shows the fibers had not debonded and that the adhesive had completely encased the carbon stand bundle. The figure also shows that the concrete substrata has formed a strong enough bond with the adhesive that it detaches with carbon strand bundle when the grove was removed for inspection.

Figure A-83: Fibers encased by Grancrete in HT-G-E-3 specimen

A.16.4 Pull Offs

Pull-off tests were not conducted on this specimen because the grooves were not large enough to fit the pull-off disk on the grooves.

A.16.5 Summary of Test Results

It was observed that the load carrying capacity is increased 62% when compared to the unstrengthened control specimen. Test results suggest that the reinforcement ratio used was capable to increase the overall load carrying capacity of the slab. The ductility was decreased by 15%. The failure was due to crushing of concrete in the maximum compression zone. This strengthening system was fully utilized because failure due to concrete crushing, indicating that this is a very good system. It should also be noted that increasing the spacing between the carbon fiber strands from a Type I to a Type 3 allowed for the cementtious material to form a better bond between the fibers, adhesive, and concrete surface, thus more fully utilizing the strengthening system. During the testing, it was observed that the flexural cracks were not propagating through the Gracrete PCW in the NSM grooves as quickly as they were propagating through the concrete on the bottom the slab. The reason for this is that the Grancrete PCW/Carbon fiber system is a much stiffer system than the concrete

surrounding it. This results in a greater tensile strength in the grooves, which resists cracking of the system. This delay in cracking of the NSM grooves can be seen in Figure A-84.

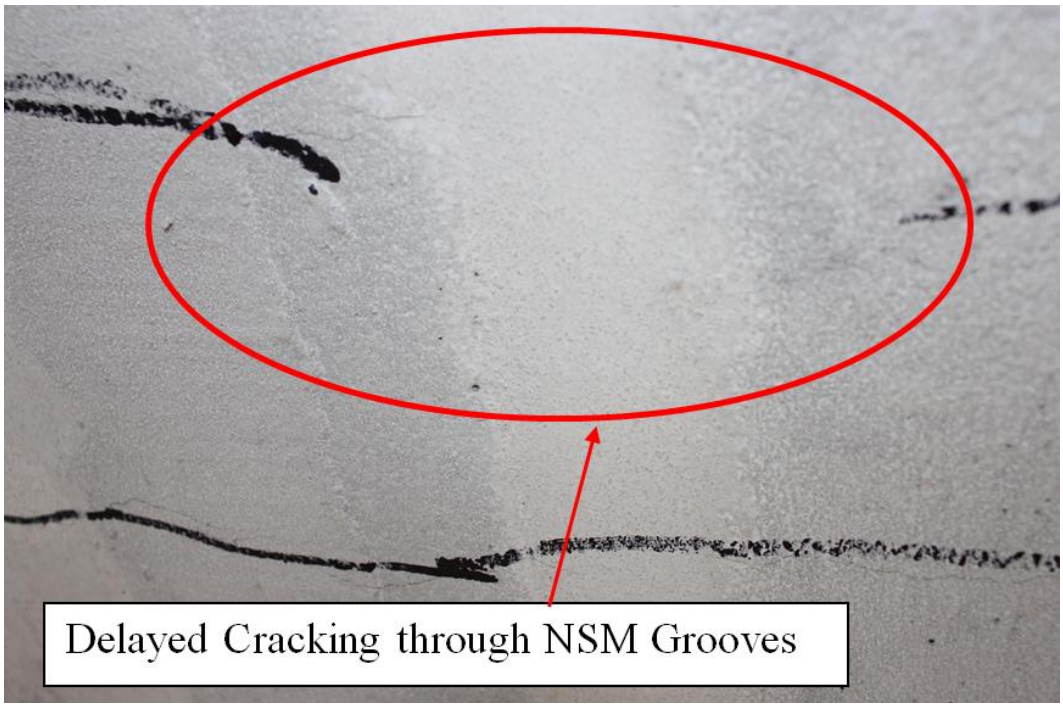

Figure A-84: Delayed Cracking through NSM FRP strips

APPENDIX B

This appendix describes the predicted values compared to the measured data of the slabs used to conduct Phase I and Phase II of the experimental program. Each specimen was given a unique strengthening ID, which is used to describe the type of fiber, type of adhesive, fiber reinforcement ratio and application technique used to strengthen the slabs. The IDs of the specimens, as well as the description of each, are shown in APPENDIX A. ACI 440.2R-08 was used to predict the ultimate load carrying capacity. The measured experimental values are compared to the predicted values in Table B-1 and Table B-2.

Table B-1: Phase I Predictions

Phase I Predictions			
	Measured	**ACI 440.2R-08 (debonding)**	**ACI 440.2R-08 (capacity)**
Slab ID	P_u *(k)*	P_u *(k)*	P_u *(k)*
G-G-E-0.25"	14.8	15.6	16.3
G-G-E-0.1"	14.8	14	14.1
C-C-E-A	19	22	21.8
C-C-E-B	20.9	22	21.8
C-E-E	20.8	22	21.8
C-G-E	20.1	22	21.8
HM-G-E-1	21.4	28.8	30.8
HT-G-E-1	21.5	26.4	31.4

Table B-2: Phase II Predictions

Phase II Predictions			
	Measured	**ACI 440.2R-08 (debonding)**	**ACI 440.2R-08 (capacity)**
Slab ID	P_u *(k)*	P_u *(k)*	P_u *(k)*
HM-E-E-3	17.5	21	21.9
HM-G-E-3	22	21	21.8
HM-N-E-3	19.6	16	21
HT-E-E-3	25.8	19.6	24.5
HT-G-E-3	24.2	19.1	23.7
HT-N-E-3	22.3	22.2	21.8